

Isolation and characterisation of bovine ultralong antibodies to SARS-CoV-2 using phage display.

Emily Jayne Park

MSc, BSc

Thesis submitted to the University of Nottingham for the degree of Doctor of Philosophy

September 2023

Abstract

The urgency for therapeutics in the arms race against SARS-CoV-2 increases with the emergence of each novel variant. Although current vaccines provide protection against severe disease in the majority of the population, there is still a great need for therapeutics for immunocompromised and severely ill patients. Broadly neutralising antibodies are highly adept at binding conserved epitopes, and, with a short developmental timescale, they are ideal candidates for antibody therapies.

In this study, consecutive immunisations were performed on two cows with Lineage A SARS-CoV-2 spike and peripheral blood mononuclear cells were isolated from the last bleed. Using this source, two bovine ultralong Fragment antigen binding (Fab) phage display libraries were constructed. Validation of the newly developed display libraries identified two Fab of interest, C13.2 and C13.7, that were subsequently cloned into a human antibody cassette and expressed in mammalian cells. Simultaneously, two rounds of biopanning were performed with the libraries against SARS-CoV-2 Lineage A trimer and SARS-CoV-2 BA.5 trimer, identifying several candidates which included C13.2 and C13.7. Full characterisation was performed on C13.2 and C13.7 through binding and neutralisation assays using spikes from different variants to assess breadth and potency. C13.2 and C13.7 were discovered to be broadly neutralising bovine antibodies. C13.2 potently neutralised pseudoviruses *in vitro* SARS-CoV-2 variants, C13.7 was less potent yet showed a greater breadth, neutralising pseudoviruses of SARS-CoV-2 variants and SARS-CoV-1.

C13.7 showed cross-reactivity to RBDs across three *Sarbecovirus* clades, warranting further investigation *in vitro, in vivo* and structural studies to determine the extent of binding and neutralisation, and ultimately the clinical potential, of this mAb. This approach identifies a pipeline for tapping into the bovine immune repertoire, which may be a powerful tool for combating rapidly emerging pathogens.

Acknowledgements

Firstly, I'd like to thank my supervisor Professor Jonathan Ball for providing me with the opportunity to complete this challenging yet rewarding project. I'd also like to thank my supervisors Dr Patrick McClure and Professor Alexander Tarr, providing invaluable guidance and support, and intellectually stimulating conversations. I'm especially grateful to Dr Richard Urbanowicz who inspired me to continue my curiosity of bovine ultralong antibodies, and for always providing exceptional support throughout my PhD journey.

A huge thank you to those who have gifted samples, making this project possible. I am eternally grateful to Dr Theocharis Tsoleridis for generating the source of B-cells, forming the foundation of this study. Thank you to Professor Pamela Bjorkman and Dr Chengcheng Fan for your work on the mAb structures and providing the panel of *Sarbecovirus* RBDs.

Thank you to the incredible National Alert and Assessment team at UKHSA, specifically Dr Mike Adams, for a fantastic placement, providing insights into bridging science and policy. To the University of Nottingham Asymptomatic Testing Service, thank you for providing the opportunity to be involved in the fight against COVID-19, the experience, and friendships I made have been invaluable.

Thanks to the Virology Research Group at the University of Nottingham, for keeping me sane, for driving me insane, and for making those painful lab days bearable. With special thanks to Jack Hill for his support at the start of this project, Dr Josh Duncan for your wealth of knowledge, Dr Joe Chappell for making me laugh, and Sophie Wartnaby for carrying me across the finish line. You're all superstars.

I'd like to thank Toby, and my family and friends around me, for your endless support, patience, and everlasting belief in me. Without you all by my side, I would have never had the strength to achieve what I have. Finally, thanks to Jack and Dougal (Appendix IV), to the cows that made this study happen, your immune systems are crazy cool.

Table of Contents

Abstract ..... **I**

Acknowledgements ..... **II**

Abbreviations ..... **XV**

Chapter 1 General Introduction ***1***

1.1. Discovery, Origin and Classification of SARS-CoV-2 ..... **1**

1.2. Insights into SARS-CoV-2 molecular biology **2**

1.2.1. SARS-CoV-2 virion and genome structure 2

1.2.2. SARS-CoV-2 life cycle 5

1.3. The immune response **9**

1.3.1. The adaptive immune response 9

1.3.2. Antibody selection 12

1.4. Immune response and targets for therapy against SARS-CoV-2 ..... **13**

1.4.1. Clinical Manifestation of SARS-CoV-2 13

1.4.2. Immune response to SARS-CoV-2 14

1.4.3. Therapies to SARS-CoV-2 19

1.4.4. Vaccines to SARS-CoV-2 20

1.5. Bovine Antibodies **22**

1.5.1. Long CDRs 22

1.5.2. Ultralong antibody formation 22

1.5.3. Bovine antibodies as therapeutics 27

1.6. Methods of antibody isolation and display **28**

1.6.1. Principles and applications of phage display 31

1.6.2. Library design 35

1.7. General Aims **36**

Chapter 2 Materials and Methodology ***38***

2.1. Preparation of samples **38**

2.2. Phagemid vector **39**

2.2.1. Phagemid modifications 40

2.3. Colony screening **44**

2.4. Library construction **45**

2.4.1. 5-alpha F'Iq E. Coli Chemically Competent Libraries 45

2.4.2. Electrocompetent TG1 libraries 46

2.4.3. HIV phage 48

2.4.4. Phage rescue and titre 49

2.5. Western Blotting and silver stain **50**

2.5.1. SDS-PAGE separation of samples and staining of SDS-PAGE 50

2.5.2. Western blotting of SDS PAGE separated samples 51

2.6. ELISA **53**

2.6.1. Phage ELISAs 54

2.6.2. IgG ELISA 56

2.6.3. MAb binding ELISAs 56

2.7. Next Generation Sequencing **.....62**

2.8. Biopanning **.....62**

2.9. Expression of chimeric mAbs **.....63**

2.9.1. Generation of chimeric mAbs using Fab subcloning and mammalian expression......64

2.10. Cell culturing **.....66**

2.10.1. Maintenance of cell lines.....66

2.10.2. Transient transfection of HEK293T cells.....67

2.10.3. Transient transfection of Expi293F cells.....67

2.10.4. Infection and Neutralisation assays.....68

2.11. Protein purification and quantification **.....70**

2.11.1. Protein G purification of Expi293F produced mAbs.....70

2.11.2. BCA assay quantification of proteins.....70

2.11.3. Endotoxin assay.....70

2.12. RBD panel expression **.....71**

2.13. mAb modifications to Fab **.....72**

2.13.1. mAb plasmid modifications.....72

2.13.2. Fab expression.....73

2.13.3. Cryo-EM structures of ultralong Fab.....73

Chapter 3 Design and construction of a bovine ultralong antibody phage display library **.....74**

3.1. Summary **.....74**

3.2. Introduction **.....74**

3.3. Aim of Chapter **.....80**

3.4. Results **.....81**

3.4.1. Development of the control phage **.....81**

3.4.1.1. Isolation of ultralong heavy and light chain from NC Cow 1......81

3.4.1.2. Cloning of HIV Fab into the phagemid vector.....82

3.4.1.3. Optimising the phage rescue protocol.....84

3.4.1.4. Validating bovine ultralong Fab phage expression.....86

.....91

3.4.2. Construction and validation of the bovine ultralong Fab library **.....92**

3.4.2.1. Construction of libraries in 5-alpha F'Iq E. coli chemically competent cells....92

3.4.2.2. Validation of expression and specificity of 5-alpha F'Iq E. coli libraries.....95

3.4.2.3. Investigating library heavy chain representation.....98

3.4.2.4. Validation of library clones by phage ELISA and western blot.....99

3.4.2.5. Validation of library diversity by NGS.....103

3.4.2.6. Construction and validation of the libraries with TG1 cells.....109

3.4.2.7. Pooling the phage libraries.....112

3.4.3. Modifications of phagemid vector **.....115**

3.5. Discussion **.....116**

3.6. Conclusion **.....124**

Chapter 4 Biopanning C13 and C18 Libraries **.....125**

4.1. Summary **125**

4.2. Introduction **125**

4.3. Aim of chapter **130**

4.4. Results **131**

4.4.1. Biopanning R1: Lineage A Trimer 131
4.4.2. Biopanning R2: SARS-CoV-2 BA.5 Trimer 137
4.4.3. Evaluation of panning titres 140
4.4.4. Evaluation of biopanning binding 142

4.5. Discussion **144**

4.6. Conclusion **149**

Chapter 5 Characterisation of chimeric ultralong antibodies 151

5.1. Summary **151**

5.2. Introduction **151**

5.3. Aim of chapter **155**

5.4. Results **156**

5.4.1. Subcloning Fab of interest into mammalian expression vector 156
5.4.2. CDRH3 sequence analysis 158
5.4.3. HEK293T expression of mAbs 158
5.4.4. Initial investigations into mAb binding and pseudovirus neutralisation 160
5.4.5. Expi293 expression of mAbs 164
5.4.6. Purification of Expi293 expressed mAbs 165
5.4.7. Quantification of mAbs 168
5.4.8. Analysing mAb expression 172
5.4.9. Characterising the binding profiles of C13.2 and C13.7 174
5.4.10. Investigating C13.2 and C13.7 binding epitopes through competition ELISA 178
5.4.11. C13.2 and C13.7 neutralisation of pseudotyped SARS-CoV variants 181
5.4.12. C13.7 binds a pan-sarbecovirus RBD epitope 188
5.4.13. Structural analysis of C13.2 and C13.7 190

5.5. Discussion **193**

5.6. Conclusion **203**

Chapter 6 General Discussion 204

Appendix I – HIV Fab fused to truncated gene 3 protein **217**

Appendix II - C13.2 and C13.7 Heavy chain in the phagemid **217**

Appendix III – RBD BCA assay and Anti-avi-tag ELISA **218**

Appendix IV – Jack and Dougal **219**

References **220**

List of Figures

Figure 1.1: Schematic of SARS-CoV-2 virion and the positive single stranded RNA genome of SARS-CoV-2: SARS-CoV-2 virion has four structural proteins: Spike (S), Nucleocapsid (N), Membrane protein (M), and Envelope protein (E). Genome: 5' cap, followed by leader sequence and the UTR. Sequentially, ORF1a, ORF1b. Non-structural proteins (NSP1–11, 12–16) are encoded by ORF1a and ORF1b, respectively. Spike protein (S) consists of S1 and S2, divided by furin cleavage site. S1 is further subdivided into N Terminal Domain (NTD), RBD, SD1 and SD2. This is followed by ORF3a, E, M, ORF6, ORF7a, ORF7b, ORF8, N, ORF10. 3' end consists of an UTR, and Poly-A tail. Source: (Zhang et al., 2021b). 4
Figure 1.2: The life cycle of SARS-CoV-2 in a host cell expressing ACE2. Briefly, the SARS-CoV-2 spike interacts with ACE2 and is endocytosed into the host cell cytoplasm. Translation of the viral polymerase is achieved through the host cell ribosome to generate a polyprotein that is subsequently cleaved by proteases. This enables continuous and discontinuous transcription for RNA and translation of viral structural proteins. S, E and M proteins combine with N and are translocated to the Golgi apparatus to form an Endoplasmic Reticulum – Golgi Intermediate Compartment (ERGIC) leading to the formation of mature virions. Subsequently, mature virions are exported out of the cell by exocytosis. Source: (Alanagreh et al., 2020). 8
Figure 1.3: Diagram of the structure of an immunoglobulin. Immunoglobulins are segregated into constant and variable regions, of which the variable comprises the antigen binding region. The variable region consists of regions of framework and complementary determining regions. Each variable segment on heavy and light chain loci are associated with a 5' leader sequence (L). The variable domains of light and heavy chains are formed from VDJ segments from the Ig heavy chain germline locus for the heavy chain, and VJ segments from Ig Kappa or Lambda light chain germline locus for the light chain. Recombination events are achieved by gene-activating machinery RAG1 and RAG2 (Ekman et al., 2009). Diagram altered from (Boyd and Joshi, 2014) using Biorender. 12
Figure 1.4: Cryo EM schematic showing classes 1-4 antibodies with the RBD (grey). N343 glycan in cyan blue. Class 1 in green, class 2 yellow, class 3 blue and class 4 pink. Source: (Barnes et al., 2020a)..... 17
Figure 1.5: Ribbon representation on human (left) and bovine (right) Fab (green) with CDRH3 regions (red). Bovine CDRH3 is comprised of a stalk and knob. Source: (Haakenson et al., 2018). 24
Figure 1.6: Schematic structure of M13 filamentous bacteriophage and its replicative cycle. Briefly, the M13 p3 interacts with the f pilus of the host cell membrane resulting in the release of single-stranded DNA into the cytoplasm. Replication occurs within a double-stranded replicative form to transcribe and translate phage proteins. Assembly and elongation occur at the host cell membrane where new phage particles are released from the membrane. (Source: (Huang et al., 2012). 34
Figure 1.7: Schematic of phage display process. Library construction was achieved by isolating RNA and synthesising cDNA. Heavy chains were amplified using germline specific primers and cloned into a phagemid vector harbouring a common bovine

light chain. The library was transformed into *E. coli* and rescued by coinfection with M13KO7 helper phage. The library was biopanned against immobilised Lineage A spike trimer and high affinity binders eluted and characterised. Created using BioRender. 37
Figure 2.1: Schematic of immunisation schedule of *Bos Taurus*. *Bos Taurus* were immunised on day 0 of the study with SARS-CoV-2 Lineage A S1, and subsequently boosted with the same immunogen on days 21 and 42. Both animals were immunised with SARS-CoV-2 Lineage A full-length spike on day 161, and then with SARS-CoV-2 Lineage A Trimer on day 235. All antigens were made soluble in Titermax Gold adjuvant. Animals were bled 7 days post immunisation. Created using BioRender. 38
Figure 2.2: Map of the pFab3 phagemid vector. The map shows the 4339 bp vector containing the origin of replication, *lac* promotor, ampicillin resistance, signal peptides, cassettes harbouring bovine (Bos) heavy and light chain insertions, and terminal gene 3 DNA. Created using SnapGene. 40
Figure 2.3: Diagram of primer use for optimising TG1 library PCR. R1 Bt IgH F 2F and IgH Rev4. R2A: VH1-7 36 F and IgH Rev4 30 BP. R2B: VH1-7 F and IgH Rev4. R3A: VH1-7 36 BP F and IgH Rev4 30 BP. 47
Figure 2.4: Heavy (left) and light (right) chain cassettes for subcloning for mammalian expression. Cassettes are prior to an f1 origin of replication, SV40 origin, neo/kan resistance, *Lac* promotor, ampicillin resistance, and CMV promotor. Created using SnapGene. 64
Figure 3.1: Phage formats proposed by George Smith. Minor coat protein p3 has three systems: 3 where the recombinant gene is fused to the genome resulting in expression of recombinant g3p only, 33 where the wild-type and recombinant gene 3 are fused to the genome resulting in both expressed, and 3+3 where the recombinant g3p is maintained separately from the wild-type phage genome. Major coat protein p8 has 3 systems: 8, 88, and 8+8, reflecting those of p3, yet expression is on the major coat protein. (Jaroszewicz et al., 2022). 77
Figure 3.2: Amplification of ultralong heavy and light chains from plasmids harbouring a HIV antibody. Lane 1: 10 Kb DNA Marker (M), Lane 2: Ultralong heavy chain at approximately 550 base pairs (H), Lane 3: Light chain at approximately 380 base pairs (L), Lane 4: negative control (N/C). 82
Figure 3.3: PCR colony screen of E. coli cells for phagemid ligation of light and heavy antibody chains. A) Lanes 9-12, 15, and 16 negative colonies that did not contain the light chain. Lanes 13 and 14 were positive for light chain ligation into the phagemid (red arrow). B) Lanes 1, 2, 4, 5, 7, and 8 contained the light chain only. Lane 3 did not contain heavy or light chains. Lane 6 was positive for heavy chain ligation (red arrow) into PFAB3 L.14. M = 10 Kb DNA molecular marker, N/C = negative control. 84
Figure 3.4: Optimisation of MOI of bacteria to helper phage ratio. Bars represent ratios 10:1, 1:1, 1:2 of bacteria to helper phage, recorded as phage titre cfu/mL. 10:1 bacterium to helper phage yielded a mean titre of 5×10^9 cfu/mL whereas an excess of helper phage. 2:1 bacterium to helper phage obtained a mean yield of 5.98×10^{12} cfu/mL. 1:1 bacterium to helper phage obtained a mean titre of 1.95×10^{13} cfu/mL. Statistical significance determined by Kruskal Wallis test with Dunn's multiple comparisons test. N=7. P = < 0.01. Error bars represent standard deviation. 86

Figure 3.5: Anti -Fd reduced protein expression of HIV phage and Ficolin control phage. HIV phage (Lane 2) and Ficolin control phage (Lane 3) was analysed by western blot under reducing conditions using an anti-Fd antibody. Band at 55 kDa inferred as Wild-type (WT) g3p, and band at 40 kDa as recombinant g3p (heavy chain fused to truncated g3p) Other bands present at 12 and 20 kDa are reduced products expressed by the phage and detected by Anti-FD. 87
Figure 3.6: ELISA to determine the binding of the HIV phage to HIV protein gp140, measured in OD_{405} nm. The HIV phage bound to gp140 at a mean OD_{405} nm of 2.4. The negative control phage (N/C phage) showed low binding to gp140 with a mean OD_{405} nm of 0.2. Controls were trialled to assess the ELISA design, none showed significant binding to gp140 compared to the HIV phage. The HIV phage bound to uncoated wells at a mean OD_{405} nm of 3.1. Statistical significance by One way ANOVA with Tukey's multiple comparisons, N=2, p = <0.0001. Error bars demark standard deviation. 89
Figure 3.7: HIV phage binding was specific to HIV proteins compared to SARS-CoV-2 Lineage A trimer. A) HIV phage bound to gp140 at a mean OD_{405} nm value of 1.78, and gp120 at 2.5. Statistical significance by Unpaired T test, N=2, p = <0.05. B) HIV phage bound to gp120 at a mean OD_{405} nm value of 1.7 compared to SARS-CoV-2 Lineage A trimer at 1.1. A positive control showed strong binding to SARS-CoV-2 Lineage A trimer at a mean OD_{405} nm value of 2.8 compared to the HIV phage which bound at a mean OD_{405} nm value of 1.1. Controls were trialled to assess the ELISA design, none showed significant binding to gp120 compared the HIV phage, the HIV phage to SARS-CoV-2 Lineage a trimer or SARS-CoV-2 Lineage A trimer when compared the positive control. Statistical significance by One way ANOVA with Tukey's multiple comparisons, N = 2, ** p = <0.05, **** p > 0.0001. Error bars demark standard deviation. 91
Figure 3.8: Digestion of PFAB3 L.14 and amplification of ultralong antibody heavy chains from C13 and C18. A) Lane 1: marker, Lane 2: digested PFAB3 L.14 band at 6,000 base pairs B) Lane 1: marker, Lane 2: C13 band between 500 and 600 base pairs, Lane 3: C18 band between 400-500 base pairs, band at 800 base pairs suspected to be non-specific. M = 10 Kb DNA molecular marker. 92
Figure 3.9: Colony PCR screen of trial heavy chain library transformations into 5-alpha F'Iq E. coli cells. A) Heavy chain colony screen of 2.5 μL cloning reaction, and B) Heavy chain colony screen of 10 μL cloning reaction. Both reactions show eight colonies positive for heavy chains from C13, ranging from 500 to 550 base pairs, and eight colonies positive for heavy chains from C18, all around 490 base pairs. B) The HIV heavy chain was cloned simultaneously, all eight colonies are positive with the HIV heavy chain around 550 base pairs. A+B) M = 10 Kb DNA molecular marker, N/C = negative control. 94
Figure 3.10: Anti -FD reduced protein expression of C13 and C18 phage libraries, and HIV control phage. The phage libraries (Lane 2: C13, Lane 3: C18) and HIV phage (Lane 4) were analysed by western blot under reducing conditions using an anti Fd antibody. Band at 55 kDa inferred as wild-type (WT) g3p. Bands around 40 kDa inferred as recombinant g3p (heavy chain fused to truncated g3p). Other bands present at 12 and 20 kDa are reduced products expressed by the phage and detected by Anti-FD. The molecular marker (Lane 1: M) shown in kDa. 95
Figure 3.11: Phage ELISA of each phage library binding to target protein as captured or direct coating, measure as OD_{405} nm. A) C13 phage library binding to neutravidin

captured biotinylated SARS-CoV-2 Lineage A trimer compared to C13 phage library binding to neutravidin only. C18 phage library binding to neutravidin captured biotinylated SARS-CoV-2 Lineage A trimer compared to C18 phage library binding to neutravidin only. Table to the right demarks assay design. Controls were trialled to assess the ELISA design, none showed significant binding to neutravidin captured biotinylated SARS-CoV-2 Lineage A trimer compared to the phage libraries or SARS-CoV-2 Lineage A trimer compared to the libraries. Statistical significance by One way ANOVA with Tukey's multiple comparisons, N=2, p = <0.0001. Error bars demark standard deviation. B) C13 and C18 phage Library binding to a high concentration of directly coated SARS-CoV-2 Lineage A trimer compared to a phage that was known to not exhibit binding to SARS-CoV-2 Lineage A trimer. Statistical significance by One way ANOVA with Dunnett's multiple comparisons, N=2, p = <0.05. Error bars demark standard deviation. 97

Figure 3.12: Colony PCR Screen of colonies of the libraries generated by linearising the vector and amplification using new primers PFAB3 COL F and PFAB3 COL R. A) C13 library colony screen of colonies 1-10. Bands at 800 base pairs or above contain a heavy chain. Bands around 400 base pairs did not contain a heavy chain. B) C18 library colony screen of colonies 1-9. All colonies were positive with bands showing at approximately 800 base pairs. A+B) M = 10 Kb DNA molecular marker, N/C = negative control. 99

Figure 3.13: ELISA to determine the binding of C13 and C18 library to SARS-CoV-2 Lineage A trimer, measured as OD_{405} nm. A) Phage ELISA to show binding of 18 clones, nine from C13 and nine from C18, to SARS-CoV-2 Lineage A Trimer, compared to background binding of a light chain only phage. Dotted line represents background binding at a mean OD_{405} nm of 0.2. Nine clones showed greater binding to the target compared to the light chain only phage. Statistical significance in binding by One Way ANOVA, and Dunnett's multiple comparisons test to background binding, N=2, p = <0.05. B) C13.2, C13.3, C13.6 and C13.7 showed strong binding to SARS-CoV-2 Lineage A trimer with mean OD_{405} nm values of between 1.6-1.8 compared to the binding of gp120 where mean OD_{405} nm values ranged between 0.4 and 0.7 to the HIV phage. Binding to SARS-CoV-2 trimer was statistically significant compared to gp120 for the four phage clones. Statistical significance by One way ANOVA with Tukey's multiple comparisons, N=2, * p= <0.05, ***p= <0.001, ****p= <0.0001. Error bars demark standard deviation. 101

Figure 3.14: Protein expression of C13 and C18 phage libraries, HIV phage, C13.2 and C13.7. The phage libraries (Lane 2: C13, Lane 3: C18), HIV phage (Lane 4), C13.2 phage (Lane 5), C13.7 phage (Lane 6) and wild-type M13 (Lane 7) were analysed by western blot under reducing conditions using A) an anti Fd antibody and B) an anti g3p antibody. Band at 55 kDa inferred as wild-type (WT) g3p and bands between 40 and 50 kDa and inferred as recombinant g3p (heavy chain fused to truncated g3p). Other bands present in A at 12 and 20 kDa are reduced products expressed by the phage and detected by Anti-FD. Other bands present in B at 11, 28, 30 and 38 kDa are reduced fragments of g3p or of Fab fragments fused to g3p. A+B) M = molecular marker, shown in kDa. 102

Figure 3.15: Investigating primer bias. Alignment of 24 unique sequences with 1 to 5 base pair mismatches to the VH1-7 germline-specific primer. Bases coloured T in green, G in yellow, A in red and C in blue. 104

Figure 3.16: NGS analysis of heavy chains from C13 and C18 libraries produced in 5-alpha F'Iq E. coli. A) C13 library PCR (AI), COL (AII), and PHAGE (AIII) number of heavy chain sequences, and of these, the number of unique amino acid sequences, for each CDRH3 length. B) C18 library PCR (BI), COL (BII), and PHAGE (BIII) number of heavy chain sequences, and of these, the number of unique amino acid sequences, for each CDRH3 length. The y axes have different scales for ease of visualisation.....109
Figure 3.17: Phage ELISA binding of each library constructed against SARS-CoV-2 Lineage A trimer, measured as OD_{405} nm. Libraries were generated by transforming in 5-alpha F'Iq E. coli cells (5-alpha F'Iq E. coli libraries) showed the high levels of binding to SARS-CoV-2 Lineage A trimer. Libraries generated by extending the heavy chain amplification primers and transforming into TG1 cells (TG1 extended primers libraries) showed the least binding to SARS-CoV-2 Lineage a trimer. Libraries generated from optimising the extended primer PCR and transforming into TG1 cells (TG1 PCR optimised 2023 libraries) showed higher levels of binding to SARS-CoV-2 Lineage A trimer compared to the TG1 extended primers libraries, however, was not as high as the 5-alpha F'Iq E. coli libraries. Error bars demark standard deviation, N=2. 112
Figure 3.18: NGS analysis of heavy chains from C13 and C18 libraries combined. A) C13 library ALL PHAGE number of heavy chain sequences, and of these, the number of unique amino acid sequences, for each CDRH3 length. B) C18 library ALL PHAGE number of heavy chain sequences, and of these, the number of unique amino acid sequences, for each CDRH3 length. The y axes have different scales for ease of visualisation.....114
Figure 3.19: Alignments of SDM modifications to the phagemid showing nucleotides and amino acid sequence 5' to 3'. A) Amber stop codon addition followed by glycine linker and His tag. The top sequence shows the original PFAB3 L.14, and bottom sequence shows the phagemid containing the amber stop codon. B) Gene 3 deletion and addition of His tag and glycine linker, top sequence represents the original PFAB3 L.14, middle sequence displays the desired insertion, and bottom sequence displays the phagemid containing the gene 3 deletion. 116
Figure 4.1: Colony PCR of R1 biopanning. Left: C13R1 clones 1-8, positive colonies 2, 4, 6 and 7 (red arrows). Right: C18R1 clones 1-8, positive colonies 1, 3, 4 and 6 (red arrows). Positive colonies for heavy chains produced a band at 800 base pairs, negative colonies absent of heavy chains produced a band at 400 base pairs. M = 10 Kb DNA molecular marker, N/C = negative control.....133
Figure 4.2: Phage binding ELISA of R1 enriched clones from C13 and C18 libraries to SARS-CoV-2 Lineage A trimer, measured as OD_{405} nm. Phage ELISA to evaluate the binding of R1 biopanning clones to SARS-CoV-2 Lineage A trimer, measured as OD_{405} nm. The combined libraries (ALL PHAGE) were trialled alongside clones as positive controls. Clones of C13 showed higher binding, as did the combined library, compared to C18 clones and C18 combined library respectively. Clonal variation was observed between clones with identical sequences, for instance C13R1.2 and C13R1.4 whereby C13R1.4 showed greater binding. C13R1.4 exhibited the highest binding to the target out of all the clones whereas clone C13R1.6 showed the lowest binding to the target. Libraries were tested for binding against an irrelevant glycoprotein, HIV gp120, as a negative control. Negative controls showed minimal binding to gp120. Error bars mark standard deviation, N=2. 137

Figure 4.3: Colony PCR of R2 biopanning. Left: C13R2 clones 1-8, positive colonies 1, 2, 4, 5, 6 and 7 (red arrows). Right: C18R2 clones 1-8, positive colonies 2, 6 and 8 (red arrows). Positive colonies for heavy chains produced a band at 800 base pairs, negative colonies absent of heavy chains produced a band at 400 base pairs. M = 10 Kb DNA molecular marker, N/C = negative control.....137
Figure 4.4: Bar chart of phage titres, measured as cfu/mL. A) Normalised input of combined libraries (ALL PHAGE) to 1 x 10^{11} cfu, R1 eluted libraries, and R1 amplified libraries for C13 and C18. B) Normalised input of R1 amplified libraries to 1 x 10^{11} cfu, R2 eluted libraries and R2 amplified libraries for C13 and C18.....141
Figure 4.5: Phage ELISA binding of pre-panned, R1 and R2, normalised to 10^{11} cfu, of each library to SARS-CoV-2 Lineage A and BA.5 trimers, measured as OD_{405} nm. A) Comparison of C13 pre-panned combined library, R1 library, R2 library to SARS-CoV-2 Lineage A trimer. B) Comparison of C13 pre-panned combined library, R1 library, R2 library to SARS-CoV-2 BA.5 trimer. C) Comparison of C18 pre-panned combined library, R1 library, R2 library to SARS-CoV-2 Lineage A trimer. D) Comparison of C18 pre-panned combined library, R1 library, R2 library to SARS-CoV-2 BA.5 trimer. A-D) C13.2 phage as a positive control for Lineage A trimer, or negative control for BA.5 trimer. Statistical significance by One Way ANOVA and Tukey's multiple comparisons test, N=2, **p = <0.05, *** p = <0.001, **** p = <0.0001. Error bars demark standard deviation. 143
Figure 5.1: Subcloning of Fab from phagemids of interest for mammalian expression. A) PCR linearisation of a heavy chain plasmid, positive products produced bands at 6000 base pairs for annealing temperatures 67.5, 69.4 and 70.7°C. B) Amplification of C13.2 and C13.7 heavy chains for subcloning. Positive products produced a band at 500 base pairs. (C). Colony PCR screen of C13.2 heavy chain positive colonies 1, 2, 3, 4, 6 and 7 at 1,800 base pairs. D) Colony PCR screen of C13.7 heavy chain positive colonies 1-8 at 1,800 base pairs. A-D) M = 10 Kb DNA molecular marker, N/C = negative control.....157
Figure 5.2: mAb CDRH3 sequence analysis. A) mAb C13.2. B) mAb C13.7. Annotated knob and stalk, and VDJ regions, showing base pairs and translated amino acids using Geneious Prime Version 2021 2.2.....158
Figure 5.3: IgG ELISA concentration interpolation of HEK293T expressed mAbs. Top: Absorbance measured at OD_{405} nm and concentration measured in μg/mL. Concentration of mAbs interpolated from a non-linear fit to standards of a known concentration, represented as a dotted line at the dilution used to determine concentrations. Error bars demark standard deviation, N=2. Bottom: Table showing interpolation of mAb concentration from HEK293T expression, displaying mean optical density (OD) at 405 nm, interpolated X value, dilution factor and concentration in μg/mL.....159
Figure 5.4: Binding ELISA curves to SARS-CoV-2 variants for mAbs C13.2, C13.7 and 18.99, measured as portion of binding (%). Binding curves of proportion of binding (%), whereby 100% was the highest optical density at 405 nm, and wells with no mAb as 0%. Curves generated from a non-linear fit of normalised, 3-fold dilution series of mAb C13.2, C13.7 and 18.99 (isolated from C18 by single B-cell sorting) starting at 2.5 μg/mL. Curves were generated for SARS-CoV-2 lineage A trimer, full length spike (FL), and RBD; Alpha (B.1.1.7) full length spike (FL); Beta (B.1.351) full length (FL), and Omicron (B.1.1.529) trimer. Error bars demark standard deviation, N=2. Concentration and EC_{50} values (below) measured in μg/mL.....162

Figure 5.5: Single point neutralisation assay of mAbs C13.2 and C13.7 to SARS-CoV-2 variants. Pseudovirus neutralisation by each mAb at a concentration of 1μg/mL, measured as portion of uninhibited control (%) for pseudotyped SARS-CoV-2 variants Lineage A, Alpha (B.1.1.7), Beta (B.1.351), Gamma (P1), Delta (B.1.617.2) and Omicron (B.1.1.529). Error bars demark standard deviation, N=3. 163
Figure 5.6: IgG ELISA concentration interpolation of Expi293 expressed mAbs. Top: Absorbance measured at OD_{405} nm and concentration measured in μg/mL. Concentration of mAbs interpolated from a non-linear fit to standards of a known concentration, represented as a dotted line, at the dilution used to determine concentrations. Error bars demark standard deviation, N=2. Bottom: Table showing interpolation of mAb concentration from Expi293 expression, displaying mean optical density OD_{405} nm, interpolated X value, dilution factor and concentration in μg/mL. 165
Figure 5.7: Affinity purification of mAbs. Flow through and elution measured by ultraviolet absorbance at 280 nm (mAU) demarked by a blue line, and conductivity (mS/cm) demarked by a red line. A) Overview of C13.2 purification. Flow through increased mAU to over 900 for 260 mL, followed by a sharp decrease on buffer exchange to wash. A sharp peak at 280 mL reaching 950 mAU shows elution of sample from the column. Conductivity at 9.3 mS/cm for 280 mL sharply decreased to 4 mS/cm during sample elution. Conductivity returned to 9.3 mS/cm after sample was completely eluted from the column. B) C13.2, elution peak at 950 mAU. Sample elution occurred over 12 fractions, demarked as T1-T12. C) C13.7, elution peak at 1100 mAU. Elution peak denoted by an increase in mAU and decrease in conductivity. Sample elution occurred over 14 fractions, demarked as T1-T14. 167
Figure 5.8: Silver stain of reduced C13.2 mAb purification fractions compared to pure C13.2 mAb, flow through and wash. Banding pattern from silver staining of reduced proteins from C13.2 fractions, Pure C13.2, flow through (FT) and wash. Three bands were present in the fractions and pure sample, the band at 55 kDa inferred as the heavy chain, 28 kDa the light chain, and the middle 45 kDa double bands as heavy-chain derived products. Left: molecular marker in kDa. The FT contained faint bands from the supernatant proteins.....168
Figure 5.9: BCA assay for analysis and interpolation of total protein quantification of mAbs. A) C13.2. B) C13.7. Linear regression of standards from a known concentration, measured at OD_{562} nm. Y = mx + c derived from linear regression on the graph was used to interpolate total protein. Table shows mean OD_{562} nm, estimated interpolated concentration, dilution factor and concentration recorded in μg/mL and mg/mL (circled interpolation used). 170
Figure 5.10: IgG ELISA interpolation of purified Expi293 expressed mAbs. A) C13.2. B) C13.7. Absorbance measured at OD_{405} nm and concentration measured in μg/mL. Concentration of mAbs interpolated from a non-linear fit to standards of a known concentration, represented as a dotted line, at the dilution used to determine concentrations. Error bars demark standard deviation, N=2. Tables below each graph display mean optical density OD_{405} nm, interpolated X value, dilution factor and concentration in μg/mL and mg/mL. 171
Figure 5.11: Silver stain of reduced purified C13.2 (left) and C13.7 (right). The thick intense band at 55 kDa inferred as heavy chain and faint band at 28 kDa the light chain. Bands at 30, 35, 37, 40 and 45 kDa in C13.2 inferred as heavy chain derived

products. Bands at 37, 38, and 45 kDa in C13.7 inferred as heavy chain derived products. Molecular marker (M) in kDa. 172
Figure 5.12: Western blot of mAbs C13.2 and C13.7, reduced, detecting expression of A) antibody light chains, at 28 kDa, and B) antibody heavy chains, at 55 kDa. Additional bands at 35, 40 and 45 kDa in B were heavy chain derived by products. Molecular marker (M) in kDa. 173
Figure 5.13: Binding ELISA curves to SARS-CoV-2 variants for mAbs C13.2 and C13.7. Binding curves of proportion of binding (%), whereby 100% was the highest optical density at 405 nm, and wells with no mAb as 0%. Curves generated from a non-linear fit of normalised, 5-fold dilution series of A) C13.2 mAb, and B) C13.7 mAb. Concentration measured in μg/mL. Curves were generated against SARS-CoV-2 lineage A trimer, full length spike (FL), S1, and RBD; Alpha (B.1.1.7) full length spike (FL); Beta (B.1.351) full length (FL), Omicron (B.1.1.529) trimer, and BA.5 (RBD). Error bars demark standard deviation, N=2. 175
Figure 5.14: ACE2 ELISA curves to SARS-CoV-2 Lineage A spike proteins for mAbs C13.2 and C13.7. Binding curves of proportion of ACE2 binding (%), whereby 100% was the highest optical density at 405 nm, and wells with no ACE2 as 0%. Curves generated from a non-linear fit of normalised ACE2 binding during a 5-fold dilution series of C13.2 mAb and C13.7 mAb diluted in soluble ACE2 for A) Lineage A trimer, B) Lineage A full length (FL), C) Lineage A RBD. Concentration measured in μg/mL. Error bars demark standard deviation, N=2. 178
Figure 5.15: Screening colonies of C13.2 and C13.7 heavy chain plasmid Fc deletion to Fab. A) C13.2 H Fab clones 1-8. Positive colonies, 1, 2, 4-8 produced a band around 1000 base pairs whereas the negative colony 3, with full Fc, produced a band around 2000 base pairs. B) C13.7 H Fab clones 1-8. All colonies were positive producing a band around 1000 base pairs. A+B) M = 10 Kb DNA molecular marker. N/C = negative control. 179
Figure 5.16: Competition ELISA between A) C13.2 mAb and C13.7 Fab, B) C13.7 mAb and C13.2 Fab, C) C13.2 and C13.7 mAb against the Fab panel (gifted by Dr. Theocharis Tsoleridis) measured as mean optical density at 405 nm. A-B) Non-linear curves analysed as proportion of mAb binding (%) measured at concentration of mAb (μg/mL) diluted in excess Fab (1:25), compared to uninhibited mAb (A: C13.2 or B: C13.7). Error bars demark standard deviation, N=2. C) Mean optical density measured at OD405 nm, colour coded to reflect potential additive effects (green) or inhibition (red), yellow neutral. Uninhibited mAbs served as comparison EC_{50}. MAb against autologous Fab served as inhibition control. 181
Figure 5.17: C13.2 Pseudovirus neutralisation assay. Pseudoviruses tested SARS-CoV-2: Lineage A, Alpha (B.1.1.7), Beta (B.1.351), Gamma (P1), Delta (B.1.617.2), Omicron (B.1.1.529), BA.5, XBB, and SARS-CoV-1: Frankfurt strain. Non-linear curves from normalised RLU data to positive and negative cell only controls, analysed as neutralisation (%) from a 5-fold dilution series of mAb (μg/mL). IC_{50}s ranged between 3-289 ng/mL. VSVg served as a negative control. Error bars demark standard deviation, N=3. Goodness of fit: $R_2 > 0.92$, except XBB where $R_2 = 0.7$. 183
Figure 5.18: C13.7 Pseudovirus neutralisation assay. Pseudoviruses tested SARS-CoV-2: Lineage A, Alpha (B.1.1.7), Beta (B.1.351), Gamma (P1), Delta (B.1.617.2), Omicron (B.1.1.529), BA.5, XBB, and SARS-CoV-1: Frankfurt strain. Non-linear curves from normalised RLU data to positive and negative cell only controls and analysed as neutralisation (%) from a 5-fold dilution series of mAb (μg/mL). IC_{50}s ranged between

11 and 1062 ng/mL. VSVg served as a negative control. Error bars demark standard deviation, N=3. Goodness of fit: $R_2 > 0.9$, except XBB where $R_2 = 0.8$ and Omicron BA.1 where $R_2 = 0.78$. 184
Figure 5.19: C13.7 mAb binding to Sarbecovirus RBD panel and SARS-CoV-2 RBD variants. A) Sarbecovirus RBD binding curves as proportion of binding (%), whereby 100% was the highest optical density and 0% wells without mAb. Curves generated from a non-linear fit of normalised, 4-fold dilution series of C13.7 mAb (μg/mL). EC_{50}s ranged between 34 and 74 ng/mL. B) SARS-CoV-2 RBD variants binding curves as proportion of binding (%), whereby 100% was the highest optical density and 0% wells without mAb. Curves generated from a non-linear fit of normalised, 4-fold dilution series of C13.7 mAb (μg/mL). EC_{50}s ranged between 38 and 86 ng/mL C) Phylogenetic tree of Sarbecovirus RBD strains and their clades (Fan et al., 2022). D) Comparison of Sarbecovirus RBD panel and SARS-CoV-2 RBD variants EC_{50}s analysed as unpaired T test. Significance at $P > 0.05$. A-B) Error bars demark standard deviation, N=2. 189
Figure 5.20: C13.2 mAb binding to Sarbecovirus RBD panel and SARS-CoV-2 RBD variants. A) Sarbecovirus RBD Binding curves as proportion of binding (%), whereby 100% was the highest optical density and 0% wells without mAb. Curves generated from a non-linear fit of normalised, 4-fold dilution series of C13.2 mAb (μg/mL). B) SARS-CoV-2 RBD variants Binding curves as proportion of binding (%), whereby 100% was the highest optical density and 0% wells without mAb. Curves generated from a non-linear fit of normalised, 4-fold dilution series of C13.2 mAb (μg/mL). A-B) Error bars demark standard deviation, N=2. 190
Figure 5.21: EM densities of single-particle cryo-EM structures of C13.2. and C13.7. A) C13.2 (orange)-spike (grey) complex shown from the side (left) and top (right). B) C13.2 as cartoon diagrams of the CDRH3 structure (left), and C13.2 Fab (light blue) interaction with the SARS-CoV-2 Lineage A RBD (grey) (right). C) C13.7 as cartoon diagram of Fab, light chain (blue) and heavy chain (yellow) with the CDRH3 protruding from the Fab. 192

List of Tables

Table 2.1: Primers used for light chain amplification and phagemid modifications. 41
Table 2.2: Colony Screening primers. 44
Table 2.3: Primers for heavy chain amplifications, linearisation of phagemid and Gibson assembly primers. 49
Table 2.4: Details of Western blot experiments. Sample preparation, primary antibody, and secondary antibody. 52
Table 2.5: SARS-CoV-2 antigens for ELISAs. 54
Table 2.6: Details of Phage ELISAs. Coat, block, analyte, primary antibody, secondary antibody and analysis. N/C = negative control. 55
Table 2.7: Details of IgG ELISA to determine mAb concentration. Coat, block, analyte, secondary antibody and analysis. 56
Table 2.8: Details of mAb binding ELISAs. Coat, block, analyte, secondary antibody, and analysis. P/C = Positive Control. N/C = negative control. 58

Table 2.9: Primers for Linearisation and amplification for subcloning of Fab for mammalian expression. 65
Table 4.1: IMGT analysis of R1 heavy chain positive colonies. V-gene and allele, D-gene and allele, J-gene and allele, CDR3 length and CDR3 amino acid sequence for each positive clone of C13 R1 (A) and C18 R1 (B). 134
Table 4.2: IMGT analysis of R2 heavy chain positive colonies. V-gene and allele, D-gene and allele, J-gene and allele, CDR3 length and CDR3 amino acid sequence for each positive clone of C13 R2 (A) and C18 R2 (B). 139
Table 5.1: Summary of C13.2 and C13.7 mAb binding and neutralisation data to SARS-CoV-1 and SARS-CoV-2 variants. Measured as EC_{50} for binding data and IC_{50} for neutralisation data, measured as μg/mL. NA = not applicable, ND = no data. Colours represent spectrum of EC_{50}/ IC_{50} with green dictating low values and red as high values. 187

Abbreviations

ACE2	Human Angiotensin-Converting Enzyme 2
AID	Activation-Induced Cytidine Deaminase
AmpR	Ampicillin resistance
ANOVA	Analysis of Variants
APC	Allophycocyanin
APS	Ammonium Peroxodisulfate
ARDS	Acute Respiratory Distress Syndrome
BCA	Bicinchoninic acid
BCR	B cell receptor
bnAbs	Broadly neutralising Antibodies
BSA	Bovine Serum Albumin
cDNA	Complementary DNA
CDR	Complementary Determining Regions
CDRH3	Complementary Determining Region Heavy Chain 3
COVID-19	Coronavirus Infectious Disease 2019
CoVs	Coronaviruses
D	Diversity
DH	Diversity Heavy
DNA	Deoxyribonucleic Acid
DNTPs	Deoxynucleotide Triphosphate
DMEM	Dulbecco's modified Eagle's medium
E	Envelope
EC_{50}	Half maximal effective concentration
EGFR	Epidermal Growth Factor Receptor
ELISA	Enzyme Linked Immunoabsorbant Assay
ERGIC	Endoplasmic Reticulum – Golgi Intermediate Compartment
Fab	Fragment antigen binding
FACS	Fluorescence-Activated Cell Sorting
FBS	Foetal Bovine Serum
Fc	Fragment crystallisable
FL	Full-Length
FR	Framework
FSG	Fish Skin Gelatin
FT	Flow Through

Fv	Fragment variable
GDP	Gross Domestic Product
G3p	Gene 3 protein
G8p	Gene 8 protein
HCMV	Human Cytomeglovirus
HEK293T	Human Embryonic Kidney 293T
HIV	Human Immunodeficiency Virus
HRP	Horseradish Peroxidase
IC_{50}	Half maximal inhibitory concentration
IgH	Immunoglobulin Heavy chain
IgL	Immunoglobulin Light chain
IMGT	ImMunoGeneTics
IPA	Isopropanol
J	Joining
KLD	Kinase, Ligase, DPNI
M	Membrane
mAbs	Monoclonal Antibodies
MERS-CoV	Middle Eastern Respiratory Syndrome Coronavirus
$MgCl_2$	Magnesium Chloride
MHC	Major Histocompatibility Complex
MOI	Multiplicity of Infection
MPBST	Phosphate Buffered Saline, TWEEN20, Milk
mRNA	Messenger Ribonucleic acid
N	Nucleocapsid
NaCl	Sodium Chloride
NaH_2PO_4	Monosodium phosphate
$NaPO_4$	Sodium Phosphate
NEAA	Non-Essential Amino Acids
NGS	Next Generation Sequencing
NHEJ	Nonhomologous DNA End-Joining
NSP	Non-Structural Protein
NTD	N Terminal Domain
ORF	Open Reading Frame
PAMPS	Pathogen Associated Molecular Patterns
PBMCs	Peripheral Blood Mononuclear Cells
PBS	Phosphate Buffered Saline
PBST	Phosphate Buffered Saline, TWEEN20
PCR	Polymerase Chain Reaction
PEI	Polyethyleneimine
PHEIC	Public Health Emergency of International Concern
pIII	p3
pNPP	p-Nitrophenyl phosphate
pp	Polyprotein
PVDF	Poly(vinylidene fluoride)
pVIII	p8
RAG	Recombination gene-activating machinery
RBD	Receptor Binding Domain
RdRp	RNA-dependent RNA polymerase
RF	Replicative Form
RLU	Relative Light Units
RNA	Ribonucleic acid
RSS	Recombination Signal Sequences
RSV	Respiratory Syncytial Virus

RTC	Replicase Transcriptase Complex
S	Spike
SARS-CoV-2	Severe Acute Respiratory Syndrome Coronavirus 2
SARS-CoV-1	Severe Acute Respiratory Syndrome Coronavirus 1
scFv	Single chain variable Fragment
sdFv	Single domain Fragment variable
SDS	Sodium Dodecyl Sulfate
SDS-PAGE	Sodium Dodecyl Sulphate-Polyacrylamide Gel Electrophoresis
SLE	Systemic lupus erythematosus
TCR	T cell receptor
TdT	Terminal deoxynucleotidyl transferase
TEMED	Tetramethylethylenediamine
TLR	Toll-Like Receptors
TMPRSS2	Transmembrane Protease, Serine 2
TRS	Transcriptional Regulatory Sequences
UTR	Untranslated Region
V	Variable
VH	Variable Heavy
VLP	Virus Like Particle
VSVg	Vesicular Syncytial Virus glycoprotein
W.H.O.	World Health Organisation
WT	Wild-Type

Chapter 1 General Introduction

1.1. Discovery, Origin and Classification of SARS-CoV-2

The seventh member of documented human coronaviruses, Severe Acute Respiratory Syndrome Coronavirus 2 (SARS-CoV-2) was discovered as the aetiological agent responsible for Coronavirus Infectious Disease 2019 (COVID-19). First reports in December 2019 documented the emergence in the Hubei Province of China; presenting as "pneumonia of an unknown aetiology," with four cases linked to the Huanan Seafood Wholesale Market (Wang et al., 2020b). Two zoonotic spillovers from the family *Coronaviridae,* SARS-CoV-1 and MERS-CoV, have caused outbreaks within the last two decades (De Wit et al., 2016), suspected to have bat origins and intermediate hosts before crossing the species barrier into humans (Li et al., 2005). *Coronaviridae* virions are classically recognised by distinctive club-shaped spike projections emerging from the surface of the virion, a similarity shared by all coronaviruses, appearing as a solar corona, hence termed Coronavirus (Fehr and Perlman, 2015). The family is subdivided into four distinct families: *Alphacoronavirus, Betacoronavirus, Gammacoronavirus, and Deltacoronavirus*, of which SARS-CoV-2 is categorised as a *Betacoronavirus* (Li, 2016).

Early whole-genome surveillance of SARS-CoV-2 confirmed similarities with bat-like Coronaviruses (CoVs) bat-SL-CoVZC45, bat-SL-CoVZXC21 (Lu et al., 2020a), RaTG13, RmYN01 and RmYN02 (Zhou et al., 2020b), suggesting a *Hipposideros* or *Rhinolophus* origin. Similarities were also noted between SARS-CoV-2 and pangolin coronavirus genomes (85.5% to 92.4%) (Lam et al., 2020), particularly in the Receptor Binding Domain (RBD), which may implicate pangolins as hosts for SARS-CoV-2. Indeed, reverse zoonosis has been recorded in Syrian hamsters, American mink and white-tailed deer. More recent work on SARS-CoV-2's origins suggest two independent zoonotic

transfers to humans, forming Lineage A and Lineage B (Pekar et al., 2022, Worobey et al., 2022).

Since the beginning of the pandemic 6,958,499 cumulative deaths from COVID-19 have been reported to the World Health Organisation (W.H.O) (September 2023) (W.H.O, 2023). Globally, the pandemic has had vast impacts on the economy. In order to combat the transmission of COVID-19, worldwide restrictions were imposed on the public through governmental control. In the UK, three 'lockdowns' were instigated by the government, replaced with tiered systems for restricting movement and gatherings, and then switching to control of movement through vaccine passports (Usman et al., 2023). Worldwide, Gross Domestic Product (GDP) decreased by 3.4%, and unemployment rose to 6.57% in 2020, thought to be a consequence of the COVID-19 pandemic (Department, 2023). Extensive research on the ongoing pandemic has emphasised a need for understanding and tackling future health threats, particularly where they may be catalysed by a vast immunologically naïve reservoir (Roltgen and Boyd, 2021).

1.2. Insights into SARS-CoV-2 molecular biology

1.2.1. SARS-CoV-2 virion and genome structure

The SARS-CoV-2 virion is approximately 125 nm in diameter, harbouring a single-stranded positive sensed Ribonucleic Acid (RNA) genome. The 30 kb genome consists of 14 Open Reading Frames (ORFs) encoding 27 proteins, flanked by a 5' capped messenger RNA (mRNA) leader sequence and a 3' poly-A tail with nested sub-genomic mRNAs. The Untranslated Regions (UTR) at the 5' and 3' termini contain loop structures for transcription and replication. The long polyprotein, encoding the replicase enzyme, comprises more than two-thirds of the genome. Preceding the structural proteins, ORF1 consists of two non-structural proteins ORF1a and ORF1b. During replication, ORF1ab is cleaved by viral proteinases to produce Non-Structural Proteins (NSP) NSP1-NSP16 which are conserved throughout the *Betacoronavirus* family (Khailany

et al., 2020). SARS-CoV-2 virion contains four major structural proteins, the spike (S) surface glycoprotein, Nucleocapsid protein (N), Membrane protein (M), small envelope protein (E); and eight accessory proteins (Figure 1.1). The smallest of the structural proteins is the envelope protein which is involved in the assembly and release process of mature virions (Naqvi et al., 2020). In addition to the envelope protein, the nucleoprotein which is highly conserved between coronaviruses, also plays a significant role in assembly by packaging the viral RNA into the ribonucleocapsid (Neuman and Buchmeier, 2016). The nucleocapsid is structurally bound to the viral RNA, enabling translocation to the endoplasmic reticulum during replication. This protein is heavily phosphorylated, and this is speculated to aid in replication by enhancing its affinity to the nucleic material of the virus (Fehr and Perlman, 2015). The most abundant structural protein is the membrane protein. Responsible for the virion shape by promoting the membrane curvature (Neuman et al., 2011), the membrane protein functions in conjunction with other structural proteins to package the RNA (Tang et al., 2020). The latter of the genome comprises accessory proteins, and a Transcriptional Regulatory Sequence (TRS) necessary for expression (Fehr and Perlman, 2015). The non-structural proteins, expressed through ribosomal frameshifting of non-structural genes, are involved in numerous roles including replication, viral assembly and viral pathogenesis (Xue, 2014). For instance, NSP12 encodes the RNA dependent

polymerase (Zanotto et al., 1996) and NSP14 has proofreading capabilities to maintain replication fidelity (Sariol and Perlman, 2020).

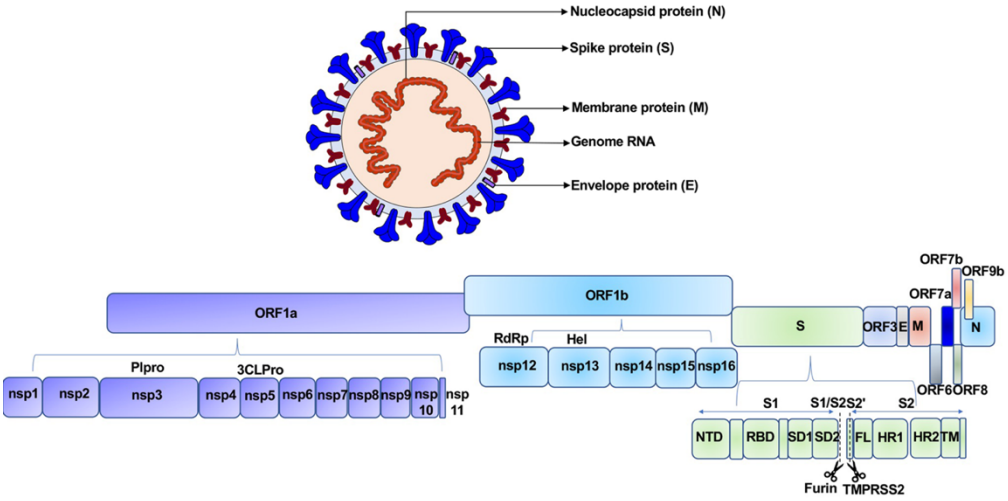

Figure 1.1: Schematic of SARS-CoV-2 virion and the positive single stranded RNA genome of SARS-CoV-2: SARS-CoV-2 virion has four structural proteins: Spike (S), Nucleocapsid (N), Membrane protein (M), and Envelope protein (E). Genome: 5' cap, followed by leader sequence and the UTR. Sequentially, ORF1a, ORF1b. Non-structural proteins (NSP1–11, 12–16) are encoded by ORF1a and ORF1b, respectively. Spike protein (S) consists of S1 and S2, divided by furin cleavage site. S1 is further subdivided into N Terminal Domain (NTD), RBD, SD1 and SD2. This is followed by ORF3a, E, M, ORF6, ORF7a, ORF7b, ORF8, N, ORF10. 3' end consists of an UTR, and Poly-A tail. Source: (Zhang et al., 2021b).

The spike glycoprotein, classed as a type 1 transmembrane protein, protrudes from the lipid bilayer as a homotrimer and is extensively covered in N-glycan caps. Each virion carries approximately 24 trimers (Ke et al., 2020). The 150 kDa protein is functionally divided into S1 which harbours the RBD composed of residues imperative to target the host cell binding (Lu et al., 2020a, Hoffmann et al., 2020, Wrapp et al., 2020b), and S2 responsible for cell membrane fusion (Wang et al., 2020b). Studies by Coutard et al., Walls et al., and Jaimes et al. (Coutard et al., 2020, Walls et al., 2020, Jaimes et al., 2020) were some of the first to demonstrate that SARS-CoV-2 exhibits a unique furin cleavage site, located between S1 and S2, to activate fusion machinery and

mediate membrane fusion (Peacock et al., 2021). The S1 subunit consists of two subdomains, consisting of the core RBD domain (SD1), and external subdomains (SD2). Together, these subdomains cap the S2 fusion machinery and can transiently 'breathe' using hinge-like motions to form two conformations, 'up' and 'down', or 'open' and 'closed'. In an 'open' or 'up' state the RBD is exposed. In contrast, in a 'closed, 'down' prefusion conformation, the receptor binding sites remain occluded. These states have been recorded for singular or multiple monomers (Wrapp et al., 2020b, Walls et al., 2020).

Cell entry is mediated by an interaction between SARS-CoV-2 S and human Angiotensin-Converting Enzyme 2 (ACE2) (Wang et al., 2020a, Wan et al., 2020, Hoffmann et al., 2020, Coutard et al., 2020, Walls et al., 2020, Wrapp et al., 2020b, Chen et al., 2020), a characteristic shared with a related coronavirus, SARS-CoV-1, responsible for the 2002 outbreak in the Guangdong Province of Southern China (Wang et al., 2020d). SARS-CoV-2, however, appears to have enhanced transmissibility over its predecessors, attributed to an increased affinity between the virus and ACE2 (Wan et al., 2020). An enhanced transmission and an immunologically naïve reservoir quickly escalated the situation from a Public Health Emergency of International Concern (PHEIC) on the 30th of January 2020, to a pandemic status by the 11th of March 2020.

1.2.2. SARS-CoV-2 life cycle

Cell attachment and entry are mediated through a complex interaction between S and the ACE2 receptor. ACE2 is predominantly found on type II alveolar cells in the respiratory tract, where it is highly expressed, but also found systemically distributed throughout the body. For instance, ACE2 is located on cells within the upper oesophagus, myocardial cells, and kidney proximal tubule cells. The clinical manifestation of systemic disease reported in SARS-CoV-2 cases is likely to be attributed to the widespread distribution of ACE2 (Xu et al., 2020).

Briefly, the S1 subunit binds to human ACE2 which triggers destabilisation within the prefusion trimer. Access to the host cell cytosol is achieved through proteolytic cleavage on the S protein by a protease, Transmembrane protease, serine 2 (TMPRSS2) (Fehr and Perlman, 2015) or by cathepsin L (Huang et al., 2006). Additional pathways have been recorded to be used by SARS-CoV-2 for cellular entry, such as C-type lectins, DC-SIGN and L-SIGN which are commonly used for pathogen recognition and intracellular adhesion, as well as phosphatidylserine receptors. These alternative receptors are relatively non-specific, thus require the presence of ACE2 for efficient infection (Jackson et al., 2022).

Following cellular entry, there is simultaneous shedding of the S1 subunit following cleavage of the furin site, this results in S2 post-fusion conformation within the host cell membrane, stabilising the spike (Benton et al., 2020). The S2 fusion complex inserts into the cell membrane enabling the release of the genome into the cytosol (Fehr and Perlman, 2015).

The viral genome consists of single-stranded positive sensed RNA, therefore, bypasses the initial process of transcription required for negative stranded RNA and DNA viruses. As the virus encodes its own replicase, this is the initial gene to be translated. The host cell ribosome binds to the capped mRNA and begins translation. A slippery sequence followed by an RNA pseudoknot between ORF1a and ORF1b results in a ribosomal frameshift, thus leading to expression of polyproteins pp1a and pp1ab. This mechanism has been hypothesised to manage replication by ensuring precise ratios of the two products. The polyproteins are associated with proteases that subsequently cleave pp1a and pp1ab to produce the NSPs. A combination of non-structural proteins forms the Replicase Transcriptase Complex (RTC) required for RNA replication.

The RNA-dependent RNA polymerase (RdRp) facilitates replication of the genome template to negative sense genomic RNA in double-membrane vesicles. The negative intermediates function as templates to generate positive sense genomic RNA to be either directly packaged into viral progeny

or to serve as discontinuous transcription of sub-genomic RNA. The latter of the two processes involves binding of the RdRp to the multiple regions of the negative sense strand for transcription of sub-genomic RNA which is sequentially translated into viral structural and accessory proteins to be assembled for the viral progeny. The method of discontinuous transcription is thought to be achieved through Transcriptional Regulatory Sequences (TRS) causing the RdRp to pause, either to continue elongation of the strand or switch to amplify a leader TRS at the 5' terminus (Sawicki et al., 2007). Given the ability of coronaviruses to undergo homologous and nonhomologous

recombination, it is proposed that RdRp strand switching is likely to play a role in viral recombinants (Keck et al., 1987).

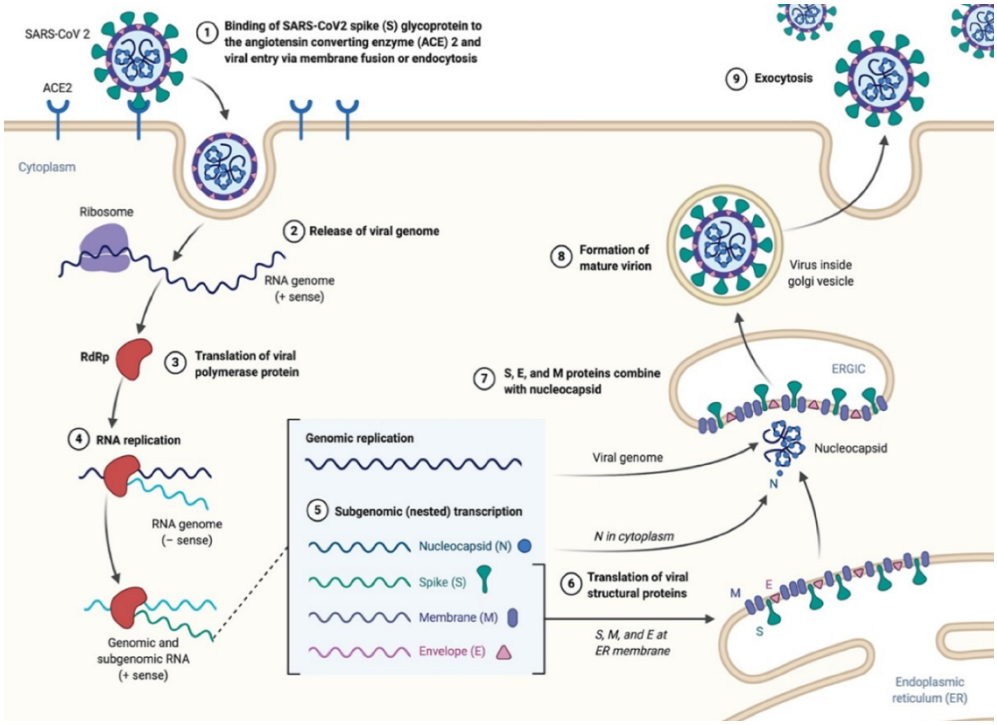

Figure 1.2: The life cycle of SARS-CoV-2 in a host cell expressing ACE2. Briefly, the SARS-CoV-2 spike interacts with ACE2 and is endocytosed into the host cell cytoplasm. Translation of the viral polymerase is achieved through the host cell ribosome to generate a polyprotein that is subsequently cleaved by proteases. This enables continuous and discontinuous transcription for RNA and translation of viral structural proteins. S, E and M proteins combine with N and are translocated to the Golgi apparatus to form an Endoplasmic Reticulum – Golgi Intermediate Compartment (ERGIC) leading to the formation of mature virions. Subsequently, mature virions are exported out of the cell by exocytosis. Source: (Alanagreh et al., 2020).

The assembly and release of viral progeny employ the endoplasmic reticulum-golgi secretory pathway. The N protein is encapsulated with the positive-strand RNA genome and assembled with structural proteins S, E, and M in an endoplasmic reticulum golgi intermediate compartment. Subsequently,

matured virions are trafficked to the host cell membrane in a golgi vesicle, and progeny virions are trafficked to the host cell surface and egress by exocytosis (Fehr and Perlman, 2015) (Figure 1.2).

1.3. The immune response

The immune system forms the defence against harmful pathogens such as bacteria, fungi, parasites, and viruses. The characteristic response to pathogens is generated through two systems: the innate and adaptive immune response. The first line of defence is initiated through the innate immune system which responds within 96 hours of an encounter with a pathogen or foreign material. The innate immune system is categorised by physical and anatomical barriers, effector cells, antimicrobial peptides, mediators such as cytokines, and cellular receptors (Aristizábal and González, 2013). The adaptive immune system initiates under circumstances where pathogens have evolved to circumvent innate defences. A specified, tailored response is required; therefore, the adaptive response employs antibodies and T-cells following the acquisition of pathogen recognition. This second line of defence forms characteristic long-term immunological memory for rapid recall upon future pathogen encounters (Gourley et al., 2004).

1.3.1. The adaptive immune response

The adaptive immune response is driven by lymphocytes, a class of white blood cells derived from progenitor cells within the bone marrow. The lymphocytes are subdivided into B-cells and T-cells, each expressing an antigen receptor on the cell surface known as either a B-Cell Receptor (BCR)/membrane-bound immunoglobulin or T-Cell Receptor (TCR).

Immunoglobulins are a defining feature of the adaptive immune response, forming a characteristic ‘Y’ shape molecule (Figure 1.3). These proteins roughly weigh 150 kDa and are subdivided into the Fragment antigen binding (Fab), comprising heavy and light chains, and Fragment crystallisable (Fc)

regions, consisting of heavy chain only. Each chain is further subdivided into constant and variable regions. The variable consists of Complementary Determining Regions (CDR) and Framework Regions (FR). The variable regions of the heavy and light chains form the antigen binding sites (Hozumi and Tonegawa, 2004). Of these regions, the third CDR of the heavy chain (CDRH3) often has the greatest contact with the target antigen. To this end, antibody formation requires methods of diversity to obtain specificity to their complementary antigen.

In pro-B-cells, differentiated from hematopoietic stem cells, allelic exclusion assures that each mature B-cell produces antibodies of a single specificity. This is achieved by ensuring only one allele is expressed. For instance, a single heavy chain (IgH), is paired with a single light chain (IgL), as either kappa or lambda (Putnam, 1969).

During the maturation of lymphocytes in the primary lymphoid organs, V(D)J recombination occurs whereby exons are arranged into three segments, Variable (V), Diversity (D) and Joining (J). VDJ genes from the heavy chain locus are utilised to produce the heavy chain, and V and J genes on the light chain locus form the light chain. Gene segments are flanked by conserved Recombination Signal Sequences (RSS). RSS are composed of non-conserved 12 or 23 base pairs between a palindromic heptamer and a nonamer. This 12 or 23-base pair non-conserved Deoxyribonucleic Acid (DNA) is referred to as the 12/23 rule. The process of VDJ recombination is determined by a recombinase consisting of two proteins, RAG1 and RAG2 which catalyse recombination. The recombinase recognises RSS flanking each of these segments, generating inversions or deletions of gene segments. Inversions or deletions are specified by the orientation of the two flanking RSS and are carried out by Nonhomologous DNA End-Joining (NHEJ) proteins (Bassing et al., 2002). Additional diversity is generated through cleavage of DNA hairpins which lead to palindromic insertions (P nucleotides) at coding points and by Terminal deoxynucleotidyl transferase (TdT) leading to N regions at signal points, known as junctional imprecision (Roth, 2014).

Affinity maturation of antibodies occurs in antigen-activated germinal centres of secondary lymphoid organs and is initiated by Activation-Induced Cytidine Deaminase (AID). This results in somatically hypermutated antibodies. AID acts on both heavy and light genes, targeting single-stranded DNA of rearranged genes. The enzyme deaminates cytosines into deoxy-uracil (U), this change generates an estimated high mutation rate of six orders of magnitude, hypermutating the DNA (Pilzecker and Jacobs, 2019). RGYW and WRCY motifs are preferentially mutated (Larsen et al., 2014). Finally, class switching of antibodies occurs when activated B-cells switch the antibody isotype depending on the effector function required (Stavnezer et al., 2008), for instance, switching to IgG for immunological memory. This region-specific form of recombination forms deletions, altering constant regions of exons in IgH, thus impacting effector functions.

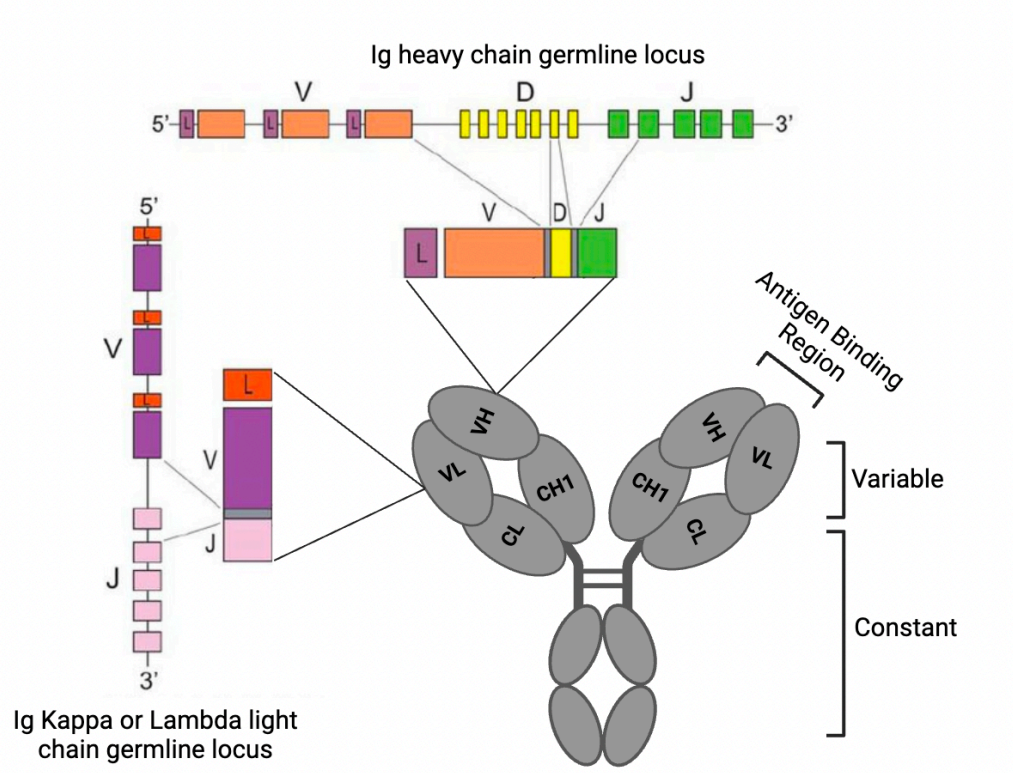

Figure 1.3: Diagram of the structure of an immunoglobulin.
Immunoglobulins are segregated into constant and variable regions, of which the variable comprises the antigen binding region. The variable region consists of regions of framework and complementary determining regions. Each variable segment on heavy and light chain loci are associated with a 5' leader sequence (L). The variable domains of light and heavy chains are formed from VDJ segments from the Ig heavy chain germline locus for the heavy chain, and VJ segments from Ig Kappa or Lambda light chain germline locus for the light chain. Recombination events are achieved by gene-activating machinery RAG1 and RAG2 (Ekman et al., 2009). Diagram altered from (Boyd and Joshi, 2014) using Biorender.

1.3.2. Antibody selection

On pathogen exposure, antigens, or Pathogen-Associated Molecular Patterns (PAMPs) interact with naïve B-cells which survey the environment for antigens in the secondary lymphoid organs. A complementary antigen B-cell interaction occurs by the selection of a specific BCR leading to downstream

processing and presentation on Major Histocompatibility Complex (MHC) class II molecules (Kwak et al., 2019).

The activated B-cells interact with primed antigen-specific T follicular helper cells (TfH cells) at the T-cell/B-cell border whereby B-cell differentiation commences. This process is commonly known as clonal selection, a principle theory in adaptive immunity (Jerne, 1955). The B-cell either differentiates into either germinal independent memory B-cells, germinal centre B-cells, or short-lived plasma cells. Germinal B-cells enter the dark zone of germinal centres and they undergo clonal expansion whereby selected cells proliferate and experience somatic hypermutation. Fully matured B-cells migrate to the light zone of germinal centres where they encounter presented antigens on follicular dendritic cells and interact with T follicular helper cells. The B-cells terminate in multiple fates such as differentiating into memory B-cells, long-lived plasma cells which secrete antibodies or re-enter into the dark zone as germinal centre B-cells (Akkaya et al., 2020).

1.4. Immune response and targets for therapy against SARS-CoV-2

1.4.1. Clinical Manifestation of SARS-CoV-2

Manifesting as a spectrum, the clinical manifestation of SARS-CoV-2 greatly varies from asymptomatic infections to Acute Respiratory Distress Syndrome (ARDS) (Li et al., 2020). Inhalation and engagement of viral particles to ACE2 receptors within nasal cavity epithelial cells give rise to a SARS-CoV-2 infection. Typically, the virus replicates for 1-2 days in the upper respiratory tract. This phase is usually asymptomatic for the host. The symptomatic phase occurs during the subsequent 2-14 days, clinically manifesting as a cough, fever, shortness of breath, tiredness, and pharyngitis, as the virus migrates to the lower respiratory tract. In severe cases, an overactive proinflammatory response occurs leading to viral sepsis which can be accompanied by pulmonary oedema and ARDS. Prior organ disorders and those at high risk

such as immunocompromised and diabetics are more susceptible to multiorgan failure (Shah et al., 2020).

1.4.2. Immune response to SARS-CoV-2

COVID-19 presents as a disease of great heterogeneity and can manifest as a systemic disease. Studies focusing on immune contexts and correlates of protection have attempted to categorise the individual responses through distinct disease profiles (Canas et al., 2023), memory B-cell subsets (Oliviero et al., 2020, Mathew et al., 2020), and antibody classifications (Wilson et al., 2020, Barnes et al., 2020b).

Primarily, the innate immune response is activated upon recognition of foreign viral particles by pathogen pattern recognition receptors such as Toll-Like Receptors (TLRs) 3, 7 and 8. This triggers the interferon cascade in order to suppress viral replication (Prompetchara et al., 2020). A multitude of studies revealed that in certain cases that there is an imbalance in innate host inflammatory mediators driven by SARS-CoV-2 (Blanco-Melo et al., 2020, Wang et al., 2020e, Del Valle et al., 2020). This has been associated with a severe COVID-19 phenotype, yet not observed in mild and moderate disease phenotypes, and is expected to be a result of a dysregulated interferon response (Hadjadj et al., 2020).

The humoral immune response is marked by systemic antibody responses and B-cell recruitment and activation. Naïve and potentially pre-existing B-cells are recruited and activated upon reinfection. The first, may differentiate into extrafollicular, short-lived plasma cells and memory B-cells, or enter germinal centres where they are subjected to multiple rounds of somatic hypermutation and affinity maturation. The latter may be activated as memory cells proceeding antigen recognition and CD4+ T helper cells. Pre-existing immunity has been reported as transient cross-reactivity, mainly regarding memory CD4+ T cells, directed towards the conserved epitopes within the spike between common cold coronaviruses (Grifoni et al., 2020, Le

Bert et al., 2020, Braun et al., 2020, Mateus et al., 2020, Sariol and Perlman, 2020). On the other hand, CD8+ T cells are correlated with effective clearance of virus in mild disease, and are stimulated upon vaccination, yet are impaired in severe disease and associated with lymphopenia (Grifoni et al., 2020, Moss, 2022).

SARS-CoV-2 infection generates durable B-cell responses in most cases. Asymptomatic to mild infections are suspected to exhibit ongoing germinal centre responses in memory B-cells, suggesting continued somatic mutations within Variable Heavy (VH) and Variable Light (VL) genes. This mechanism is achieved by the retention of antigens on immune complexes on follicular dendritic cells (Gaebler et al., 2021, Sakharkar et al., 2021, Sokal et al., 2021, Wang et al., 2021b). B and T-cell responses (Dan et al., 2021, Wajnberg et al., 2020, Gaebler et al., 2021) were found in asymptomatic individuals despite records of lower antibody titres (Vanshylla et al., 2021, Graham et al., 2021), highlighting the importance of cell-mediated immunity in the response to SARS-CoV-2 infection (Cox and Brokstad, 2020). In contrast, severe disease is speculated to generate a robust extrafollicular B-cell response which could explain high levels of proinflammatory cytokines and antibody titres. Data suggests that the early B-cell response in severe COVID-19 stimulates naïve B-cells which differentiate into plasmablasts with limited somatic hypermutation (Roltgen and Boyd, 2021), likely to be due to an impaired germinal centre response (Kaneko et al., 2020). Despite this, circulating T helper cells within the severely infected were recorded to be robust (Zhang et al., 2021a).

Antibodies, the core of the humoral immune response, play a crucial role in immune mechanisms such as neutralisation, phagocytosis, the complement cascade, and antibody-dependent cell-mediated cytotoxicity. Antibodies combat a range of pathogens by creating diversity, specifically in variable regions. SARS-CoV-2 generates the characteristic production of IgG, IgA and IgM within a two-week time frame in response to a coronavirus infection (Iyer

et al., 2020). The predominant antibody response is directed at the spike of the virus (Brouwer et al., 2020, Piccoli et al., 2020, Robbiani et al., 2020, Suthar et al., 2020), particularly the RBD, although, antibodies to N Terminal Domain (NTD) (McCallum et al., 2021b) and to N (Brochot et al., 2020) have also been documented. Seroconversion has been recorded to occur at a median time of 11 to 13 days post-symptom onset for RBD (Iyer et al., 2020, Long et al., 2020). An increase in disease severity appears to increase this rate of seroconversion to six to eight weeks (Roltgen et al., 2020). Antibody responses associated with immunological memory are reported to target the S2 and recorded to be less potent, likely attributed to the conservation between human common cold coronaviruses and SARS-CoV-2 (Anderson et al., 2021, Ng et al., 2020, Nguyen-Contant et al., 2020). The heterogeneity of disease severity witnessed among individuals infected with COVID-19 is speculated to be caused by the magnitude of antibody and T-cell response, and the pre-existing immunological memory (Stephens and McElrath, 2020).

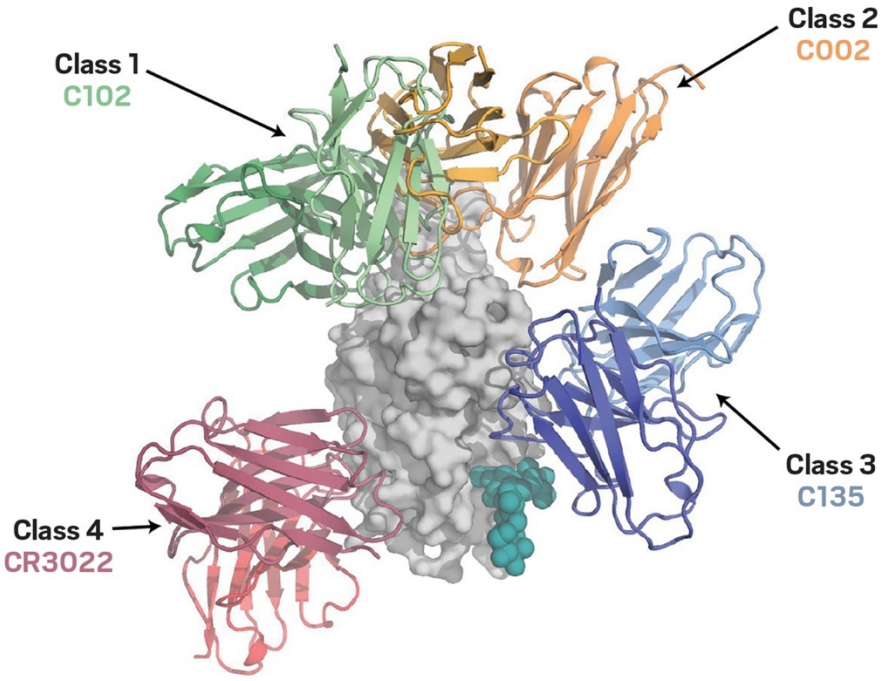

Figure 1.4: Cryo EM schematic showing classes 1-4 antibodies with the RBD (grey). N343 glycan in cyan blue. Class 1 in green, class 2 yellow, class 3 blue and class 4 pink. Source: (Barnes et al., 2020a).

The antibody response to SARS-CoV-2 from convalescent serum has been categorised into either four distinct classes (Barnes et al., 2020a), or defined by epitopes (Piccoli et al., 2020), based on the recognition of the RBD (Figure 1.4). Predominantly, recurrent ACE2 blocking neutralising antibodies have heavy chains encoded by germlines VH3-53 or VH3-66 (Ju et al., 2020, Seydoux et al., 2020, Rogers et al., 2020, Cao et al., 2020, Zost et al., 2020), likely to be attributed to germline-encoded residues that form a common binding mode within the RBD (Barnes et al., 2020b, Hurlburt et al., 2020). Another documented antibody germline isolated from convalescent donors was VH3-30 (Robbiani et al., 2020). Of the four classes, class 1 antibodies hinder the SARS-CoV-2 spike by binding RBDs in the 'up' conformation. These antibodies are noted to have shorter CDR3 regions. Examples include C102, C105 and CC12.3. By comparison, class 2 antibodies recognise RBDs in both

'up' and 'down' conformations and are also encoded by the germline VH3-53. Examples of these antibodies are C144, COVA2-39, LY-CoV555 and C002. This class has been described to exhibit longer CDRH3 regions, for instance, C144 bridges within CDRH3 lock adjacent RBDs in a down conformation, directly competing with ACE2. Class 3 antibodies vary from class 1 and class 2 antibodies in that they bind outside of the ACE2 binding site, examples include Sotrovimab (S309 epitope) (Pinto et al., 2020) and C135. Class 4 antibodies bind a cryptic epitope on 'up' RBDs. Despite being described to be less potent neutralisers, these antibodies have been recorded to broadly neutralise *betacoronaviruses* such as SARS-CoV-1, RaTG13, and Pangolin 17 (Shrestha et al., 2021, Barnes et al., 2020b). Examples include CR3022, S304 and S2X259 (Tortorici et al., 2021, Focosi et al., 2022).

Antibody durability of IgM has been recorded to decline within 3 months in most individuals; however, IgG can last at least 1 year after a natural infection (Carvalho et al., 2022). Antibody durability to SARS-CoV-2 was impacted by both vaccination, with an estimated over 70% of the world's population having been vaccinated (Edouard Mathieu, 2020), and by reinfection of novel variants. Novel variants that evolved throughout the pandemic reduced the durability of immunity to infection, with studies predicting a high level of reinfection between 3 and 63 months after infection (Townsend et al., 2021). Tracking of immune escape variants during the pandemic highlighted regions of antibody escape susceptibility. The first was the introduction of D614G from the original Lineage A Wuhan strain, recorded to enhance transmissibility (Yurkovetskiy et al., 2020). Subsequent substitutions, particularly in the RBD, enhanced viral binding and evaded antibody responses (Plante et al., 2021). Examples include mutations at E484, present in both P1 (Brazil, Gamma) and B.1.351 (South Africa, Beta), followed by mutations in residues L452, L455, F456, G485, F486, and F490 (Edara et al., 2021, Zhou et al., 2021). Mutations associated with enhanced affinity for ACE2 were noted to evade neutralising antibody responses, for instance, the mutation of N501Y, present in variants B.1.1.7 (UK, Alpha), B.1.351 and P1.

Recorded as the most pathogenic of variants, B.1.617.2 (India, Delta), contained two mutations L452R and T478K that decreased antibody efficacy for both vaccinated and naturally infected individuals (Planas et al., 2021). Superseding the Delta variant was the emergence of a newer variant with over 30 mutations in the spike protein, B1.1.529 (South Africa, Omicron), recorded to have increased molecular flexibility, thus increasing infectivity and evading antibody neutralisation (Chakraborty et al., 2022). More recent subvariants of Omicron, XBB and BQ.1 are recorded to exhibit enhanced immune evasion capabilities for both vaccinated and naturally infected individuals (Uraki et al., 2023a).

1.4.3. Therapies to SARS-CoV-2

A plethora of therapeutics have been developed to combat SARS-CoV-2. Antivirals such as Molnupiravir, Paxlovid, Ivermectin, and Remdesivir, which act as replication inhibitors, were proven to reduce disease severity (Singh et al., 2021, Wang et al., 2020c, Caly et al., 2020). Antivirals, however, are most effective when delivered at a certain time point to reduce peak viral load, require multiple doses for consecutive days, and are heavily reliant on rapid diagnostics with a low level of detection (Singh and de Wit, 2022). In the early days of the pandemic, convalescent plasma was thought to be an effective treatment (Group, 2021), however, studies generated mixed results. Host-directed therapies such as Dexamethasone and Baricitinib have also been proven to reduce mortality by 13-21%, yet also require timely administration for maximum effectiveness. The most extensively developed treatment, however, has been the production of mAbs. With over 80 commercially approved, monoclonal Antibodies (mAbs) are associated with a high confidence of safety despite rapid development from discovery to trials (Marovich et al., 2020). Pertinent to cellular entry, the interface between host cells and the spike has been a key target for antibody-based therapeutics during the COVID-19 pandemic. Many of the mAbs licenced for use for SARS-CoV-2 treatment were isolated from convalescent donors, thus exhibiting high specificity to the strains with which the donors were infected, however,

often reduced in neutralisation potency against a novel variant. For instance, the initial success of mAbs Casirivimab and Imdevimab (REGN-COV2) was hindered by the emergence of Delta (B.1.617.2) and Omicron (B.1.1.529). Resistance, such as E406 mutations, to the majority of commercially available mAbs emerged both through treatment and from immunity drivers within the population (Dejnirattisai et al., 2022). Further mutations such as L452R, E484D/K/Q, F490S/L and Q493R/K reduced neutralisation of Bamlanivimab (LY-CoV555 and LY-CoV016), produced by Eli Lilly, (Starr et al., 2021b). MAb neutralisation was reduced following the emergence of Omicron, resulting in the authorisation of Bebtelovimab (LY-CoV1404) (Westendorf et al., 2022). Bebtelovimab was effective against BA.2.12.1 and BA.4/5 (Wang et al., 2022), however, is reported to have reduced efficacy against recent variants BQ.1.1 or XBB. Additionally, Sotrovimab (S309 epitope) is reported to have reduced efficacy towards these new variants (Imai et al., 2023, Driouich et al., 2023).

1.4.4. Vaccines to SARS-CoV-2

A key response to the pandemic was the rapid production of vaccines in a short developmental time scale (Krammer, 2020). Vaccines ranged from adenoviral-vectored, DNA, inactivated, attenuated, Virus Like Particle (VLP), recombinant vaccines, and RNA vaccines. Of those that became rapidly licenced for use were ChAdOx1 nCoV-19, developed from a Chimpanzee adenovirus vector expressing the full-length spike glycoprotein, and mRNA vaccines, BNT162b2 (Pfizer-BioNTech) and mRNA-1273 (Moderna), delivering the genetic material rather than expressing the antigen itself. Vaccinations to SARS-CoV-2, whether they present mRNA or foreign antigen to the immune system, induced a robust antibody response in most individuals, which when boosted elicited an enhanced response. Vaccination has been recorded to increase class switching of antibodies (Laidlaw and Ellebedy, 2022, Goel et al., 2021a) and induced a germinal centre response composed of pre-existing B-cell reactive to seasonal coronaviruses and naïve recruited B-cells specific to SARS-CoV-2 spike protein. The presence of these B-cells 15 weeks post-vaccination suggests ongoing affinity maturation (Turner et al., 2021).

Findings were consistent that a hybrid immunity, consisting of natural and vaccinated immunity, generated better protection from reinfection, a likely consequence of the re-activation of memory B-cells (Gazit et al., 2022, Callaway, 2021, Goldberg et al., 2022). Recall of memory B-cells is critical upon re-exposure to SARS-CoV-2. In individuals who had a natural infection, a singular dose of mRNA-based vaccine was sufficient to reach peak humoral immunity (Goel et al., 2021a, Lozano-Ojalvo et al., 2021). Despite these findings, antibody levels have proven to decay over time, from both natural infection and vaccination, leaving individuals susceptible to reinfection (Zhou et al., 2021, Goldberg et al., 2022, Perez-Alos et al., 2022). Multiple studies record the evasion of natural and vaccine induced antibodies by the emergence of viral variants, which have impacted the durability of antibody-mediated immunity (Zhou et al., 2021, Liu et al., 2021, McCallum et al., 2021a, Wibmer et al., 2021, Chen et al., 2021). Recent studies suggest variant XBB.1.5, a subvariant of XBB, despite sharing similar amino acids within the RBD, can evade humoral immunity from both natural infection and vaccine, however, a dose of bivalent vaccine of BA.5 was proven to improve humoral immunity (Uraki et al., 2023b). Booster doses are likely to induce high antibody titres, however, may not increase the specificity of the B-cell response and, therefore may have little impact on escape variants (Goel et al., 2021b).

Current vaccines predominantly protect the lower respiratory tract, protecting from symptomatic disease, but may enable transmission through viral shedding in the upper respiratory tract. Indeed, a vaccine applied intranasally inducing sterilising immunity is highly desirable, however, few vaccines can be administered this way (Krammer, 2020). This suggests a need to regularly update vaccines or develop broadly neutralising mAbs, targeting conserved regions, to maintain or extend humoral immunity. Until then, protection from severe disease will be therefore highly reliant on somatically mutated memory B-cell reactivation towards specific viral variants (Tong et

al., 2021), which may not be possible for those who cannot receive the vaccines and/or are immunocompromised.

1.5. Bovine Antibodies

1.5.1. Long CDRs

CDRs harbouring long paratope features have been recorded for camelid, shark, bovine, chickens, and recently humans (Prabakaran and Chowdhury, 2020). Camelid (VHH) and shark (VNAR) antibodies vary from that of chickens, bovine and humans, by lacking a light chain. These single-domain or nanobodies are reported to exhibit breadth and potency (Hmila et al., 2008, Stijlemans et al., 2004), and have recently been employed against SARS-CoV-2 (Wrapp et al., 2020a). By comparison, chicken, human and bovine antibodies have similar features, conveying breadth and potency, however, the structures are formed on the heavy chain of full antibodies (Haakenson et al., 2018, Wu et al., 2012). To date, the longest human CDRH3 recorded, PG16, at 28 amino acids, is a broadly neutralising antibody to Human Immunodeficiency Virus (HIV) from an African donor (Walker et al., 2009), thus suggesting long CDRs are a requisite for antibody breadth.

1.5.2. Ultralong antibody formation

Initial studies by Berens *et al.* (Berens et al., 1997) identified the unique length of the bovine heavy chain while analysing lymphoid tissue. One sequence discovered, F18M, was found to have 51 amino acids in the CDRH3. Following this, a plethora of studies have revealed multiple sequences of long CDRH3s (Deiss et al., 2019, Liljavirta et al., 2014, Ma et al., 2016, Wang et al., 2013) from a range of different species of cattle (Walther et al., 2016). Further studies by Saini et al. (Saini et al., 1999) and Walther et al. (Walther et al., 2013) proved these long antibodies to be fully functional in all isotypes, with three sub-isotypes of bovine IgG and two sub-isotypes of IgM recorded.

Cattle immune repertoires have deviated from the standard mechanism of antibody recombination and therefore have reduced germline combinatorial diversity. The bovine heavy chain locus, found on chromosome 21, contains a

limited number of functional variable segments. To date, 12 variable genes exist appertaining to a singular subgroup, IgHV1 (Lopez et al., 1998, Niku et al., 2012, Berens et al., 1997).

With only 10 to 12 functional variable heavy chain genes, 23 diversity heavy chain genes (16 of which are functional), and 12 junctional heavy chain genes (data from ImMunoGeneTics – IMGT (Alamyar, 2010)), rearrangement is compensated through excessive somatic hypermutation by AID in lymphoid tissue of foetal bovine ileal Peyer's patches in the gut and spleen. Bioinformatic studies indicate theoretically up to 920 possible recombination events of VDJ, this is drastically lower in comparison to the possible human antibody recombination events of 6,762 (Walther et al., 2016).

A subset of these antibodies, possess ultralong CDRH3s, recorded to exceed 70 amino acids in length (Berens et al., 1997, Lopez et al., 1998, Saini et al., 2003, Zhao et al., 2006), and comprise around 15% of the antibody repertoire. These antibodies have been coined as "Ultralong antibodies". Although long CDR3s have been recorded in other species such as dolphins, camels, and sharks, CDR3 lengths are not attained to the length observed in cattle (Saini et al., 2003, Decanniere et al., 1999, Stanfield et al., 2004, Nguyen et al., 2000).

Genomic studies have identified a specific set combination of VDJ germlines, IgHV1-7, IgHD8-2 and IgHJ2-4 (Deiss et al., 2019, Koti et al., 2008, Wang et al., 2013), that are predisposed to form ultralong antibodies. This length of the CDRH3 forms an unusual paratope structure consisting of a β-ribbon 'stalk' supporting a disulphide-rich 'knob' that protrudes from the antibody (Figure 1.5). The chains forming the knob are often cysteine-rich, enabling the formation of globular loops or folds through the generation of disulphide bridges (Wang et al., 2013). The bridges are suspected to enable stabilisation for the formation of weak molecular interactions, such as hydrogen bonds, which often take time to form (Vadnais and Smider, 2016). The evolution of such structures has been scrutinised, with theories of their evolution relating to excessive rumen microorganism exposure, lack of placental transfer of immunoglobulins (Staley and Bush, 1985) or experiencing multiple infections with close related strains enabling the formation of cross-protective responses (Deiss et al., 2019).

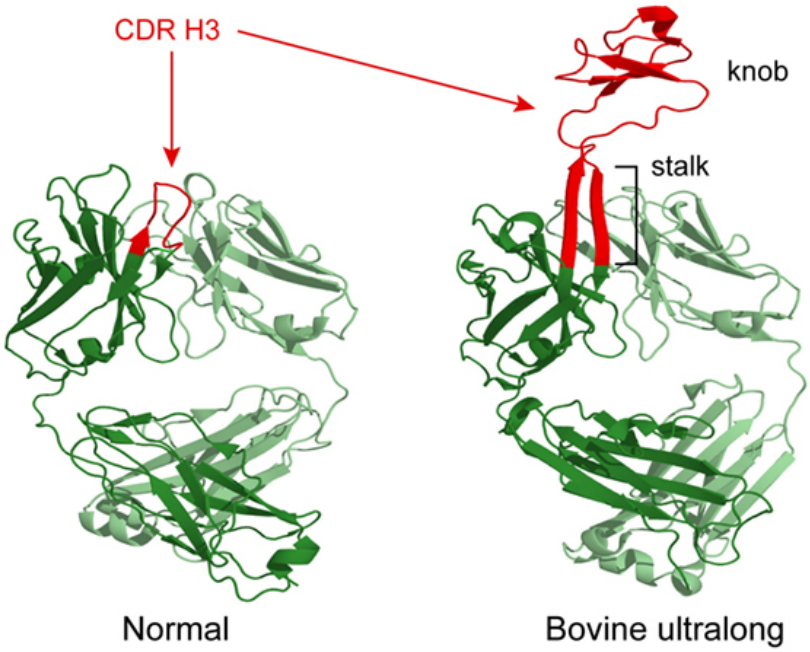

Figure 1.5: Ribbon representation on human (left) and bovine (right) Fab (green) with CDRH3 regions (red). Bovine CDRH3 is comprised of a stalk and knob. Source: (Haakenson et al., 2018).

IgHV1-7 is found in nearly all reported ultralong antibodies, however, its use is not limited to ultralong antibodies and has been documented to be utilised with shorter DH regions (Deiss et al., 2019). This V gene segment has a high level of germline conservation in the CDR1 and CDR2 suggesting a structural requirement to support the ultralong structure (Stanfield et al., 2018). IgHV1-7 has a duplication of eight nucleotides at the 3' end, altering the reading frame which results in a longer V region, this is recognised by amino acid residues TTVHQ (See Chapter 5, Figure 5.2A), forming the ascending β strands. The ascending and descending β strands of the stalk are encoded at the V-D and D-J joints. These joints are largely conserved to form the structural basis of the stalk, however, it has been reported that short nucleotide sequence insertions may be inserted at the V-D junction, providing an additional method for diversity (Koti et al., 2010).

Cluster 2 of the diversity segment is characterised by 48 amino acids harbouring four cysteines and multiple GYG motifs, with sequence bias towards amino acids such as tyrosine (35%), glycine (31%), and serine (15%) (Wang et al., 2013). Interestingly, the diversity germline IgHD8-2, commonly associated with ultralong antibodies, is thought to have arisen through genomic deletion within cluster 2. The deletion is suspected to have fused two Diversity Heavy (DH) regions while maintaining the 5' and 3' RSS. The product of this is a DH region with multiple short repeating motifs. These tandem repeats are suspected to generate substantial diversity for this DH region (Safonova and Pevzner, 2020). IgHD8-2 features somatic hypermutation hotspots 'RGYW' or 'WRCY' as well as 38 codons that can be mutated to a cysteine residue with a singular nucleotide change, increasing the potential number of disulphide bridges within CDRH3, thus diversifying the disulphide pattern in ultralong antibodies (Wang et al., 2013). Flanking IgHD8-2 in cluster 2 are IgHD5-2 and IgHD6-2, of which IgHD6-2 sequences share a conserved cysteine with IgHD8-2, which is present in all ultralong CDRH3 antibodies (Smider and Smider, 2020). This cysteine forms a structural disulphide bond at the base of the ultralong CDRH3 stalk (Wang et al., 2013,

Stanfield et al., 2018) suggesting ultralong antibodies may also be generated from this DH cluster. Class switch recombination relies on AID as a mechanism to change antibody isotypes, which occurs during the transcription of antibodies. During this process, double-strand breaks occur to switch the constant region and replacement involves NHEJ. As mutational hotspots are found in proximity within IgHD8-2, it is suspected that NHEJ may cause insertions and deletions within this ultralong D region, similar to the mechanism for class switching (Haakenson et al., 2018).

This limitation of variation within the V region is heavily compensated by alterations between V-D and D-J, but most importantly through somatic hypermutation within the diversity region both pre and post-antigen exposure. The product generated can accommodate substantial structural diversity such as disulphide bridge patterns, loop structures, and variations in stalk residues, length, and orientation. Studies like Svilenov et al. (Svilenov et al., 2021) highlight the importance of the structure of the stalk in providing stability, expression and folding, despite noting that the knob can act as an individual entity.

Bos Taurus mount a strong adaptive response despite having limited variation in the variable gene (Berens et al., 1997, Sinclair et al., 1997, Lopez et al., 1998, Saini et al., 2003, Zhao et al., 2006, Wang et al., 2013). Studies from Wang *et al.* (Wang et al., 2013) and Stanfield et al. (Stanfield et al., 2016) were the first to upload bovine ultralong Fabs BLV1H12, BLV5B8, B11, E03 and A01 to the Protein Data Bank. Comparison of these sequences shows commonalities such as high numbers of amino acids within the CDRH3, containing from one to four disulphide bridges, and are paired with the same minimally mutated λ light chain germline (Stanfield et al., 2018, Saini et al., 2003). Notably, the β stalk varies in length between these Fabs but appears to extend at a similar angle. The knob, however, is estimated to twist by up to 60°. Interestingly, these studies have highlighted residues that are thought to be conserved to support the knob architecture. Such residues include the Cys^{H92} defining the beginning of the CDRH3, $Tryptophan^{H103}$ defining the end

of the CDRH3, Glutamine or Asparagine found 6 residues prior to Tryptophan^{H103}, and Histidine or Tyrosine found 4 residues prior to the terminal Tryptophan^{H103} (Stanfield et al., 2018).

The unusual structure of knob and stalk in ultralong antibodies provides remarkable diversity in the bovine repertoire enabling binding to occluded epitopes which may be inaccessible to conventional antibodies, therefore may exhibit greater specificity to their complementary antigen.

1.5.3. Bovine antibodies as therapeutics

In recent years, the focus of therapeutics has shifted to the use of mAbs and broadly neutralising Antibodies (bnAbs) with substantial affinity maturation from specific B-cells, and therefore, often reliant on repeated antigen exposure from immunisations.

Recognised by their unique ability to bind to occluded epitopes (Prabakaran and Chowdhury, 2020, Sok et al., 2017, Burke et al., 2022), bovine ultralong antibodies have increased in interest in the last decade for their potential applications including their uses as therapeutics. Ultralong antibodies enable bovine to rapidly mount a robust immune response, particularly to broadly neutralising epitopes, following exposure to an antigen. Sok et al. (Sok et al., 2017) discovered a bovine ultralong antibody, NC Cow 1, to HIV. This antibody was found within 77 days of the study and achieved a neutralisation breadth across 79% of cross clade isolates. The ultralong CDRH3 is suspected to combat the challenging footprint of the HIV envelope by navigating through the glycan shield covering conserved epitopes on the glycoprotein that are utilised for CD4 binding. The breadth was speculated to be attributed to the binding of a small number of residues deep within the CD4 binding site. Broadly neutralising antibodies are typically a product of repeated immunisation and in HIV patients broadly neutralising antibodies have only been recorded to be established years after infection (Schanz et al., 2014, Andrabi et al., 2018). Further supporting this notion that these paratope structures are crucial for antigen binding, an antibody targeting bovine viral

diarrheal virus was modified to remove the knob, resulting in the abolishment of virus binding (Wang et al., 2013). Studies have since proven the autonomous functionality of the knob (Pekar et al., 2021). Since then, broad and potent ultralong antibodies have been discovered against a plethora of targets, for instance, Foot-and-Mouth disease (Li et al., 2019), complement component C5 (Macpherson et al., 2021b), cancer-associated receptor tyrosine kinase Epidermal Growth Factor Receptor (EGFR) (Pekar et al., 2021), and more recently to *Sarbecovirus* spike proteins through a naïve bovine library (Burke et al., 2022). Studies suggest ultralong bovine CDRH3s are highly versatile, particularly when modified to reduce the immunogenicity such as functioning as a chimeric antibody enabling Fc effector functions, as well as performing alone as a 'knobbodies' (Macpherson et al., 2021a), providing options for therapeutic design.

This unique paradigm may be harnessed to provide an approach in rapidly generating immune diversity for diagnosis, or, if in high potency, therapeutics against challenging disease agents following exposure of a pathogen (Zhao et al., 2003), especially if known to have cross-reactivity with closely related strains. High throughput discovery and isolation techniques are therefore highly desirable for their isolation.

1.6. Methods of antibody isolation and display

As of November 2019, pre-pandemic, over 80 mAbs have been approved for use across the US, with an increase of mAbs in the late-stage commercial clinical pipeline of around 20% within the last year, excluding COVID-19 antibodies (Valldorf et al., 2022). The global monoclonal antibody market is expected to reach 292 billion by 2026 according to the Monoclonal Antibodies (MAbS) Global Market Report 2023. A particular mAb, Humira (Adalimumab), approved in 2012, for the treatment of rheumatoid arthritis and TNFα-mediated chronic inflammatory diseases, has been recorded as the most profitable entity, with mAb treatments filling the majority of the top 10 drugs

by global sales (Urquhart, 2020). These mAbs have been discovered in a range of technologies and methods such as hybridoma, phage display, bacterial display, yeast surface display, mammalian surface display, ribosome display, and B-cell selection. Most systems support a wide range of antibody formats; however, full IgG expression is predominantly achieved through mammalian expression due to the complex nature of immunoglobulins (Dyson et al., 2020). For alternative display systems, antibody fragments are commonly used either as Fab (de Haard et al., 1999) or single chain variable Fragments (scFv) (Vaughan et al., 1996). Technologies of antibody display rely on sources of universal or immune libraries, and more recently transgenic animals (Bruggemann et al., 2015). Immune libraries are commonly derived from the immunisation of animals (Sok et al., 2017), humans (Cai and Garen, 1995), or convalescent recovered individuals (Duan et al., 2005). Immune libraries have experienced pre-selection and therefore typically contain an abundance of high affinity binders, thus ideal candidates for mAb selection (Valldorf et al., 2022). Conversely, universal libraries, either naïve, semi-synthetic, or synthetic, may be utilised against multiple targets (Weber et al., 2014, Frenzel et al., 2016, Hoet et al., 2005).

Library display can be achieved through multiple systems. Bacterial expression systems employ the cellular surface for the display of antibodies or antigens, commonly using lipoproteins (Mazor et al., 2007). For instance, Lpp-OmpA of *E. coli* (Francisco et al., 1993). In addition to *E. coli,* gram-positive Staphylococcus genus has been used for antibody display (Cavallari, 2017). This system provides fast-growing rates, cost-effectiveness, and high yield over alternative systems (Valldorf et al., 2022).

Yeast display, pioneered in 1997 (Boder and Wittrup, 1997), predominantly uses the a-agglutinin complex subunits Aga1p and Aga2p to display antibodies. Successfully known for the generation of Sintilimab, a mAb treatment for Hodgkin's lymphoma, yeast display provides a high throughput method for antibody display (Hoy, 2019). Yeast display has also been

successfully used in combination with immunised cattle to isolate an antibody to EGFR (Pekar et al., 2021).

Mammalian expression maintains a popular system for antibody display with the specific advantage of ensuring correct folding, glycosylation, and post-translational modification of antibodies. Typically, the antibody is fused to a transmembrane domain through the C termini of the heavy chain. Transient transfection can then be employed to generate the library. Mammalian systems have been utilised in the recent pandemic and identified promising candidates (Burke et al., 2022). Despite the advantages, drawbacks include a reduced library size and limited expression of antibodies from transiently transfected cells.

Cell-free systems such as ribosome display work by coupling the fusion library to the corresponding mRNA (Yan and Xu, 2006). The main advantage of this system is that host transformation efficiency does not limit display and therefore can produce libraries of up to 10^{15}. Moreover, additional diversity can be incorporated through error-prone Polymerase Chain Reaction (PCR) amplification (Valldorf et al., 2022).

Discovered in 1975, hybridoma technology fuses the host's B-cells with immortal cancerous cell lines such as myeloma cells (Kohler and Milstein, 1975). The main advantage of this methodology is that the resultant cell line, which can be cryopreserved, will produce antibodies limitlessly. Issues of immunogenicity can occur when using animal hybridomas, for instance, mice. To overcome this, antibody systems switched to transgenic mice and single human B-cell techniques (Chen and Murawsky, 2018). This technique has been further developed to improve the transformation process. For instance, using CpG oligonucleotide, a TLR ligand which acts as an activator for memory B-cells, recorded to increase efficiencies to between 30-100% (Traggiai et al., 2004).

Single B-cell antibody selection requires a multistep process linking to antibody display. A selection of B-cells are first isolated and detected,

commonly by fluorochrome-labelled antigens via Fluorescence-Activated Cell Sorting (FACS) or by antigen-coated beads. The heavy and light chains are isolated individually and subcloned into vectors for expression (Adler et al., 2018). This system benefits in preserving natural pairings of heavy and light chains, removes the cost of cell fusions experienced with hybridoma technology (Bradbury et al., 2018), as well as FACS modifications, such as dual staining and gating, leading to the selection of antigen-specific B-cells (Prashar et al., 2022).

The most extensively applied system of displaying antibodies is phage display. Phage display technology is the generation of a library of a diverse phage clone population whereby each clone carries a unique foreign DNA insert, hence resulting in its expression on the surface. To date, there are 14 marketed therapeutic mAbs discovered or modified through this system. Of these and the most well-known is the previously mentioned Adalimumab. In addition, commercially important mAbs such as Belimumab (LymphoStat-B) for Systemic Lupus Erythematosus (SLE), Ramucirumab for Stomach cancer and non-small-cell lung carcinoma, and Ixekizumab for psoriasis, are all candidates derived from phage display (Valldorf et al., 2022). Phage display is known for its ease of generating libraries of great diversities with impressive yields allowing the selection of antibodies with low nanomolar affinities (Valldorf et al., 2022).

1.6.1. Principles and applications of phage display

Phage display increased in popularity in the mid-1980s, revolutionising the engineering of peptides and proteins (Tikunova and Morozova, 2009). The novel technology was first demonstrated through experiments by George Smith, who successfully expressed exogenous proteins on the surface of an M13 filamentous bacteriophage. Smith fused a portion of EcoRI endonuclease into the minor capsid protein, pIII (p3), leading to the incorporation of the hybrid capsid protein into the phage. This led to the display of the foreign protein on the phage surface. He discovered that chimeric EcoRI fused p3 could bind to antibodies against EcoRI endonuclease (Smith, 1985).

Furthermore, the peptide or protein displaying phage particles could be enriched to a specific ligand by affinity through a method coined 'biopanning' (Parmley and Smith, 1988). By immobilising EcoRI endonuclease antibodies, Smith showed that phage particles expressing EcoRI endonuclease could be enriched more than 1000-fold. This experiment led to the key concepts underpinning phage display: there is a direct physical link between genotype and phenotype, and this method could be harnessed for the development of large library repertoires (Kay et al., 1996). Since the 1990s, the display of antibodies, or their fragments, has been the preferred technology for the selection of specific properties and targets. Facilitated by biopanning, peptides and proteins of high affinity and specificity can be selected for almost any target (Tikunova and Morozova, 2009). Phage display success has been recorded in the selection of zinc fingers (Choo and Klug, 1994), peptides (Parmley and Smith, 1988), hormones (Bass et al., 1990), and antibodies (Frenzel et al., 2016). Increasingly antibodies have been employed as molecular shuttles for toxic agents, therefore phage display can also be used to provide a scaffold in the search for high affinity antibodies as delivery systems (Zambrano et al., 2022).

Phage display utilises bacteriophages, referred to as phage, which are viruses that can infect bacteria and are abundantly found in nature. There are a variety of bacteriophages that exist, however, the M13 filamentous phage is the most widely used for antibody and peptide display due to an extremely malleable phage coat (Kay et al., 1996). Filamentous phage are elongated viruses bearing the F plasmid for fertility. With 98% genome similarity to all filamentous phage, they are highly adept for modification purposes (Aghebati-Maleki et al., 2016). Exogenous DNA engineering of up to 12 kb has been documented to not have an impact on filamentous phage functionality (Marintcheva, 2017).

M13 is a cylindrical virus comprising of a 6,407 base single-stranded genome, segregated into nine genes which encode five capsid proteins (Figure 1.5). Of the five capsid proteins, phage display systems commonly utilise the major

capsid protein, pVIII (p8), encoded by gene 8, and the minor capsid protein, pIII (p3), encoded by gene 3. Fusion to the major capsid protein appears restricted to shorter amino acids, such as those ranging between six to eight amino acids in length (Kishchenko et al., 1994). On the contrary, sequences fused to gene 3 can be much longer and therefore an ideal candidate for antibody expression. Fusions are added to the N terminus as the C terminal domain is required for integration into the phage coat and infectivity (Kay et al., 1996).

As shown in Figure 1.6, infection of *E. Coli* is initiated by the tip of the F pilus and TolA of the bacterium interacting with p3, resulting in depolymerisation of pilin subunits. Major capsid proteins merge with the membrane and the phage genome is translocated to the cell cytoplasm. Host resident proteins convert the single-stranded phage DNA into a supercoiled double-stranded Replicative Form (RF). This product serves as a template for transcription and translation, initiated by protein p2. When protein p5 reaches a high concentration, newly synthesised single-stranded DNA is sequestered into new phage particles rather than following the RF cycle. Transfer of capsid proteins occurs at the bacterial envelope. Capsid proteins assemble around the DNA to form a cylindrical structure consisting of the major coat protein, p8. Elongation of the phage particle is terminated by the addition of g3p and g6p. A conformational change from these proteins enables the release of the phage particle from the host cell (Webster, 1996).

In the instance of a host harbouring a phagemid encoding the recombinant gene 3, a 'helper' phage is employed, introducing both wild-type gene 3 and assembly genes through superinfection. The helper phage is defective in replication but encodes the full complement of capsid genes. The expression of a phagemid is tightly regulated through self-maintenance and selected expression whereby the phagemid behaves as a plasmid and is only expressed via a helper phage (Kay et al., 1996). This is driven by high copies of intact M13 origin, which out-competes helper phage plasmid packaging. In this instance, a superinfected host cell harbours the phagemid and the helper phage vector containing assembly genetics, leading to the expression of both

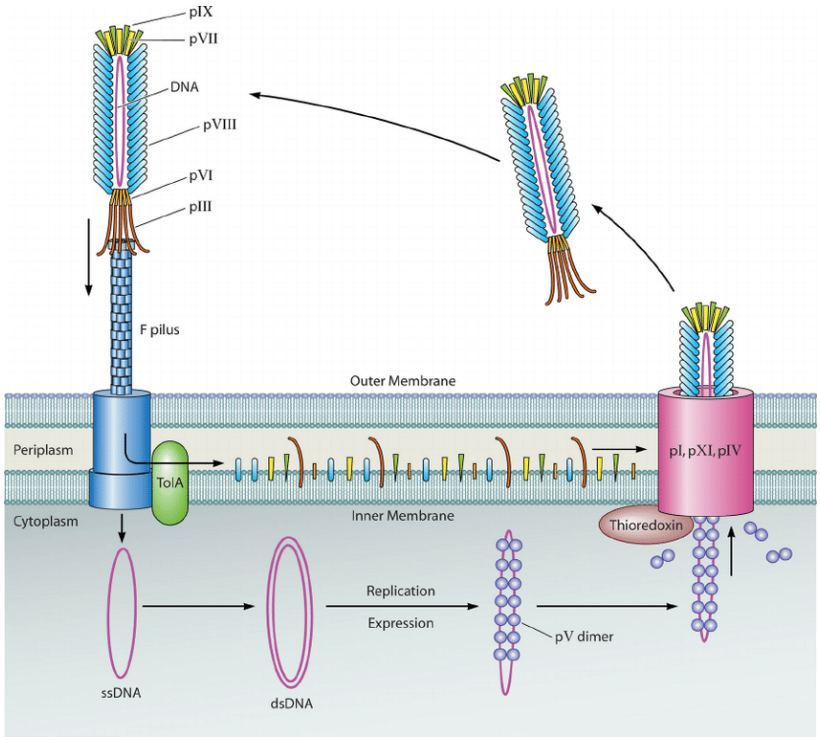

Figure 1.6: Schematic structure of M13 filamentous bacteriophage and its replicative cycle. Briefly, the M13 p3 interacts with the f pilus of the host cell membrane resulting in the release of single-stranded DNA into the cytoplasm. Replication occurs within a double-stranded replicative form to transcribe and translate phage proteins. Assembly and elongation occur at the host cell membrane where new phage particles are released from the membrane. (Source: (Huang et al., 2012).

wildtype and recombinant proteins on the capsid protein (Ledsgaard et al., 2018).

1.6.2. Library design

In more recent years, experiments have harnessed the phage expression system through cloning vectors known as 'phage vectors', or more recently 'phagemids', due to their enhanced flexibility (Breitling et al., 1991). Phagemid systems combine features of phage and plasmid consisting of the replication of origin, packaging signal of the phage, and the gene expression systems of the chosen plasmid. Library design can be modified to alter valency, these are known as filamentous phage-based vector systems. There are six major formats for filamentous display, three for gene 3, p3 expression, and the remaining three refer for gene 8, p8 expression, referring to the major and minor capsid proteins, respectively. P3 expression can be in formats 3, 33, or 3+3, and p8 as 8, 88 or 8+8, allowing for fusions to be directly with the genome or remain separately on a phagemid. These systems determine valency by altering the relationship between avidity and affinity. These formats are further discussed in Chapter 3, including vector modifications to alter protein expression. Phage display has been instrumental in the research of antibodies and their epitopes with the ability to generate large phage libraries of over 10^{12} phage molecules and antibody repertoires of great diversity.

Most recently, phage display has played an important role in identifying potential mAbs for diagnostics and therapeutics for SARS-CoV-2. For example, phage display was used for screening of potent neutralising antibodies using convalescent patient sera (Pan et al., 2021, Zhou et al., 2022, Kim et al., 2022), and of peptides for rapid and accurate detection of SARS-CoV-2 (Yang et al., 2022). The success of mAbs obtained through phage display is attributed to the versatility of library construction, and ensuring a highly representative and diverse library, to be panned against singular or multiple targets.

1.7. General Aims

Since the beginning of the SARS-CoV-2 pandemic, considerable advances have been made to adapt therapeutics and treatment to each emerging novel variant. With the emergence of three *Betacoronavirus* spillovers occurring within the last two decades, the urgency for pandemic preparedness and response is dependent on the rapid identification and employment of broadly neutralising antibodies. Phage display is a proven method for the rapid identification of monoclonal antibodies, therefore employing this technique with the breadth of bovine ultralong immune libraries, elicited from immunisation, provides an avenue for the rapid deployment of broadly neutralising mAbs against, new, challenging pathogens.

The aim at the outset of this project was to construct a phage display system for a bovine ultralong Fab library, targeting SARS-CoV-2 Lineage A trimer. A schematic of the process can be viewed in Figure 1.7. The success of library

construction led to the formation of a second aim whereby antibodies of interest were to be isolated and characterised.

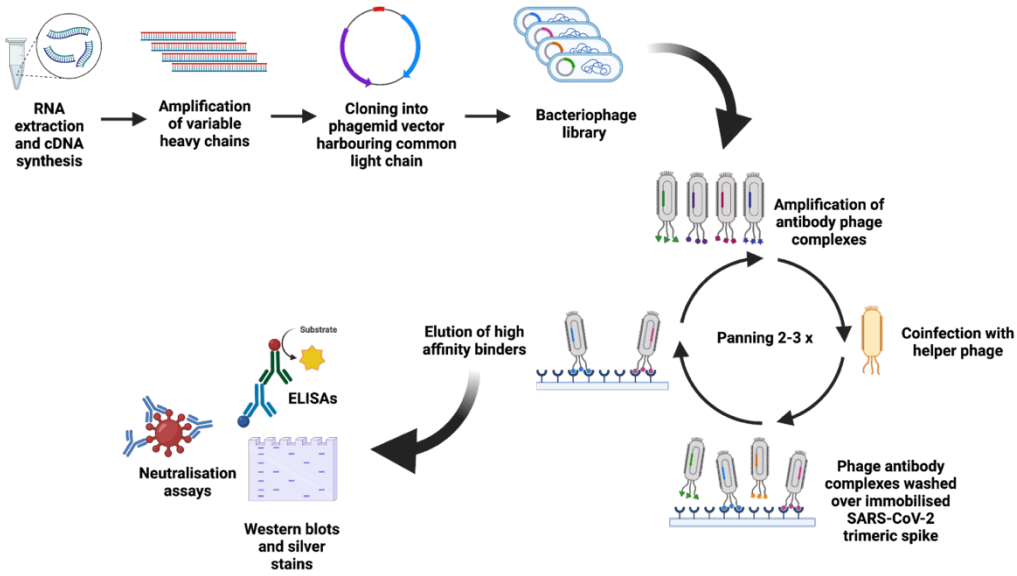

Figure 1.7: Schematic of phage display process. Library construction was achieved by isolating RNA and synthesising cDNA. Heavy chains were amplified using germline specific primers and cloned into a phagemid vector harbouring a common bovine light chain. The library was transformed into *E. coli* and rescued by coinfection with M13KO7 helper phage. The library was biopanned against immobilised Lineage A spike trimer and high affinity binders eluted and characterised. Created using BioRender.

Chapter 2 Materials and Methodology

2.1. Preparation of samples

Samples used in this study were previously collected by Dr. Richard Urbanowicz and Dr. Theocharis Tsoleridis. All animal experiments were approved by and carried out in strict accordance with the University of Nottingham's experiments and ethics committees and complied with the Home Office of Great Britain and Northern Ireland's Animals (Scientific Procedures) Act 1986.

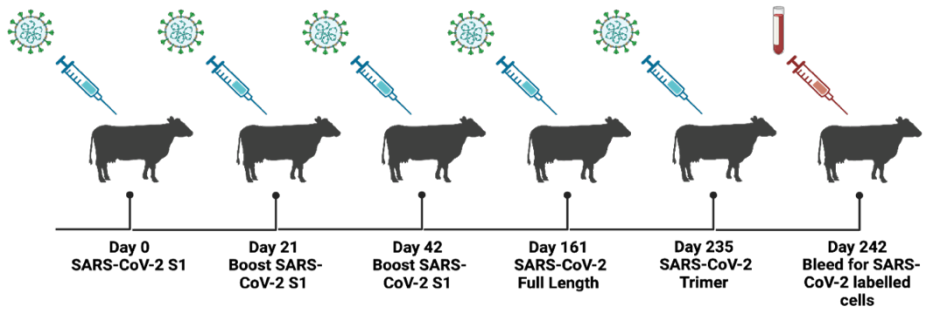

Figure 2.1: Schematic of immunisation schedule of *Bos Taurus*. *Bos Taurus* were immunised on day 0 of the study with SARS-CoV-2 Lineage A S1, and subsequently boosted with the same immunogen on days 21 and 42. Both animals were immunised with SARS-CoV-2 Lineage A full-length spike on day 161, and then with SARS-CoV-2 Lineage A Trimer on day 235. All antigens were made soluble in Titermax Gold adjuvant. Animals were bled 7 days post immunisation. Created using BioRender.

In this study, two 2-year-old Holstein-Friesian cows (*Bos Taurus*, School of Veterinary Science, Sutton Bonington, University of Nottingham) '202818' and '402813', hereby named 'C18' and 'C13', respectively, were immunised with various forms of Lineage A SARS-CoV-2 spike glycoprotein. Figure 2.1 refers to the immunisation schedule whereby initial immunisations were with S1 and full-length (FL) spike prior to a singular dosage of SARS-CoV-2 spike trimer

glycoprotein (The Native Antigen Company: SARS-CoV-2 Spike Glycoprotein (S1), Sheep Fc-Tag (HEK293): REC31806; SARS-CoV-2 Spike Glycoprotein (Full-Length), His-Tag (CHO): REC31868; SARS-CoV-2 Spike Glycoprotein (Trimeric), His-Tag (CHO): REC31871). Initial processing and flow cytometry of samples was managed and performed by Dr Theocharis Tsoleridis who kindly provided bulk cell sorts used in this study. Briefly, serum was harvested at the latest time point, day 242, 7 days post immunisation for spike-specific Peripheral Blood Mononuclear Cells (PBMCs), in accordance with Grant et al.'s study (Grant et al., 2012). PBMCs were incubated with biotinylated SARS-CoV-2 Lineage A trimer spike and dual stained with Allophycocyanin (APC) and Phycoerythrin-conjugated to streptavidin. FACS was employed to sort the bulk of the cells to select for spike-specific PBMCs. C18 yielded approximately 4,000 cells and C13 yielded approximately 4,200 cells.

2.2. Phagemid vector

The phagemid, pSD3, previously gifted by Professor Kevin Gough, was altered by Professor Jonathan Ball to express a cassette with P*st*I and B*mt*I restriction sites for cloning of bovine variable heavy and light chains, as shown in Figure 2.2. Expression was tightly controlled and selected for by the presence of a *Lac* promotor and ampicillin resistance (AmpR). The cassette was slotted into the vector downstream to the *Lac* promotor and CAP binding site; therefore, enabling transcription control using media containing the catabolite repressor, glucose. The cassette encoded a bovine light chain leader sequence followed by a P*st*I restriction site which was used for ligating a common bovine light chain, taken from NC Cow 1 (Sok et al., 2017) (of which the germline, IgLV1-47, is frequently paired with ultralong heavy chains) into the phagemid. Further downstream to the light chain, encodes a pelB signal peptide followed by bovine ultralong heavy chain framework and B*mt*I restriction site as a cloning site for the bovine ultralong heavy chain libraries. Following the heavy chain fragment was a truncated gene 3 for the expression

of the Fab region on the minor capsid protein. The presence of the amino terminal 36 kDa of gene 3 protein (g3p) is crucial for the infectivity of the phage particle and so this was incorporated into the vector. The phagemid bears an f1 origin and is maintained as a plasmid within the bacterial cell, however, required co-infection with a helper phage to produce functioning phage particles.

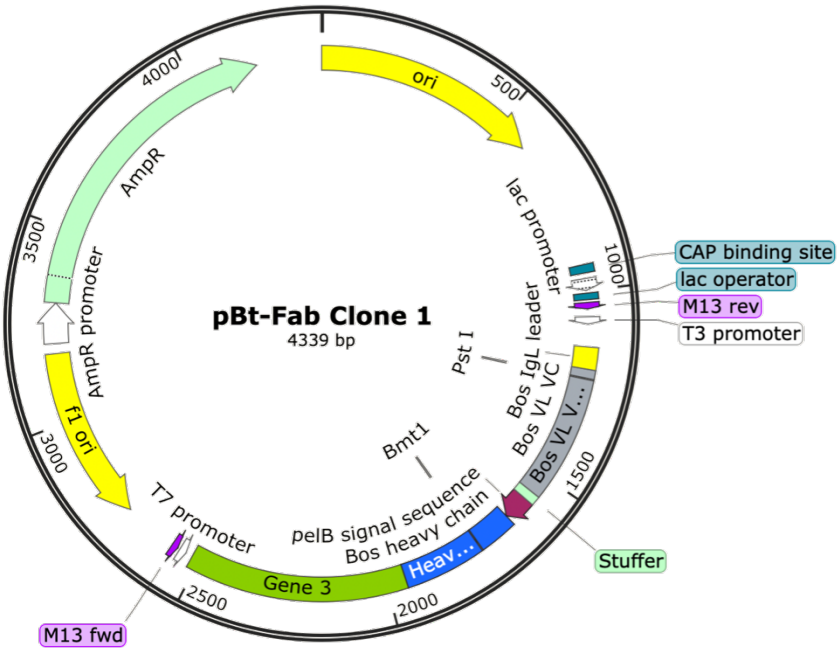

Figure 2.2: Map of the pFab3 phagemid vector. The map shows the 4339 bp vector containing the origin of replication, *lac* promotor, ampicillin resistance, signal peptides, cassettes harbouring bovine (Bos) heavy and light chain insertions, and terminal gene 3 DNA. Created using SnapGene.

2.2.1. Phagemid modifications

Given ultralong antibodies are frequently paired with a minimally mutated light chain, a common light chain was maintained during heavy chain shuffling. The phagemid was modified to contain this common light chain at the P*st*I restriction site. This was achieved by amplifying a known bovine light chain sequence from NC Cow 1 (Sok et al., 2017) that naturally pairs with a bovine ultralong heavy chain.

To amplify this light chain from a plasmid designed by Professor Jonathan Ball, a PCR was set up using a 25 μL reaction using 1 unit of Hotstar Taq polymerase (Qiagen: 203205), 10 μM deoxynucleotide triphosphates (DNTPs), 10 pM of VL1-47 F and IgL Rev primer (Table 2.1), and 10X buffer, for 40 cycles at 95 °C for 15 minutes, 20 seconds at 63°C, 72°C for 30 seconds and a final extension of 72°C for 5 minutes. Samples were prepared for visualisation by the addition of 10% FastDigest Green Buffer (10x) (Thermo Fisher: B72) and loading into a 2% agarose gel containing ethidium bromide, alongside 3.5 μL GeneRuler DNA 1Kb Ladder Mix (Thermo Fisher: SM0331). Products were visualised following gel electrophoresis for 42 minutes at 90 volts. The pFab3 vector was digested using P*st*I (NEB: R0140S) according to manufacturer's protocol. Subsequently, the light chain was ligated into the vector and transformed using In-Fusion HD Cloning Kit (Takara Bio: 638917), following the cloning enhancer protocol in the manufacturer's instructions. In this instance, 100 ng of digested vector and 1μL cloning enhanced PCR product was used. The ligation was gently pipetted into 25 μL of Stellar competent *E. coli* cells (Takara Bio: 636763, genotype: *F–, endA1, supE44, thi-1, recA1, relA1, gyrA96, phoA, Φ80d lacZΔ M15, Δ (lacZYA - argF) U169, Δ (mrr - hsdRMS - mcrBC), ΔmcrA, λ*–) and rested on ice for 30 minutes prior to transformation using heat shock at 42°C for 45 seconds. Transformations were rested on ice for the following 2 minutes then 250 μL of SOC media was added and transformants shaken at 37°C for 1 hour. 75 μL of this was plated on selection appropriate agar plates and grown at 37°C overnight. Colonies were screened using M13 F and M13 R primers as described in section 2.3 (Table 2.2).

Table 2.1: Primers used for light chain amplification and phagemid modifications.

Primer name	Sequence (5'- 3')	Reaction	Section
VL1-47 F	GTGCTGACTCAGCCATCA	Common Light chain amplification for Phagemid	2.2.1 2.7.1
IgL Rev	GGGACTTGGGCTGACCCAGG	Common Light chain amplification for Phagemid	2.2.1 2.7.1
Q5SDM pFAB3 F	ATACCCGTACGACGTTCCGGACTA CGCTCCTTAGGGCGGCGGCTCT	Amber stop codon modification	2.2.1
Q5SDM pFAB3 R	GCGCCATGGTGATGGTGATGGTGA GAGCCGCCGCCAGCGGGTGATG	Amber stop codon modification	2.2.1
Q5SDM HISHAXG3 P F	ATACCCGTACGACGTTCCGGACTA CGCTTCTTAACACCGGTACCCA	Gene 3 deletion modification	2.2.1
Q5SDM HISHAXG3 P R	GCGCCATGGTGATGGTGATGGTGA GAGCCGCCGCCAGCGGGTGATG	Gene 3 deletion modification	2.2.1

The phagemid vector was later modified to contain an amber stop codon at the junction between the heavy chain and gene 3 to enable production of soluble Fab in *E. coli* bacterial cells. Production of soluble Fab could then be achieved when the phagemid is transformed into non-amber suppressor strains. During the translation of the protein the stop codon is read, and translation is terminated. In amber suppressor strains, such as TG1 (Genotype: *[F' traD36 proAB lacIqZ ΔM15] supE thi-1 Δ(lac-proAB) Δ(mcrB-hsdSM)5(rK - mK -)*), the bacteria carry a mutation in the tRNA preventing termination of translation, thus forming a recombinant protein generated from the gene of interest fused to gene 3 (Noren et al., 1989).

As an alternative, for usage without the requirement of non-suppressor and suppressor strains, soluble Fab expression was achieved by mutation to incorporate a traditional stop codon, in this instance TAA, to be read when transformed into protein expressing *E. coli*.

In both instances, a Glycine-Serine linker and histidine tag was followed by a stop codon. Site-directed mutagenesis was achieved using Q5 Site-Directed Mutagenesis Kit (NEB: E0554) with the primers Q5SDM pFAB3 F and Q5SDM pFAB3 R for amber stop codon modification, and Q5SDM HISHAXG3P F and Q5SDM HISHAXG3P R for gene 3 deletion, in Table 2.1, following manufacturer's procedure. Each reaction was performed as a 25 μL reaction using 12.5 μL of Q5 Hot Start High-Fidelity 2X Master Mix and 0.5 micromolar of each primer for 25 cycles at 98 °C for 30 seconds, 20 seconds at 72°C, for the insertion of the amber stop codon, and 68°C for the gene 3 deletion, followed by extensions at 72°C for 3 minutes for the insertion, and 2 minutes for the deletion. A final extension of 72°C for 5 minutes completed the reaction. Products were visualised using gel electrophoresis as previously described and colonies sequenced using M13 Forward and Reverse primers (section 2.3). Subsequently, products were Kinase, Ligase, DPNI (KLD) treated (NEB: M0554S) following manufacturers' protocol and transformed into 25 μL 5-alpha F'Iq *E. coli* (NEB: C2992, Genotype: *F´ proA+B+ lacIq Δ(lacZ)M15 zzf::Tn10 (TetR) / fhuA2Δ(argF-lacZ)U169 phoA glnV44 Φ80Δ(lacZ)M15 gyrA96 recA1 relA1 endA1 thi-1 hsdR17*). Expression in this cell type enables catabolite repression by glucose as it possesses *Lac Iq*, therefore expression of the phagemid can be regulated with the presence or absence of glucose. 5 μL of KLD (NEB: M0554S) treated product was transformed as previously described for the light chain phagemid transformation. 75 μL of this was plated on selection appropriate agar plates and grown at 37°C overnight. Colonies were screened using M13 Forward and Reverse primers as described in section 2.3 (Table 2.2).

Both approaches served as a potential alternative to subcloning into mammalian expression to analyse Fab characteristics.

2.3. Colony screening

Colony screening was achieved using colony PCR. Reactions were performed in 15 μL reactions using 1 unit of Hotstar Taq polymerase, 10 μM dNTPs, 10X buffer, and 10 pM of each primer (Table 2.2) for 35 cycles at 95 °C for 15 minutes, 20 seconds annealing, 72°C for 1 minute 30 seconds and a final extension of 72°C for 5 minutes. Products were visualised using gel electrophoresis as previously mentioned and sequenced using primers in Table 2.2. Overnight cultures of positive colonies were prepared using 5 mL of LB agar supplemented with 100 μg/mL ampicillin, inoculated with a singular colony, and shaken at 37°C overnight at 225 rpm. The DNA was purified from the overnight culture using GenElute Plasmid Miniprep Kit (Sigma: PLN70), following manufacturer's procedure, with an elution volume of 50 μL, quantified by nanodrop and sequenced using primers in Table 2.2.

Table 2.2: Colony Screening primers.

Primer name	Sequence (5'- 3')	Reaction	Annealing temperature
M13 Forward	TGTAAAACGACGGCCAGT	Colony PCR for light chain in phagemid	55°C
M13 Reverse	CAGGAAACAGCTATGAC	Colony PCR for light chain in phagemid	55°C
pFAB3 col F	AGTTACAGCTGCGAGGTCA	Colony PCR of phagemid	62°C
pFAB3 col R	TACGTTGCAGGTGAAGGTCT	Colony PCR of phagemid	62°C
T7 F	TAATACGACTCACTATAGGG	Colony PCR for subcloning into pCDNA	60°C
BGH R	TAGAAGGCACAGTCGAGG	Colony PCR for subcloning into pCDNA	60°C

2.4. Library construction

Isolation of RNA of samples from section 2.1 was achieved using GenElute Mammalian Total RNA Miniprep kit according to manufacturers' protocol. Subsequently, complementary DNA (cDNA) was synthesised using 'RNA to cDNA EcoDry Premix Random Hexamer Kit' (Takara Bio: 639546), according to manufacturers' protocol.

2.4.1. 5-alpha F'Iq E. Coli Chemically Competent Libraries

Antibody heavy variable gene amplification was carried out using primer set listed in Table 2.3. For C13 cDNA amplification, a 20 μL reaction was performed using 1 unit of Hotstar Taq polymerase, 10 μM dNTPs, 10 pM of primers VH1-7 F and IgH Rev4, and 10X buffer for 45 cycles 95 °C for 15 minutes, 20 seconds at 62°C, 72°C for 30 seconds and a final extension of 72°C for 5 minutes. For amplification of C18 cDNA, a semi-nested PCR was performed. The initial round (R1) was performed as a 15 μL reaction using 1 unit of Hotstar Taq polymerase, 10 μM dNTPs, 10 pM of primers Bt IgH F2 F and IgH Rev4 (Table 2.3), and 10X buffer for 35 cycles 95 °C for 15 minutes, 20 seconds at 60°C, 72°C for 30 seconds and a final extension of 72°C for 5 minutes. For round 2, a 15 μl reaction was performed using 1 unit of Hotstar Taq polymerase, 10 μM dNTPs, 10 pM of VH1-7 F and IgH Rev4, and 10X buffer for 35 cycles 95 °C for 15 minutes, 20 seconds at 62°C, 72°C for 30 seconds and a final extension of 72°C for 5 minutes. Products were visualised using gel electrophoresis as previously mentioned. Products were then purified using NEB Monarch PCR & DNA Cleanup Kit (5 μg) (NEB: T1030S) according to manufacturer's protocol.

Library construction was modified to linearise the pFab3 L.14 phagemid for ligation of the heavy chain library to eliminate incomplete digestion. The reaction was carried out as a 20 μL reaction using 1 unit of Q5 High Fidelity polymerase (NEB: M0491S) 10 μM DNTPs, 10 pM of primers pFAB3 L.14 F and pFAB3 L.14 R (Table 2.3), and 10X for 35 cycles 98 °C for 10 seconds, 30

seconds at 66°C, 72°C for 1 minute 53 seconds and a final extension of 72°C for 2 minutes. The product was treated with DPNI (NEB: R0176S) and purified using Monarch® PCR & DNA Cleanup Kit (5 µg), following manufacturer's protocols, to remove methylated DNA, and then visualised using gel electrophoresis as mentioned previously.

The heavy chain and linearised phagemid were ligated using In-Fusion cloning, at a molar ratio of 2:1 insert to vector, following manufacturer's instructions. Phagemids were propagated into 5-alpha F'Iq chemically competent *E. coli* cells, an aliquot of culture was reserved to generate a titre to calculate transformation efficiency. Efficiencies were calculated as below. The remaining culture was spread on square 25x25cm^2 culture dishes containing 2XYT agar, supplemented with 100 µg/mL ampicillin (phagemid selection) and 10 µg/mL tetracycline (cell phenotype selection), to limit competition between clones. Plates were incubated at 37°C overnight.

$$Transformation\ efficiency = \frac{number\ of\ transformants/ug\ of\ DNA}{(\frac{First\ dilution\ in\ ul}{Total\ transformants + recovery\ media\ in\ ul}\ x\ \frac{Plated\ in\ ul}{dilution\ volume})}$$

A subset of clones were screened the following day by colony PCR (Section 2.3) using primers PFAB3 COL F and PFAB3 COL R (Table 2.2) to validate the success of the ligation and transformation. Libraries were subsequently rescued and titred using the protocol outlined in section 2.4.4, with the addition of tetracycline to media and agar plates for selection of 5-alpha F'Iq *E. coli* cell phenotype.

2.4.2. Electrocompetent TG1 libraries

To improve the cloning efficiency and thus aiming to increasing representation of diversity, libraries were re-constructed using TG1 electrocompetent cells. TG1 colonies lack *RecA* and *end1* mutations and therefore are incompatible with In-Fusion cloning. To overcome this, cloning was altered to accommodate Gibson Assembly. As recommended by

manufacturer, the original primers used for generating the chemically competent 5-alpha F'Iq *E. coli* library were extended to be between 20 and 40 base pairs (Table 2.3: VH1-7 36 BP F and IgH Rev4 30 BP). Initially, the PCR to amplify heavy chains from cDNA was carried out as described for the chemically competent library, however using the extended primers. Screening colonies and sequencing of the transformants suggested a reduction in source representation. To overcome this, three rounds of PCR were carried out with each product trialled neat, 1:10, 1:100 and 1:1000. Round 3A was performed with the brightest dilution band from round 2B. Each round was performed as 1 unit of Hotstar Taq polymerase, 10 μM DNTPs, and 10X buffer, and 1 μL template, for 35 cycles for R1 and 45 cycles for R2, and R3 at 95 °C for 15 minutes, 20 seconds annealing, 72°C for 30 seconds and a final extension of 72°C for 5 minutes.

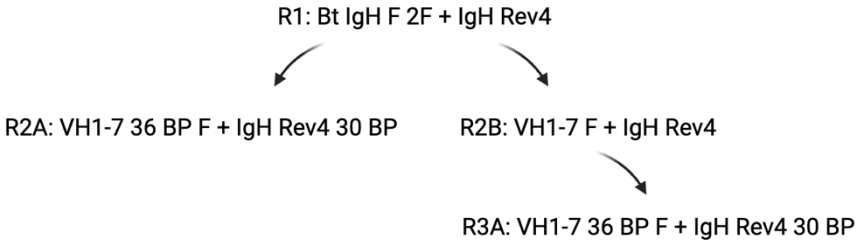

Figure 2.3: Diagram of primer use for optimising TG1 library PCR. R1 Bt IgH F 2F and IgH Rev4. R2A: VH1-7 36 F and IgH Rev4 30 BP. R2B: VH1-7 F and IgH Rev4. R3A: VH1-7 36 BP F and IgH Rev4 30 BP.

Products were visualised by gel electrophoresis, and column purified as previously described. Products were sent for Next Generation Sequencing (NGS) analysis and those showing the highest diversity between rounds 2A and 3A were selected for generating the TG1 library.

A 20 μL reaction was prepared. Using the equation below, the molar ratio was calculated to use 123 ng of library insert (approximately 500 bp) to 41 ng of

linearised vector (approximately 5,000 bp), equating to around 0.369 pmols and 0.015 pmols, respectively.

$$pmols = \frac{(weight\ in\ nanograms)\ x\ 1000}{(base\ pairs\ x\ 650\ daltons)}$$

10 µL of Gibson Assembly Mastermix 2x (NEB: E2611L) was added to the reaction and volume made to 20 µL with deionised H_2O. The reaction was carried out at 50°C for 15 minutes, followed by heat inactivation at 70 °C for 15 minutes to inactivate the ligase. Ligations were diluted three-fold as recommended by Lucigen in order to reduce arcing. A total of 5.46 ng of each ligation was added to 25 µL of thawed TG1 cells (Lucigen: Cambridge Bioscience: 60502-1), and incubated for 10 minutes on ice, then transferred into a pre-chilled electroporation cuvette (Invitrogen P41050; 0.1 cm). Conditions for electroporation were 1.8 kV Voltage, 25 µF capacitance, and 200 Ω resistance. Cuvettes were placed on ice and 975 µL of prewarmed Recovery media (Lucigen: 80026-1) added before transferring to a 1.7 mL Eppindorf and shaken for 1 hour at 37°C to allow outgrowth of any transformants. Time coefficient (milliseconds) and voltage (V) results were consistent, with voltage around 1780-1800 volts and time coefficient of between 4.6 and 4.9 seconds. An aliquot of transformants was serially diluted and 100 µL plated on 2XYT 2% Glucose (40% w/v) Ampicillin 100 µg/mL ampicillin (2XYT GA) plates. The remaining culture was spread on square 25x25cm^2 2XYT GA agar culture dishes and incubated at 37°C overnight. Transformation efficiency and screening of colonies were carried out as previously described.

2.4.3. HIV phage

A control was generated to optimise the phage production process. A known ultralong heavy chain sequence (Sok et al., 2017), was ligated into the phagemid vector at the B*mt*I site. This heavy chain was derived from an antibody that targets HIV and so the control is hereby referred to as the HIV phage control. The heavy chain was amplified from the plasmid using a

reaction similar to the 5-alpha F'Iq *E. coli* library construction, except with a codon-optimised primer, VH1-7 NCI F (Table 2.3).

Table 2.3: Primers for heavy chain amplifications, linearisation of phagemid and Gibson assembly primers.

Primer name	Sequence (5'- 3')	Reaction
VH1-7 NCI F	TTGAGCGACAAGGCTGTCGGCTGGGTTCGA	Amplification of HIV Heavy chain codon optimised
IgH Rev4	GAGTTCCAGGTCACGGTCA	Amplification of HIV Heavy chain
VH1-7 F	TTGAGCGACAAGGCTGTAGGCTG	Amplification of heavy chains
Bt IgH F2 F	ACTGTGGACCCTCCTCTTTG	R1 of semi nested PCR
pFAB3 L.14 F	GCGTGACCTGGAACTCG	Linearisation of phagemid
pFAB3 L.14 R	CAGCCTTGTCGCTCAATGA	Linearisation of phagemid
VH1-7 36 BP F	CTCTGGATTCTCATTGAGCGACAAGGCTGTAGGCTG	Extended primers for Gibson assembly
IgH Rev4 30 BP	TCAGGGCACCCGAGTTCCAGGTCACGGTCA	Extended primers for Gibson assembly

2.4.4. Phage rescue and titre

The rescue and titre protocols were modified from methods of McCafferty and Johnson (McCafferty and Johnson, 1996) and Diebolder and Krawczyk (Diebolder and Krawczyk, 2018).

Phagemids were 'rescued' using the M13KO7 helper phage (NEB: N0315S). M13KO7 is a derivative of M13 harbouring an M13 origin of replication containing P15A and kanamycin resistance. In the presence of an f1 harbouring phagemid, the single-stranded genetic material of the phagemid is preferentially packaged and secreted. Libraries spread on square 25x25cm^2 culture dishes and incubated overnight were scraped into 25 mL of 2XYT GA

and grown to log phase (OD_{600} = 0.5) followed by addition of an optimised amount of helper phage. The culture was co-infected, static, for 45 minutes at 37°C before centrifuging at 3000 xg for 10 minutes and the supernatant containing glucose discarded. Bacterial pellets were resuspended in glucose free media to enable transcription of phagemid DNA. Cultures were shaken at 30°C, 5x culture volume aeration, for 14-18 hours. Prior to harvesting phage particles, the bacterial cells were pelleted and supernatant aspirated into a fresh falcon tube for the addition of 1/6th mL of cold Polyethylene Glycol precipitation solution (20% PEG8000, 2.5 M NaCl). This was incubated at 4°C overnight. The following day the recombinant phage was harvested by centrifugation at 4000 xg for 10 minutes and resuspended at 1/100th the starting volume using Phosphate Buffered Saline (PBS).

Phage particles were titred by infecting log-phase TG1 for 30 minutes standing at 37°C and subsequently serially diluted in 2XYT GA media prior to plating on 2XYT GA and grown at 37°C overnight. The following day, colonies were counted and Colony forming units per microlitre (Cfu/μL) calculated as below:

$$cfu = \frac{Number\ of\ colonies}{\mu l\ (the\ volume\ of\ phages\ used)\ x\ (dilution)}$$

Titres were compared by Kruskal Wallis and Dunn's multiple comparison test on GraphPad Prism version 9 for macOS (Graphpad Software, San Diego, USA).

2.5. Western Blotting and silver stain

2.5.1. SDS-PAGE separation of samples and staining of SDS-PAGE

Western blot and silver stain Sodium Dodecyl Sulphate-Polyacrylamide Gel Electrophoresis (SDS-PAGE) acrylamide gels were made in house. The resolving gel was prepared to 12% with 2.5 mL H_2O, 3 mL 30% acrylamide:

bisacrylamide (37.5:1) (Sigma: A3699), 1.9 mL 1.5 M Tris (pH 8.8), 37.5 μL 20% (w/v) Sodium Dodecyl Sulfate (SDS, Sigma: L3771), 50 μL 30% (w/v) Ammonium Peroxodisulfate (APS, ITW reagents) and 11.25 μL Tetramethylethylenediamine (TEMED, Sigma: T9281), and loaded into a Mini-PROTEAN® Tetra Handcast System (Bio-rad: 1658001FC). The resolving gel was set for 20 minutes with 500 μL 100% Isopropanol (IPA) added to the top to ensure the gel was set evenly. The stacking gel was prepared to 5%, with 1.2 mL H_2O, 0.42 mL 30% acrylamide:bisacrylamide (37.5:1), 0.32 mL 1.5 M Tris (pH 6.8), 12.5 μL 20% (w/v) SDS, 8.5 μL 30% (w/v) APS and 5 μL TEMED. This was added to the resolving gel once the IPA was washed away with dH_2O and set for 20 minutes. Samples were prepared to a set volume with loading buffer (4X Laemmi sample buffer (Bio-rad: 161-0747) in the presence or absence of 2-mercaptoethanol (Sigma: M-7522) mix, then heat denatured at 95°C for 10 minutes. Samples were loaded into the gel and resolved in 1x Running buffer (1L; 25 mM Trizma base, 192 mM glycine, 0.1% SDS), initially at 70 volts for 20 minutes for proteins to clear the stacking gel, then at 150 volts for 60 minutes. Samples were run alongside Spectra Multicolour Broad Range Protein Ladder (ThermoFisher: 26623).

For silver stain, resolved gels were developed using ProteoSilver Silver Stain Kit (Sigma: PROTSIL1-1KT) following manufacturer's protocol.

2.5.2. Western blotting of SDS PAGE separated samples

Following electrophoresis separation of proteins, samples were transferred to Amersham™ Hybond® P Western blotting membranes, (Polyvinylidene Fluoride) PVDF (Cytiva: 10600029). The membrane was activated by soaking in methanol for two minutes, followed by chilled 1x Towbin buffer (1L; 25 mM Trizma base, 192 mM glycine, 20% Methanol, p*H* 8.3) for 10 minutes. The gel and blotting papers were soaked in 1x Towbin buffer for 5 and 10 minutes, respectively. Proteins were transferred using a Transblot SD Semi-dry transfer cell (Bio-rad) by sandwiching the gel on top of the membrane in 6 layers of blotting paper, under a current of constant 100 mA for 1 hour. Visible markers

of the ladder determined the success of the transfer, and the molecular markers were drawn over on the membrane using a pencil for downstream visualisation. The membrane was subsequently blocked overnight in a blocking buffer consisting of Phosphate Buffered Saline, TWEEN20 (PBST (0.1%)) and 10% milk powder (MPBST), and stored at 4°C.

The following day, the membrane was blocked for a subsequent 30 minutes in fresh blocking buffer and placed on a rocker and incubated with primary and secondary antibodies for 1 hour each and washed three times of 10-minute washes with PBST (0.1% T) in between each incubation. Membranes were developed in Pierce™ ECL Western Blotting Substrate (Thermofisher: 32106) and incubated for 1 minute. Proteins were detected using a G:Box (Syngene) and visualised by chemiluminescent detection of oxidised luminol from the HRP. Details of western blot experiments in Table 2.4.

Table 2.4: Details of Western blot experiments. Sample preparation, primary antibody, and secondary antibody.

Western blot	Sample preparation	Primary antibody	Secondary antibody
Phage	18 μL sample and 6 μL of loading buffer with reducing agent	Anti FD Bacteriophage antibody produced in rabbit (Sigma: B7786) diluted 1:1000 in MPBST (5% milk, 0.1% TWEEN20)	Anti-Rabbit IgG (whole molecule)–Peroxidase antibody produced in goat (Sigma: A0545), diluted 1:5,000 MPBST (5% milk, 0.1% TWEEN20)
mAb Light chains	9 μL sample and 3 μL of loading buffer with and without reducing agent.	Mouse anti-Human Lambda Light Chain Secondary Antibody (Thermo Fisher: MA5-11590) diluted to 1:1000 in MPBST (5% milk, 0.1% TWEEN20)	Anti-Mouse IgG (whole molecule)–Peroxidase antibody produced in goat (Sigma: A4416) diluted to 1:4000 in MPBST (5% milk, 0.1% TWEEN20)
mAb Heavy chains	9 μL sample and 3 μL of loading buffer with and without reducing agent.	N/A	Goat anti Human FC specific HRP (Sigma: AP113P) diluted to 1:1000 in MPBST (5% milk, 0.1% TWEEN20)

2.6. ELISA

A Maxisorp 96-well plate (Nunc, Thermofisher Scientific: 4442404) was coated with antigen overnight at 4°C. Wells were washed five times with 200 μL PBST (0.1%), as standard, for each subsequent wash step. To reduce non-specific binding, wells were blocked with 200 μL blocking buffer for 2 hours at room temperature. Wells were washed and analyte added in duplicate, 50 μL per well, for 1 hour at room temperature. Wells were washed again, and the primary antibody was added at 50 μL per well and incubated for 1 hour at room temperature. A secondary antibody was added at 50 μL per well and incubated for 1 hour at room temperature. Subsequently, wells were washed to remove any unbound analyte. The assay was developed using 50 μL per well of SIGMAFAST™ p-Nitrophenyl phosphate (pNPP) Tablets (Sigma: N2770) and absorbance read at an optical density of 405 nm, using a Fluorostar Omega microplate reader (BMG Labtech, Aylesbury, UK), in 5-minute intervals until saturation was reached. Analyses of results were carried out using GraphPad Prism version 9 for macOS (Graphpad Software, San Diego, USA).

Table 2.5: SARS-CoV-2 antigens for ELISAs.

SARS-CoV-2 Antigen	Product name: number	Company
Lineage A Trimer	SARS-CoV-2 Spike Glycoprotein (Trimeric), His-Tag (CHO): REC31871	Native Antigen
Lineage A S1	SARS-CoV-2 Spike Glycoprotein (S1), Sheep Fc-Tag (HEK293): REC31806	Native Antigen
Lineage A FL	SARS-CoV-2 Spike Glycoprotein (Full-Length), His-Tag (CHO): REC31868	Native Antigen
Lineage A RBD	SARS-CoV-2 Spike Glycoprotein (S1) RBD, His-Tag (HEK293): REC31882	Native Antigen
Alpha FL (B.1.1.7)	SARS-CoV-2 (B.1.1.7) Stabilized Spike Glycoprotein (Full-Length), His-Strep-Tag (HEK293): REC31924	Native Antigen
Beta FL (B.3.351)	SARS-CoV-2 (B.1.351/501.V2) Stabilized Spike Glycoprotein (Full-Length), His-Strep-Tag (HEK293): REC31926	Native Antigen
Omicron Trimer (B.1.1.529)	SARS-CoV-2 (B.1.1.529/Omicron) Stabilized Spike Glycoprotein (Trimeric), His-Strep-Tag (HEK293): REC32008	Native Antigen
BA.5 RBD	SARS-CoV-2 Spike Trimer Protein, His Tag (BA.5/Omicron) (MALS verified): SPN-C522e-50ug	Acro biosystems

2.6.1. Phage ELISAs

Enzyme Linked Immunoabsorbant Assays (ELISAs) were performed to quantify phage binding to SARS-CoV-2 Lineage A antigens (Table 2.5). Phage ELISA and Phage Binding ELISAs were performed as described in Table 2.6 to determine whether binding was glycoprotein specific.

Table 2.6: Details of Phage ELISAs. Coat, block, analyte, primary antibody, secondary antibody and analysis. N/C = negative control.

ELISA	Coat (in bicarbonate buffer.	Block	Analyte	Primary antibody	Secondary antibody	Analysis
Phage	5 µg/mL Lineage A SARS-CoV-2 Trimer or SARS-CoV-2 BA.5 trimer (Table 2.5)	4% Bovine Serum Albumin (BSA), PBST 0.1% TWEEN 20).	Phage particles normalised to 1 x 10^{10} cfu in blocking buffer. N/C: PBST (0.1% TWEEN20).	M13 phage coat protein g8p Monoclonal Antibody (RL-ph2) (Invitrogen: MA1-06604), was diluted to 1:1000 in blocking buffer.	Anti-Mouse IgG (whole molecule) –Alkaline Phosphatase antibody produced in goat (Sigma: A3562) at a dilution of 1:2000 in blocking buffer.	One way Analysis of Variants (ANOVA) and Dunnett's or Tukey's multiple comparison test.
Phage Binding	5 µg/mL SARS-CoV-2 Lineage A trimer (Table 2.5) 5 µg/mL HIV gp120 (Native Antigen: Human Immunodeficiency Virus gp120 Protein [HIV-1/Clade B (89BZ_167)]).	4% Bovine Serum Albumin (BSA), PBST 0.1%).	Phage particles normalised to 1 x 10^{10} cfu in blocking buffer. N/C: PBST (0.1% TWEEN20).	M13 phage coat protein g8p Monoclonal Antibody (RL-ph2) (Invitrogen: MA1-06604), was diluted to 1:1000 in blocking buffer.	Anti-Mouse IgG (whole molecule) –Alkaline Phosphatase antibody produced in goat (Sigma: A3562) at a dilution of 1:2000 in blocking buffer.	One way ANOVA and Tukey or Dunnett's multiple comparisons test between gp120 and SARS-CoV-2 Lineage A trimer for each phage clone OR Unpaired T test.

2.6.2. IgG ELISA

IgG ELISA was carried out to determine the concentration of expressed chimeric mAbs (Table 2.7). MAb concentrations were determined from a known standard curve.

Table 2.7: Details of IgG ELISA to determine mAb concentration. Coat, block, analyte, secondary antibody and analysis.

ELISA	Coat	Block	Analyte	Secondary antibody	Analysis
IgG	10 μg/mL Anti-Human IgG (Fc specific) antibody produced in goat (Sigma: I2136) in bicarbonate buffer.	MPBST (5% Milk, 0.1% TWEEN20)	P/C: IgG from IgG1, Lambda from human myeloma plasma (Sigma: i5029), starting at a concentration of 20 μg/mL and diluting 2-fold for 15 serial dilutions in PBST (0.1% TWEEN20) N/C: PBST (0.1% TWEEN20).	Anti-Human Lambda Light Chains (Bound and Free) –Alkaline Phosphatase antibody produced in goat (Sigma: A2904), diluted 1:2,000 in PBST (0.1% TWEEN20)	Sigmoidal dose-response curve from the standard and X values interpolated.

2.6.3. MAb binding ELISAs

Binding ELISAs were performed for mAb binding characterisation, ACE2 binding, RBD panel binding, and competition ELISAs (Table 2.8). Binding ELISAs were performed for mAbs against SARS-CoV-2 antigens from variants of concern (Table 2.5). The ACE2 binding ELISA was initially optimised by analysing ACE2 concentrations from 10 μg/mL to 0.156 μg/mL to SARS-CoV-2 Lineage A trimer. The optimal concentration, 2.5 μg/mL, determined by EC_{50} was used as a diluent for mAb dilutions. Subsequently, ACE2 binding ELISAs

were performed to determine potential ACE2 inhibition of binding to SARS-CoV-2 antigens in the presence of mAbs of interest. Additionally, mAbs of interest were trialled for binding against an RBD panel. The RBD panel was gifted by Dr. Chengcheng Fan (Caltech, USA), and consisted of 14 *Sarbecovirus* RBDs from various bat clades, and 8 human SARS-CoV-2 RBDs. Finally, mAb binding was trialled in competition with Fab. A panel of 16 Fabs, of which 14 were discovered by Dr. Theocharis Tsolderidis, were tested against mAbs to determine inhibition or enhancement as single points. 14 of the Fab panel were tested for binding to SARS-CoV-2 Lineage A trimer, carried out by Dr. Theocharis Tsolderis, in an attempt to calculate EC_{50}s. However, as the Fabs were not purified, it was decided to use Fabs excess to saturated binding. Stock concentrations of each Fab were prepared at a dilution of double the saturation, at 1:12.5, in PBST (0.1%). The mAbs of interest were diluted to double their EC_{50}s in PBST (0.1%), based on their binding curves against SARS-CoV-2 Lineage A Trimer as described previously in section 2.10.1. Fab and mAb were diluted 1:1, bringing the concentration of mAb to its EC_{50} and the Fab to 1:25. For competition curves, Fabs were used at an over-saturated dilution of 1:25, and used as diluent for mAbs. Heterologous curves were generated for observations between mAb and an alternative Fab, autologous curves acted as a positive control between mAb and its Fab version, and an uninhibited mAb curve was generated as a negative control.

Table 2.8: Details of mAb binding ELISAs. Coat, block, analyte, secondary antibody, and analysis. P/C = Positive Control. N/C = negative control.

ELISA	Coat (in bicarbonate buffer)	Block	Analyte	Secondary antibody	Analysis
mAb Binding	0.5 µg/mL SARS-CoV-2 antigen (Table 2.5)	MPBST (5% Milk, 0.1% TWEEN20)	mAb serially diluted in PBST (0.1%) four-fold starting at a concentration of 2.5 µg/mL for 7 points. N/C: PBST (0.1% TWEEN20).	Anti-Human IgG (γ-chain specific)–Alkaline Phosphatase antibody produced in goat (Sigma: A3187) diluted 1:2,000 in PBST (0.1% TWEEN20).	Proportion of uninhibited control (%) relative to the maximum binding (2.5 µg/mL antibody concentration) and minimum binding negative control)). The EC50 was calculated using a non-linear analysis and selecting for preferred model between [Agonist] vs. response -- Variable slope (four parameters) and [Agonist] vs. response (three parameters).
ACE2	0.5 µg/mL Lineage A SARS-CoV-2 antigen (Table 2.5)	MPBST (5% Milk, 0.1% TWEEN20)	2.5 µg/mL of ACE2 (Native Antigen: REC31876) in PBST (0.1%). mAb serially diluted in PBST (0.1% TWEEN20) four-fold in ACE2/PBST starting at a concentration of 2.5 µg/mL for 7 points. P/C: ACE2/PBST (0.1% TWEEN20) N/C: PBST (0.1% TWEEN20).	Monoclonal Anti-Goat/sheep –Alkaline Phosphatase antibody produced in mouse (Sigma: A8062), diluted 1:2,000 in PBST (0.1% TWEEN20).	Proportion of uninhibited control (%) relative to the maximum binding (positive control) and minimum binding (negative control). The EC50 was generated using non-linear analysis and selecting for preferred model between [Agonist] vs. response -- Variable slope (four parameters) and [Agonist] vs. response (three parameters).

ELISA	Coat (in bicarbonate buffer)	Block	Analyte	Secondary antibody	Analysis
RBD Binding	5 μg/mL of RBD antigen	MPBST (5% Milk, 0.1% TWEEN20)	mAb four-fold serially diluted in PBST (0.1% TWEEN20) starting at 2.5 μg/mL for 7 points. P/C: Avi Tag Monoclonal Antibody (1D11D10) (Thermo Fisher: A01738-40), at 2.5 μg/mL PBST (0.1% TWEEN20). N/C: irrelevant antibody, IgG1, Lambda from human myeloma plasma, at 2.5 μg/mL PBST (0.1% TWEEN20).	mAb: mAb detection, 50 μL of Anti-Human IgG (γ-chain specific)–Alkaline Phosphatase antibody produced in goat, diluted 1:2,000 in PBST (0.1% TWEEN20). P/C: Anti-Mouse IgG (whole molecule)-Alkaline Phosphatase, diluted 1:2,000 in PBST (0.1% TWEEN20). N/C: Anti-Human Lambda Light Chains (Bound and Free) –Alkaline Phosphatase antibody produced in goat, diluted 1:2,000 in PBST (0.1% TWEEN20).	Proportion of uninhibited control (%) relative to the maximum binding (mAb at 2.5 μg/mL) and minimum binding (PBST (0.1%) only). Curves were generated using non-linear analysis and selecting for preferred model between [Agonist] vs. response -- Variable slope (four parameters) and [Agonist] vs. response (three parameters) Unpaired T test was carried out between Sarbecovirus RBD strains and Human SARS-CoV-2 RBD variants.

ELISA	Coat (in bicarbonate buffer)	Block	Analyte	Secondary antibody	Analysis
Fab Binding	0.5 μg/mL SARS-CoV-2 Lineage A trimer (Table 2.5)	MPBST (5% Milk, 0.1% TWEEN20)	Five-fold serial dilution of Fab in PBST (0.1% TWEEN20) for 7 points. N/C: PBST (0.1% TWEEN20).	Anti-Human Lambda Light Chains (Bound and Free) –Alkaline Phosphatase antibody produced in goat (Sigma: A2904), diluted 1:2,000 in PBST (0.1% TWEEN20).	Proportion of uninhibited control (%) relative to the maximum binding (Neat Fab) and minimum binding negative control)). The EC50 was calculated using a non-linear analysis and selecting for preferred model between [Agonist] vs. response -- Variable slope (four parameters) and [Agonist] vs. response (three parameters).
Competition single point	0.5 μg/mL SARS-CoV-2 Lineage A Trimer (Table 2.5)	MPBST (5% Milk, 0.1% TWEEN20)	Fab were prepared at a dilution of 1:12.5, in PBST (0.1% TWEEN20). The mAbs diluted to double their EC_{50}s in PBST (0.1% TWEEN20). Fab and mAb were diluted two-fold, bringing the concentration of mAb to its EC_{50} and the Fab to 1:25.	Anti-Human IgG (γ-chain specific)–Alkaline Phosphatase antibody, diluted 1:2,000 in PBST (0.1% TWEEN20).	Mean Optical density readings measured, and a matrix was generated.

ELISA	Coat (in bicarbonate buffer)	Block	Analyte	Secondary antibody	Analysis
Competition: Curves	0.5 μg/mL SARS-CoV-2 Lineage A Trimer (Table 2.5)	MPBST (5% Milk, 0.1% TWEEN20)	Heterologous curves: a four-fold serial dilution of mAb in alternative Fab (1:25) diluted in PBST (0.1% TWEEN20) starting at 2.5 μg/mL for 7 points. Autologous curves: a four-fold serial dilution of mAb in own Fab (1:25) diluted in PBST (0.1% TWEEN20) was prepared, starting at 2.5 μg/mL for 7 points. Uninhibited curves: a four-fold serial dilution of mAb in PBST (0.1% TWEEN20) starting at 2.5 μg/mL for 7 points. N/C: PBST (0.1% TWEEN20).	Anti-Human IgG (γ-chain specific)–Alkaline Phosphatase antibody, diluted 1:2,000 in PBST (0.1% TWEEN20).	Proportion of uninhibited control (%) relative to the maximum binding (mAb at 2.5 μg/mL) and minimum binding (PBST (0.1%) or Fab only). Curves were generated using non-linear analysis and selecting for preferred model between [Agonist] vs. response -- Variable slope (four parameters) and [Agonist] vs. response (three parameters).

2.7. Next Generation Sequencing

Validation of library diversity was achieved using NGS (Genewiz EZ amplicon service, AZENTA Life Sciences). Samples were prepared by PCR amplification using VH1-7 F and IgH Rev4 or extended primers (Table 2.3), following the reaction stated in 2.4.1 and 2.4.2 to amplify heavy chains, except in this instance, the template added was 1 μL of the initial PCR product, 1 μL transformed colony library, or 1 μL phage library, and the total of each reaction volume was 100 μL. Template was diluted between 1:100 and 1:10,000, and validated with gel electrophoresis as reported in section 2.2.1. Products were column purified using Monarch® PCR & DNA Cleanup Kit (5 μg) as described in manufacturers protocol and visualised using gel electrophoresis to ensure the presence of product. Data were analysed using Geneious Prime Version 2021 2.2 (https://www.geneious.com). Illumina sequences were imported, paired reads set, trimmed using BBDuk, and merged. Sequences were mapped to the VH1-7 F primer and trimmed at the 5' and 3' to form sequences from VH1-7 to framework 4. Unique sequences were extracted and sequences shorter than 270 base pairs removed. Sequences were matched against the IMGT/V-QUEST version: 3.6.0 (22 March 2023) database to identify CDRH3 lengths and sequences.

2.8. Biopanning

The biopanning protocol was adapted and modified from two sources (Philipp and Adalbert, 2017, Solemani Zadeh et al., 2019, Diebolder and Krawczyk, 2018). A Maxisorp 96-well plate (Nunc, Thermofisher Scientific: 4442404) was coated directly with 5 μg/mL Lineage A SARS-CoV-2 Trimer in bicarbonate buffer (Table 2.5) overnight at 4°C. Wells were washed five times with 200 μL PBST (0.1%), as standard, for each subsequent wash step. To reduce non-specific binding, wells were blocked with 3% Bovine Serum Albumin (BSA), (Sigma: A3059), in PBST at 200 μL per well, for two hours at room temperature. For the second round of biopanning, an alternative blocking

buffer of 3% Gelatin from cold water fish skin (FSG) (Sigma: G7041) was used. Blocking buffers were chosen from optimisation of this blocking step. Simultaneously, phage libraries were preincubated in a blocking buffer to 1 x 10^{11} cfu. In parallel, 10 mL of 2XYT was inoculated with 2 mL overnight culture TG1 and grown at 37°C, 250 rpm to log phase at an OD_{600} of 0.5. TG1 cells were maintained by plating on M9 minimal media, supplemented with 25% glucose, 20% Magnesium Chloride ($MgCl_2$) and 100mg/mL Thiamine-hydrochloride, for selection of the F episome. After blocking, wells were washed and blocked phage libraries were added for 1 hour at room temperature with gentle agitation. To remove low affinity binders, wells were washed alternating with PBS and PBST, increasing the concentration of TWEEN20 from 0.1-1.0%, by 0.1%, for each alternate wash. For the subsequent panning rounds, washing steps were increased to 20 steps with PBST, increasing concentration in alternative washes from 0.1-2%, by 0.1% each time. High affinity binders from each library were eluted in 100 μL 0.2 M glycine pH 2.2 for 8 to 10 minutes, then neutralised using 15 μL per well of 1 M Trizma hydrochloride (Tris HCL) pH 9.1 and aspirated into a 1.7 mL eppindorf. To ensure all phage particles were collected, 100 μL of log phase TG1 was added to the wells. Simultaneously, eluted phage were added to 500 μL of log phase TG1. Both cultures were incubated at 37°C for 30 minutes static and then 30 minutes shaking, then combined. A serial dilution in 2XYT GA media to 10^{-4} was generated for both libraries and plated on 2XYT GA agar to determine the titre, while the remaining culture was spread on square plates to reduce competition between clones. The following day, the titre was calculated as in section 2.4.4, and phage particles rescued and amplified as previously described.

2.9. Expression of chimeric mAbs

Two phage clones from library C13 exhibited high levels of binding over the other clones (C13.2 and C13.7 phage). These Fabs of interest were therefore

subcloned into a mammalian expression vector to form chimeric mAbs consisting of a human Fc region, and a bovine Fab region.

2.9.1. Generation of chimeric mAbs using Fab subcloning and mammalian expression.

The Fab was ligated into pCDNA3 vectors harbouring heavy and light chain cassettes designed by Professor Jonathan Ball (Figure 2.4). The light chain vector, pBt IgL, was digested at the B*mt*I restriction site using the restriction enzyme B*mt*I according to manufacturer's procedure. The light chain, amplified using VL1-47 and Bos IgL Rev (Table 2.9), could be seamlessly cloned into the light chain vector at the B*mt*I restriction site. The heavy chain amplified from the phagemid required additional segment of DNA upstream for cloning into the pBt IgH vector. This was achieved 1 unit of Hotstar Taq polymerase, 10 μM DNTPs, 10 pM of an internal reverse primer and a newly designed forward primer to give a 15 bp overhang complementary to pBt IgH (Bos infusion F, Bt IgH Rev3, Table 2.9), and 10X buffer for 45 cycles 95 °C for

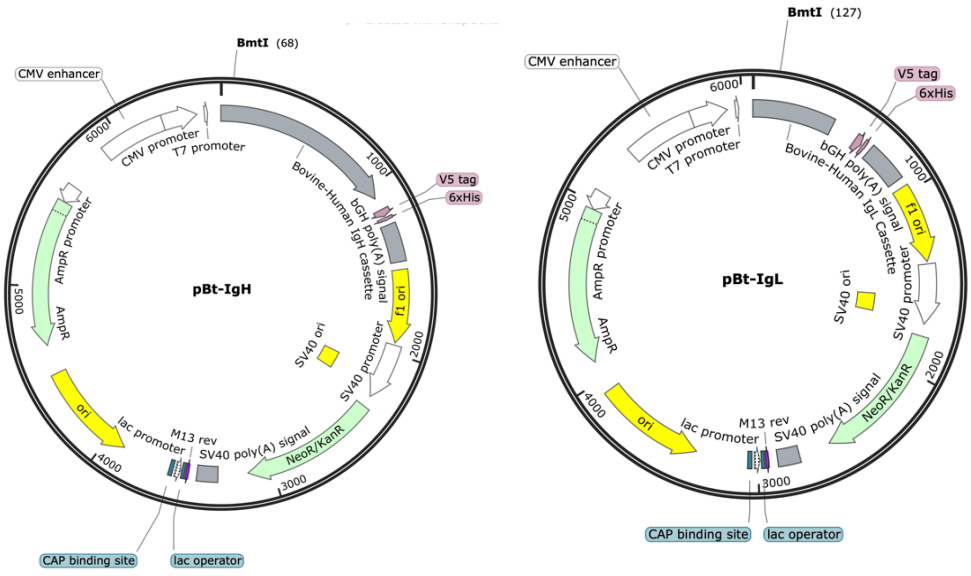

Figure 2.4: Heavy (left) and light (right) chain cassettes for subcloning for mammalian expression. Cassettes are prior to an f1 origin of replication, SV40 origin, neo/kan resistance, *Lac* promotor, ampicillin resistance, and CMV promotor. Created using SnapGene.

15 minutes, 20 seconds of annealing at 62°C and an extension at 72°C for 1 minute. A final extension of 72°C was carried out for 5 minutes. A plasmid of pBt IgH containing a heavy chain was linearised to delete the DNA downstream of the VH1-7 site. This was carried out as a 25 μL reaction comprising of 12.5 μL of Q5 Hot Start High-Fidelity 2X Master Mix, 0.5 micromolar of Bos vector F and Bos vector R (Table 2.4), and 1 μL of plasmid diluted 1:100. The reaction proceeded as an initial cycle at 98°C for 30 seconds followed by 35 cycles of 98°C for 10 seconds, 68°C for 30 seconds, and 72°C for 4 minutes and 30 seconds. This was followed by a final extension of 72°C for 2 minutes and visualised using gel electrophoresis as previously mentioned. The product was treated with DPNI following manufacturers procedure, and column purified. The amplified heavy chain with a 15 bp overhang could then be seamlessly cloned into the vector. Products were ligated using In-Fusion cloning, with a molar ratio of 2:1, and transformed into Stellar competent *E. coli* cells (Takara Bio: 636763) previously described (Section 2.2.1). The following day, the colonies were screened by colony PCR (Section 2.3) using T7 F and BGH R primers (Table 2.2), and plasmids extracted and sequenced.

Table 2.9: Primers for Linearisation and amplification for subcloning of Fab for mammalian expression.

Primer name	Sequence (5'- 3')	Reaction
VL1-47 F	GTGCTGACTCAGCCATCA	Common Light chain amplification for pBt IgL
IgL Rev	GGGACTTGGGCTGACCCAGG	Common Light chain amplification for pBt IgL
Bos vector F	TGGTCACCGTCTCCTCAGCCT	Linearisation of pBt IgH
Bos vector R	TGAGAATCCAGAGGCCGTGCA	Linearisation of pBt IgH
Bos infusion F	GCCTCTGGATTCTCATTGAGCGACAAGG CTGTAGGCT	Amplification of heavy chain for subcloning into pCDNA

Bt IgH Rev3	AGGCTGAGGAGACGGTGACCA	Amplification of heavy chain for subcloning into pCDNA
pBt_H_Fab_F	CATCATCACCATCACCATTGAG	Fc deletion of heavy chain pCDNA
pBt_H_Fab_R	GTGGGTCTTGTCGCAGCT	Fc deletion of heavy chain pCDNA

2.10. Cell culturing

2.10.1. Maintenance of cell lines

Human Embryonic Kidney 293T (HEK293T) and Vero E6 cell lines were maintained in Dulbecco's Modified Eagle's Medium (DMEM) (Gibco: 41965-039) supplemented with heat inactivated 10% foetal bovine serum (FBS) and 1% Non-Essential Amino Acids (NEAAs) (Gibco: 11140-050). Expi293F cells (Gibco: 13481059), for high yield protein production, were maintained in Expi293 Expression Medium. Cells were passaged bi-weekly and discarded after a maximum passage of 50 or 30, for HEK293T and Vero E6, and Expi293F, respectively.

Briefly, passaging of HEK293T and Vero E6 involved aspirating the spent media from the cells and washed with Dulbeccos PBS (Sigma: D8537). Cells were subsequently incubated with prewarmed Trypsin, at 0.05% Trypsin-EDTA (Thermo Fisher: 25300062) for 5 minutes and 0.25% Trypsin-EDTA (Thermo Fisher: 25200-072) for 10 minutes, for HEK293T and Vero E6, respectively. To neutralise the Trypsin, fresh DMEM was added to the cells and transferred to a 50 mL falcon for centrifuging at 300 xg for 7 minutes in a swinging bucket centrifuge to pellet the cells. The media was aspirated, discarded and the pellet resuspended in fresh media. 10 μL of cells were transferred to a haemocytometer for counting. Cells were diluted to an appropriate concentration and seeded into T75 cell culture flasks (Corning: 430639). Cells were maintained by incubation at 37°C and 5% CO_2.

Passaging of Expi293F cells was carried out by Dr. Joseph Chappell following manufacturers Expi293 Expression System User Guide. Briefly, 10 μL of cell suspension was added to 10 μL of Trypan blue and placed on a haemocytometer to calculate cell viability density. Following protocol recommendations, a calculated volume of cells was transferred to pre-warmed Expi293 Expression Medium in a non-baffled Erlenmeyer flask. Cells were incubated at 37°C on an orbital shaker platform with 8% CO_2.

2.10.2. Transient transfection of HEK293T cells

To generate pseudoparticles or chimeric mAbs, a transient transfection of HEK293T cells was carried out. HEK293T cells were seeded at a density of 1.5 x 10^6 24 hours prior to the transfection in a 10 cm^2 Corning Primaria dish (Corning: 353803). On the day of transfection, plasmids were diluted with Opti-MEM Reduced serum medium (Gibco: 31985-047) and combined with the transfection reagent, polyethyleneimine (PEI). For pseudovirus particle production, MLV-gag/pol, luciferase reporter, and SARS-CoV-2 spike glycoprotein plasmids (provided by Dr Joshua Duncan) were mixed with Opti-MEM at a concentration of 2 μg of each plasmid to a total of 300 μL. A second mix consisting of 24 μl PEI (1 mg/mL) and 276 μl Opti-MEM was added to each plasmid mix and incubated at room temperature for 1 hour. Media was aspirated from the plates and 7 mL of Opti-MEM was added gently to the dishes. The plasmid/PEI mixes were then added to plates in a dropwise motion and incubated for 6 hours at 37°C and 5% CO_2. Following this incubation, the media was replaced with 10 mL supplemented DMEM and incubated for 72 hours at 37°C and 5% CO_2. Cell supernatant was harvested and filtered through a 0.45 μM filter for immediate use or stored at 4°C for 1 week. For mAb production, the above protocol was optimised to use 4 μg of heavy and light chain plasmid only.

2.10.3. Transient transfection of Expi293F cells

The day prior to transfection, cells were seeded at a density of 2.5-3 x 10^6 viable cells and allowed to grow overnight. On the day of transfection, the

cells were counted and should have reached a density of 4.5 x 10^6 cells per mL. The culture was adjusted to bring the density of cells to 3 x 10^6 per mL using fresh, pre-warmed Expi293 Expression Medium. The molecular ratios of plasmid were calculated depending on the culture total volume. For example, 1 μg/mL of DNA was required, therefore a 200 mL culture required 66.66 μg of heavy chain plasmid in combination with 133.333 μg of light chain plasmid for a ratio of 2:1. Plasmids were diluted in Opti-MEM accordingly, and a second mixture consisting of ExpiFectamine 293 Reagent (Gibco: A14524) and Opti-MEM was made according to the recommendations in the Expi293 Expression System User Guide. The ExpiFectamine 293 Reagent and Opti-MEM mix was incubated at room temperature for 5 minutes before combining with the plasmid and Opti-MEM mix and incubated for 20 minutes at room temperature. This solution was added dropwise to the culture while swirling. Transfected cultures were incubated at 37°C and humidified atmosphere of 8% CO2 on an orbital shaker. The next day, enhancers were added to the culture following the procedure in the manufacturer's guide. 5–7 days post-transfection, the secreted proteins were harvested by centrifuging and retaining the supernatant. The supernatant was either purified immediately or stored at -20°C.

2.10.4. Infection and Neutralisation assays

Vero E6 cells were seeded at 10,000 cells per well in a Costar white bottomed 96-well plate (Corning: 3917) 24 hours prior to the infection and neutralisation assays. For infection assays, media was aspirated and pseudovirus particles added at 100 μL per well in triplicates to the plate. After 4 hours of incubation at 37°C and 5% CO_2, pseudovirus particles were replaced with 250 μL DMEM added to each well and incubated for a further 72 hours. Media was discarded and 50 μL of cell lysis buffer (Promega: E1531) was added to each well and incubated on a rocker at room temperature for 10-15 minutes. The assay was developed by injecting 50 μL Luciferase substrate (Promega: E1500) into each well and immediately reading luminescence at 3600 gain using a Fluorostar Omega microplate reader. For

single point neutralisation assays, mAbs were diluted 1:1 at a final concentration of 1 μg/mL in pseudovirus particles, incubated at room temperature for 1 hour, then added 100 μL per well in triplicate to the seeded Vero E6 plate. After 4 hours of incubation at 37°C and 5% CO_2, the media was removed and replaced with 250 μL fresh DMEM was added to each well and incubated for a further 72 hours and then read as protocol previously described for infection assays. For neutralisation assays, a five-fold serial dilution of each mAb was generated by diluting in Dulbeccos PBS, starting at 200 μg/mL in a V bottomed 96 well microtitre plate (Thermo Fisher: 612V96). Pseudovirus particles were added to each well to generate a 10-fold dilution of the mAb, bringing the starting concentration of the curve to 20 μg/mL. A separate well consisting of PBS diluted in pseudovirus served as a positive control. The V bottomed plate was incubated at room temperature for 1 hour prior to adding 100 μL per well in triplicate to the seeded Vero E6 plate. After 4 hours of incubation at 37°C and 5% CO_2, the media was removed and replaced with 250 μL fresh DMEM was added to each well and incubated for a further 72 hours. Development of the assays were carried out using the Luciferase assay system as described for infection assays, except for SARS-CoV-2 pseudovirus particles a gain of 3800 was used, and 2000 for Vesicular Syncytial Virus (VSVg) control pseudoparticles. Infectivity of pseudovirus particles, measured as Relative Light Units (RLU), was normalised to positive and negative controls, calculated as proportion of uninhibited control (%) relative to the maximum infectivity (positive control) and minimum infectivity (ΔEnvelope pseudovirus particles). The IC_{50} for curves was calculated on GraphPad Prism by transforming the data as Y = 100 - (normalised value), using the non-linear analysis and selecting for preferred model between [Inhibitor] vs. response -- Variable slope (four parameters) and [Inhibitor] vs. response (three parameters).

2.11. Protein purification and quantification

2.11.1. Protein G purification of Expi293F produced mAbs

The purification of mAbs was carried out using an ÄKTA start protein purification system (Cytiva: 29022094) with HiTrap Protein G column (Cytiva: 17040501). The harvested Expi293F supernatant to be purified was diluted two-fold in binding buffer (100 mM $NaPO_4$, pH 7.0; 1L) and 0.2 μM filtered. The sample was loaded onto the column and flow through retained. The column was washed with binding buffer prior to eluting with elution solution (200 mM glycine, pH 2.7; 500 mL). Fifteen 1 mL fractions were collected and neutralised with 200 μL of neutralisation buffer (1M Tris, pH 9.0; 200 mL). An aliquot of each fraction was retained for validation by silver stain. Fractions covering the mAU elution peak were stored at 4°C or pooled into an Amicon Pro Purification System with 100 kDa Amicon Ultra-0.5 Device (Merck: ACS510024) and centrifuged to concentrate fractions. The column was washed 3 times with Dulbeccos PBS and transferred to a 2 mL Zeba Spin Desalting Column (Thermo Fisher: 89890). The buffer was exchanged to Dulbeccos PBS in the spin column following manufacturer's protocol to remove excess glycine from the elution step.

2.11.2. BCA assay quantification of proteins

To quantify the purified mAbs and *Sarbecovirus* RBD proteins, a range of mAbs dilutions were prepared and compared to a standard curve of BSA using Pierce BCA Protein Assay Kit (Thermo Fisher: 23227), following manufacturer's protocol. The assay was read at 562 nm using a Fluorostar Omega microplate reader after 30 minutes of developing at 37°C. Results were analysed on GraphPad Prism by calculating a simple linear regression and interpolating X values.

2.11.3. Endotoxin assay

The mAbs of interest were prepared for *in vivo* studies and so an endotoxin assay was carried out on all samples. The mAbs to be analysed were diluted in Dulbeccos PBS and compared to an endotoxin standard curve from the

Pierce™ Chromogenic Endotoxin Quant Kit (Thermo Fisher: A39552S). The assay was carried out following manufacturer's procedure and read at 405 nm using a Fluorostar Omega microplate reader. Results were analysed on GraphPad Prism by calculating a simple linear regression and interpolating X values.

2.12. RBD panel expression

The RBD panel was gifted by Dr. Chengcheng Fan (Caltech, USA), and consisted of 14 *Sarbecovirus* RBDs from various bat clades, and eight human SARS-CoV-2 RBDs. DNA was transformed into Stellar *E. coli* competent cells, overnights prepared from the transformants, and the following day plasmids extracted, as previously described in section 2.2.1. Dr. Joshua Duncan transfected HEK293T with 4 μg of each plasmid, using an alternative transfection reagent, Lipofectamine and P3000. Briefly, plasmids were mixed with p3000, followed by the addition of Lipofectamine 3000 following manufacturers recommendations, and incubated at room temperature for 20 minutes. This mix was added to cells at a density of 3 x 10^6 with Opti-MEM media and incubated for 6 hours, subsequent steps were carried out as described in section 2.10.2.

Harvested supernatant was purified using Ni-NTA His Bind Resin (Merck: 70666) and Amicon Pro Purification System with a 10 kDa Amicon Ultra-0.5 Device (Merck: ACS510024). Briefly, 200 μL of resin was added to the Amicon Pro Purification System with an exchange device, and the storage buffer was removed through centrifugation and flow through discarded. All centrifugation steps were carried out at 1000 xg for 1 minute in a swinging bucket rotor. 500 μL of 1x Binding buffer (50 mM NaH_2PO_4 pH 8, 0.3 M NaCl, 10 mM Imidazole) was added to the exchange device and centrifuged. 9000 μL of the sample was added to the exchange device and incubated for 60 minutes at room temperature with gentle agitation prior to centrifuging. 1.5 mL of Wash Buffer (50 mM NaH_2PO_4 pH 8, 0.3 M NaCl, 20 mM Imidazole) was

added to each exchange device, centrifuged, and flow through discarded. Samples were eluted by inserting the 10 kDa Amicon Ultra-0.5 Device onto the exchange device and returning the device to the collection tube. 1.5 mL of Elution Buffer (50 mM NaH_2PO_4 pH 8, 0.3 M NaCl, 25 mM Imidazole) was added, and the resin was gently resuspended and incubated for 5 minutes at room temperature. The sample was centrifuged at 4,000 xg for 15 minutes in a swinging bucket rotor to elute all of the sample. The filter was washed twice with PBS and centrifuged at 4000 xg for 1 minute to remove excess elution buffer.

To validate RBD expression and to determine the protein concentration, a silver stain was carried out on one of the samples and BCA assay for all samples, as previously described in sections 2.5 and 2.11.2, respectively.

2.13. mAb modifications to Fab

2.13.1. mAb plasmid modifications

Heavy chain plasmids of mAbs were modified to remove the CH2 region in order to produce Fab versions of mAbs. This was achieved with a 25 μL SDM reaction. The reaction was performed as 12.5 μL Q5 Hot Start High-Fidelity 2X Master Mix, 0.5 μM of primers pBt_H_Fab_F and pBt_H_Fab_R (Designed by Dr. Theocharis Tsoleridis, Table 2.9), plasmid diluted 1:100 in nuclease free water and made up to 25 μL with nuclease free water. An initial temperature of 98°C for 10 seconds, followed by 25 cycles at 98 °C for 30 seconds, 20 seconds at 64°C, and extension at 72°C for 3 minutes and 30 seconds. A final extension of 72°C for 2 minutes completed the reaction. Products were visualised using gel electrophoresis, sequenced using T7 Forward and BGH Reverse primers, treated with KLD and transformed as described in section 2.2.1. Colonies were screened by colony PCR and sequenced using T7 Forward and BGH Reverse primers as previously mentioned in section 2.3.

2.13.2. Fab expression

Expression of Fab was carried out by Dr. Joseph Chappell by transfecting a 25 mL culture of Expi293F cells. The transfection was performed as described in section 2.10.3, with 16.67 μg of light chain plasmid, and 8.33 μg of modified heavy chain plasmid from section 2.9.1.

2.13.3. Cryo-EM structures of ultralong Fab

Cryo-EM structures of ultralong Fab were performed by Dr. Chengcheng Fan, Division of Biology and Biological Engineering, California Institute of Technology, Pasadena, CA, (Caltech).

Chapter 3 Design and construction of a bovine ultralong antibody phage display library

3.1. Summary

Phage display has rapidly become a popular technique for the identification of antibodies due to its versatility in experimental design and ability to generate high yields. A control HIV phage was generated for the purpose of validating the biopanning and optimising the process. Library design and construction were optimised to support the display of a B-cell pool of bovine ultralong antibodies on g3p of the M13 bacteriophage. Libraries were validated throughout construction to maintain source representation.

3.2. Introduction

Therapeutic mAbs have proven to be successful in treating widespread disease and have since made an impact in the SARS-CoV-2 pandemic (Pan et al., 2021, Zhou et al., 2022, Kim et al., 2022). Their rapid isolation and employment may be vital for future pandemic threats. High throughput screening of candidates is therefore highly desirable. Phage display is a versatile option for antibody selection, with the option to fuse antibody or antibody fragments to M13 bacteriophage coat proteins depending on the desired valency (Jaroszewicz et al., 2022).

The popularity of the M13 bacteriophage for phage display is clear in the literature (Bazan et al., 2012, Tikunova and Morozova, 2009, Griffiths and Duncan, 1998, Smith, 1985, Smith and Petrenko, 1997). To obtain optimal efficiency for M13 phage display, classical display systems were designed using vectors, which could be modified for integration of the desired fusion protein. Designing a phage display library requires careful consideration of vector design such as which coat protein to express on, fusion to all or limited copies of coat protein, and whether fusion is to the native genome or through a separate entity such as a phagemid (Smith and Petrenko, 1997). The most

common systems focus on the major coat protein, p8 and minor coat protein, p3. The most abundant protein, p8, forms a flexible protein cylinder of 2700 20° tilted monomers that conceals the DNA. P3 forms five molecules at the end of the particle, consisting of 406 amino acids, of which the amino-terminal portion is involved in infection as an adsorption protein.

Phage display formats 3, 33, 8, and 88 are based on the natural phage genome (Figure 3.1). Display on pVI, pVII, and pIX have also been employed but are far less utilised (Simons et al., 1981, Loset et al., 2011, Kara et al., 2020). Initial formats include 3 or 8 vector display systems where the fusion protein is directly incorporated into the genome as single-stranded DNA. The resulting fused protein is found on all copies of the coat protein. Alternatively, 33 or 88 vector displays contain the wild-type phage gene 3 or 8 protein and recombinant gene 3 or 8 protein within the genome, leading to the simultaneous expression of both proteins on a phage particle (Parmley and Smith, 1988, Cwirla et al., 1990, Clackson et al., 1991, Swimmer et al., 1992). This is designed to ensure the viability of phage (Parmley and Smith, 1989), and, in the context of 33 systems where longer peptides and proteins can be expressed, there is significantly lower valency (Chang et al., 2020). These systems, albeit marked for their ease of use, are noted to have their drawbacks such as loss of infectivity in p3 fusion proteins, and affinity issues associated with polyvalent display. To address these drawbacks, 3+3 and 8+8 systems were designed (Breitling et al., 1991), whereby recombinant fusions are maintained on a 'phagemid', and helper phage, defective in origin replication, are employed for packaging and assembly, chromosome replication, and egress from host cells. In this system, the display is similar to 33 and 88 formats, whereby the phage harbours two copies of the p3 or p8 gene, both wild-type and recombinant. The phagemid commonly contains genes for antibiotic selection, coat protein, cloning sites for insertion of antibody fragments, and M13 origin of replication but lacks genes for complete functional phage. The presence of intact M13 replication origin, present in the phagemid but not the helper phage, results in preferential

packaging of phagemids over helper phage. Helper phage dependent 8+8 and 3+3 vector systems have individual benefits. 8+8 systems utilising the major capsid protein benefit from high valency and low-affinity ligand display. The display of peptides on gene 8 protein is known for applications in diagnostics and vaccine design (Liu et al., 2016) (Meola et al., 1995). In contrast, the 3+3 system offers monovalency due to expression of a singular copy of recombinant p3. Generally, p3 is more widely used for complex proteins over p8 due to steric hindrance. Low valency and dual expression of wild-type and recombinant proteins removes the avidity effect of the polyvalent display, thus enabling higher affinity selection (Lowman et al., 1991, Sidhu, 2001, Smith and Petrenko, 1997). The main benefit of this system is the ability to distinguish between modest and high affinity binders. This system is well known for its uses in antibody epitope selection (Kay et al., 1996, Scott and Smith, 1990) and expression of various antibody formats over the years (Smith and Petrenko, 1997, Winter et al., 1994, Hoogenboom et al., 1991, Dooley et al., 2003, Mandrup et al., 2013, Abraham et al., 1996).

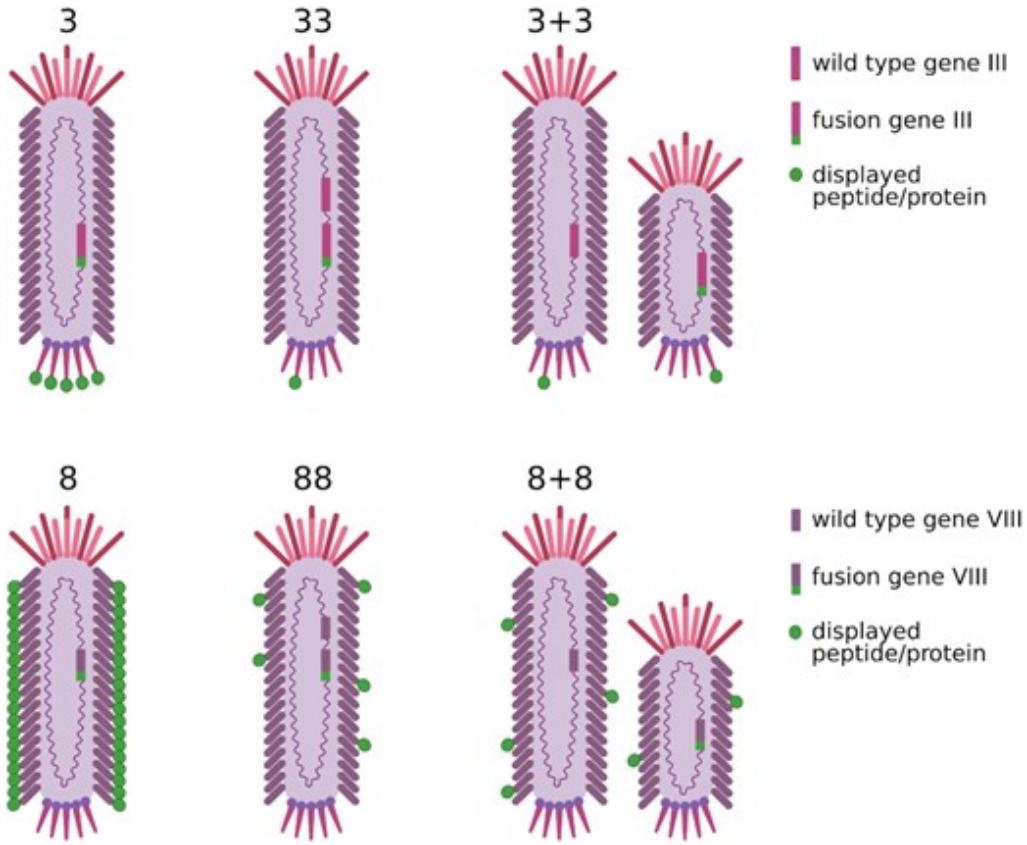

Figure 3.1: Phage formats proposed by George Smith. Minor coat protein p3 has three systems: 3 where the recombinant gene is fused to the genome resulting in expression of recombinant g3p only, 33 where the wild-type and recombinant gene 3 are fused to the genome resulting in both expressed, and 3+3 where the recombinant g3p is maintained separately from the wild-type phage genome. Major coat protein p8 has 3 systems: 8, 88, and 8+8, reflecting those of p3, yet expression is on the major coat protein. (Jaroszewicz et al., 2022).

Alternative formats of filamentous phage include the indirect display of p3 (for displaying cDNA), pVI, pVII and pIX display, landscape phages and selectively infective phage (SIP), which are described elsewhere (Jaroszewicz et al., 2022).

Phagemid vectors are widely used due to their high level of versatility. This system is often preferable over phage vector designs due to a high level of genetic stability, thus allowing for long stretches of exogenous DNA to be

expressed (Hoogenboom et al., 1991). Furthermore, these systems benefit from modifications and inducible promotor control. Perhaps the most popular modification is the addition of an amber-stop codon (TAG) between the fusion antibody gene and gene 3 on the phagemid. The resulting phagemid can be transformed into amber suppression strains or non-amber suppressor strains of *E. coli* for controlling the expression of soluble Fab (Valldorf et al., 2022). For instance, in suppressor strains, such as TG1, the stop codon is suppressed resulting in the expression of recombinant coat proteins. On the contrary, in non-suppressor strains like HB2151, the stop codon is translated resulting in the expression of antibody fragments unfused to the coat protein (Hoogenboom et al., 1991). In addition, phagemid vectors commonly possess a *Lac* operon for control of expression. A host cell expressing *Lac* I_q in combination with glucose as a catabolite repressor negatively regulates the translation of recombinant proteins to prevent the production of phage particles. The absence of glucose, and thus translation of the gene, results in the expression of recombinant clones that may have a growth advantage. This inducible control ensures library diversity (Diebolder and Krawczyk, 2018).

Library construction can be derived from natural sources or can be synthetically derived. Natural sources are subdivided into universal (naïve) libraries or immunised libraries. Universal libraries are derived from healthy unimmunised sources, whereas immune libraries typically come from immunised sources. For example, Marks et al*.* formulated a naïve, universal library of scFv from peripheral blood lymphocytes for two donors, discovering antibodies to haptens and autoantigen-specific antibodies (Marks et al., 1991). Universal libraries, however, do not experience affinity maturation, and thus often exhibit moderate affinity compared to those that are immunised. To circumvent this, semi-synthetic (Barbas et al., 1992), or synthetic libraries can be produced by processes that favour maturation affinity, for example, *in vitro*, or in-silico modelling (Raybould et al., 2019) which can be used to modify a peptide or protein of interest (Barderas et al., 2008). A semi-synthetic library generated by Nissim et al*.* encoding 50 VH

genes and random CDR3 inserts up to 36 base pairs, was altered to be fully synthetic (Griffiths et al., 1994), and utilised against a range of antigens (Nissim et al., 1994). Instead, immune libraries are usually generated from convalescent donors, however, immune libraries can be made hyperimmune from repeated immunisation and isolating variable regions to identify high affinity binding mAbs (Noy-Porat et al., 2020). Moreover, immunised libraries contain antibodies that have experienced affinity maturation and glycosylation by the immune system and therefore may have better biophysiological attributes in comparison to synthetically derived antibodies which are more likely to have self, or poly reactivity (Spencer et al., 2012, Kaleli et al., 2019).

A variety of antibody formats, such as Fab, scFv, Fragment variable (Fv), and single domain Antibody (sdAb), can be displayed (Sellmann et al., 2020, de Haard et al., 1999, Solemani Zadeh et al., 2019). For scFv, variable heavy and light chain regions are fused with a peptide linker fused to g3p (Crameri and Suter, 1993). Despite the majority of scFv forming monomers, dimers and trimers have been recorded to form, interfering with selection (Griffiths et al., 1993). Alternatives such as Fv, or sdAb, are optimal systems for antibodies that do not have light chains, such as VHH camelid antibodies. On the other hand, Fab fragments consisting of variable regions of light chain and heavy chain with constant domain CH1, are fused to g3p by either the heavy or light chain. Fab fusions have less of a tendency to dimerise (Griffiths and Duncan, 1998) and are thought to be more stable. The first phage displayed antibody library was constructed by McCafferty *et al.* 1990 (McCafferty et al., 1990), displaying the variable regions of anti-lysozyme antibody on p3 using an fd-tet vector. Antibody phage display was also independently discovered by Breitling and Dübel (Breitling et al., 1991) and Lerner and Barbas (Barbas et al., 1991).

Due to conservation within variable domains, species-specific consensus sequences have been used for the design of PCR primers, thus enabling the preparation of immune, non-immune and synthetic antibody repertoires

genes by PCR (McCafferty and Johnson, 1996). The construction of Fab libraries can be conducted in a variety of ways. One approach is sequential antibody chain cloning (Kugler et al., 2015) to add in heavy and light chain repertoires. Alternatively, heavy and light chain repertoires can be added concurrently using type two restriction enzymes (Nelson and Valadon, 2017). Another technique uses overlap extension PCR to generate splicing events (Davies et al., 1995), commonly used for the generation of scFv libraries (Jaroszewicz et al., 2022).

In this study, the design was selected to accommodate a bovine immune ultralong Fab library for isolation of high affinity binders to SARS-CoV-2 Lineage A trimer. The antibody format was selected based on studies that support the expression of a light chain in combination with a heavy chain library for optimal binding of antigen. This appears to be important in the bovine repertoire, with multiple sources stating the use of lambda light chain germlines V30 and V47, suspected to contain structural features that optimise ultralong heavy chain binding (Arun et al., 1996, Pasman et al., 2010, Saini et al., 2003, Ramirez Valdez et al., 2023). A format of 3+3 was decided as optimal for selecting high affinity binders from monovalent display.

3.3. Aim of Chapter

The work described in this chapter aimed to develop and optimise a phagemid phage display system to represent bovine ultralong Fab antibodies, from a source of bulk sort B-cells raised against multiple SARS-CoV-2 Lineage A antigen immunisations, on p3 of M13 bacteriophage. This study maximised the discovery of high affinity antibodies by repeated immunisations, resulting in hyperimmune sources. Validation of immune repertoire representation was achieved using NGS to ensure bias was limited through the process. A control HIV phage was generated for the purpose of optimising the process and validating the biopanning.

3.4. Results

3.4.1. Development of the control phage

3.4.1.1. Isolation of ultralong heavy and light chain from NC Cow 1.

A positive control, subsequently termed HIV phage, was prepared prior to the construction of the bovine ultralong library. This control phage was intended for validating biopanning following the successful construction of the bovine ultralong libraries. Plasmids designed by Professor Jonathan Ball, containing a bovine antibody light and ultralong heavy chain sequences to an epitope of HIV published by Sok et al. (Sok et al., 2017), were used to PCR amplify the heavy and light chains (Figure 3.2). The heavy chain was amplified using an IgHV1-7 germline-specific forward primer, codon optimised, and a reverse primer that would generate 15 base pair homology arms for seamless cloning into the phagemid at the B*mt*I restriction site using InFusion cloning. As expected, the resulting product was approximately 550 base pairs. Following sequencing, the band present at 200 base pairs in the heavy chain amplification was suspected to be primer dimer products whereby nonspecific annealing and primer elongation events occurred during amplification. The light chain was amplified by primers that generated a product with homology arms for cloning into the phagemid at the P*st*I restriction site. This product, as expected, yielded a band of around 390 base pairs.

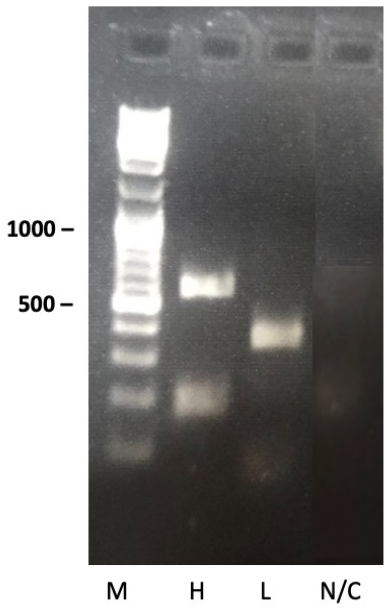

Figure 3.2: Amplification of ultralong heavy and light chains from plasmids harbouring a HIV antibody. Lane 1: 10 Kb DNA Marker (M), Lane 2: Ultralong heavy chain at approximately 550 base pairs (H), Lane 3: Light chain at approximately 380 base pairs (L), Lane 4: negative control (N/C).

3.4.1.2. Cloning of HIV Fab into the phagemid vector

Ultralong bovine heavy chains are frequently paired with a minimally mutated light chain. This enabled the use of the HIV light chain as a constant for library heavy chain shuffling (sequential chain insertion). InFusion cloning technology enables cloning of multiple fragments into a vector in one reaction, however, as the light chain was common for the library this enabled the production of a new phagemid containing the common light chain, ready for insertion of a heavy chain library. The light chain was cloned into the P*st*I restriction site of the phagemid and transformed into 5-alpha F'I*q* Competent *E. coli.* Expression in this cell type allows for high transformation efficiency for toxic gene cloning and enables catabolite repression by glucose as it possesses *Lac* Iq, therefore, expression of the phagemid can be regulated with the presence or absence of glucose. Following the transformation of the light chain, 16 clones were

screened for positive colonies using M13 F and R primers (Figure 3.3A). Colonies 13 and 14 were positive, shown by a band at the desired product size of around 2,500 base pairs. The negative colonies, 1-8 (data not shown), 9-12 and 15 and 16, contained M13 F and R sites and therefore produced a band, however, band size was around 380 base pairs smaller than the positive colonies containing the light chain. Following sequencing, colony 14 yielded the desired sequence, thus the phagemid, PFAB3 L.14, was purified and used for subsequent cloning of the control heavy chain. PFAB3 L.14 was digested using B*mt*I restriction enzyme and the control ultralong heavy chain ligated and transformed. Figure 3.3B presents the colony screen from this experiment. Colonies 1, 2, 4, 5, 7 and 8 did not contain the heavy chain but contained the light chain, producing a band at 2,500 base pairs, whereas colony 3 did not contain either heavy or light chains, producing a band smaller than the other colonies at 2,000 base pairs. Colony 6, the only positive colony, was 500 base pairs larger than colonies 1, 2, 4, 5, 7 and 8, and 880 base pairs larger than colony 3, producing a band around 3,000 base pairs. Sequencing of colony 6 confirmed that it contained the control heavy chain insert.

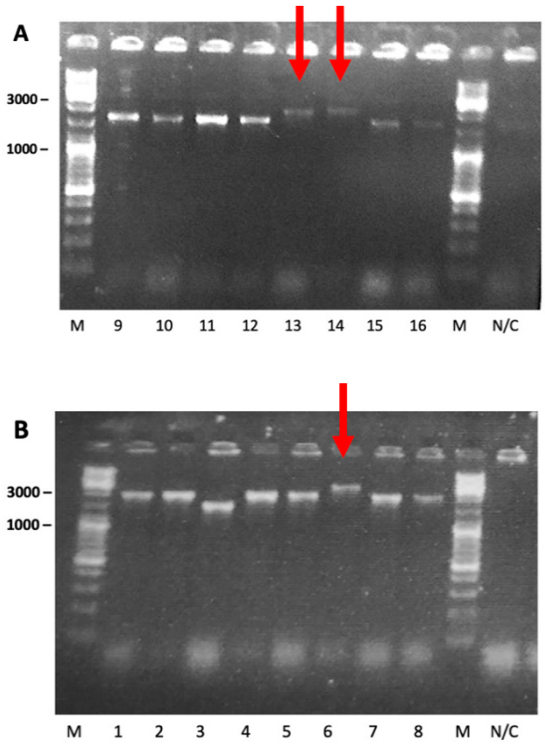

Figure 3.3: PCR colony screen of *E. coli* cells for phagemid ligation of light and heavy antibody chains. A) Lanes 9-12, 15, and 16 negative colonies that did not contain the light chain. Lanes 13 and 14 were positive for light chain ligation into the phagemid (red arrow). B) Lanes 1, 2, 4, 5, 7, and 8 contained the light chain only. Lane 3 did not contain heavy or light chains. Lane 6 was positive for heavy chain ligation (red arrow) into PFAB3 L.14. M = 10 Kb DNA molecular marker, N/C = negative control.

3.4.1.3. Optimising the phage rescue protocol

Developing an effective library requires the optimisation of phage rescue protocol to obtain maximum phage yields. To avoid bias, transformed cells harbouring phagemids were grown on 25x25 cm^2 square culture plates with selective media. Although not a prerequisite for phage display, solid media is thought to reduce competition experienced by liquid cultures. Generally, cells expressing exported products grow at an optimal temperature of 30°C and so this temperature was maintained through the rescue process, except during

coinfection with helper phage where infection occurs optimally at 37°C (McCafferty and Johnson, 1996). Prior to infection, transformed cells were grown to mid-log phase for expression of F pilus. This assured all *E. coli* can be infected with helper phage. To ascertain mid-log phase was achieved, the optical density was measured at 600 nm following 2-2.5 hours of incubation at 30°C. An OD_{600} nm of between 0.4-0.6 was deemed as mid-log phase (Nilsson et al., 2000). To produce infectious phage particles bearing the fusion protein, a ratio was calculated between bacterial cells and helper phage based on the Multiplicity of Infection (MOI). Initial studies by McCafferty et al. (McCafferty and Johnson, 1996) suggested a ratio of 1:1 of helper phage to bacteria, however, the more recent studies of Diebolder and Krawczyk (Diebolder and Krawczyk, 2018) recommend an MOI of 20:1. As higher levels of helper phage have been recorded to break, or release, F pili from *E. coli* (O'Callaghan et al., 1973), the ratio was optimised (Figure 3.4). A ratio of 10:1 bacterium to helper phage obtained a mean yield of 5×10^9 cfu/mL whereas an excess of helper phage (1:2 bacteria to helper phage) obtained a higher mean titre of 5.98×10^{12} cfu/mL. A 1:1 ratio obtained a mean titre of 1.95×10^{13} cfu/mL. To achieve maximum yields, a slight excess of helper phage was used (1:1.25 bacteria: helper phage).

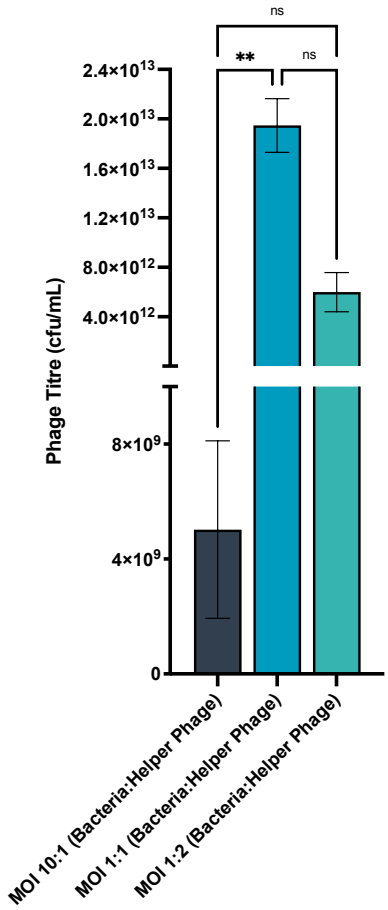

Figure 3.4: Optimisation of MOI of bacteria to helper phage ratio. Bars represent ratios 10:1, 1:1, 1:2 of bacteria to helper phage, recorded as phage titre cfu/mL. 10:1 bacterium to helper phage yielded a mean titre of 5 x 10^9 cfu/mL whereas an excess of helper phage. 2:1 bacterium to helper phage obtained a mean yield of 5.98 x 10^{12} cfu/mL. 1:1 bacterium to helper phage obtained a mean titre of 1.95 x 10^{13} cfu/mL. Statistical significance determined by Kruskal Wallis test with Dunn's multiple comparisons test. N=7. P = < 0.01. Error bars represent standard deviation.

3.4.1.4. Validating bovine ultralong Fab phage expression

To confirm that phage display on g3p could support the expression of ultralong bovine antibodies, the HIV phage was produced through the optimised phage rescue protocol. To ascertain the expression of Fab on phage particles, a western blot was performed detecting the coat proteins of M13

with an anti FD antibody (Figure 3.5). Protein expression of the HIV phage was compared to a recombinant g3p phage targeting ficolin, gifted by Dr. Alexander Tarr. The proteins were reduced, thus a band consisting of heavy chain fused to a truncated g3p was expected to form at approximately 40 kDa (Appendix I). As previously described, the phagemid system expresses wild-type and recombinant g3p simultaneously. In this system, the expression of wild-type g3p expression safeguards the infectivity of the phage (Bratkovic, 2010). Contrary to the recombinant g3p which is truncated, wild-type g3p was at full size, at around 55 kDa. In Figure 3.5, a band can be observed around 40 kDa in the HIV Phage as recombinant g3p and a fainter band at 55 KDa, inferred as wild type g3p. The control phage has an intense band at 55 kDa

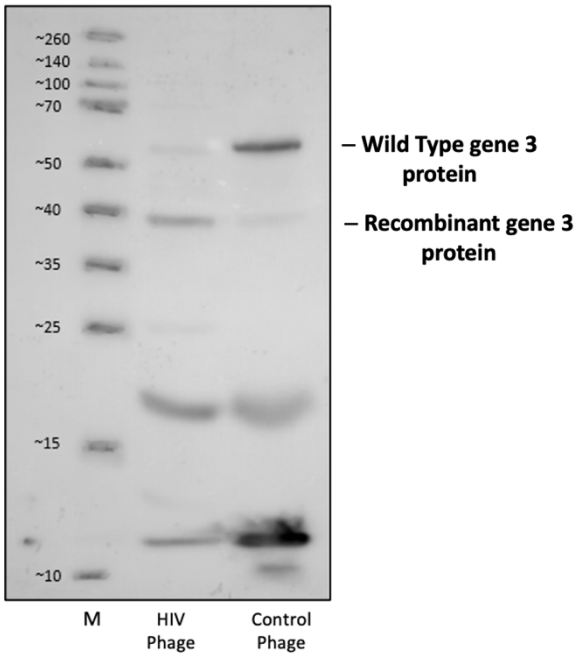

Figure 3.5: Anti -Fd reduced protein expression of HIV phage and Ficolin control phage. HIV phage (Lane 2) and Ficolin control phage (Lane 3) was analysed by western blot under reducing conditions using an anti-Fd antibody. Band at 55 kDa inferred as Wild-type (WT) g3p, and band at 40 kDa as recombinant g3p (heavy chain fused to truncated g3p) Other bands present at 12 and 20 kDa are reduced products expressed by the phage and detected by Anti-FD.

and a fainter band at 39 kDa. Other bands observed in Figure 3.5 at 12 and 20 kDa are reduced products expressed on the coat of the phage and detected by Anti-FD.

Having confirmed the expression of gene 3 proteins through the phage rescue protocol, it was necessary to confirm that the HIV phage was expressing recombinant gene 3 protein, thus displaying the HIV Fab. This was achieved by confirming the HIV phage activity to HIV protein gp140 in an ELISA.

To identify binding, a bait of gp140 (lacking transmembrane domain compared to gp120) was used (Figure 3.6), in accordance with various controls. The binding of the HIV Phage to gp140 was significant ($p = <0.0001$) compared to the negative control phage, previously used in Figure 3.5. The HIV phage and negative control phage yielded a mean OD_{405} nm of 2.4 and 0.2, respectively. Three controls validated the assay, removing a layer of the ELISA to ensure binding was not due to non-specific binding to the elements of the assay. The lower part of Figure 3.6 indicates what layers were removed for the controls. The HIV Phage showed high levels of binding to the uncoated wells, reaching a mean OD_{405} nm of 3.1, suggesting that the HIV phage was binding non-specifically to the plastic of the plate. Phage particles are notoriously sticky, with non-specific binding recorded to various components of screening systems such as the solid phase, capture reagents and blocking agents (Vodnik et al., 2011). Navigating around false positives is a requirement for producing an effective screen of phage with true affinity to the target. To ensure that the binding observed of the HIV phage to gp140 in Figure 3.6 was true and not due to non-specific binding of uncoated plastic, a

trial of blocking agents in combination with the HIV phage were tested (data not shown). A blocking agent of 2% BSA in PBS reduced background non-specific binding to below 0.2 at a mean OD_{405} nm, thus was used as the blocking agent for subsequent phage ELISAs.

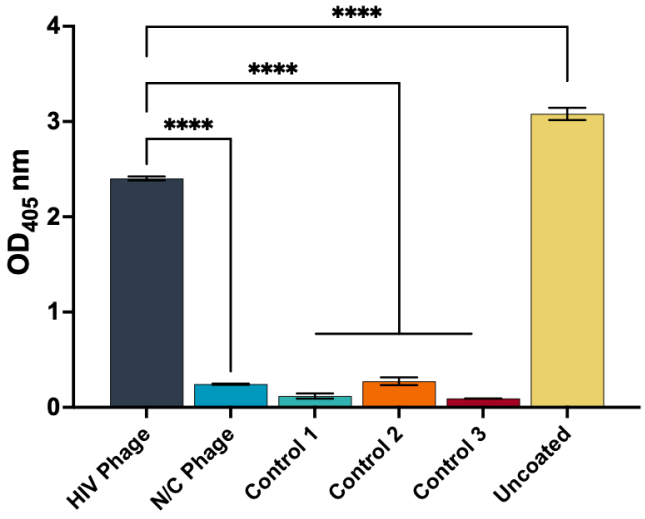

	gp140	Phage	Anti FD
HIV Phage	+	+	+
N/C phage	+	+	+
Control 1	+	-	-
Control 2	+	-	+
Control 3	+	+	-
Uncoated	-	+	+

Figure 3.6: ELISA to determine the binding of the HIV phage to HIV protein gp140, measured in OD_{405} nm. The HIV phage bound to gp140 at a mean OD_{405} nm of 2.4. The negative control phage (N/C phage) showed low binding to gp140 with a mean OD_{405} nm of 0.2. Controls were trialled to assess the ELISA design, none showed significant binding to gp140 compared to the HIV phage. The HIV phage bound to uncoated wells at a mean OD_{405} nm of 3.1. Statistical significance by One way ANOVA with Tukey's multiple comparisons, N=2, p = <0.0001. Error bars demark standard deviation.

In order to verify binding was specific to the HIV glycoprotein, two ELISAs were performed (Figures 3.7A and B). The HIV phage was tested for binding against the HIV glycoprotein trimer, gp120. The HIV phage showed strong binding to gp140 and gp120, with mean OD_{405} nm values of 1.78 and 2.5, respectively (Figure 3.7A). Binding was significant ($p = <0.05$) to gp120 over gp140. This was expected as the HIV Fab displayed on the phage was raised against the HIV trimer. To determine that this binding was glycoprotein specific, the HIV phage was tested for binding against an irrelevant glycoprotein, SARS-CoV-2 Lineage A trimer. Despite showing some binding to SARS-CoV-2 Lineage A trimer (mean OD_{405} nm of 1.1), the HIV phage showed significant binding ($p = <0.05$) to gp120 (mean OD_{405} nm of 1.7) (Figure 3.7B). However, due to the 'stickiness' of the control phage to SARS-CoV-2 Lineage A trimer, it could not be used as intended as a negative control in the biopanning. A positive control of a characterised SARS-CoV-2 specific Fab phage showed significant binding (mean OD_{405} nm of 2.8) to SARS-CoV-2 Lineage A trimer ($p = <0.0001$) in comparison to the HIV phage (mean OD_{405} nm of 1.1). The detection antibody was altered to an Anti M13 gene 8 major coat protein to reduce background noise in the assay. Four controls validated the assay, removing a layer of the ELISA to ensure binding was not due to non-specific binding to the new element of the assay. The lower part of Figure 3.7B indicates what layers were removed for the controls.

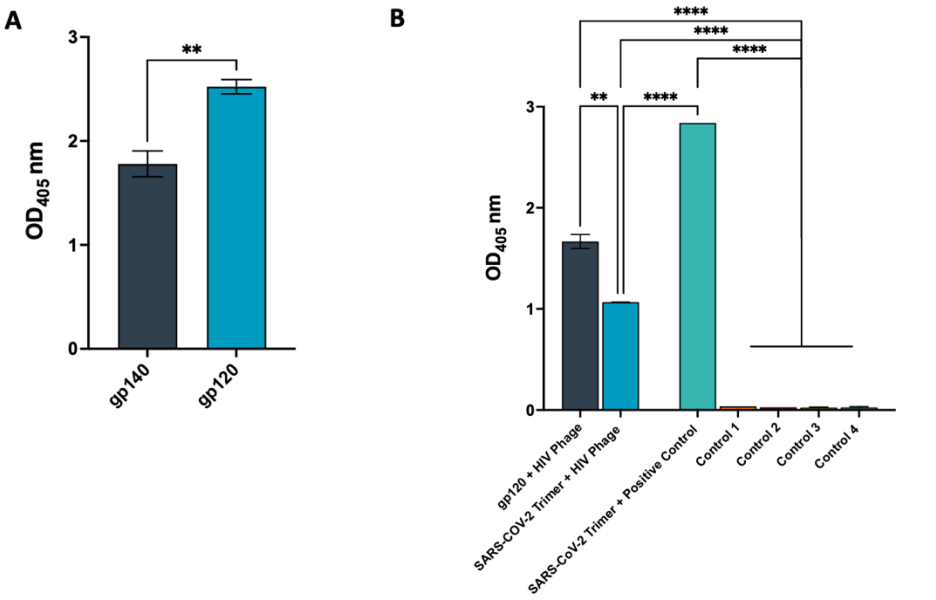

	gp120	SARS-CoV-2 Trimer	Phage	Anti g8p
Control 1	+	-	-	+
Control 2	-	+	-	+
Control 3	+	-	+	-
Control 4	-	+	+	-

Figure 3.7: HIV phage binding was specific to HIV proteins compared to SARS-CoV-2 Lineage A trimer. A) HIV phage bound to gp140 at a mean OD_{405} nm value of 1.78, and gp120 at 2.5. Statistical significance by Unpaired T test, N=2, p = <0.05. B) HIV phage bound to gp120 at a mean OD_{405} nm value of 1.7 compared to SARS-CoV-2 Lineage A trimer at 1.1. A positive control showed strong binding to SARS-CoV-2 Lineage A trimer at a mean OD_{405} nm value of 2.8 compared to the HIV phage which bound at a mean OD_{405} nm value of 1.1. Controls were trialled to assess the ELISA design, none showed significant binding to gp120 compared the HIV phage, the HIV phage to SARS-CoV-2 Lineage a trimer or SARS-CoV-2 Lineage A trimer when compared the positive control. Statistical significance by One way ANOVA with Tukey's multiple comparisons, N = 2, ** p = <0.05, **** p > 0.0001. Error bars demark standard deviation.

3.4.2. Construction and validation of the bovine ultralong Fab library

3.4.2.1. Construction of libraries in 5-alpha F'Iq E. coli chemically competent cells

Following the establishment of the HIV phage control, the construction began of bovine ultralong Fab libraries from two bovine (C13 and C18) bulk sort B-cells raised against multiple SARS-CoV-2 Lineage A antigen immunisations (previously described in Chapter 2, section 2.1). This was done by RNA isolation and cDNA synthesis of the bulk sorted cells. The light chain phagemid, PFAB3 L.14 was digested at the B*mt*I restriction site and analysed

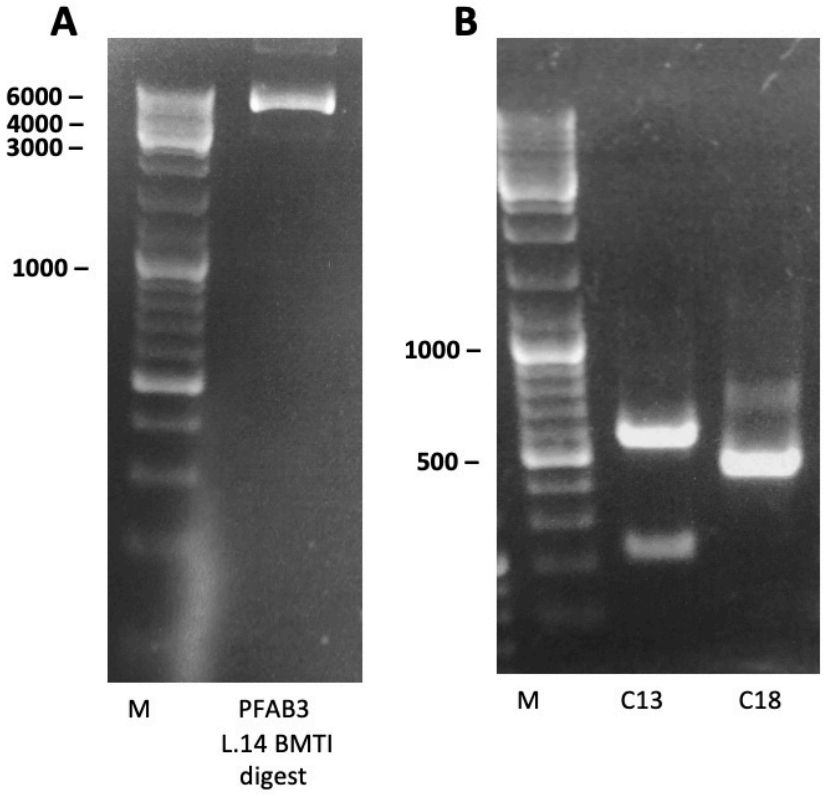

Figure 3.8: Digestion of PFAB3 L.14 and amplification of ultralong antibody heavy chains from C13 and C18. A) Lane 1: marker, Lane 2: digested PFAB3 L.14 band at 6,000 base pairs B) Lane 1: marker, Lane 2: C13 band between 500 and 600 base pairs, Lane 3: C18 band between 400-500 base pairs, band at 800 base pairs suspected to be non-specific. M = 10 Kb DNA molecular marker.

by gel electrophoresis (Figure 3.8A). A bright band was observed at 6000 base pairs confirming digestion of the phagemid.

Heavy chains from C13 and C18 cDNA were PCR amplified with germline-specific VH1-7F and IgHRev4 primers. This generated a thick band between 500-600 base pairs for C13 and a thick band between 400-500 base pairs for C18 (Figure 3.8B). Band thickness and intensity indicate the presence of multiple heavy chains of similar sizes which clustered during electrophoresis. The band present at 200 base pairs in C13 was suspected to be primer dimers whereby nonspecific annealing and primer elongation events have occurred during amplification. The band present at 800 base pairs in C18 is suspected to be non-specific.

4,200 B-cells were obtained from C13 and 4,000 B-cells from C18, of which 10-15% are likely to be ultralong. Using this percentage, approximately 630 sequences were required to represent C13 and 600 for C18. With a transformation efficiency of 1-3 x 10^9 cfu/μg DNA, 5-alpha F'Iq *E. coli* 5-alpha F'Iq *E. coli* were deemed adequate for transforming the library for source representation. A cloning experiment was designed with a molecular ratio that could accommodate for multiple single inserts. A trial 2.5 μL ligation was transformed, and colonies were screened for heavy chains using germline specific VH1-7F and IgHRev4 primers. Cloning of the HIV heavy chain was performed simultaneously during this trial as a control. All clones were positive for heavy chains, forming bands around 500 base pairs (Figure 3.9A). Variations within band sizes around 500 base pairs implied the presence of heavy chains with varying CDHR3 lengths. For example, C13 colony 6 band appears lower than the other bands and lower than 500 base pairs therefore likely to carry a shorter heavy chain. The cloning reaction was scaled to 10 μL in an attempt to ensure all sequences had an equal chance of ligating into the vector. Figure 3.9B shows the colony screen of the larger cloning experiment, with all colonies containing a heavy chain. Similar to the small-scale experiment, there was variation between band sizes. Both experiments show that band sizes are generally smaller for C18, below 500 base pairs, compared

to C13, in which most bands were above 500 base pairs, except for C13 colony 6 in the 2.5 μL cloning reaction (Figure 3.9A). However, increasing ligation reaction size had little to no impact on cloning efficiency, with 2.5 μl reaction obtaining 1.3 x 10^5 and 2 x 10^5 for C13 and C18, respectively,

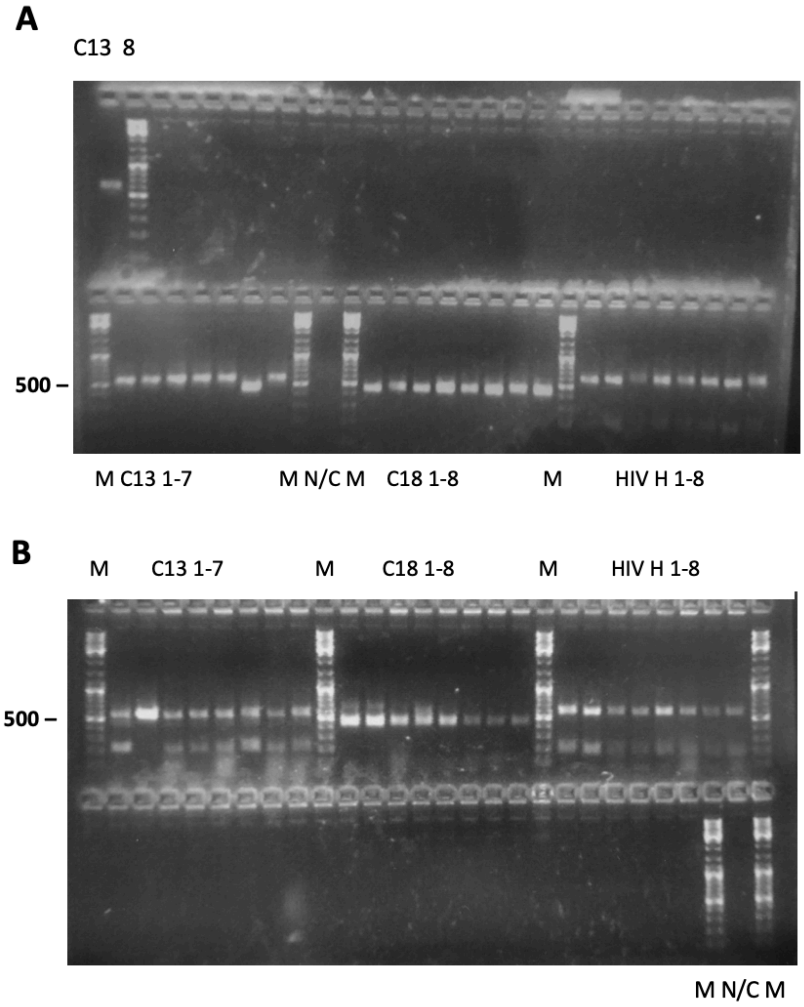

Figure 3.9: Colony PCR screen of trial heavy chain library transformations into 5-alpha F'Iq *E. coli* cells. A) Heavy chain colony screen of 2.5 μL cloning reaction, and B) Heavy chain colony screen of 10 μL cloning reaction. Both reactions show eight colonies positive for heavy chains from C13, ranging from 500 to 550 base pairs, and eight colonies positive for heavy chains from C18, all around 490 base pairs. B) The HIV heavy chain was cloned simultaneously, all eight colonies are positive with the HIV heavy chain around 550 base pairs. A+B) M = 10 Kb DNA molecular marker, N/C = negative control.

compared to 10 µl reaction obtaining 1.37 x 10^5 and 1.24 x 10^5 for C13 and C18, respectively.

3.4.2.2. Validation of expression and specificity of 5-alpha F'Iq E. coli libraries

Phage particles were rescued and titred, and the libraries were validated by western blot. The HIV phage was run as a comparison. Figure 3.10 shows a similar pattern to Figure 3.5, whereby libraries C13 and C18 present bands of around 40 kDa as recombinant g3p, and the thick band at 55 kDa as wild type g3p. Other bands observed in Figure 3.10 at 12 and 20 kDa are reduced products expressed by the phage and detected by Anti-FD.

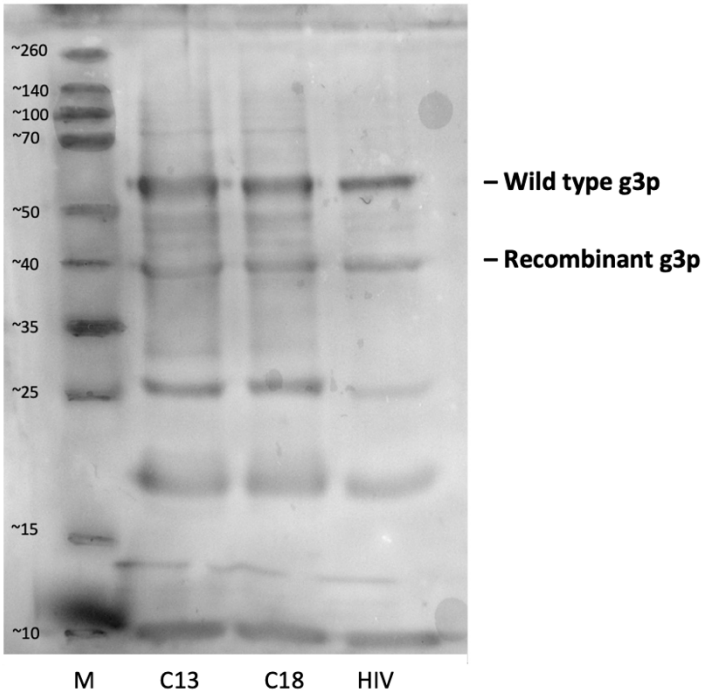

Figure 3.10: Anti -FD reduced protein expression of C13 and C18 phage libraries, and HIV control phage. The phage libraries (Lane 2: C13, Lane 3: C18) and HIV phage (Lane 4) were analysed by western blot under reducing conditions using an anti Fd antibody. Band at 55 kDa inferred as wild-type (WT) g3p. Bands around 40 kDa inferred as recombinant g3p (heavy chain fused to truncated g3p). Other bands present at 12 and 20 kDa are reduced products expressed by the phage and detected by Anti-FD. The molecular marker (Lane 1: M) shown in kDa.

After confirming the expression of the libraries, the reactivity to the target was tested. This was achieved by performing an ELISA. This was similar to the ELISA performed for the HIV phage but changed the target to the SARS-CoV-2 Lineage A trimer. Immobilisation of the target protein using capture proteins is commonly used for phage biopanning. To explore this, the phage ELISA was altered to neutravidin capture of the target, biotinylated SARS-CoV-2 Lineage A trimer. Five controls validated the assay, removing a layer of the ELISA to ensure binding was not due to non-specific binding to the elements of the assay. Figure 3.11A shows C13 library exhibiting high binding to wells coated with both capture and target protein, at a mean OD_{405} nm of 2.8, but also to wells containing capture proteins only, at a mean OD_{405} nm of 1.3. This trend was exaggerated in C18 library where wells of neutravidin only showed a similar level of binding to the wells containing capture and target protein. The wells containing capture and target protein reached a mean OD_{405} nm of 2.6, which was not significantly different to wells only containing the capture protein at a mean OD_{405} nm of 2.5. Therefore, the binding that was observed in Figure 3.11A could not be confirmed to be specific to SARS-CoV-2 Lineage A trimer. To circumvent this, a direct coat of SARS-CoV-2 trimer at a high concentration was tested in an attempt to fully saturate the wells with the target protein. Since the blocking buffer had been optimised, the binding observed was predicted to be specific to SARS-CoV-2 trimer. A caveat of this is the possibility that the well may not be fully saturated and thus some of the binding observed may be from non-specific binding to the plastic. Figure 3.11B shows binding of C13 library to a high concentration of SARS-CoV-2 Lineage A trimer at a mean OD_{405} nm of 2.5, and C18 library at a mean OD_{405} nm of 2.9, which were both significant ($p = <0.05$) when compared to an irrelevant phage.

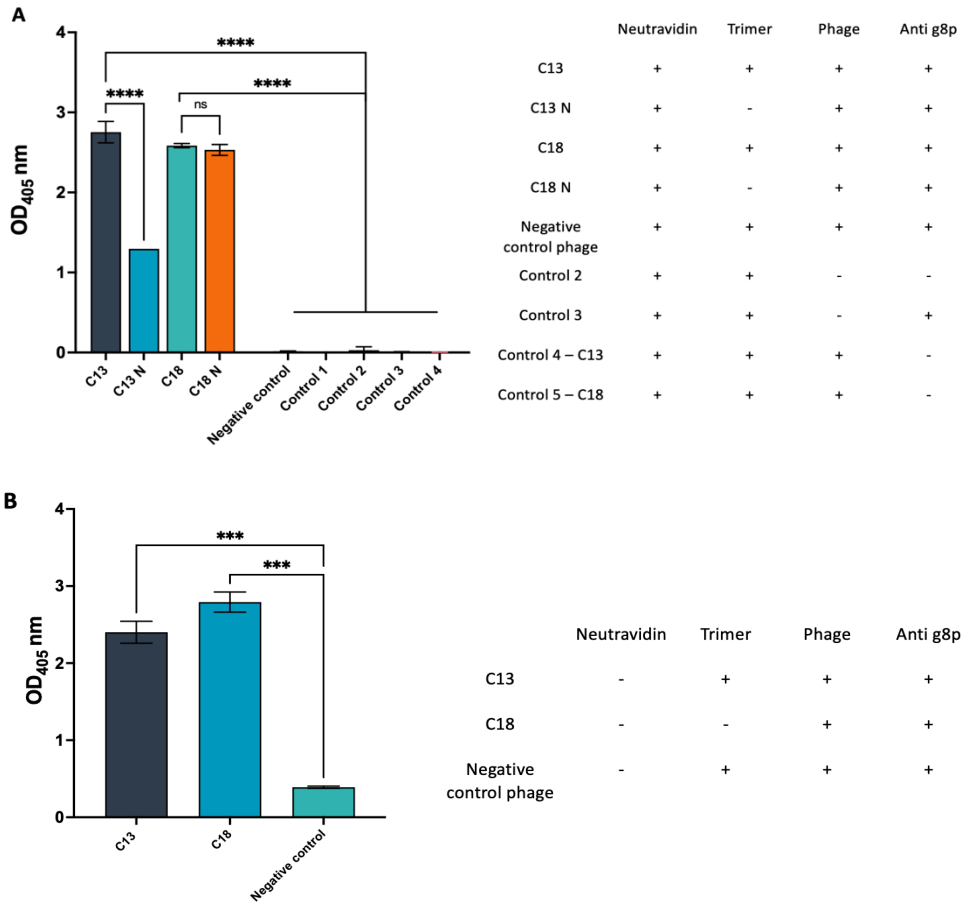

Figure 3.11: Phage ELISA of each phage library binding to target protein as captured or direct coating, measure as OD_{405} nm. A) C13 phage library binding to neutravidin captured biotinylated SARS-CoV-2 Lineage A trimer compared to C13 phage library binding to neutravidin only. C18 phage library binding to neutravidin captured biotinylated SARS-CoV-2 Lineage A trimer compared to C18 phage library binding to neutravidin only. Table to the right demarks assay design. Controls were trialled to assess the ELISA design, none showed significant binding to neutravidin captured biotinylated SARS-CoV-2 Lineage A trimer compared to the phage libraries or SARS-CoV-2 Lineage A trimer compared to the libraries. Statistical significance by One way ANOVA with Tukey's multiple comparisons, N=2, p = <0.0001. Error bars demark standard deviation. B) C13 and C18 phage Library binding to a high concentration of directly coated SARS-CoV-2 Lineage A trimer compared to a phage that was known to not exhibit binding to SARS-CoV-2 Lineage A trimer. Statistical significance by One way ANOVA with Dunnett's multiple comparisons, N=2, p = <0.05. Error bars demark standard deviation.

3.4.2.3. Investigating library heavy chain representation

To further this work, individual clones were rescued and sequenced to assess the diversity and representation of heavy chains in the phage libraries. A high proportion of sequenced clones showed the presence of phagemids lacking heavy chains (data not shown). A high number of colonies from transforming the digested phagemid confirmed incomplete digestion (data not shown) and so to overcome this, primers were designed to PCR linearise the phagemid vector at the B*mt*I restriction site. Removal of the template following linearisation, and use of this product in future cloning experiments was predicted to result in the transformation of clones that only had a ligated insert into the vector. The libraries were re-constructed using the linearised vector.

New colony screening primers were designed to determine whether the linearisation had been successful. These primers flanked the B*mt*I restriction site therefore would produce bands of two different sizes depending on whether the insert was successfully ligated into the vector. Phagemid vectors containing a heavy chain were expected to produce a band between 800 and 1000 base pairs, whereas vectors without a heavy chain would generate a band of around 400 base pairs. In Figure 3.12, C13 colonies 1, 2, 3, 5-8 and 10 all contain a heavy chain insert with bands around 800 base pairs. Colony 4 failed to amplify. To note, colonies 1 and 10 appear slightly lower in size compared to the other positive colonies and therefore likely carried a smaller heavy chain. Colony 9 showed the presence of a clone lacking a heavy chain, forming a band around 400 base pairs. The colony screen from library C18 showed that all nine colonies carried a heavy chain, as shown by a band around 800 base pairs. The above aimed to remove any light chain only clones during the cloning, however, the presence of colony 9 indicated that this method could not fully prevent this, therefore these phagemids were likely to be carried through the phage rescue. This was confirmed by a colony screen

following the rescue and subsequent titre of phage libraries whereby one out of eight screened clones was absent for a heavy chain (data not shown).

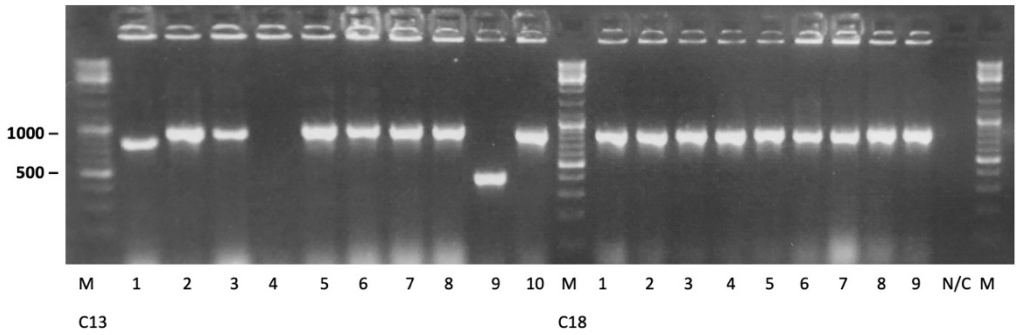

Figure 3.12: Colony PCR Screen of colonies of the libraries generated by linearising the vector and amplification using new primers PFAB3 COL F and PFAB3 COL R. A) C13 library colony screen of colonies 1-10. Bands at 800 base pairs or above contain a heavy chain. Bands around 400 base pairs did not contain a heavy chain. B) C18 library colony screen of colonies 1-9. All colonies were positive with bands showing at approximately 800 base pairs. A+B) M = 10 Kb DNA molecular marker, N/C = negative control.

3.4.2.4. Validation of library clones by phage ELISA and western blot

After confirmation that most clones carried a heavy chain insert, a selection of phage clones were individually rescued and a phage ELISA was performed against SARS-CoV-2 Lineage A trimer. Binding was compared to a phagemid lacking a heavy chain insert; therefore, the binding significance could be attributed to the heavy chain. Out of the nine clones from library C13, five showed significant binding when compared to a light chain only phage (***p= <0.001, ****p= <0.0001). Of the five clones, C13.2, C13.3, C13.6 and C13.7 showed the highest binding, ranging mean OD_{405} nm values of 2-2.3. Generally binding to SARS-CoV-2 Lineage A trimer for C18 library clones was lower, yet four clones showed significant binding (* p= <0.05, ***p= <0.001, ****p= <0.0001) compared to a light chain only phage, with mean OD_{405} nm values ranging 0.35-0.56 (Figure 3.13A). A subsequent phage ELISA was performed, comparing the binding of the four highest binders from C13 to

SARS-CoV-2 Lineage A trimer and an irrelevant glycoprotein, HIV gp120. Binding was significant to SARS-CoV-2 Lineage A trimer compared to gp120 for phage clones C13.2, C13.3, C13.6 and C13.7 (****p= <0.0001). For example, the mean OD_{405} nm values for C13.2 phage to SARS-CoV-2 Lineage A trimer was 1.9 compared to 0.49 for gp120 (Figure 3.13B), establishing that the binding was specific to the SARS-CoV-2 Lineage A trimer glycoprotein.

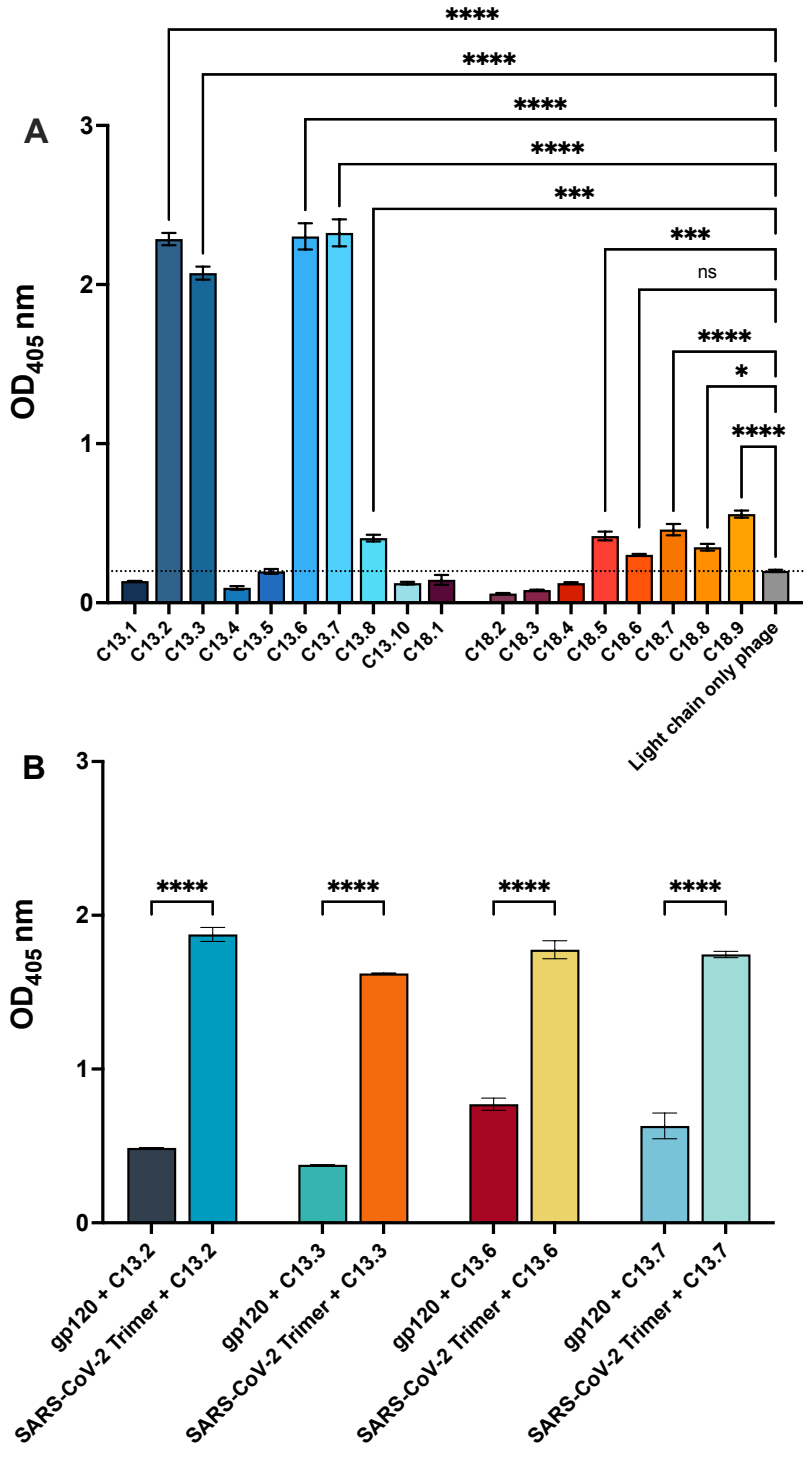

Figure 3.13: ELISA to determine the binding of C13 and C18 library to SARS-CoV-2 Lineage A trimer, measured as OD_{405} nm. A) Phage ELISA to show binding of 18 clones, nine from C13 and nine from C18, to SARS-CoV-2 Lineage A Trimer, compared to background binding of a light chain only phage. Dotted line represents background binding at a mean OD_{405} nm of 0.2. Nine clones showed greater binding to the target compared to the light chain only phage. Statistical significance in binding by One Way ANOVA, and Dunnett's multiple comparisons test to background binding, N=2, p = <0.05. B) C13.2, C13.3, C13.6 and C13.7 showed strong binding to SARS-CoV-2 Lineage A trimer with mean OD_{405} nm values of between 1.6-1.8 compared to the binding of gp120 where mean OD_{405} nm values ranged between 0.4 and 0.7 to the HIV phage. Binding to SARS-CoV-2 trimer was statistically significant compared to gp120 for the four phage clones. Statistical significance by One way ANOVA with Tukey's multiple comparisons, N=2, * p= <0.05, ***p= <0.001, ****p= <0.0001. Error bars demark standard deviation.

Expression of the libraries, and C13.2 and C13.7 phage clones of interest were validated by detecting coat proteins (Figure 3.14A) and g3p (Figure 3.14B) using western blot to ensure individual clone and library expression. In Figure 3.14A, a similar pattern to previous anti FD western blots (Figures 3.5 and 3.10) was observed, whereby the intense band at 55 kDa was inferred as a wild-type g3p, and bands between 40 and 50 kDa inferred as heavy chain fused to truncated g3p. Library bands were thicker than C13.2 phage and C13.7 phage as expected for multiple bands of varying heavy chain lengths The helper phage M13KO7 was run as a control alongside to compare g3p expression. A similar banding pattern can be seen in the wild-type control (M13KO7) compared to libraries, HIV phage and C13.2 and C13.7 phage clones. Other bands observed in Figure 3.14A at 12 and 20 kDa are reduced products expressed by the phage and detected by anti Fd. To confirm that this band was g3p and not a different coat protein, Figure 3.14B shows a second western blot, detecting g3p, whereby the same band at 55 kDa confirmed

that this band was wild type g3p. Library, C13.2 and C13.7 phage bands appear fainter, around 40 to 50 kDa. The wild-type M13 g3p was not detected in the g3p western blot (data not shown), this was due to low signal which is why the band appeared fainter in the anti FD western blot (Figure 3.14A). This was similar for the HIV phage which showed a reduced signal in both blots. Other bands observed in Figure 3.14B are likely to be fragments of g3p or fragments of gene 3 fused to heavy chain.

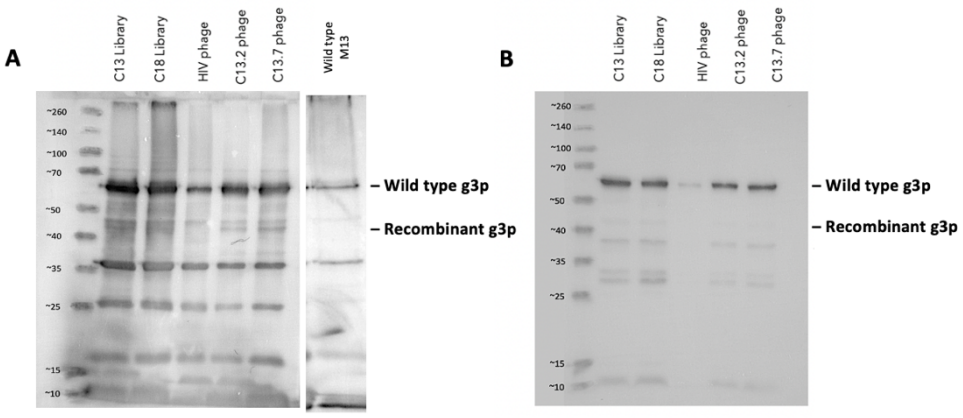

Figure 3.14: Protein expression of C13 and C18 phage libraries, HIV phage, C13.2 and C13.7. The phage libraries (Lane 2: C13, Lane 3: C18), HIV phage (Lane 4), C13.2 phage (Lane 5), C13.7 phage (Lane 6) and wild-type M13 (Lane 7) were analysed by western blot under reducing conditions using A) an anti Fd antibody and B) an anti g3p antibody. Band at 55 kDa inferred as wild-type (WT) g3p and bands between 40 and 50 kDa and inferred as recombinant g3p (heavy chain fused to truncated g3p). Other bands present in A at 12 and 20 kDa are reduced products expressed by the phage and detected by Anti-FD. Other bands present in B at 11, 28, 30 and 38 kDa are reduced fragments of g3p or of Fab fragments fused to g3p. A+B) M = molecular marker, shown in kDa.

Sanger sequencing of the phage clones in Figure 3.13B showed that C13.2 and C13.6 were identical, as were C13.3 and C13.7. Sequences of C13.2 and C13.7 can be found in Appendix II. Diversity of the library required investigating. Further screening of the libraries showed multiple identical sequences, 12 out of 20 sequences unique for C13 and 15 out of 20 sequences unique for C18 (data not shown). Therefore, the diversity of the libraries was suspected to be low.

3.4.2.5. Validation of library diversity by NGS

As technologies have advanced, NGS has increased in popularity for its applications in Phage Display. NGS enables a deep analysis of the library composition, allowing for library characterisation and validation of representation. The direct link between phenotype and genotype can be employed to select potential binders by following a specific sequence through panning rounds (Yang et al., 2017). Moreover, NGS can serve as an identifier of rare clones which may be underrepresented within a phage pool (Zambrano et al., 2022). Here, NGS was employed to verify the levels of diversity of heavy chains and to analyse any skewing to certain sequences. As it was suspected that diversity was low from initial sanger sequencing, thus may not be representative of the source, the VH1-7 germline-specific primer was investigated to determine if this was the cause of any bias.

The germline-specific heavy chain primer was scrutinised against the day 242 unsorted antibody repertoire (previously described Chapter 2, section 2.1), to ensure sequence selection was not biased. The primer was screened against an NGS dataset obtained by Dr. Theocharis Tsoleridis. Out of 132,000 sequences, 5,500 were derived from the germline IgHV1-7, of which 843 were spike reactive from the B-cell sort to SARS-CoV-2 Lineage A trimer. The germline-specific heavy chain primer matched 797 of these sequences suggesting 90% of IgHV1-7 antibodies would be amplified. Figure 3.15 represents the 10% of sequences that would not be amplified by the germline-specific heavy chain primer as they contained bases which did not correspond to the primer. For example, the first base of sequence 22 was a C

compared to the primer that starts with a T. Some sequences such as sequence number 10 contain five base pairs which do not match the primer. Increasing degeneracy of the primer was considered, however, this may result in the amplification of other germlines by reducing the specificity, therefore VH1-7 primer was suited for its specificity to the germline, yet it should be noted that certain VH1-7 sequences, such as those in Figure 3.15, would not be amplified.

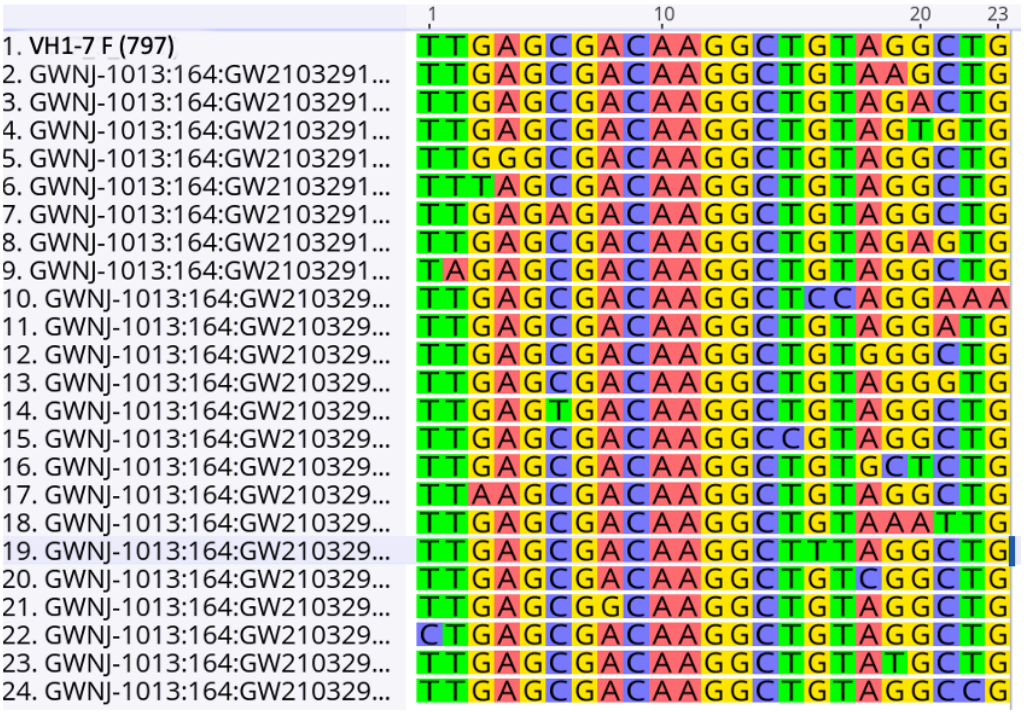

Figure 3.15: Investigating primer bias. Alignment of 24 unique sequences with 1 to 5 base pair mismatches to the VH1-7 germline-specific primer. Bases coloured T in green, G in yellow, A in red and C in blue.

To verify the diversity of the library, and to determine any skewing, NGS was performed at three points during the construction of the library. NGS was performed on the amplification of heavy chains using VH1-7F and IgHRev4 primers, to assess library representation at each stage. The three points were: initial PCR products of cDNA amplification (hereby called PCR), heavy chain PCR products amplified from the transformed library (hereby called COL), and heavy chain PCR products amplified from the phage library expressing unique heavy chains (PHAGE). This study focused on ultralong antibodies present in

the library and their unique sequences, therefore, the number of unique nucleotide sequences for each CDRH3 length was identified and how many of these sequences contained a unique amino acid profile. Figure 3.16 shows the analysis of these points for each library, identifying the number of unique sequences based on nucleotide (Number of sequences) and of those sequences, the unique amino acid protein sequence of the CDRH3 (unique CDRH3) for each CDHR3 length. For C13 library, the initial profile of heavy chains (Figure 3.16AI: PCR) shows a large range of CDRH3 lengths starting from 11 amino acids up to 67. Sequences with smaller CDRH3 lengths were less represented within the population, yet had more unique sequences, compared to some of the longer CDRH3 sequences. For example, CDHR3 lengths of 61 and 63 amino acids were detected the most in Figure 3.16AI with 216 sequences recorded sequences with a CDRH3 of 61 amino acids and 71 for sequences with a CDRH3 of 63 amino acids. Interestingly, sequences of these CDRH3 lengths contained few unique amino acid sequences. There are two explanations for this trend. There was skewing to these sequences, and or, these identical sequences were well represented in the B-cell population. This pattern across CDRH3 lengths was not continued to the transformed colonies (Figure 3.16AII) whereby only 7 different CDRH3 lengths were recorded. Those with 61 and 63 amino acids were still well represented, however, shorter CDHR3 sequences were not carried forward. This pattern was also found for Figure 3.16AIII therefore library representation was lost during the cloning step (Figure 3.16A).

Analysis of C18 library confirmed a similar trend. However, compared to C13 library, C18 library had fewer sequences with long CDRH3s to begin with. CDRH3 lengths ranged from five amino acids to 64 amino acids. More sequences contained unique amino acids in the CDRH3 across the entire CDRH3 lengths. Like C13 library, sequence representation was skewed to certain CDRH3 lengths. For instance, 14,751 sequences had a CDRH3 of 20 amino acids, and 3,535 sequences had a CDRH3 length of 27 amino acids (Figure 3.16BI). Most of these sequences were not unique for these CDRH3

lengths. The range of CDRH3 lengths was reduced in the Figure 3.16BII data, with sequences only recorded for CDRH3 lengths 16, 17, 20, 22, 24, 26 and 27. CDRH3 lengths of 20 and 27 were well represented in Figure 3.16BII, likely due to skewing to these sequences, and or, these identical sequences were well represented in the B-cell population. Identical sequences of 17 amino acids in the CDRH3 increased in number, thus decreased in number of unique sequences, in the dataset Figure 3.16BII compared to Figure 3.16BI. This trend was reflected in the Figure 3.16BIII therefore it was concluded that library representation was also lost in the cloning step for C18 library (Figure 3.16B).

A

AI

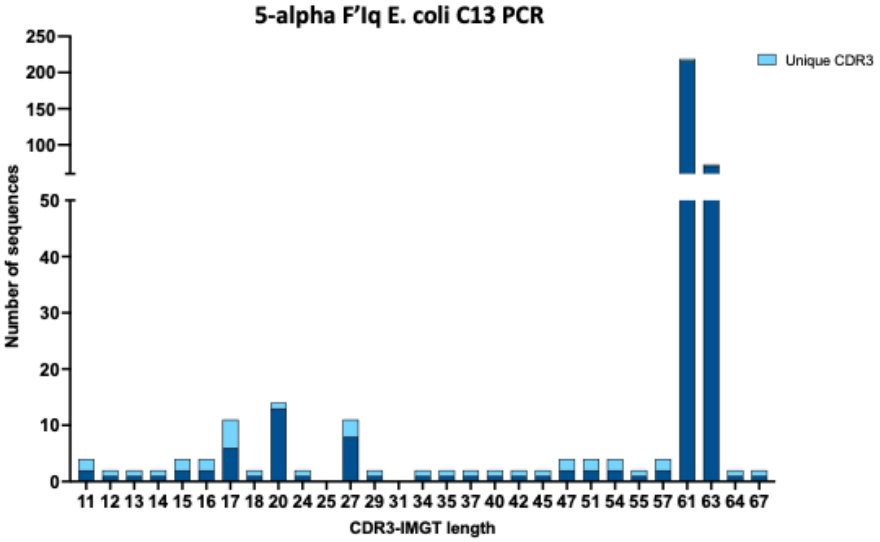
5-alpha F'Iq E. coli C13 PCR
Unique CDR3
Number of sequences
250
200
150
100
50
40
30
20
10
0
11 12 13 14 15 16 17 18 20 24 25 27 29 31 34 35 37 40 42 45 47 51 54 55 57 61 63 64 67
CDR3-IMGT length

AII

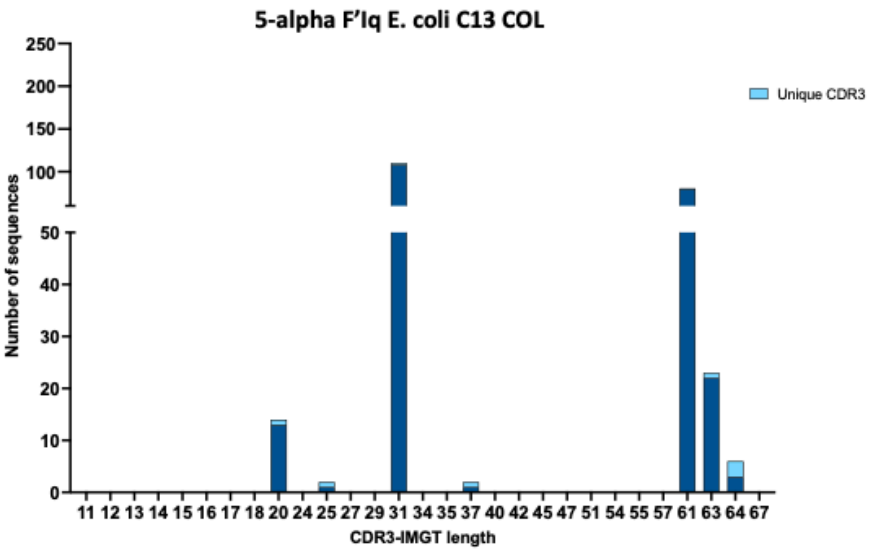
5-alpha F'Iq E. coli C13 COL
Unique CDR3
Number of sequences
250
200
150
100
50
40
30
20
10
0
11 12 13 14 15 16 17 18 20 24 25 27 29 31 34 35 37 40 42 45 47 51 54 55 57 61 63 64 67
CDR3-IMGT length

AIII

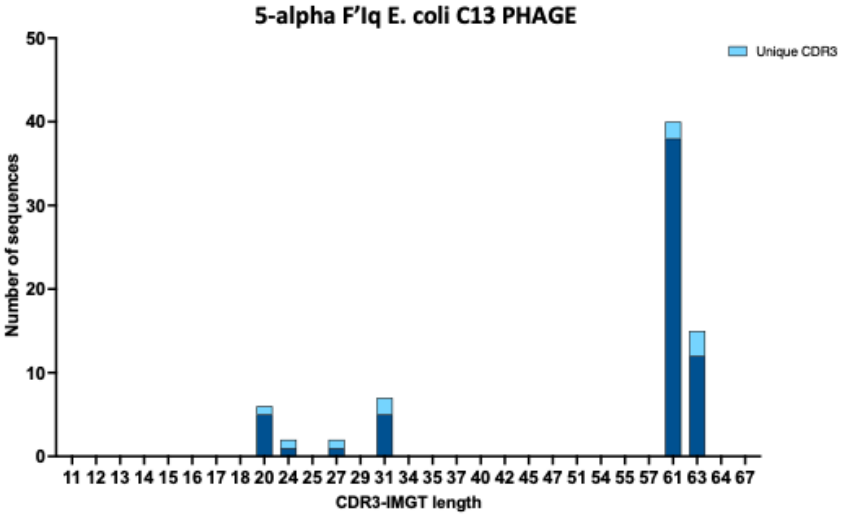
5-alpha F'Iq E. coli C13 PHAGE
Unique CDR3
Number of sequences
50
40
30
20
10
0
11 12 13 14 15 16 17 18 20 24 25 27 29 31 34 35 37 40 42 45 47 51 54 55 57 61 63 64 67
CDR3-IMGT length

B

BI

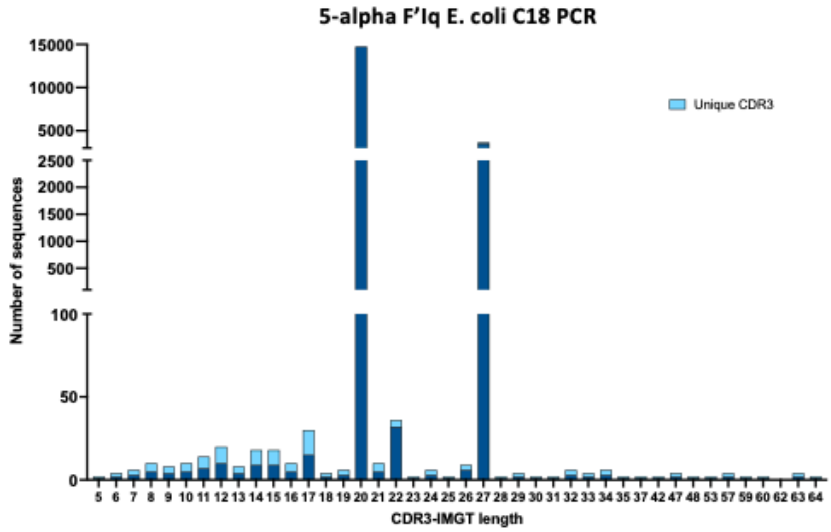
5-alpha F'Iq E. coli C18 PCR
Unique CDR3
Number of sequences
15000
10000
5000
2500
2000
1500
1000
500
100
50
0
5 6 7 8 9 10 11 12 13 14 15 16 17 18 19 20 21 22 23 24 25 26 27 28 29 30 31 32 33 34 35 37 42 47 48 53 57 59 60 62 63 64
CDR3-IMGT length

BII

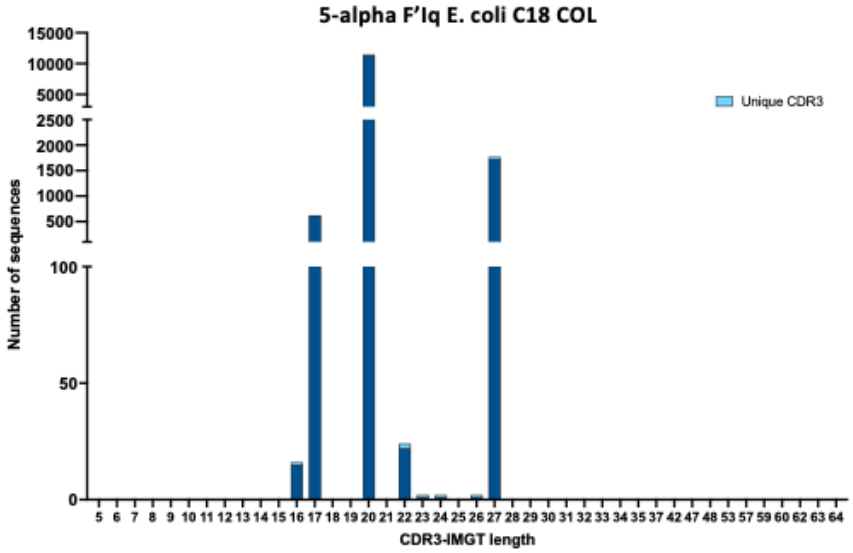
5-alpha F'Iq E. coli C18 COL
Unique CDR3
Number of sequences
15000
10000
5000
2500
2000
1500
1000
500
100
50
0
5 6 7 8 9 10 11 12 13 14 15 16 17 18 19 20 21 22 23 24 25 26 27 28 29 30 31 32 33 34 35 37 42 47 48 53 57 59 60 62 63 64
CDR3-IMGT length

BIII

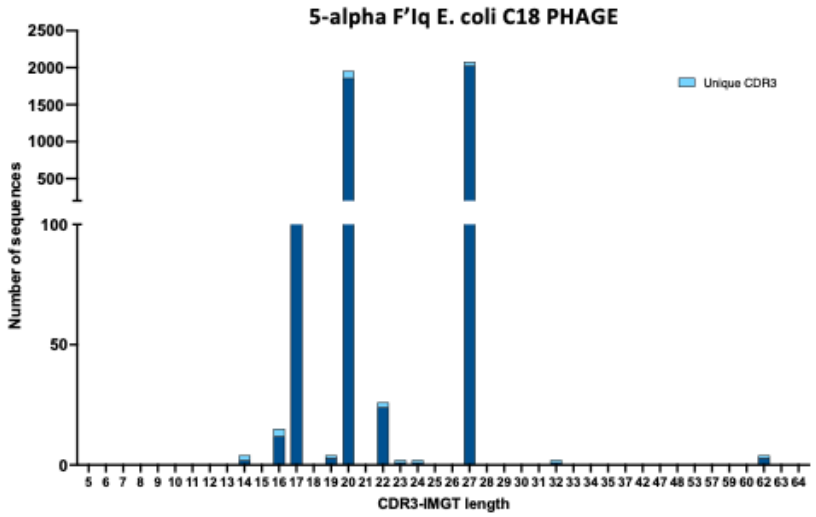
5-alpha F'Iq E. coli C18 PHAGE
Unique CDR3
Number of sequences
2500
2000
1500
1000
500
100
50
0
5 6 7 8 9 10 11 12 13 14 15 16 17 18 19 20 21 22 23 24 25 26 27 28 29 30 31 32 33 34 35 37 42 47 48 53 57 59 60 62 63 64
CDR3-IMGT length

Figure 3.16: NGS analysis of heavy chains from C13 and C18 libraries produced in 5-alpha F'Iq *E. coli*. A) C13 library PCR (AI), COL (AII), and PHAGE (AIII) number of heavy chain sequences, and of these, the number of unique amino acid sequences, for each CDRH3 length. B) C18 library PCR (BI), COL (BII), and PHAGE (BIII) number of heavy chain sequences, and of these, the number of unique amino acid sequences, for each CDRH3 length. The y axes have different scales for ease of visualisation.

3.4.2.6. Construction and validation of the libraries with TG1 cells

Libraries transformed in 5-alpha F'Iq *E. coli* showed a reduction in representation and so to overcome this the construction libraries were altered in attempt to increase the heavy chain representation. Cloning in chemically competent cells was likely reducing the chances of representation of the rarer clones within the population due to lower cloning efficiencies, therefore, clones highly represented in the population were more likely to be successfully cloned, and rarer clones least likely to be successfully cloned. The cloning was altered to transform libraries into TG1 electrocompetent cells, raising the cloning efficiency, to increase the chances of rarer clones being represented. To accommodate this alteration, ligation of heavy chains was performed using Gibson Assembly as InFusion cloning was incompatible with these cells. The original VH1-7 and IgHRev 4 primers were extended to accommodate this. This generated heavy chain PCR products with homology arms between 30 and 40 base pairs. These arms were complementary to upstream and downstream segments of the phagemid at the B*mt*I site, thus allowing for seamless cloning of inserts into the phagemid. Cloning efficiencies yielded 1.5×10^7 /μg DNA and 3.5×10^6 /μg DNA for C13 and C18, respectively. However, NGS analysis of the cDNA amplification using the extended primers reduced initial diversity compared to the VH1-7 and IgHRev 4 primers. In C13 the PCR amplification of cDNA, using VH1-7 and IgHRev 4

primers, 29 different CDRH3 lengths were identified, however, amplification of cDNA using the extended primers reduced this to 14 different CDRH3 lengths. In C18 the PCR amplification of cDNA using VH1-7 and IgHRev 4 primers 42 different CDRH3 lengths were identified yet amplification using the extended primers reduced this to 3 different CDRH3 lengths (data not shown). In an attempt to gain library representation using the extended primers, various combinations of heavy chain PCR amplifications of cDNA were performed (data not shown), the reactions are described in Chapter 2, Figure 2.3. NGS analysis was performed on each PCR product, and each presented a unique NGS profile of CDHR3 lengths, skewing to various sequences. As not one product contained the desired representation, products were pooled for Gibson assembly ligation and transformation into TG1 for the construction of libraries. This generated two libraries, C13 TG1 PCR optimised library 2023 and C18 TG1 PCR optimised library 2023.

The binding of each library was analysed through ELISA. The 5-alpha F'Iq *E. coli* phage libraries showed little diversity and thus did not represent the library sources, showing skewing to certain sequences within the population and a reduction in range of CDRH3 lengths (Figure 3.16). The sequences that were well represented in this library were discovered to confer high levels of binding therefore the binding of the libraries, C13 5-alpha F'Iq *E. coli* and C18 5-alpha F'Iq *E. coli* were likely due to the dominance of these clones within the library (Figure 3.17). Libraries were reconstructed into TG1 electrocompetent cells to increase the cloning efficiency and thus increase the chances of representation of rarer sequences in the population. The amplification of the cDNA using the extended primers resulted in a reduction of source representation when comparing cDNA amplification using the original primers (data not shown). The phage libraries generated from this (C13 and C18 TG1 extended primers libraries) showed a reduction in binding to SARS-CoV-2 Lineage A, therefore heavy chain sequences that bound to SARS-CoV-2 Lineage A trimer were lost during the construction of these libraries. The amplification of the cDNA using the TG1 extended primers was

optimised to achieve a higher level of representation. Pooling of optimised PCR products increased cDNA representation compared to the TG1 extended primers amplification of the cDNA (data not shown). Phage libraries for the pooled optimised PCR products were generated (TG1 PCR optimised libraries 2023) and also tested for binding against SARS-CoV-2 Lineage A trimer. There was an increase of TG1 PCR optimised libraries 2023 in binding to SARS-CoV-2 Lineage A trimer compared to the TG1 extended primers libraries (Figure 3.17). However, binding was less for the TG1 PCR optimised libraries 2023 compared to the 5-alpha F'Iq *E. coli* libraries, which could be a caveat of extending the primers, thus losing representation of certain sequences that the primers did not anneal well to.

Representation of cDNA could not be achieved during construction of the phage library with 5-alpha F'Iq *E. coli* cells and generating a phage library with extended primers saw a reduction in cDNA representation yet this method was better at maintaining levels of representation through the process. In order to achieve maximum representation, all phage libraries of varying diversity were combined.

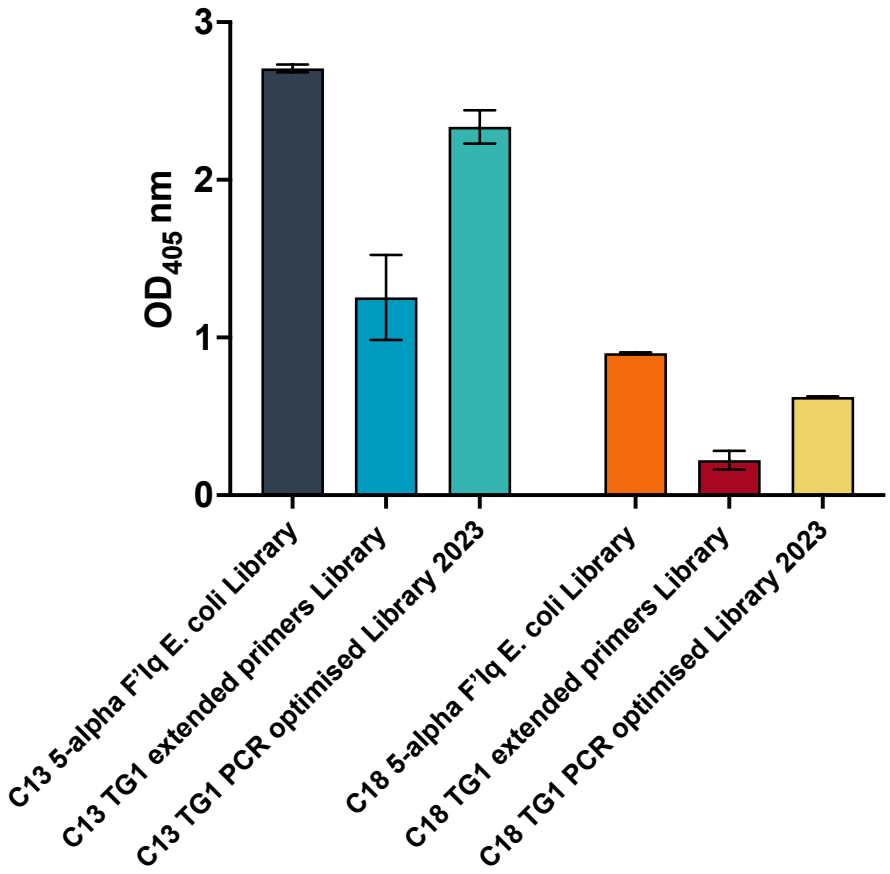

Figure 3.17: Phage ELISA binding of each library constructed against SARS-CoV-2 Lineage A trimer, measured as OD_{405} nm. Libraries were generated by transforming in 5-alpha F'Iq *E. coli* cells (5-alpha F'Iq *E. coli* libraries) showed the high levels of binding to SARS-CoV-2 Lineage A trimer. Libraries generated by extending the heavy chain amplification primers and transforming into TG1 cells (TG1 extended primers libraries) showed the least binding to SARS-CoV-2 Lineage a trimer. Libraries generated from optimising the extended primer PCR and transforming into TG1 cells (TG1 PCR optimised 2023 libraries) showed higher levels of binding to SARS-CoV-2 Lineage A trimer compared to the TG1 extended primers libraries, however, was not as high as the 5-alpha F'Iq *E. coli* libraries. Error bars demark standard deviation, N=2.

3.4.2.7. Pooling the phage libraries

To generate a library with as much source representation, the phage libraries were pooled and NGS analysis was performed to determine representation

(ALL PHAGE). The number of different CDRH3 lengths in C13 5-alpha F'Iq *E. coli* PHAGE (Figure 3.16A) was only six, compared to the C13 ALL PHAGE which had 19 different CDRH3 lengths (Figure 3.18A). There was more variation in representation across the CDRH3 lengths, and there was less skewing to sequences with 61 or 63 amino acids in the CDRH3. Certain sequences, however, were likely to have a higher representation in the source population, for instance, sequences with 20, 24, 25, 31, 61 and 63 amino acids in the CDRH3, which did not contain many unique sequences. In contrast, the C18 ALL PHAGE library did not improve from combining the libraries with sequences of 20 amino acids in the CDRH3 dominating the library (Figure 3.18B). This CDRH3 length contained many identical sequences, although this was observed for cDNA amplification using the original VH1-7 and IgHRev 4 primers (Figure 3.16B C18 PCR) and, therefore, it is likely that this clone dominated the B-cell sort.

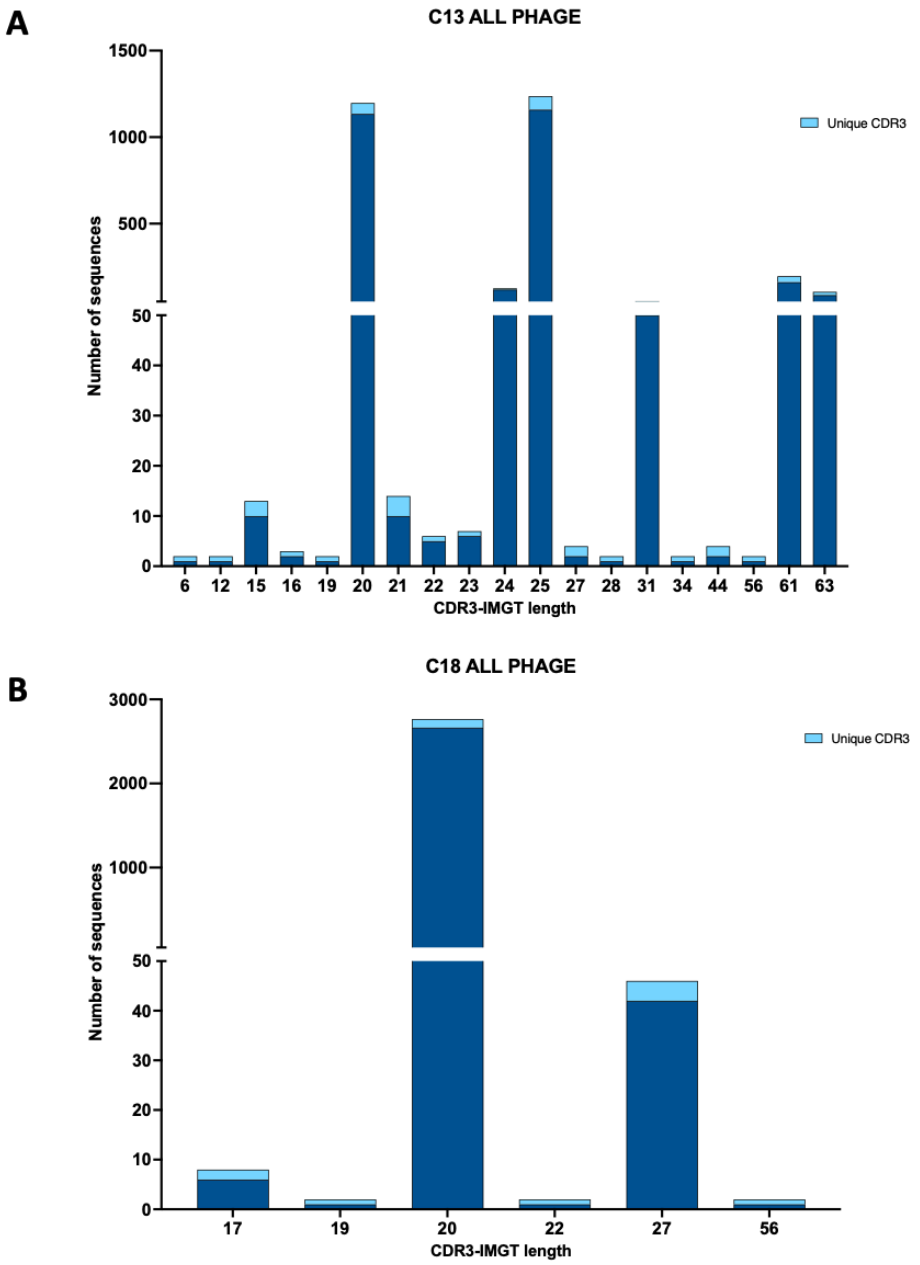

Figure 3.18: NGS analysis of heavy chains from C13 and C18 libraries combined. A) C13 library ALL PHAGE number of heavy chain sequences, and of these, the number of unique amino acid sequences, for each CDRH3 length. B) C18 library ALL PHAGE number of heavy chain sequences, and of these, the number of unique amino acid sequences, for each CDRH3 length. The y axes have different scales for ease of visualisation.

3.4.3. Modifications of phagemid vector

Phagemids are commonly modified to contain an amber stop codon. This modification enables rapid characterisation of phage clones using soluble Fab as a prior step to cloning a Fab of interest into full antibody constructs. The presence of amber stop codons between the coding regions of the antibody fragment and p3 enables continuous translation (Smith, 1985). In suppressor strains, such as TG1 used in this study, the codon is read as a glutamine hence displaying antibody fragments on p3. Conversely, direct transformation of desired phagemid into non-suppressor strains such as HB2151 or BL21 (DE3) where the amber stop codon is read as stop, the antigen fragment is produced as a soluble entity that can be directly utilised for characterisation (Kumar et al., 2019).

Site-directed mutagenesis of the phagemid vector, PFAB3 L.14, was performed to generate soluble Fab. The first experiment resulted in an insert of the amber stop codon, attached to a glycine linker and His tag for downstream processing such as protein purification. This produced a phagemid named PFAB3_AMB which when compared to the original PFAB3 L.14 vector has this insert (Figure 3.19A). Simultaneously, the phagemid was mutated with another set of primers to delete gene 3, which when transformed into standard *E. coli* competent cells would generate the production of soluble Fab. Figure 3.19B shows the mutated phagemid, PFAB3_XG3P, with the heavy chain leading into a His tag and glycine linker followed by a stop codon. The original PFAB3 L.14 follows directly into gene 3 from the heavy chain.

In this methodology, phage of interest were individually rescued and titred to determine the binding potential, and subsequently, antibody fragments subcloned into a full antibody construct vector to identify individual characteristics of the antibody. Nevertheless, follow-up studies to this one may benefit from an amber stop codon within the PFAB3 vector for rapid characterisation of clones.

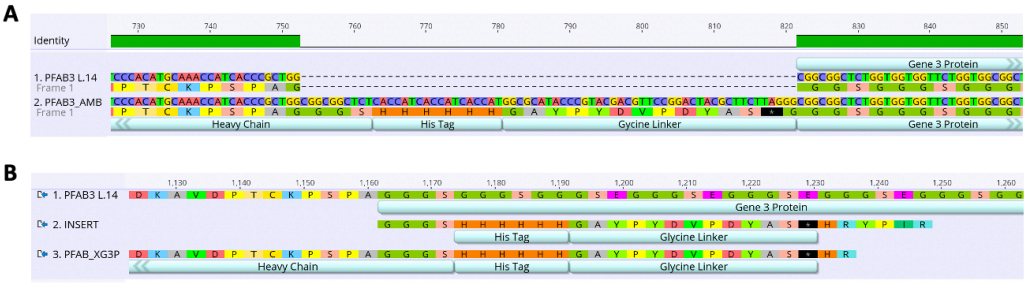

Figure 3.19: Alignments of SDM modifications to the phagemid showing nucleotides and amino acid sequence 5' to 3'. A) Amber stop codon addition followed by glycine linker and His tag. The top sequence shows the original PFAB3 L.14, and bottom sequence shows the phagemid containing the amber stop codon. B) Gene 3 deletion and addition of His tag and glycine linker, top sequence represents the original PFAB3 L.14, middle sequence displays the desired insertion, and bottom sequence displays the phagemid containing the gene 3 deletion.

3.5. Discussion

With the recent interest in bovine ultralong antibodies as potential therapeutics, a system optimised for their isolation is highly desirable. Phage display remains a popular tool for monoclonal antibody discovery as it is highly versatile to optimise display for high affinity selection against a variety of targets. This study aimed to optimise a phage display system for the isolation of bovine ultralong antibodies and maximised the discovery of high affinity antibodies by repeated immunisations, resulting in a hyperimmune library, with a population of cells sorted by their reactivity to SARS-CoV-2 Lineage A trimer. This chapter discusses the production of the HIV control phage, derived from a bovine ultralong HIV chain (Sok et al., 2017) and the subsequent construction of a bovine ultralong Fab library targeting SARS-CoV-2. The two ultralong bovine libraries were optimised for source representation.

The HIV control phage was primarily generated as a control for biopanning purposes, but also served as a template to optimise the phage protocol. Successful cloning of the light and ultralong heavy chain of the HIV antibody, as demonstrated in Figure 3.3, resulted in a phagemid containing bovine light and paired ultralong heavy chain. Filamentous phage growth is reliant on the capsid proteins, therefore long inserts, for instance, can lead to instability of the fused protein and gene deletion. Extreme alteration of the capsid proteins can impact propagation, be toxic to the host cell, or disrupt the integrity of the capsid during egress from the cell (Zhao et al., 2016). More importantly, cytoplasm expression can result in impaired conformation, reduction of disulphide bridges, and ultimately loss of antibody biological function (Bratkovic, 2010, Gagic et al., 2016). As ultralong heavy chains are long, complex inserts, it was unknown whether the expression would be successful. The HIV control phage confirmed the possibility of displaying ultralong bovine Fab on g3p of the M13 bacteriophage. The expression was validated by western blot, Figure 3.5, and ELISA, Figure 3.6. Protein analysis by western blotting identified a band at 55 kDa as wild-type g3p, and a band at 39 kDa as the truncated g3p fused to the heavy chain. To distinguish between these two bands the phagemid could be modified to display a tag between Fab and g3p, this tag could then be detected with an antibody, thus detecting recombinant g3p. A similar approach was carried out using an SV5 tag in Chasteen et al.'s study (Chasteen et al., 2006), therefore, wild-type g3p would not produce a band as these proteins would not contain the tag. This could aid in the confirmation of recombinant protein expression. Once expression was confirmed, the rescue of phage particles was optimised to achieve the maximum yields and reduce any potential loss from this step, this was important to optimise prior to library construction. An investigation into ratios of helper phage during coinfection resulted in obtaining high titres of 10^{13} cfu/mL of phage, as shown in Figure 3.4, using a ratio of 1.25 helper phage to 1 bacterial cell which was used for subsequent library construction. Expression of recombinant phage particles was supported by the activity of the HIV phage, which showed highly specific binding to HIV glycoproteins

gp120 and gp140 (Figures 3.6 and 3.7), confirming activity of the Fab to its target antigen. Unfortunately, the HIV phage showed higher than background binding to SARS-CoV-2 Lineage A trimer, thus could not be used as anticipated as a negative control in the biopanning procedure.

Pertinent to establishing an effective Fab phage display system is the removal of potential bias, achieving specificity, and validating diversity to confirm sample representation. Bias, non-specificity and loss of diversity can arise during amplification, assembly, cloning of genes, and the transformation of phagemids. In order to optimise these elements, several aspects of the phage protocol were optimised.

Initial construction of each library was achieved through digesting the PFAB3 L.14 phagemid, which carried the common light chain, at the B*mt*I restriction site and amplifying the source heavy chains using ultralong germline specific primers, VH1-7 and IgHRev 4 (Figure 3.8). The primers amplified the heavy chains and added a 15 base pair homology arm that was complementary to the sense and antisense sequence of the phagemid at the B*mt*I restriction site for InFusion cloning. InFusion cloning supports the integration of multiple single inserts in a singular step, whereby homology arms are trimmed back at the 3' ends during the reaction, allowing for seamless cloning into a vector when transformed into cells that contain DNA repair mechanisms (McClure et al., 2016). The molecular ratios were calculated in the cloning step to represent the ultralong heavy chains in the source. Here, 4,200 B-cells were obtained from C13 and 4,000 B-cells from C18, of which 10-15% are likely to be ultralong. Using this percentage, approximately 630 sequences were required to represent C13 and 600 for C18. With a transformation efficiency of 1-3 x 10^9 cfu/µg DNA, 5-alpha F'Iq *E. coli* were deemed adequate for transforming the library for source representation. Initial observations from a heavy chain colony screen of a small InFusion reaction of transformed libraries showed that C18 heavy chains were overall smaller fragments to C13 suggesting the presence of CDRH3s of fewer amino acids. On the other hand, the majority of C13 bands appeared above 500 base pairs, at a similar band

size to that of the HIV phage heavy chain of 61 amino acids, thus likely to contain longer CDRH3s. Reaction size was increased for source representation by increasing the likelihood of ligation of rarer heavy chains into the phagemid. However, increasing ligation reaction size had little to no impact on cloning efficiency, with both reactions obtaining similar yields (Figure 3.9).

Bias during the process was reduced by the growth of transformed colonies on solid media, thus removing competition between clones. This was carried out throughout the process in order to avoid reductions in diversity during consecutive amplifications (Castel et al., 2011). One of the main challenges of bias in a phagemid system is the presence of 'bald' phages, recorded to result in up to 90% of rescued phage bearing no displayed antibody. The helper phage employed for this study, M13KO7, preferentially packages single-stranded phagemid DNA in the presence of a phagemid bearing a wild-type M13 or f1 origin, thus reducing the output of bald phages. Nevertheless, non-valid inserts from stop codons and indels are unpreventable, permitting integration of helper phage coat protein which can be amplified as selection-unrelated contaminants during panning (Zambrano et al., 2022). A possible solution is to use a tryptic helper phage such as KM13. Treatment with trypsin following a selection round eliminates bald phages, therefore, fusion proteins are retained and continue to be propagated (Barbas et al., 2001).

Libraries were validated for Fab expression on g3p by western blot and compared to the HIV phage which presented a similar banding pattern. In Figure 3.10, library bands around 39 kDa appear more intense and thicker for the libraries, yet less intense a band wild-type g3p, likely due to a greater expression of wild type g3p than recombinant g3p on each particle. The specificity of the libraries was determined through ELISA, ascertaining whether binding was true to the target or non-specific to capture proteins such as neutravidin and avidin analogues, plastics (Figure 3.6A and Figure 3.11), or blocking agents (data not shown). Capture proteins and plastic motifs, have been reported as decoys, leading to false positives during the selection process (Vodnik et al., 2011, Zambrano et al., 2022). Removal of

these decoys ensures accurate selection and subsequent amplification of phage clones with true affinities to the target.

Since establishing diversity could not be achieved with a singular control phage, the libraries were evaluated for their representation of the source. Individual clones from each library were sequenced to assess the diversity and representation of heavy chains in the phage libraries. In the initial library produced, a high proportion of sequenced clones showed the presence of phagemids lacking heavy chains as a result of incomplete digestion of the phagemid vector during the cloning procedure. To overcome this, the libraries were re-constructed. Primers were designed to linearise the phagemid vector at the B*mt*I restriction site. Similar to the heavy chain PCR products, the linearised, amplified phagemid contained homology arms complementary to the heavy chains for seamless InFusion cloning. New colony screening primers flanking the B*mt*I restriction site were designed to determine whether the linearisation had been successful (Figure 3.12). Although light chain-only colonies were present, they were greatly reduced compared to the first library (data not shown). The reconstructed libraries were validated once more by western blot, this time employing an antibody to g3p simultaneously alongside the anti FD blot to reduce background bands from other reduced phage coat proteins. As expected, the bands present in each sample of Figure 3.14A above 50 kDa, reflected the band observed in Figure 3.10, as wild-type g3p, and a much fainter band between 40-50 kDa for recombinant g3p (heavy chain fused to truncated g3p). Notably, bands for the libraries appear less discrete to C13.2 and C13.7 phage clones, thus suspected to be the presence of recombinant g3p of varying CDRH3 lengths.

A subset of phage from each re-constructed naïve library were individually rescued and trialled for binding against SARS-CoV-2 Lineage A trimer (Figure 3.13A). Eight out of 18 clones showed significant binding (* p= <0.05, ***p= <0.001, ****p= <0.0001), indicating that the SARS-CoV-2 Lineage A trimer-specific sort had pre-enriched the libraries as expected. The specificity of the highest binders was evaluated by a phage ELISA against an irrelevant

glycoprotein, gp120. Data from Figure 3.13B show significant binding (****p= <0.0001) of each phage clone to SARS-CoV-2 Lineage A trimer compared to HIV gp120, confirming the specificity of these phage clones towards SARS-CoV-2 Lineage A trimer. Due to high levels of binding, these clones were further investigated. Sequencing of phage heavy chains revealed clones with identical sequences. C13.2 matched C13.6, and C13.3 matched C13.7. A possible explanation for this is that the germline-specific primer was causing primer bias to certain sequences within the source population. An alternative explanation was that certain sequences were highly represented within the B-cell population and, or the diversity of the libraries was low.

To investigate the first explanation, the heavy chain primer was examined for bias during amplification. The primer was screened against an NGS dataset obtained by Dr. Theocharis Tsoleridis. The primer matched to 90% of IgHV1-7 antibodies, therefore, 10% of sequences would not be amplified by the germline-specific heavy chain primer as they contained bases which did not correspond to the primer (Figure 3.15). Modification of the primer to increase degeneracy and using a set of primers were considered, however, due to limited variation within the heavy chain germline, degeneracy or using multiple primers could increase the risk of selecting alternative germlines (Berens et al., 1997, Lopez et al., 1998, Niku et al., 2012). The small primer bias could not explain the little diversity observed within the libraries so to determine whether there was loss of source representation during the library construction, NGS analysis was performed.

The libraries were sequenced using NGS across three points. The sequences were prepared in Geneious prime and mapped to VH1-7 F primer as a reference, unique sequences extracted, and analysed through the IMGT-HIGH VQUEST database (Alamyar, 2010). For each CDRH3 amino acid length, the number of unique nucleotide sequences and unique CDRH3 amino acids were recorded. The diversity in the PCR product (Figure 3.16AI and BI) was not reflected in the transformed phagemids for each library (Figure 3.16AII and BII), thus not carried forward when rescuing phage particles (Figure 3.16AIII

and BIII). A possible explanation for this is the lower cloning efficiency of chemically competent cells to electrocompetent cells. The library required representation of 4,200 B-cells for C13 and 4,000 B-cells for C18. As this study aimed to represent the source, a library 10 times greater, 10^4 was required to ensure source representation, assuming each B-cell cDNA sequence is amplified similarly. Electrocompetent cells are the preferred cell type for the construction of phage libraries with efficiencies recorded up to $\geq 4 \times 10^{10}$ cfu/µg DNA for commercial kits (Chai et al., 2020). As TG1 cell lines lack *recA1* and *endA* mutations, they are incompatible with Infusion cloning. To circumvent this issue, the ligation mechanism was modified to Gibson assembly, which mirrors infusion cloning, however, contains a ligase instead of relying on host cell ligase to repair nicked DNA. This ligation can then be used in cell lines without *recA1* and *endA* mutations. The cloning reaction for each library was optimised by extending the current primers to increase overhangs to between 20 and 40 base pairs as recommended by the manufacturer.

Amplification of cDNA with the extended primers did not represent the cDNA amplification by the original primers therefore the extended primer amplification of cDNA was optimised. NGS analysis of each optimised PCR showed varying levels of skewing, however, none of the products generated the same representation of the original cDNA amplification with VH1-7 and IgHRev 4 primers. A likely explanation for this is that extending primers may influence the hybridisation of the DNA and be less efficient at annealing to the target. Other possible explanations for this include cDNA degradation from multiple freeze-thaw cycles and, or, low copies of certain sequences, therefore a reduced likelihood of their amplification.

As the original primers would not generate a homologous arm long enough for products to clone into the phagemid, the optimised PCR products were pooled to represent the source diversity. The pooled PCR products were cloned using Gibson assembly, transformed into TG1 cells and phagemids rescued to produce phage particles. An ELISA was performed to determine

which library showed the greatest binding to the target, SARS-CoV-2 Lineage A trimer (Figure 3.17). The 5-alpha F'Iq *E. coli* libraries showed the greatest binding, however, that was likely due to over-representation of phage clones C13.2 and C13.7, which showed strong binding individually to the SARS-CoV-2 Lineage A trimer. This was, indeed, further supported by analysis of NGS data where such as C13.2 and C13.7 were highly represented within the C13 5-alpha F'Iq *E. coli* library. To obtain maximum representation, all phage libraries produced, and known to exhibit binding to SARS-CoV-2 Lineage A trimer, were combined and analysed by NGS (Figure 3.18). The representation of C13 ALL PHAGE is increased in comparison to the 5-alpha F'Iq *E. coli* phage library (Figure 3.16 C13 PHAGE). In contrast, the C18 library appears to have decreased in representation but retained CDR3s of longer lengths. As the goal of this project was focused on ultralong antibodies, both libraries were taken forward for biopanning.

The use of NGS in this project provided a useful tool for validating sample source representation and identifying rarer clone sequences that may have been lost during the library construction (Zambrano et al., 2022). However, the maximum read of Illumina EZ amplicon service could cover was a sequence of 500 base pairs, thus a large proportion of sequences from these data sets could not be merged. Illumina services covering longer reads were considered but decided against due to the cost-effectiveness of the project. Furthermore, this study's analysis was reliant on the integrity of the IMGT database, which may misidentify sequence gene germlines. Therefore, future advances in NGS technology and its costs, as well as the expansion and validation of databases, are thought to be beneficial for the analysis of phage display studies in the future.

Phagemid systems are highly versatile and readily modifiable for desired characteristics. The ease of producing soluble Fab in a single step by switching cell lines (Figure 3.19), enables the rapid characterisation of clones. In this study, clones with high affinity to SARS-CoV-2 Lineage A trimer, C13.2 and C13.7 phage, were taken forward for subcloning into a human chimeric

antibody construct for characterisation. Amber stop codon and gene 3 deletion modifications, however, may have a use for identifying bovine ultralong candidates from libraries to various disease agents in the future.

3.6. Conclusion

Phage display has proven a useful tool with a high level of adaptability to suit experimental design. Its advantages such as low propagation costs, ease of handling with the availability of commercial kits to aid in library formation, enable the production of large libraries without compromising on diversity. Here a phage display system was optimised for the display of bovine ultralong Fab on M13 bacteriophage g3p. A HIV control phage expressing bovine ultralong Fab on g3p aided in optimising the process prior to the construction of libraries. Validation steps of western blotting, ELISAs and NGS analysis determined source representation of the bulk sorted, B-cell ultralong bovine repertoires specific to SARS-CoV-2 Lineage A trimer throughout library construction. This discussion identifies two libraries that may be employed for high throughput screening of bovine ultralong antibodies, describes the discovery of two phage clones of interest through library validation, and identifies several steps for improvement of library construction to establish source representation and diversity.

Chapter 4 Biopanning C13 and C18 Libraries

4.1. Summary

Facilitated by the biopanning process, peptides and proteins of high affinity and specificity can be selected for almost any target. The experimental design for biopanning was optimised to select for high affinity binders against SARS-CoV-2 trimer antigens from phage display libraries C13 and C18, previously produced from a source of enriched B-cells to SARS-CoV-2 Lineage A trimer, in Chapter 3. Two bovine ultralong phage clones carrying Fab of interest, C13.2 and C13.7, identified during validation (Chapter 3) were selected in different panning rounds (Chapter 4), and extensively characterised (Chapter 5). This results chapter focussed on the employment of higher diversity libraries in the biopanning process, for selection of high affinity Fab to SARS-CoV-2 Lineage A trimer and SARS-CoV-2 BA.5 trimer.

4.2. Introduction

A major concept of phage display is affinity enrichment through a process termed 'Biopanning'. Initially in 1988, displayed peptides fused to the surface of filamentous bacteriophage were selected for by this process. In 1990, advances in phage display technology extended to expression of functional antibody fragments on the surface of the phage, producing an antibody-phage complex which could be enriched by washing a phage display library over immobilised antigens (McCafferty et al., 1990). This uncovered some key principles of biopanning. Firstly, specific binders could be isolated out of a pool of irrelevant clones. Secondly, this system enabled the relative enrichment of high affinity clones over those with lower affinities (McCafferty, 1996). Biopanning typically follows the construction of a suitable library and the selection of a target. Fundamentally, biopanning consists of three main steps: incubation of the library with the target to capture the binding phage, washing away of non-binding phage, and elution of bound

phage (Sparks et al., 1996). This process is traditionally carried out in multiple rounds to select for the highest binding phage. Biopanning rounds can be altered on stringency to select binding phage with a spectrum of affinity to the target. To efficiently perform biopanning, an understanding of controlling affinity, diversity and specificity is required (McCafferty, 1996).

A high-quality library is necessary for representing the diversity of the source. The display system has a strong influence on the biopanning process with multiple options of display valency. As discussed in Chapter 3, two libraries were generated from a hyperimmune source, displaying ultralong bovine Fab on g3p through a phagemid system. On the M13 bacteriophage, five copies of g3p are found, in comparison to the abundance of g8p with up to 2700 copies. Display on a singular protein, such as on one of five g3p, results in high affinity selection, in comparison to display on g8p where multiple proteins are expressed simultaneously, clustered, increasing avidity. Since the aim of this study was to display ultralong bovine Fab to SARS-CoV-2 Lineage A trimer, and isolate high affinity binders, g3p display was selected over g8p display due to its ability to harbour long amino acid fusions (Bazan et al., 2012). A phagemid format, carrying gene 3 fusions on a separate entity, was selected over phage vector display since phage vectors can potentially result in polyvalent display, which can favour low affinity high avidity binding events (Ledsgaard et al., 2018). Conversely, display on a phagemid format commonly results in the expression of one recombinant g3p out of five (Hoogenboom et al., 1998), thus reducing valency and ultimately resulting in discrimination between low and high affinity binders during selection. Chapter 3 described different approaches to generate a library from $4x10^3$ antigen-sorted B-cells obtained from two cows immunised with SARS-CoV2 spike protein constructs. Generated phage libraries containing levels of diversity were combined to increase library representation of the source prior to panning. Despite controlling display by selecting a vector system, clonal variation is an uncontrollable factor that can influence display levels. The expression of the display may be attributed to translational, transportation, or stability

differences of the fusion to g3p. For instance, selection and amplification bias can occur for clones that are well expressed and therefore those clones that express well are more likely to form a greater contribution to the repertoire (McCafferty, 1996, Barbas et al., 1991, Lowman et al., 1991).

In conjunction with library quality, the target's quality can affect the panning efficiency. In Chapter 3, various targets were tested to assess the binding of the HIV phage. Initial trials of using lysates, produced from cells transfected with a plasmid containing the HIV gp120 full length trimer, showed high levels of background non-specific binding (data not shown) and thus purified proteins were selected for target usage in the phage ELISA and for biopanning of libraries. For biopanning, displayed libraries are commonly subjected to the target antigen via adsorption to an immobilised surface for a set incubation time. Surfaces used for biopanning include nitrocellulose (Hawlisch et al., 2001), polystyrene tubes (Hust et al., 2002), magnetic beads (McConnell et al., 1999) and microtiter plates (Russo et al., 2018) with high binding surfaces such as Maxisorp. The main disadvantage of immobilisation is that it can result in conformational changes of the target antigen such as denaturation or distortion. Furthermore, target antigens may not preferentially bind in the correct orientation. Therefore, panning against incorrectly immobilised antigens may result in the isolation of high affinity binders to distorted antigens and low affinity to the desired native antigen. Typically, this is addressed by streptavidin or neutravidin capture of biotinylated antigen which lifts the antigen from the surface, thus improving display. However, biotinylating comes with its caveats such as ensuring the correct biotin-antigen ratio, decreasing antigen binding regions, and antigen aggregation (Ledsgaard et al., 2018). Alternative methods of panning against a target can be achieved by the target antigen being in solution, expressing the target on cells, liposomes, nanoparticles, virus-like particles, or expressing *in vivo* (Tikunova and Morozova, 2009, Ledsgaard et al., 2022b).

When optimising the panning rounds, panning efficiency can be influenced by the concentration of the phage library added, and the incubation time of the library with the target. Studies by McCafferty et al. discovered that high phage inputs could reduce the portion of the proportion of binding. They theorised that a high concentration of phage can form aggregates upon binding, thus incoming phage cannot associate due to steric hindrance. The authors suggest that 1.5 x 10^{10} of phage particles would be sufficient to saturate a 100 μL well, at 90 mm^2, and therefore recommended that this concentration of phage library is optimal for biopanning (McCafferty, 1996). During each panning round, manipulation of stringency, such as in wash steps, results in an affinity equilibrium. Wash steps act to remove non-binders whereas phage harbouring complementary motifs to the target are sterically and electrostatically bound. During the first selection round, stringency is often low and increased for subsequent rounds to allow for the dissociation of low-affinity binders. Higher stringency washes performed on amplified subpopulations often result in the isolation of the binders with the highest affinity. Wash steps are commonly performed using TWEEN20 solutions, which increase in concentration with subsequent panning rounds (Solemani Zadeh et al., 2019, Vodnik et al., 2011). Stringency can be increased by decreasing concentration of the target. This acts to isolate binding phage with the highest of affinities and slowest dissociation rates to the target (Ledsgaard et al., 2022a). Generally following wash steps, bound phage are eluted with drastic pH change or enzymatic digestion, but can be eluted with basic solutions, chaotropic agents, or competition with other antibodies or antigen (Hoogenboom, 2002). Elution by pH is traditionally carried out by incubating glycine-HCL pH 2.2 and neutralising with a tris-based solution of pH>9. This results in denaturation of the Fab releasing the phage from the target without impacting the infectivity of the phage. The addition of log phase bacteria results in infection by the eluted phage for subsequent rescue of the phage from infected bacteria cells. Alternatively, trypsin can be used which causes proteolytic cleavage of bound phage. This can be beneficial in the removal of non-specific binding wild-type phage as this process renders them non-

infectious (Kristensen and Winter, 1998). Eluted phage are amplified and titred for submission to another panning round. This process retains high affinity clones, which can be lost to incomplete recovery. Technological advances have allowed for the development of systems such as RISE (rescue and in situ selection and evaluation) which allow for rescued phage progeny to be directly captured by the target in a single step, and URSA (ultra rapid selection of antibodies) which can perform up to five selection rounds per day (Vanhercke et al., 2005, Hogan et al., 2005). Furthermore, BIAcore chip sensors which work on surface plasmon resonance can be employed to optimise wash and elution steps, thus limiting selection to a singular round, reducing the experimental time (Malmborg et al., 1996). Ultimately, stringency acts as a selective pressure and can be adapted for the isolation of recombinant phage with varying affinities.

In performing successive panning followed by elution and amplification, phage of high affinity are enriched. Generally, three rounds of panning have been recorded to be sufficient to isolate high affinity binders from libraries of up to 10^9 clones (Sparks et al., 1996). In addition to traditional panning rounds, subtractive selection can be used prior to selection. For example, panning against a known decoy can remove non-specific binders from the library, enhancing subsequent panning efficiencies. Finally, matrices of biopanning rounds, also known as cross panning, can be used to enrich antibody fragments to closely related strains of a particular pathogen (Ledsgaard et al., 2022b, Bradbury et al., 2011, Zhang et al., 2003).

Screening of phage of interest is traditionally achieved by classical ELISA, yet more recently screening has been achieved through NGS. When comparing these two methods, the yield varies the most. NGS-guided screens yield hundreds of enriched and rare clones at a rapid rate, whereas classical ELISA can be repetitive and time-consuming, identifying the few top enriched clones and where they bind, but can result in the loss of rare binders. On the other hand, NGS screening can result in limited reads, and requires a rescue step to isolate clones, in comparison to ELISA where screening provides the whole

read and clones can be isolated from the media after elution (Zambrano et al., 2022). Following the identification of phage of interest through either classical ELISA, NGS or a combination of the two methods, characterised clones of interest can be further optimised by second-generation phage libraries, known for their successes in improving antibody affinities (Barbas et al., 1994). Second-generation phage libraries aim to increase affinity maturation to the target by modifying a library of enriched clones. Vectors are usually modified during this process to distinguish between the original library and secondary library vectors. Several methods have been employed to generate affinity maturation, for example, directed mutagenesis, error-prone PCR, and DNA shuffling. Site-directed or random mutagenesis can be performed on variable regions of antibodies (Hawkins et al., 1992), specifically on CDRs (Lowe et al., 2012). In contrast, error-prone PCR introduces mutagenesis by lacking proofreading activities, thus resulting in novel proteins which may harbour mutations resulting in an enhanced affinity (Abou-Nader and Benedik, 2010). Finally, DNA shuffling usually involves chain shuffling, whereby a heavy or light chain of interest is constant, and the alternative chain is shuffled with a full repertoire from the pre-panned library (Marks et al., 1991).

Despite options to improve panning outcomes, there are various implications for selection which cannot be controlled. As previously mentioned, clonal variation can act on display, but also between clones. Variation can occur between level of expression and stability, even if each clone has the same affinity. Moreover, if one clone exhibits a higher growth rate, there will be increased progeny phage in the population for that clone (McCafferty, 1996).

4.3. Aim of chapter

In Chapter 3, validation of the initial library, by selecting between 10 and 20 clones, identified that the libraries required optimising. Of the clones selected, C13.2 and C13.6 were identical, as were C13.3 and C13.7. From this

point onwards, the project followed two avenues simultaneously. Clones C13.2 and C13.7 were taken forward for characterisation and the libraries were checked for quality using NGS at various points during construction. Once a level of reasonable diversity was established, each library was biopanned against SARS-CoV-2 trimer antigens from two variants, Lineage A and BA.5 with the aim of isolating cross-reactive high affinity binders. C13.2 and C13.7, initially identified through the first library validation, were also identified through the different rounds of the panning, suggesting the approach worked. This chapter discusses the biopanning approach and analysis of clones selected in each round of panning.

4.4. Results

4.4.1. Biopanning R1: Lineage A Trimer

The pooled libraries were validated before panning (data not shown). A subset of eight colonies from each library were selected for colony PCR to determine heavy chain inserts. Light chain-only clones were present in around 30-40% of the clones screened for C13 and C18, respectively. This was expected as combining libraries to increase overall representation, previous 5-alpha F'Iq *E. coli* libraries, which contained light chain-only clones, would also be included. PCR products from clones positive for a heavy chain insert were sequenced and all sequences were unique from each other suggesting a level of diversity had been reached (data not shown).

Biopanning was performed using a high concentration of target antigen immobilised directly to the surface of a 96-well plate. The source in which the libraries were constructed from had previously experienced enrichment through the sorting of spike-specific B-cells by FACS. Round 1 (R1) of biopanning sought to further enrich the combined libraries to SARS-CoV-2 Lineage A trimer. In a 96-well plate, 1 x 10^{11} pre-blocked phage were incubated with 5 μg/mL of direct immobilised SARS-CoV-2 Lineage A trimer for 1 hour. Following wash steps, bound phage were eluted under low pH

conditions, and neutralised with a high pH solution. Eluted phage were incubated with log phase TG1 *E. coli* for infectivity to occur. After an incubation period, the infected log phase bacteria were titred and plated. A subset of eight colonies from each library were selected for colony PCR to determine heavy chain inserts (Figure 4.1). Light chain-only clones were expected from combining libraries to increase overall representation of which 5-alpha F'Iq *E. coli* libraries contained a high number of light chain-only clones. As the primers used flanked the B*mt*I restriction site, bands would be produced for colonies positive and negative for heavy chains. For those with heavy chains present, a band around 800 base pairs were expected, and for those absent of heavy chains, thus only containing a light chain, a band of around 400 base pairs was expected. Four colonies from each library were positive for heavy chains, presenting as bands of varying lengths, around 800 base pairs (Figure 4.1). In C13, positive clones were C13R1.2, C13R1.4, C13R1.5, C13R1.6, and C13R1.7. In C18, positive clones were C18R1.1, C18R1.3, C18R1.4, and C18R1.6. Bands lower than this were noted to lack heavy chains (C13R1.8, C18R1.2, C18R1.5, C18R1.7, and C18R1.8), except for

colony C13.R1.5, which was predicted to harbour a short CDRH3. C13R1.1 failed to amplify.

To unearth the sequence variation of the positive clones, the clones were sequenced and analysed using the IMGT database. IMGT database characterisation of library sequences included information on the variable, joining, diversity genes, and the CDRH3 length and amino acid sequence. Ultralong in this study was deemed above 50 amino acids in the CDRH3. All C13 sequences were derived from the ultralong germline IgH1-7, which was expected as the germline-specific primer VH1-7 was used to amplify cDNA (Table 4.1A). This variable germline was paired with diversity region IgHD8-2 and joining region IgHJ2-4, which are commonly paired with IgHV1-7 for ultralong antibodies. The exception was C13R1.7 which was analysed as IgHD6-2 rather than IgHD8-2, however, this was suspected to be a misidentification of the IMGT database. C13R1.2 and C13R1.4 were identified as identical sequences that matched the sequence of C13.2 phage identified during library validation in Chapter 3. These clones harboured the longest

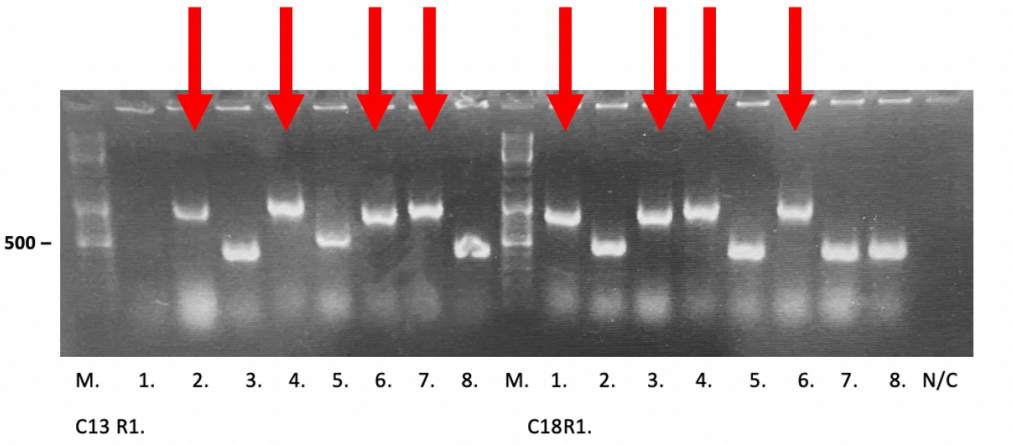

Figure 4.1: Colony PCR of R1 biopanning. Left: C13R1 clones 1-8, positive colonies 2, 4, 6 and 7 (red arrows). Right: C18R1 clones 1-8, positive colonies 1, 3, 4 and 6 (red arrows). Positive colonies for heavy chains produced a band at 800 base pairs, negative colonies absent of heavy chains produced a band at 400 base pairs. M = 10 Kb DNA molecular marker, N/C = negative control.

CDRH3 identified from the screen at 63 amino acids. Furthermore, C13R1.7 was discovered to have the same sequence as C13.7 phage, with 61 amino acids in the CDRH3. C13R1.6, however, appeared to be a shorter CDRH3 than the other sequences with a length of 31 amino acids. This correlates with its band in Figure 4.1 which was observed to be slightly lower than the others. Unfortunately, C13R1.5, which presented as a band around 500 base pairs, thought to contain a heavy chain, could not be identified by the IMGT database. This clone was suspected to be a non-valid insert containing indels within this heavy chain fragment (Table 4.1A).

Table 4.1: IMGT analysis of R1 heavy chain positive colonies. V-gene and allele, D-gene and allele, J-gene and allele, CDR3 length and CDR3 amino acid sequence for each positive clone of C13 R1 (A) and C18 R1 (B).

A

R1	V-GENE and allele	D-GENE and allele by IMGT/JunctionAnalysis	J-GENE and allele	CDRH3 Length	CDR3
C13R1.2	Bostau IGHV1-7*01 F	Bostau IGHD8-2*01 F	Bostau IGHJ2-4*01 F	63	TTVHPRTQIPGTCPTGYSYSSGCRFGP ACSSGDCCQTYNADGLGHYKCINRDY TYTNDFYVEAW
C13R1.4	Bostau IGHV1-7*01 F	Bostau IGHD8-2*01 F	Bostau IGHJ2-4*01 F	63	TTVHPRTQIPGTCPTGYSYSSGCRFGP ACSSGDCCQTYNADGLGHYKCINRDY TYTNDFYVEAW
C13R1.5	Bostau IGHV1-7*01 F				
C13R1.6	Bostau IGHV1-7*01 F	Bostau IGHD8-2*01 F	Bostau IGHJ2-4*01 F	31	TTVHCTNGYVYGSYGCYSNLLFYDSAL GVDAW
C13R1.7	Bostau IGHV1-7*01 F	Bostau IGHD6-2*01 F	Bostau IGHJ2-4*01 F	61	ATVHQKTEHSCRNGYVYHSDYTCHAD SVVDGCCCLRASGEVRDCYYHREAPT VTYQFYVDAW

B

R1	V-GENE and allele	D-GENE and allele by IMGT/JunctionAnalysis	J-GENE and allele	CDRH3 Length	CDR3
C18R1.1	Bostau IGHV1-7*01 F	Bostau IGHD4-1*01 F	Bostau IGHJ2-4*01 F	20	QRMCSYGYNCGGAEKPHLDAW
C18R1.3	Bostau IGHV1-7*01 F	Bostau IGHD4-1*01 F	Bostau IGHJ2-4*01 F	20	QRMCSYGYNCGGAEKPHLDAW
C18R1.4	Bostau IGHV1-7*01 F	Bostau IGHD4-1*01 F	Bostau IGHJ2-4*01 F	20	QRMCSYGYNCGGAEKPHLDAW
C18R1.6	Bostau IGHV1-7*01 F	Bostau IGHD4-1*01 F	Bostau IGHJ2-4*01 F	20	QRMCSYGYNCGGAEKPHLDAW

In contrast to C13, C18 library was dominated by a singular clone following R1 enrichment against the SARS-CoV-2 Lineage A trimer (Table 4.1B). The dominant sequence harboured a CDRH3 of 20 amino acids. The variable germline IgHV1-7 is not restricted to ultralong heavy chains, therefore a heavy chain with the germline IgHV1-7 can have shorter CDRH3. Identical clones of C18R1.1, C18R1.3, C18R1.4 and C18R1.6 are an example of this. The analysis

showed an alternative D gene to IgHD8-2 which is commonly paired with ultralong antibodies, which have been recorded to occur for IgHV1-7 non-ultralong heavy chains (Table 4.1). Table 4.1B analysis supports the data in Figure 4.1 whereby all positive bands (C18R1.1, C18R1.3, C18R1.4 and C18R1.6) appeared to contain a similar number of base pairs.

As the positive clones were enriched from R1 to SARS-CoV-2 Lineage A trimer, they were predicted to exhibit high binding to SARS-CoV-2 Lineage A trimer. This was assessed by performing a phage ELISA which would also determine variation in binding between each clone. As clonal variation can occur, clones that contained identical sequences were trialled for binding against each other (Figure 4.2). This identified clones that were better expressed. The combined libraries were run alongside the clones as positive controls, having previously established their binding to SARS-CoV-2 Lineage A trimer (data not shown).

The C13 combined library (C13 ALL PHAGE) displayed higher binding to SARS-CoV-2 Lineage A trimer than C18 combined library (C18 ALL PHAGE), likely to be the contribution of C13.2 phage (C13R1.2 and C13R1.4) and additional clones with high affinity to the target. Interestingly clone C13R1.4 showed greater binding to SARS-CoV-2 with a mean OD_{405} value of 1.75 compared to C13R1.2 with a mean OD_{405} value of 1.42. C13R1.7 phage (clone identical to C13.7 CDRH3) showed binding to SARS-CoV-2 Lineage A trimer, albeit less than clones C13R1.2 and C13R1.4 (clones identical to C13.2 CDRH3). Interestingly, clone C13R1.5, which likely contained a fragment rather than a full sequence of a heavy chain, showed detectable binding to SARS-CoV-2 Lineage A trimer. The light chain accompanying ultralong heavy chains is reported to be important for binding (Klewinghaus et al., 2021, Saini et al., 2003), however, the binding of this clone is likely to be non-specific. C18 R1 clones, despite harbouring the same CDHR3, had varying levels of binding suggesting clonal variation. Unexpectedly, C18R1.4 was isolated from the screen, recorded to also carry the same CDRH3, did not amplify well during the phage rescue, and therefore did not reach titres required for the phage

ELISA. This suggested that this clone was poor at expressing relative to the other clones of C18 (C18R1.1, C18R1.3, and C18R1.6).

As skewing from R1 was observed, and diversity reduced as expected from successful enrichment from biopanning, therefore continued SARS-CoV-2 Lineage A trimer screening of each library was halted and experimental design shifted to determine cross-reactive clones within the pool.

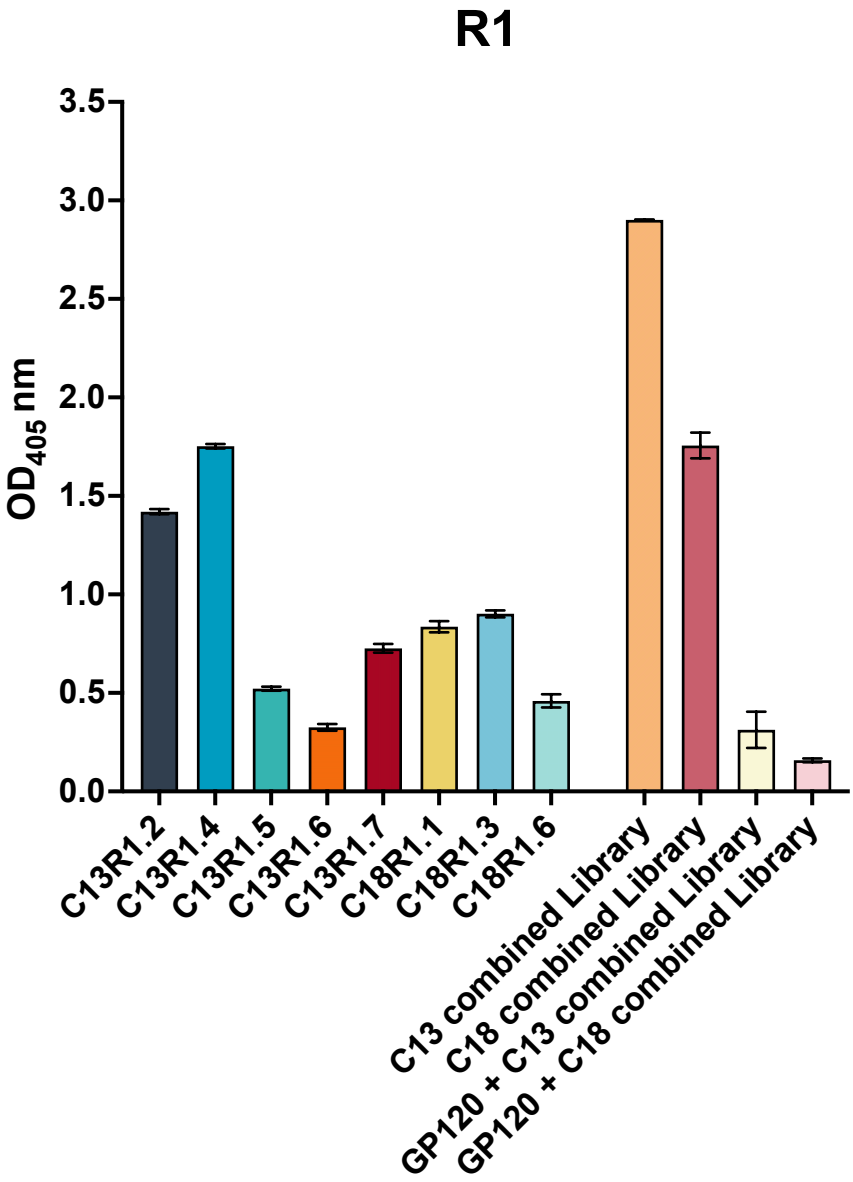

Figure 4.2: Phage binding ELISA of R1 enriched clones from C13 and C18 libraries to SARS-CoV-2 Lineage A trimer, measured as OD_{405} nm. Phage ELISA to evaluate the binding of R1 biopanning clones to SARS-CoV-2 Lineage A trimer, measured as OD_{405} nm. The combined libraries (ALL PHAGE) were trialled alongside clones as positive controls. Clones of C13 showed higher binding, as did the combined library, compared to C18 clones and C18 combined library respectively. Clonal variation was observed between clones with identical sequences, for instance C13R1.2 and C13R1.4 whereby C13R1.4 showed greater binding. C13R1.4 exhibited the highest binding to the target out of all the clones whereas clone C13R1.6 showed the lowest binding to the target. Libraries were tested for binding against an irrelevant glycoprotein, HIV gp120, as a negative control. Negative controls showed minimal binding to gp120. Error bars mark standard deviation, N=2.

4.4.2. Biopanning R2: SARS-CoV-2 BA.5 Trimer

Typically, biopanning is performed as sequential rounds against the same target with altered stringency, such as reducing the target concentration for isolating antibodies with slow dissociation rates (Ledsgaard et al., 2022a). In

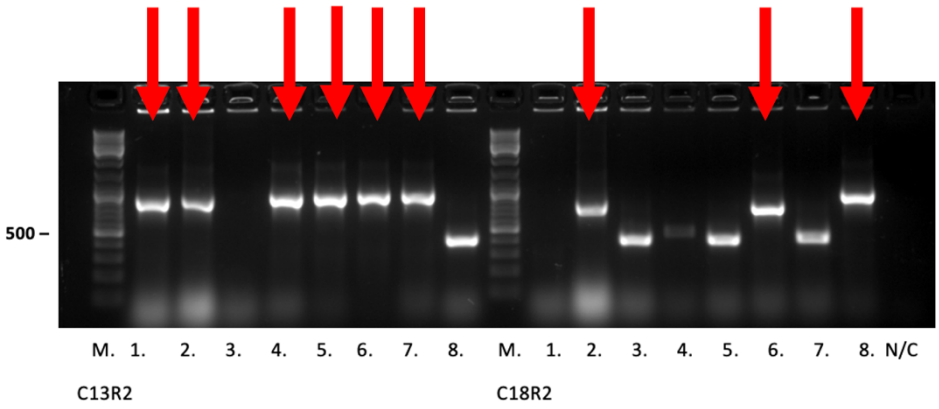

Figure 4.3: Colony PCR of R2 biopanning. Left: C13R2 clones 1-8, positive colonies 1, 2, 4, 5, 6 and 7 (red arrows). Right: C18R2 clones 1-8, positive colonies 2, 6 and 8 (red arrows). Positive colonies for heavy chains produced a band at 800 base pairs, negative colonies absent of heavy chains produced a band at 400 base pairs. M = 10 Kb DNA molecular marker, N/C = negative control.

this study, the sources received a pre-enrichment round whereby B-cells were sorted based on their reactivity to SARS-CoV-2 Lineage A trimer. R1 biopanning acted as a second enrichment round, and as skewing to specific clones was evident, such as to clones of C13.2 and C13.7, the second round of panning was altered to a closely related target. SARS-CoV-2 evolved during the pandemic, and the point in time of this study the Omicron variant BA.5 had established dominance in the UK population (GOV.UK, 2022). The second round of biopanning mirrored the first with an alteration of the target to SARS-CoV-2 BA.5 trimer. Biopanning R2 (R2) was performed on immobilised SARS-CoV-2 BA.5 trimer to select for phage clones expressing Fabs, from R1 with established affinity to SARS-CoV-2 Lineage A trimer, with cross-reactivity to the newer variant of concern SARS-CoV-2 BA.5 trimer. Analysis of eluted phage was performed as described in section 4.4.1. Figure 4.3 presents the positive and negative colonies from the PCR colony screen.

PCR of the clones from R2 showed that C13 R2 contained more clones bearing heavy chain inserts, and that the inserts were of a similar size. C18 R2, however, was observed to have less, with three of the eight screened clones bearing heavy chains of a similar molecular size, except for clone C18R2.8 which was observed to be slightly bigger than C18R2.2 and C18R2.6. Positive colonies were sequenced and analysed using IMGT database to identify heavy chains. As eluted phage from R1 was used against the target in R2, it was predicted that isolated sequences were cross-reactive to SARS-CoV-2 Lineage A trimer and SARS-CoV-2 BA.5 trimer. Table 4.2A, shows isolated sequences from C13 library R2 biopanning following the format previously described in section 4.4.1. All clones isolated matched the sequence of C13.7 phage. Since the sequence of C13.2 (C13R1.2 and C13R1.4) and C13R1.6 phage were not identified, it was theorised that these clones exhibit low or no affinity for SARS-CoV-2 BA.5 trimer. C13R2.3, C18R2.1 and C18R2.4 either failed to amplify or produced too poor a product to accurately sequence.

Table 4.2: IMGT analysis of R2 heavy chain positive colonies. V-gene and allele, D-gene and allele, J-gene and allele, CDR3 length and CDR3 amino acid sequence for each positive clone of C13 R2 (A) and C18 R2 (B).

A

R2	V-GENE and allele	D-GENE and allele by IMGT/Junction Analysis	J-GENE and allele	CDRH3 Length	CDR3
C13R2.1	Bostau IGHV1-7*01 F	Bostau IGHD6-2*01 F	Bostau IGHJ2-4*01 F	61	ATVHQKTEHSCRNGYVYHSDYTCHADSVVDGCC CLRASGEVRDCYYHREAPTVTYQFYVDAW
C13R2.2	Bostau IGHV1-7*01 F	Bostau IGHD6-2*01 F	Bostau IGHJ2-4*01 F	61	ATVHQKTEHSCRNGYVYHSDYTCHADSVVDGCC CLRASGEVRDCYYHREAPTVTYQFYVDAW
C13R2.4	Bostau IGHV1-7*01 F	Bostau IGHD6-2*01 F	Bostau IGHJ2-4*01 F	61	ATVHQKTEHSCRNGYVYHSDYTCHADSVVDGCC CLRASGEVRDCYYHREAPTVTYQFYVDAW
C13R2.5	Bostau IGHV1-7*01 F	Bostau IGHD6-2*01 F	Bostau IGHJ2-4*01 F	61	ATVHQKTEHSCRNGYVYHSDYTCHADSVVDGCC CLRASGEVRDCYYHREAPTVTYQFYVDAW
C13R2.6	Bostau IGHV1-7*01 F	Bostau IGHD6-2*01 F	Bostau IGHJ2-4*01 F	61	ATVHQKTEHSCRNGYVYHSDYTCHADSVVDGCC CLRASGEVRDCYYHREAPTVTYQFYVDAW
C13R2.7	Bostau IGHV1-7*01 F	Bostau IGHD6-2*01 F	Bostau IGHJ2-4*01 F	61	ATVHQKTEHSCRNGYVYHSDYTCHADSVVDGCC CLRASGEVRDCYYHREAPTVTYQFYVDAW

B

R2	V-GENE and allele	D-GENE and allele by IMGT/Junction Analysis	J-GENE and allele	CDRH3 Length	CDR3
C18R2.2	Bostau IGHV1-7*01 F	Bostau IGHD4-1*01 F	Bostau IGHJ2-4*01 F	20	QRMCSYGYNCGGAEKPHLDAW
C18R2.6	Bostau IGHV1-7*01 F	Bostau IGHD4-1*01 F	Bostau IGHJ2-4*01 F	20	QRMCSYGYNCGGAEKPHLDAW
C18R2.8	Bostau IGHV1-7*01 F	Bostau IGHD1-1*01 F	Bostau IGHJ2-4*01 F	27	CAKFASGDGYATCTNYYYQCAQVAYYTDW

Sequence analysis of the three positive clones from C18 library in Figure 4.3 can be observed in Table 4.2B. Clones C18R2.2 and C18R2.6 were discovered to express the same heavy chain CDRH3 amino acid sequence and can be matched to all the clones analysed in R1. Interestingly, C18R2.8 was not identified in the first round of biopanning to SARS-CoV-2 Lineage A trimer, however, was selected for in the panning against SARS-CoV-2 BA.5 trimer. The sequences selected through R2 panning did not have the standard diversity region, IgHD8-2, nor did they contain an ultralong CDRH3.

Initially, a larger screen was planned to be performed in order to extensively analyse the R2 pool from each library, however, due to time constraints this was unachievable. In addition, clones from R2 were planned to be assessed for binding against SARS-CoV-2 BA.5 trimer, like in R1 to identify clonal variation. As the aim of this study focused on ultralong antibodies, analysis of

C13.2 and C13.7 ultralong phage clones was continued. Characterisation of cross-reactive C18R2.2/C18R2.6 (identical sequences to C18R1.1, C18R1.3, C18R1.6) and C18R2.8 are recommended for continuation of this study.

4.4.3. Evaluation of panning titres

The phage titres of the pre-panned C13 and C18 combined libraries (ALL PHAGE) were 1.49 x 10^{13} cfu/mL and 1.68 x 10^{13} cfu/mL, respectively. The phage input for each round of panning was normalised to 1 x 10^{11} cfu. Figure 4.4A presents the titres obtained for R1 biopanning against SARS-CoV-2 Lineage A trimer. Elution from R1 was 2.3 x 10^{6} and 1.56 x 10^{6} cfu/mL for C13 and C18, respectively. Eluted phage was amplified for R2 biopanning. Amplified titres reached 2.07 x 10^{13} and 2.91 x 10^{13} cfu/mL for C13 and C18, respectively. After the second round of biopanning using SARS-CoV-2 BA.5 trimer as bait, 2.42 x 10^{7} for C13 and 3.1 x 10^{6} cfu/mL were eluted for the C13 and C18 libraries, respectively (Figure 4.4B). Libraries were amplified for a potential third round of biopanning. These titres reached 1.65 x 10^{13} and 1.45 x 10^{13} cfu/mL for C13 and C18, respectively. Due to time constraints, a third round of panning was not performed.

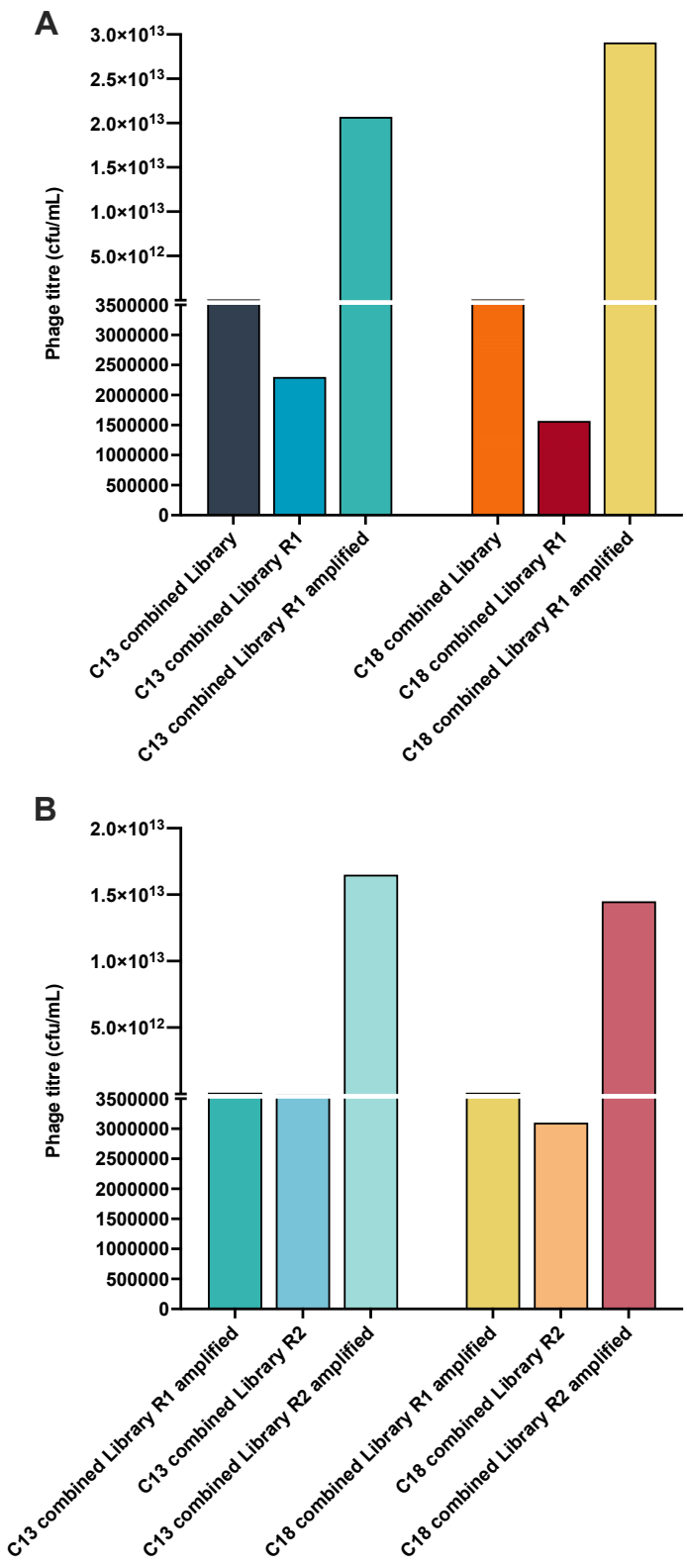

Figure 4.4: Bar chart of phage titres, measured as cfu/mL. A) Normalised input of combined libraries (ALL PHAGE) to 1 x 10^{11} cfu, R1 eluted libraries, and R1 amplified libraries for C13 and C18. B) Normalised input of R1 amplified libraries to 1 x 10^{11} cfu, R2 eluted libraries and R2 amplified libraries for C13 and C18.

4.4.4. Evaluation of biopanning binding

ELISAs were performed to evaluate the binding of the biopanning rounds, pre-panning (combined), R1 amplified eluted phage (R1) and R2 amplified eluted phage (R2), for each library (Figure 4.5). C13.2 phage served as a positive control for SARS-CoV-2 Lineage A trimer and a negative control for SARS-CoV-2 BA.5 trimer. Figures 4.5A and B refer to C13 library. As expected, in Figure 4.5A, binding to SARS-CoV-2 Lineage A trimer significantly increases from the pre-panned library to R1 ($p = <0.001$). Interestingly, panning against SARS-CoV-2 BA.5 trimer (R2) significantly increased binding to SARS-CoV-2 Lineage A trimer compared to the pre panned library, albeit less than R1 ($p = <0.001$. When this is reversed, as portrayed in Figure 4.5B, binding to BA.5 significantly increases from R1 to R2, as expected ($p = <0.001$). Furthermore, enrichment from the pre-panned library to R2 is shown to be significant ($p = <0.0001$). In Figure 4.5B, R1 enrichment to SARS-CoV-2 Lineage A trimer also increased binding to BA.5 trimer ($p = <0.001$).

Unexpectedly, these trends were not observed in C18 library, Figures 4.5C and 6D. An increase from pre-panned to R1 was expected when panning against SARS-CoV-2 Lineage A trimer, however, binding was low and non-significant. In Figure 4.5C, R2 appeared to have significant binding over the pre-panned library ($p = <0.001$). This trend was observed in Figure 4.5A, however, binding of R2 was significant over R1 in Figure 4.5C, in which enrichment was expected for this round of panning ($p = <0.001$). Notably, C18 pre panned showed greater binding to SARS-CoV-2 BA.5 trimer than SARS-CoV-2 Lineage A trimer. The binding of R1 to SARS-CoV-2 BA.5 trimer was lower which was expected as R1 was enriched towards SARS-CoV-2 Lineage A trimer Figure 4.5D). R1 to R2 showed a significant increase in binding showing enrichment ($p = <0.05$), as expected, however, the binding of R2 to SARS-CoV-2 BA.5 trimer was lower than the binding observed in the pre-panned library.

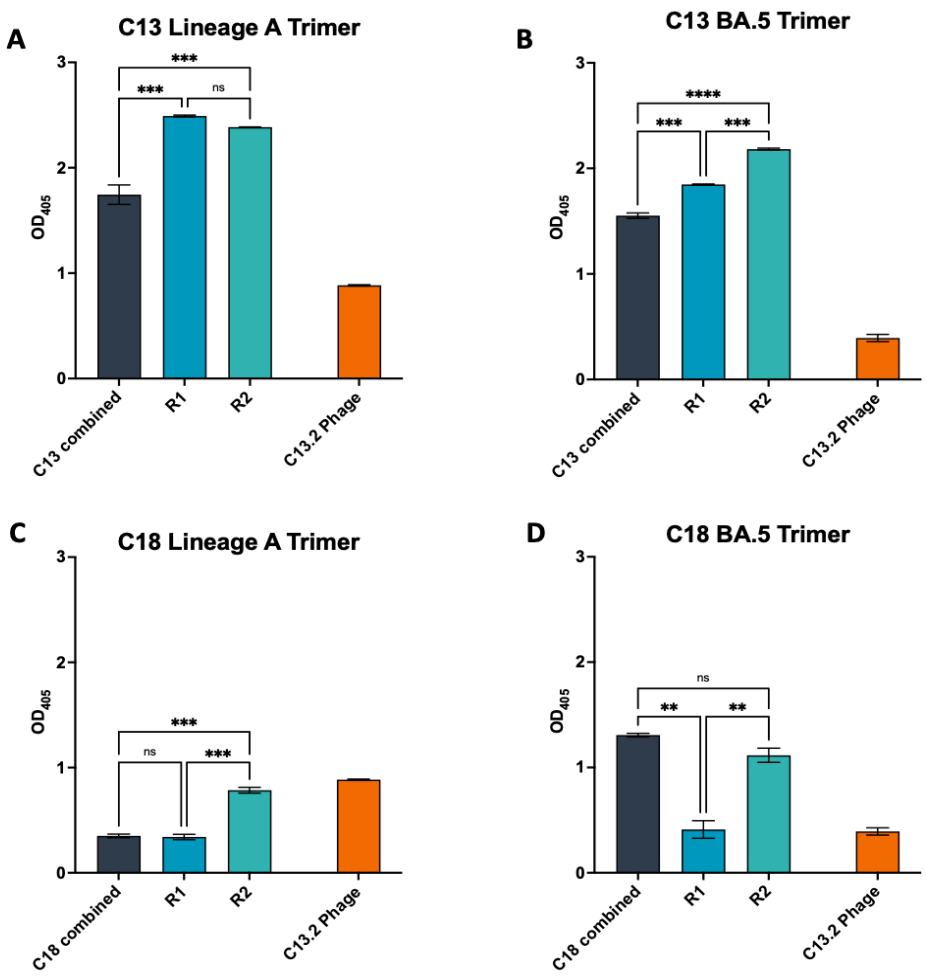

Figure 4.5: Phage ELISA binding of pre-panned, R1 and R2, normalised to 10^{11} cfu, of each library to SARS-CoV-2 Lineage A and BA.5 trimers, measured as OD_{405} nm. A) Comparison of C13 pre-panned combined library, R1 library, R2 library to SARS-CoV-2 Lineage A trimer. B) Comparison of C13 pre-panned combined library, R1 library, R2 library to SARS-CoV-2 BA.5 trimer. C) Comparison of C18 pre-panned combined library, R1 library, R2 library to SARS-CoV-2 Lineage A trimer. D) Comparison of C18 pre-panned combined library, R1 library, R2 library to SARS-CoV-2 BA.5 trimer. A-D) C13.2 phage as a positive control for Lineage A trimer, or negative control for BA.5 trimer. Statistical significance by One Way ANOVA and Tukey's multiple comparisons test, N=2, **p = <0.05, *** p = <0.001, **** p = <0.0001. Error bars demark standard deviation.

4.5. Discussion

Paramount to infection, the trimeric glycoprotein of SARS-CoV-2 has been a target for the majority of therapeutics for COVID-19. Displayed on the viral surface, the trimer is a direct target for the immune system. The first recorded strains of SARS-CoV-2, sampled between 5 January–27 April 2020, were denoted to Lineage A. Thus, this was chosen as the immunogen for the immunisation of *Bos Taurus,* and therefore the main target for biopanning the immune libraries generated in Chapter 3.

In this study, biopanning was designed to select for high affinity binders. To further work from Chapter 3, antigen immobilisation occurred directly to a 96-well plate at a high concentration of 5 μg/mL. Direct coating was selected for target immobilisation because as witnessed in this study, capturing biotinylated target resulted in the accumulation of non-specific binding of the phage. Several methods have been documented to overcome these issues, such as subtractive selection, also known as negative selection, whereby the library is washed over an immobilised contaminant to remove non-specific binders (Eisenhardt et al., 2007, Lim et al., 2019). In this study, however, a high concentration of antigen target was selected for saturation of wells, and to reduce background non-specific binding, as recommended in studies of Katakura et al., McConnell et al., and Rahbarina et al. (McConnell et al., 1999, Katakura et al., 2002, Rahbarnia et al., 2016).

Phage libraries were normalised to 1 x 10^{11} and pre-blocked in a blocking agent to reduce non-specific binding. Incubation was carried out for 1 hour with gentle agitation to encourage binding. Saturant was changed in between panning rounds to remove non-specific binding to blocking buffers, as performed by studies such as Lausten et al. and Zadeh et al. (Solemani Zadeh et al., 2019, Laustsen et al., 2017). In accordance with this, wash steps increased from 10 in R1 to 20 in R2, with each wash increasing in

concentration of TWEEN20 by 0.1%, to increase stringency. Altering these parameters aimed to reduce non-specific binding during panning.

This chapter focused on evaluating biopanning rounds. Light chain-only clones were present in around 30-40% of the clones screened for the pre-panned C13 and C18, respectively. This was expected as combining libraries to increase overall representation, previous 5-alpha F'Iq *E. coli* libraries, which contained light chain-only clones, would also be included. These clones were identified throughout panning, but did not increase in percentage, and even decreased on screening of C13 R2, suggesting there was no bias for their selection for over heavy chain clones, and that they may have reduced following increased stringency of subsequent panning rounds. Despite the presence of light chain only phage, Figure 4.1 showed that R1 selected phage clones had heavy chains of varying molecular sizing. This suggested that these heavy chains varied in their CDR3 length. During this screen, analysis of clone C13R1.5 which was thought to contain a heavy chain, harboured a non-valid insert. An advantage of the phagemid system is resistance to deletions, thus are more genetically stable (Chasteen et al., 2006), therefore a potential explanation for this clone could have arisen from a mutation during PCR.

R1 screening identified the presence of identical sequences from a relatively small screen. This could suggest that bias already existed in the pre-panned library from the enrichment of FACS. Secondly, due to this preselection, initial library diversity is likely to be lower than that of a traditional immune library. Isolation of RNA was performed on approximately 4,000 B-cells from each library and ultralong germline antibodies, comprising of 10-15% of the population, were amplified, therefore this selection had a high likelihood reducing the diversity of the source further. During this process, phage of interest C13.2 and C13.7, which were known binders to SARS-CoV-2 Lineage A trimer (Chapter 3, Figure 3.16), were identified following R1 (C13.2 = C13R1.2 and C13R1.4, C13.7 = C13R1.7). This assured that the biopanning was successful and reflected the high representation of these two sequences within the NGS ALL PHAGE dataset. Indeed, C13.7 heavy chain sequence was

found in 106 times out of 162 sequences with a CDRH3 length of 61 amino acids, and C13.2 heavy chain sequence was found 58 times out of 87 sequences with a CDRH3 length of 63 amino acids. This suggests these sequences are well represented in multiple B cells within the source. These sequences, identified originally through library validation, showed high affinity binding to SARS-CoV-2 Lineage A trimer and therefore were further investigated as chimeric mAbs. This was discussed in Chapter 5. Analysis of clones isolated from R1 showed the enrichment of specific clones (Table 4.1), and differences in levels of binding despite certain clones being identical (Figure 4.2). For instance, C13R1.2 and C13R1.4 (identical sequence to C13.2 phage), and C18R1.1, C18R1.3 and C18R1.6. and clones C13R1.2 and C13R1.4. An explanation could be that the expression level varies between clones, or alternatively, titres could vary as cfu/mL only serves as an estimation and not an accurate concentration. Out of all the clones screened, C13R1.2 and C13R1.4 (identical sequence to C13.2 phage) was an ultralong antibody which showed the highest level of binding to SARS-CoV-2 Lineage A trimer and so this clone's characterisation was continued during R2 panning.

A second panning round to SARS-CoV-2 Lineage A trimer with higher stringency would have identified which clones from R1 that had high affinities to the trimer. Thus, those with lower affinity would dissociate from the target, resulting in the elution of those with the highest affinity to the trimer. However, as FACS acted as a prior round of enrichment, and skewing to specific clones was observed following R1, the study followed the possibility of identifying a bovine ultralong Fab with cross-reactivity to different variants by harnessing the power of phage display biopanning.

First identified in early 2022, SARS-CoV-2 BA.5 became a highly transmissible sub-lineage of the Omicron variant, recorded to harbour 35 mutations in the spike protein compared to Lineage A strains, hence selected as a variant of concern. BA.5 was proven to be resistant to most monoclonal antibodies and reported causative of breakthrough infections from those with natural or passive immunity (Shrestha et al., 2022). Moreover, future variants were

predicted to stem from this variant as it established dominance (Tanne, 2022), therefore, the subsequent round target was switched to SARS-CoV-2 BA.5 trimer. This additional round of panning sought to identify high affinity binders from R1 that may have cross-reactivity to SARS-CoV-2 BA.5 trimer, thus potentially identifying broadly reactive antibodies to SARS-CoV-2.

The stringency level of the second round of panning was increased to ensure that phage binding were of high affinity. This was achieved through changing the blocking buffer and increasing the number of washes and TWEEN20 concentrations to reduce non-specific binding. Screening of C13 colonies in Figure 4.3, showed a distinct reduction of phage absent of heavy chain inserts present in R1 suggesting that the presence of these binders in the round was largely non-specific or of low affinity. Interestingly, in this library, one clone dominated the screen. Table 4.2 shows all clones screened carrying an identical heavy chain to C13.7 phage, a clone present in the validation of the library, and enriched following R1 panning, suggesting a potential Fab that had high affinity for SARS-CoV-2 Lineage A trimer and SARS-CoV-2 BA.5 trimer. In contrast, analysis of C18 R2 highlighted two clones carried through from R1 of 20 and 27 amino acids in the CDR3. C18R2.2 and C18R2.6, corresponding to all clones identified in R1, were found to be highly represented in the NGS. On the other hand, clone C18R2.8 was not identified in R1 screen, therefore may have been a rarer clone from R1 and enriched in R2. This suggests this clone may have a higher affinity for SARS-CoV-2 BA.5 trimer compared to SARS-CoV-2 Lineage A trimer.

Biopanning titres can be analysed to validate enrichment, particularly when using a singular target for multiple rounds whereby an increase in titres would be expected as enrichment occurs. Combining the rounds in the same analysis would not be valid for this experiment as the target was altered between panning rounds, thus aiming to isolate cross-reactive Fab. Therefore, titres were kept separate for each round. Investigating titres across rounds could be achieved if a third round of panning was performed against one of the baits.

Analysis of titres in Figure 4.4 served as validation of amplification of eluted phage.

Enrichment was evaluated using phage ELISA. It was predicted that when comparing R1 to the input of pre-panned libraries, an increase in binding to SARS-CoV-2 Lineage A trimer would be observed as a confirmation of enrichment. Moreover, when comparing R2 to R1, an increase in binding to SARS-CoV-2 BA.5 trimer would be expected. This was evident for C13 library, in Figure 4.5A, where significant increases in these expected trends were observed, and moreover, a significant increase of binding to SARS-CoV-2 Lineage A trimer was observed from pre-panned to R2 suggesting the presence of cross-reactive phage ($p = <0.001$). There was a slight decrease in binding to SARS-CoV-2 Lineage A trimer between R1 and R2 which was expected with target change. An increase of binding to SARS-CoV-2 BA.5 trimer between R1 and R2 was observed which was expected (Figure 4.5B). Furthermore, an increase in binding to SARS-CoV-2 BA.5 trimer was observed between pre-panned and R2 suggesting R1 enrichment to SARS-CoV-2 Lineage A trimer modestly enriched the binding activity of SARS-CoV-2 BA.5 trimer binders within the library. Despite R1 enrichment to SARS-CoV-2 Lineage A trimer, R1 showed a higher level of binding to SARS-CoV-2 BA.5 trimer than the pre-panned library, further implicating the presence of cross-reactive binders. Clones isolated from R2 were suspected to have high affinity for both targets implying that these clones may recognise conserved epitopes between the two trimers.

By contrast, C18 library did not reflect the patterns exhibited by the C13 phage library. This library was known to have reduced diversity and reduced binding from the phage ELISA in Chapter 3 (Figure 3.21). Figures 4.5C and D show reduced binding in comparison to C13 phage library, as expected. In Figure 4.5C, an increase of binding to SARS-CoV-2 Lineage A trimer between pre-panned and R1 was expected, however, binding was not significant. Additionally, R2 had significant binding to SARS-CoV-2 Lineage A trimer compared to both pre-panned and R1 ($p = <0.001$). A potential explanation

was that there could have been a contaminant in the R2 phage preparation. R2 biopanning showed a reduction of binding from pre-panned to R1 suggesting clones with binding SARS-CoV-2 BA.5 trimer were not enriched when panning against SARS-CoV-2 Lineage A trimer (Figure 4.5D). This is supported by the identification of C18R2.8 which was not found in the R1 screen. This trend, however, was reversed for R2 where binding increased for SARS-CoV-2 BA.5 trimer between R1 to R2, thereby showing enrichment. Nonetheless, the pre-panned library showed greater binding to SARS-CoV-2 BA.5 trimer than R2 which was unexpected, however, this was non-significant.

Time constraints prevented further characterisation of these libraries; however, a second-generation library was planned. The light chains of the B-cell bulk sort sources could be amplified, and the light chain library shuffled into the phagemid vector of a common heavy chain of interest. The resultant library, panned against targets of interest, may result in the identification of a clone with an affinity-enriched heavy chain from the first-generation library, and an affinity-enriched light chain from the second-generation library. This may isolate a clone with superior affinity to the target. Furthermore, this study considered panning against S2, however, S2 antibodies are recorded to be less potent so this was not explored. These options highlight further applications of phage display in the search for broadly neutralising antibodies.

4.6. Conclusion

In summary, biopanning can be altered and modified to isolate a range of antibodies on a spectrum of varying affinities. Consideration of display formats, targets and their quality, library quality, stringency, elution, and panning rounds are required for effective panning of phage display. Ultralong bovine repertoires were subjected to two rounds of biopanning against the SARS-CoV-2 Lineage A trimer and the more recent variant of concern, SARS-CoV-2 BA.5 trimer. The initial interest in ultralong C13.2 phage and C13.7

phage, identified through library validation, resulted in their characterisation. These phage clones were also identified through the biopanning process with C13.2 phage, displaying high binding to SARS-CoV-2 Lineage A trimer, and C13.7 phage, showing cross-reactivity to both SARS-CoV-2 Lineage A trimer and SARS-CoV-2 BA.5 trimer, validating the biopanning process. Non-ultralong clones of interest showing cross-reactivity, such as C18R2.2/C18R2.6 and C18R2.8 are recommended to be investigated further through their characterisation.

Chapter 5 Characterisation of chimeric ultralong antibodies

5.1. Summary

Since the SARS-CoV-2 pandemic, antibody therapies have increased in popularity as treatments for infectious diseases, with over 75 in current clinical trials against 20 infectious pathogens, and more in the preclinical pipeline (Whaley and Zeitlin, 2022). Despite this, infectious diseases remain unpredictable. The rapid emergence of novel SARS-CoV-2 variants challenged the effectiveness of current therapeutics and vaccines. Broadly neutralising therapeutics which can withstand antigenic evolution are therefore highly desirable. Research into bovine ultralong antibodies has advanced in recent years highlighting their clinical potential as diagnostics and therapeutics. Two chimeric bovine ultralong antibodies, C13.2 and C13.7, were generated and characterised. C13.7 exhibited cross-reactivity to *Sarbecovirus* and SARS-CoV-2 strains, and neutralisation of pseudotyped variants of concern *in vitro.* This chapter focuses on the characterisation of mAbs C13.2 and C13.7 to broaden our understanding of bovine ultralong antibodies and to determine their clinical potential as diagnostics and therapeutics.

5.2. Introduction

Antibody therapies are relatively well-established as treatments for cancers and autoimmune diseases, however, are not the classical choice for treating infectious diseases due to cost and complexities in production (Pelfrene et al., 2019, Saylor et al., 2009). For the short term, antibiotics, antifungals and antivirals are commonly used, yet long-term solutions often require antibody therapy. Viruses, however, are challenging to target as the infectious mechanism is often unknown (Salazar et al., 2017).

Traced back to the 20th century, serum therapy, now known as intravenous immunoglobulin, was the first recorded antibody treatment for viral agents (Stangel and Pul, 2006). Since then, antibody therapeutics and their isolation have developed. From the mid-1970s, hybridoma technology, followed by display methods of phage, ribosome, yeast, bacterial and mammalian, or cell sorting methods, were explored for selection of antibody therapies to viral agents (Valldorf et al., 2022). The success of these approaches has resulted in multiple candidates, either approved or in clinical phases, for current viral diseases. For instance, CSJ148 (Macagno et al., 2010) and MSL-109/Serivumab (Manley et al., 2011) for Human Cytomeglovirus (HCMV), MHAA4549A (Gupta et al., 2016) and CR6261 (Ekiert et al., 2009) for Influenza, VRC01 (Wu et al., 2011), 3BNC117 (Caskey et al., 2015) and Ibalizumab (US/EU approved) (Blair, 2020) for HIV, Synagis (Palivizumab; MEDI-493) (McLellan et al., 2010), Motavizumab—YTE (Robbie et al., 2013) and REGN2222 (Bournazos and Ravetch, 2017) for Respiratory Syncytial Virus (RSV), m366.6 (Hu et al., 2019) for Dengue, AR4A (Giang et al., 2012) for HCV, ZMapp (Qiu et al., 2014) for Ebola, and Rabishield (Kaza and Nathan, 2023) (EU approved) for Rabies. Several of these antibodies were modified for their use as therapeutics, such as altering Fc regions, thereby resulting in a longer half-life, or altering animal-derived antibodies to reduce the immunogenicity (Lu et al., 2020b). The latter is achieved by modifying antibodies to be humanised or chimeric. Humanised antibodies are altered by inserting CDRs of interest into human antibody scaffolds whereas chimeric antibodies retain Fab regions, from the host they are raised in, fused to human constant regions so that animal-derived Fab can bypass immunogenicity (Waldmann, 2019). Examples of chimeric antibodies include Atezolizumab, Cusatuzumab and Caplacizumab (Alfaleh et al., 2020). Occasionally, these antibodies are recognised as immunogenic despite the Fc modification, presenting challenges for their use as therapeutics. As of 2020, only one chimeric antibody, employed for the treatment of anthrax, Obiltoxaximab, was approved in US and EU for use (Greig, 2016), suggesting a need to develop and further modify current mAbs to reduce their

immunogenicity, increase their stability, and to closely mirror human-like properties, thus allowing for higher tolerance to non-human regions.

Historically, Coronaviruses are prone to zoonotic spillover events from their natural reservoirs. In the last 20 years, three reports of zoonotic respiratory *Betacoronaviruses* have been well documented, including SARS-CoV in 2002, MERS-CoV in 2011 (Perlman and Netland, 2009) and as of 2019, SARS-CoV-2. The emergence of SARS-CoV-2 resulted in vast developments in antibody therapeutics, identifying multiple candidates that could be administered immediately to provide passive protection against severe disease. MAbs are highly specific and associated with a high confidence of safety despite the speed at which they are developed at from discovery to trials. The majority of mAb candidates for SARS-CoV-2 targeted the RBD in the spike of the virion, blocking RBD–ACE2 interaction, thus preventing disease progression. However, this area was highly susceptible to variation, resulting in variants that could escape mAb neutralisation.

In the early stages of the pandemic (February 2021) the US FDA announced the emergency administration of mAbs Bamlanivimab and Etesevimab, followed by Casirivimab and Imdevimab later that year. Despite the success of mAbs in the early pandemic, the emergence of subsequent variants Beta (B.1.351) and Gamma (P1) reduced the efficacy of Bamlanivimab and Etesevimab, resulting in the removal of their approval for treatment of COVID-19. Later variants of Delta (B.1.617.2) and Omicron (B.1.1.529) impacted the efficacy of Casirivimab and Imdevimab (Widyasari and Kim, 2023). Antibody combinations or cocktails were produced to reduce the impact of escape variants, for example, Evusheld comprised of mAbs Tixagevimab and Cilgavimab. Evusheld, and individual mAbs of Bebtelovimab and Sotrovimab, retained efficacy against omicron sublineages BA.2.12.1, and BA.4/BA.5, however, a reduction of activity was recorded against more recent variants BQ.1.1 and XBB.1.5 (Imai et al., 2023, Iacobucci, 2023). Recurrent mutations at, what appeared to be, mutational hotspots in sublineages of Omicron suggest convergent evolution in response to the selective pressure

of population humoral immunity. For instance, Omicron subvariant XBB, which was derived from a breakpoint recombination event in the Omicron BA.2 subvariants, harboured the F486S mutation, whereas Omicron BA.5 harboured the mutation F486V. Convergent mutations at the hotspots are suspected to disrupt mAb activity. At the point of this study, Sotrovimab was the only mAb in the clinical pipeline retaining EC_{50}s of 806.6 ng/mL to XBB and 1238 ng/mL to BQ.1.1 (Touret et al., 2023). As these new variants establish dominance within the population, it is likely that emerging variants will derive from current dominant strains, therefore, a broadly neutralising mAb is highly desirable.

Bovine ultralong antibodies, despite representing a small subset of the repertoire, allow cattle to mount diverse antibody responses to pathogens. These antibodies are recorded to be rapidly produced in response to antigenic exposure. The ultralong CDRH3 forms a unique paratope structure protruding from the antibody, enabling binding to challenging epitopes. For instance, an ultralong bovine antibody was discovered to bind to the complex surface glycoprotein of HIV. The ultralong antibody, NC Cow 1, exhibited a cross-clade HIV neutralisation of 79% in response to HIV GP140 SOSIP Env trimer, resulting in a median IC_{50} of 28 ng/mL (Sok et al., 2017). More recently, a bovine ultralong antibody, B9, was discovered to be broadly reactive to SARS-CoV-2 and SARS-CoV (Burke et al., 2022). Furthermore, ultralong knobs are documented to function independently without a reduction in neutralisation capabilities suggesting the Fc region is not necessary for knob stability or function. Indeed, Fc receptor response has its importance in an infection, Sok et al. demonstrated transplant of the ultralong knob onto the Fc region of PG9, a broadly neutralising human antibody. The transplant was successful with a modest reduction in neutralisation breadth and potency (Sok et al., 2017). This implies bovine ultralong CDRH3s, raised against challenging disease agents, can be readily modified suggesting a promising avenue for antibody therapeutics.

Vaccines were thought to be a panacea during the SARS-CoV-2 pandemic, reducing disease severity and decreasing transmission, however, current vaccines do not produce sterilising immunity, therefore, leaving individuals such as the immunocompromised vulnerable. Immunity was recorded to be enhanced with booster vaccines, inducing high antibody titres, however, may not increase the specificity of the B-cell response and therefore have a reduced effect on escape variants (Goel et al., 2021b). Despite vaccination, reinfections have been recorded throughout the pandemic, suggesting this may have occurred (Goldberg et al., 2022, Goel et al., 2021a). Moreover, certain individuals may not mount a protective response to the vaccines, or those who are vulnerable or immunocompromised may not be able to receive the vaccine, suggesting a need for additional therapeutics.

Coronaviruses exhibit pandemic potential due to their high incidence of zoonotic transfer; therefore, it is unlikely that SARS-CoV-2 will be the last. Preparedness to future pandemics pivots on the identification of candidates targeting conserved epitopes of the *Sarbecovirus* family. This illustrates the need for complementary therapeutics, which may have a dual purpose of diagnosis and prophylaxis, with a broad spectrum of activity while retaining potency. These therapeutics will need to be rapidly deployed in response to pathogenic threats and accompany the antigenic evolution of pathogens.

5.3. Aim of chapter

Two bovine ultralong Fab were identified through validation of a phage display library, derived from B-cell enriched sources. Fab of the phage of interest was amplified and cloned into cassettes in vectors for mammalian expression of chimeric mAbs. These mAbs were characterised and analysed to determine their reactivity and *in vitro* neutralisation to pseudotyped SARS-CoV-2 variants, and potential cross-reactivity to *Sarbecovirus* RBD strains.

5.4. Results

Fab of the phage of interest were amplified and cloned into cassettes within a vector for the expression of bovine ultralong Fab on human Fc of IgG to produce chimeric mAbs. Characterisation of mAbs C13.2 and C13.7 involved analysing the CDRH3 sequences to gain an understanding of the knob and stalk and evaluating the expression and concentration of mAbs. To accurately characterise mAbs, preparations were purified prior to binding and competition ELISAs, and pseudotype neutralisation assays. Characterisation aimed to determine their reactivity, binding profile and begin to uncover their clinical potential.

5.4.1. Subcloning Fab of interest into mammalian expression vector

Validation of the initial library identified two phage clones of interest, C13.2 and C13.7. C13.2 exhibited a high level of binding to SARS-CoV-2 Lineage A trimer, and C13.7 which showed cross-reactivity to SARS-CoV-2 Lineage A and BA.5 trimer. To further this work, the Fab of the phage were amplified and cloned into cassettes for the expression of bovine ultralong Fab on human Fc, producing chimeric IgG. The light chain previously amplified for cloning into the phagemid contained homologous arms to be cloned directly into the light chain cassette. However, heavy chains amplified from the phagemids lacked an upstream segment of DNA from the heavy chain constant region required for the ligation into the heavy chain cassette. To rectify this, a plasmid containing a full heavy chain was linearised by PCR. A gradient PCR was performed, Figure 5.1A shows 67.5, 69.4, and 70.7°C annealing temperatures, with bands around 6000 base pairs, successful for plasmid linearisation. Heavy chains were PCR amplified from the phagemids of C13.2 and C13.7 using designed primers with homologous arms complementary to the PCR linearised plasmid for InFusion cloning (Figure 5.1B). This produced products at around 500 base pairs which when sequenced confirmed the desired product for both chains.

Heavy chain products were cloned using Infusion cloning and transformed. Colonies were subsequently screened by PCR. Figure 5.1C shows seven out of eight colonies positive for C13.2 heavy chain and Figure 5.1D shows all colonies positive for C13.7 heavy chain, at around 1,800 base pairs. C13.2H 5 and C13.2H 8 failed to amplify. Sequencing of clones revealed those with desired sequences, therefore these clones were amplified, and plasmids purified for mammalian expression by transient transfection.

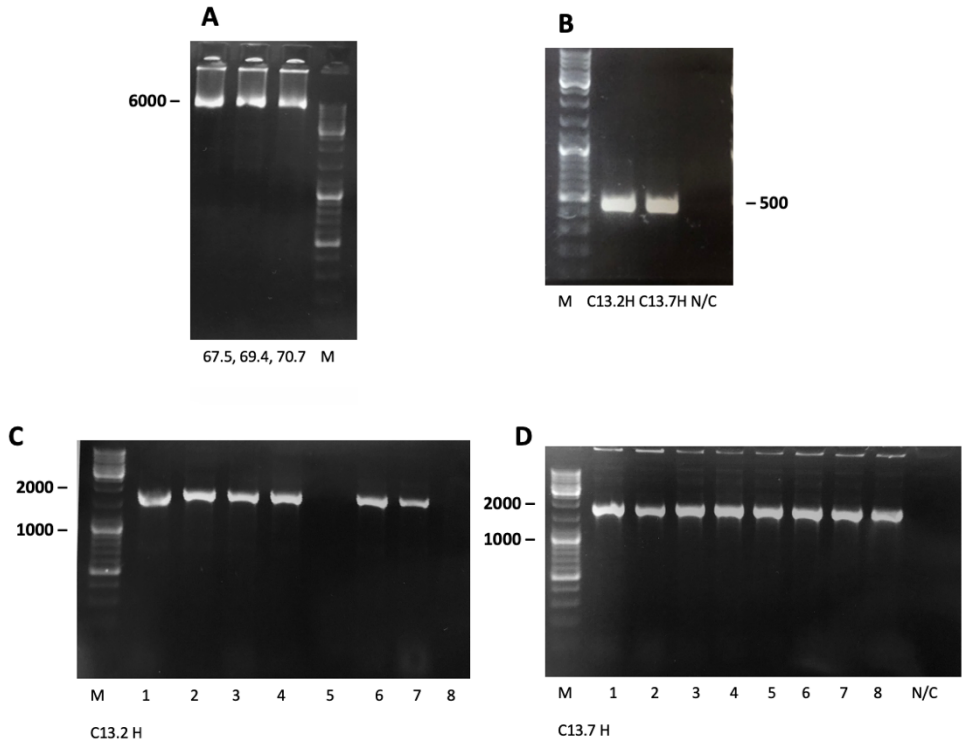

Figure 5.1: Subcloning of Fab from phagemids of interest for mammalian expression. A) PCR linearisation of a heavy chain plasmid, positive products produced bands at 6000 base pairs for annealing temperatures 67.5, 69.4 and 70.7°C. B) Amplification of C13.2 and C13.7 heavy chains for subcloning. Positive products produced a band at 500 base pairs. (C). Colony PCR screen of C13.2 heavy chain positive colonies 1, 2, 3, 4, 6 and 7 at 1,800 base pairs. D) Colony PCR screen of C13.7 heavy chain positive colonies 1-8 at 1,800 base pairs. A-D) M = 10 Kb DNA molecular marker, N/C = negative control.

5.4.2. CDRH3 sequence analysis

Initial analysis of the C13.2 and C13.7 mAb CDRH3 sequences identified that both CDRH3 sequences had six cysteines and were of variable length. Figure 5.2 subdivides each CDRH3 into each corresponding V, D and J regions, identifying the stalk which supports the knob structure. C13.2 is longer by two amino acids, with a CDRH3 of 63, compared to C13.7 CDRH3 of 61. Interestingly, C13.7 CDRH3 has three adjacent cysteines within its knob, which may form disulphide bridges with each independent cysteine, forming a complex globular structure.

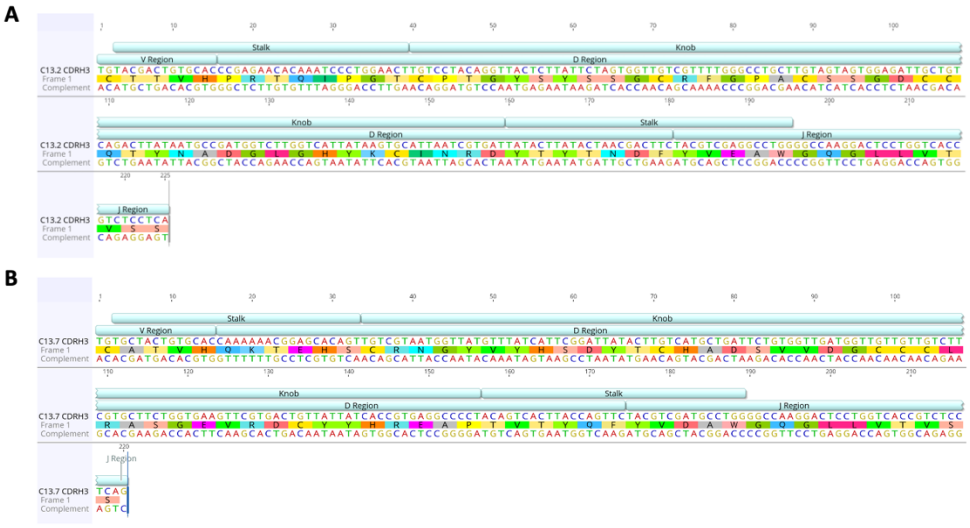

Figure 5.2: mAb CDRH3 sequence analysis. A) mAb C13.2. B) mAb C13.7. Annotated knob and stalk, and VDJ regions, showing base pairs and translated amino acids using Geneious Prime Version 2021 2.2.

5.4.3. HEK293T expression of mAbs

The chimeric mAbs were produced by transfecting HEK293T cells at a density of 3 x 10^6, with light and heavy chain plasmids to investigate the degree of expression. The IgG ELISA captured heavy chains and detected light chains, thus quantifying full IgG present in the sample. Figure 5.3 shows the

interpolation of C13.2 and C13.7 derived from a standard curve. This experiment yielded concentrations of 48 and 20 μg/mL for C13.2 and C13.7, respectively. Comparison of the concentrations to previous in-house

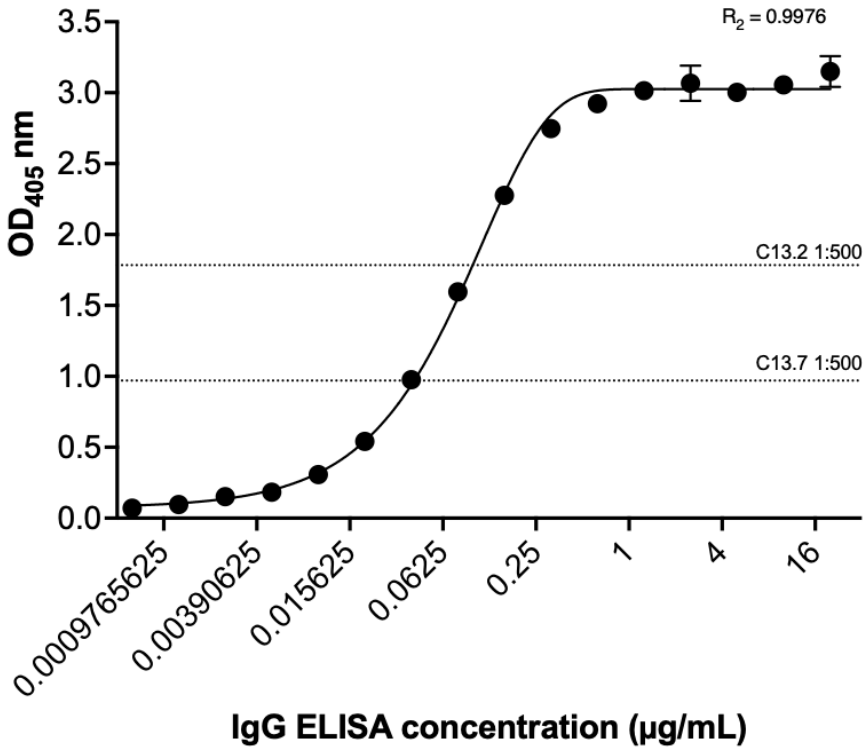

	Mean OD	Interpolated value from curve	Dilution factor	Concentration μg/mL
C13.2	1.783	0.0974	1:500	48.687
C13.7	0.970	0.0407	1:500	20.362

Figure 5.3: IgG ELISA concentration interpolation of HEK293T expressed mAbs. Top: Absorbance measured at OD_{405} nm and concentration measured in μg/mL. Concentration of mAbs interpolated from a non-linear fit to standards of a known concentration, represented as a dotted line at the dilution used to determine concentrations. Error bars demark standard deviation, N=2. Bottom: Table showing interpolation of mAb concentration from HEK293T expression, displaying mean optical density (OD) at 405 nm, interpolated X value, dilution factor and concentration in μg/mL.

expression of bovine ultralong antibodies showed that C13.2 and C13.7 expressed well in HEK293T cells.

5.4.4. Initial investigations into mAb binding and pseudovirus neutralisation

C13.2 and C13.7 demonstrated binding to SARS-CoV-2 Lineage A trimer as a Fab-phage complex, therefore binding was tested to ensure this interaction was maintained following modification to chimeric mAbs. The mAbs were tested for binding against SARS-CoV-2 Lineage A Full length (FL) spike and RBD in comparison to the trimer. MAbs were also tested for binding to full length (FL) spike of Alpha (B.1.1.7), Beta (B.1.351), and Omicron (B.1.1.529) trimer. A non-ultralong chimeric mAb, 18.99, isolated from C18 by single B-cell sorting, had high affinity to these antigens and thus was tested in comparison as a positive control. Curves observed in Figure 5.4 show that C13.2 and C13.7 exhibited higher binding to all targets tested compared to mAb 18.99. C13.2 EC_{50}s ranged between 1-33 ng/mL and had the highest binding to all targets, except for Omicron (B.1.1.529) trimer, where the EC_{50} for C13.7 was lower (34 ng/mL for C13.2 compared to 19 ng/mL for C13.7). C13.7 EC_{50}s ranged between 5-19 ng/mL for the targets tested. Interestingly, all mAbs required a higher EC_{50} to bind Omicron (B1.1.529) trimer over the other antigens, C13.7 EC_{50} was 19 ng/mL, compared to 33.6 ng/mL for C13.2 and 394.6 ng/mL for 18.99. 18.99 EC_{50}s ranged between 18-394 ng/mL for the targets tested.

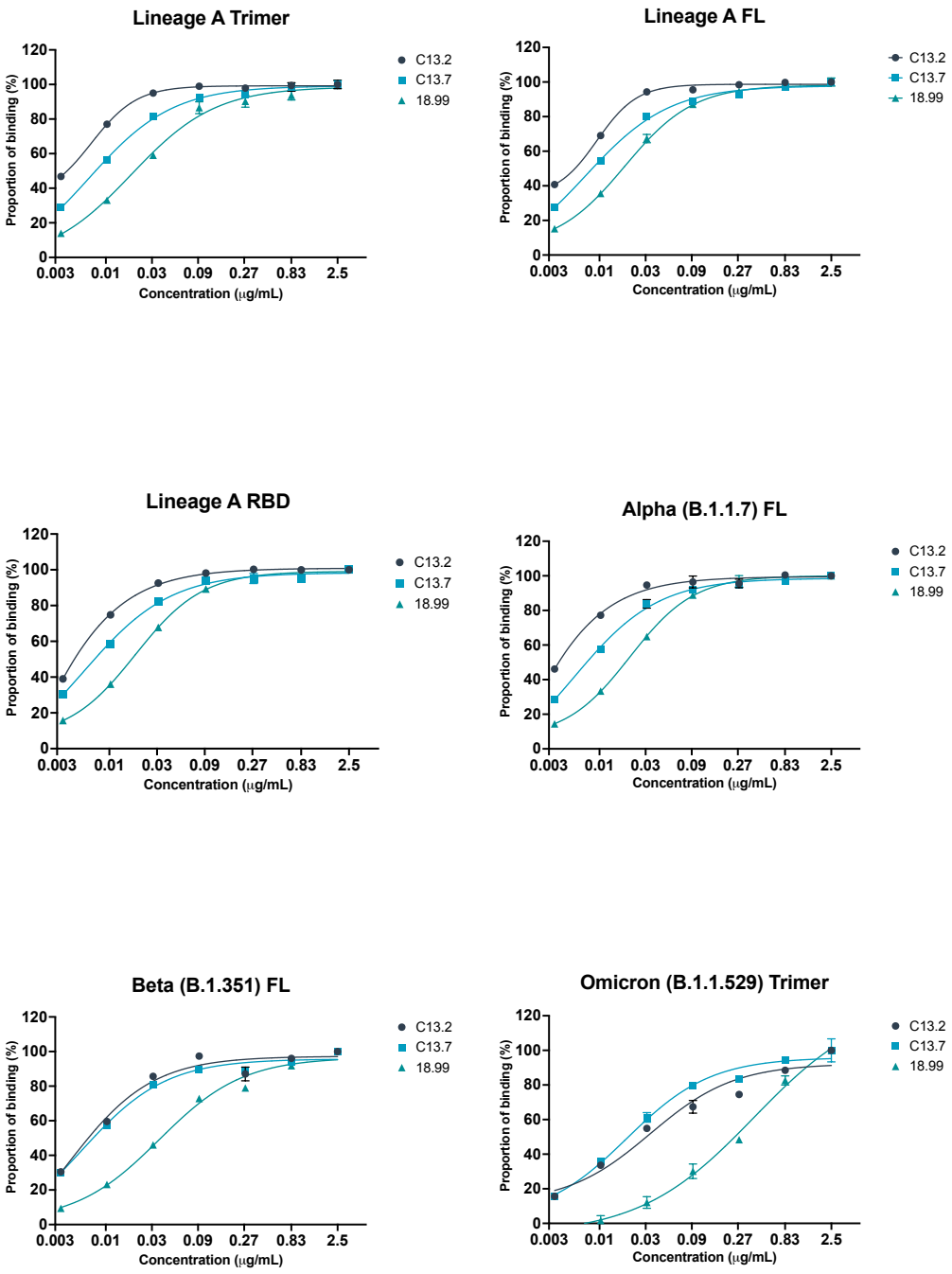

	Wuhan Trimer	Wuhan FL	Wuhan RBD	Alpha (B.1.1.7) full length spike (FL)	Beta (B.1.351) full length spike (FL)	Omicron (B.1.1.529) Trimer
C13.2	0.0071	0.0094	0.0014	0.0011	0.0041	0.0336
C13.7	0.0067	0.0072	0.0055	0.0055	0.0057	0.0192
18.99	0.0185	0.0182	0.0183	0.0207	0.0357	0.3946

Figure 5.4: Binding ELISA curves to SARS-CoV-2 variants for mAbs C13.2, C13.7 and 18.99, measured as portion of binding (%). Binding curves of proportion of binding (%), whereby 100% was the highest optical density at 405 nm, and wells with no mAb as 0%. Curves generated from a non-linear fit of normalised, 3-fold dilution series of mAb C13.2, C13.7 and 18.99 (isolated from C18 by single B-cell sorting) starting at 2.5 μg/mL. Curves were generated for SARS-CoV-2 lineage A trimer, full length spike (FL), and RBD; Alpha (B.1.1.7) full length spike (FL); Beta (B.1.351) full length (FL), and Omicron (B.1.1.529) trimer. Error bars demark standard deviation, N=2. Concentration and EC_{50} values (below) measured in μg/mL.

To determine if the binding data would be reflected in pseudovirus neutralisation, a single point pseudovirus neutralisation assay was performed for each variant of concern at the time. Pseudotyping allows for expression of viral glycoproteins onto surfaces of other viral membranes lacking the genome. The resultant cells mimic viral entry without carrying infectious material. Figure 5.5 demonstrates the proportion of neutralisation compared to an uninhibited control. No neutralisation to VSVg pseudoviruses was observed and wells containing only pseudovirus served as a positive control (data not shown). Both mAbs neutralised all pseudotyped variants at 1 μg/mL, by at least 81% and 31% for C13.2 and C13.7, respectively. C13.2 neutralised all pseudotypes with a greater potency compared to C13.7.

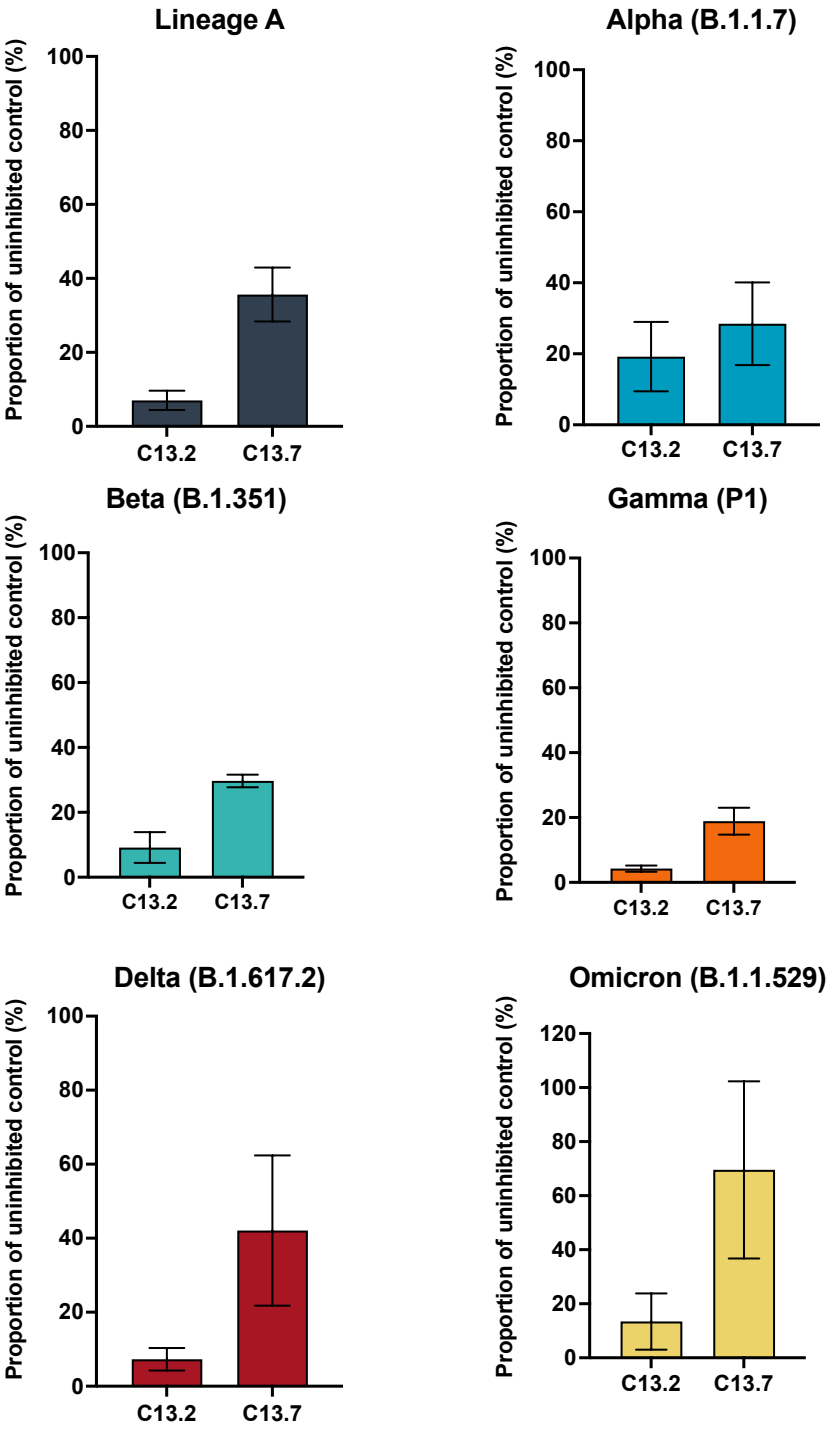

Figure 5.5: Single point neutralisation assay of mAbs C13.2 and C13.7 to SARS-CoV-2 variants. Pseudovirus neutralisation by each mAb at a concentration of 1μg/mL, measured as portion of uninhibited control (%) for pseudotyped SARS-CoV-2 variants Lineage A, Alpha (B.1.1.7), Beta (B.1.351), Gamma (P1), Delta (B.1.617.2) and Omicron (B.1.1.529). Error bars demark standard deviation, N=3.

5.4.5. *Expi293 expression of mAbs*

Further characterisation of mAbs required an increase in protein production and so expression was changed to a high-yield transient expression system in Expi293 cells.

Similar to the HEK293T expressed mAbs, an IgG ELISA was performed on the harvested mAbs produced in Expi293 cells. Yields increased by a moderate amount (Figure 5.6) with a similar cell density to HEK293T experiment, thus indicating a higher return. For instance, C13.2 was predicted to return a minimum of 2.3 mg/mL for a litre culture.

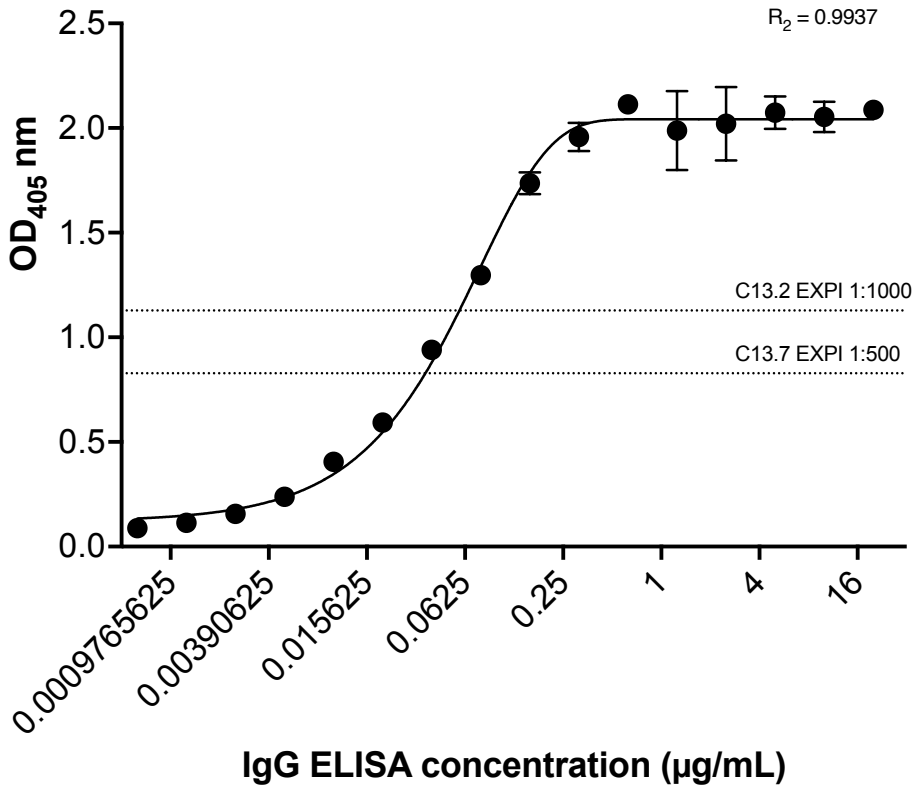

	Mean OD	Interpolated value from curve	Dilution factor	Concentration μg/mL
C13.2 EXPI 1:100	1.448	0.0928	100	9.3
C13.2 EXPI 1:500	1.273	0.0715	500	35.5
C13.2 EXPI 1:1000	1.128	0.0578	1000	58.0
C13.7 EXPI 1:100	1.474	0.0952	100	9.5
C13.7 EXPI 1:500	0.829	0.0365	500	18.5
C13.7 EXPI 1:1000	0.563	0.0204	1000	20.0

Figure 5.6: IgG ELISA concentration interpolation of Expi293 expressed mAbs. Top: Absorbance measured at OD_{405} nm and concentration measured in μg/mL. Concentration of mAbs interpolated from a non-linear fit to standards of a known concentration, represented as a dotted line, at the dilution used to determine concentrations. Error bars demark standard deviation, N=2. Bottom: Table showing interpolation of mAb concentration from Expi293 expression, displaying mean optical density OD_{405} nm, interpolated X value, dilution factor and concentration in μg/mL.

5.4.6. Purification of Expi293 expressed mAbs

Initial experiments for increasing yield were carried out on C13.2 based on the potency observed in Figure 5.5 and the level of expression which appeared to be higher than C13.7. A litre culture of Expi293 cells was transfected with heavy and light chain plasmids of C13.2. C13.7 was later produced from a 250 mL culture. Antibody preparations were purified using HiTrap Protein G Sepharose High-Performance resin columns. Protein G broadly binds a range of IgG from eukaryotic species allowing for the purification of IgG antibodies

from a solution. Figure 5.7A shows the purification output. UV absorbance, measured in mAU (blue line), remains high during sample loading and binding. Switching to the wash buffer resulted in a drastic drop in mAU, and elution marked by the affinity peak of the sample dissociating from the column into the fractions. The affinity peak is marked by a decrease in conductivity due to ionic exchange as protein dissociates from the column. A clear elution peak can be observed for C13.2, reaching an mAU of just under 1000 (Figure 5.7B). C13.7 purification generated an elution peak of just over 1000 mAU and was collected over a greater number of fractions (Figure 5.7C).

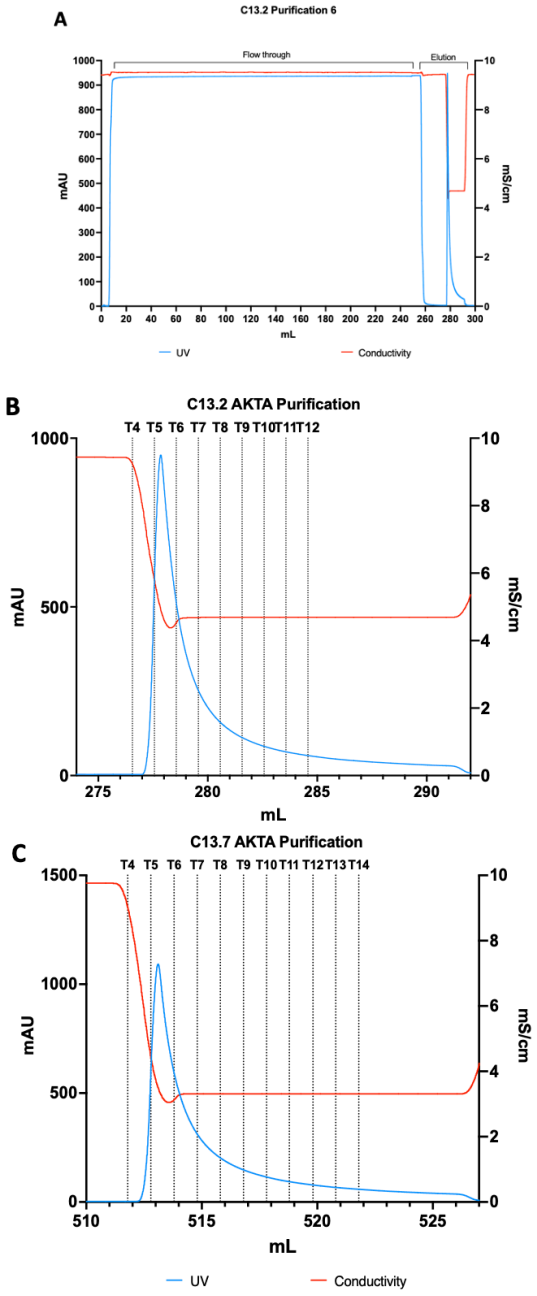

Figure 5.7: Affinity purification of mAbs. Flow through and elution measured by ultraviolet absorbance at 280 nm (mAU) demarked by a blue line, and conductivity (mS/cm) demarked by a red line. A) Overview of C13.2 purification. Flow through increased mAU to over 900 for 260 mL, followed by a sharp decrease on buffer exchange to wash. A sharp peak at 280 mL reaching 950 mAU shows elution of sample from the column. Conductivity at 9.3 mS/cm for 280 mL sharply decreased to 4 mS/cm during sample elution. Conductivity returned to 9.3 mS/cm after sample was completely eluted from the column. B) C13.2, elution peak at 950 mAU. Sample elution occurred over 12 fractions, demarked as T1-T12. C) C13.7, elution peak at 1100 mAU. Elution peak denoted by an increase in mAU and decrease in conductivity. Sample elution occurred over 14 fractions, demarked as T1-T14.

Fractions from the purification were pooled and further concentrated using molecular weight columns followed by a desalting procedure with buffer exchange columns. To confirm the elution peak in Figure 5.7A and B was the purified mAb, a silver stain was performed on the fractions and pure C13.2 (column concentrated and desalted). Figure 5.8 shows the presence of three distinct bands in all fractions. The bottom band, around 28 kDa, was identified as the light chain, and the band at 50 kDa, the heavy chain. The middle, intermediate band around 45 kDa was thought to be a heavy chain derived by-product. The flow through and wash were also retained to ensure several factors: the maximum amount of product was purified from the culture supernatant, the column did not become oversaturated, and to ensure the product was not eluted during the wash.

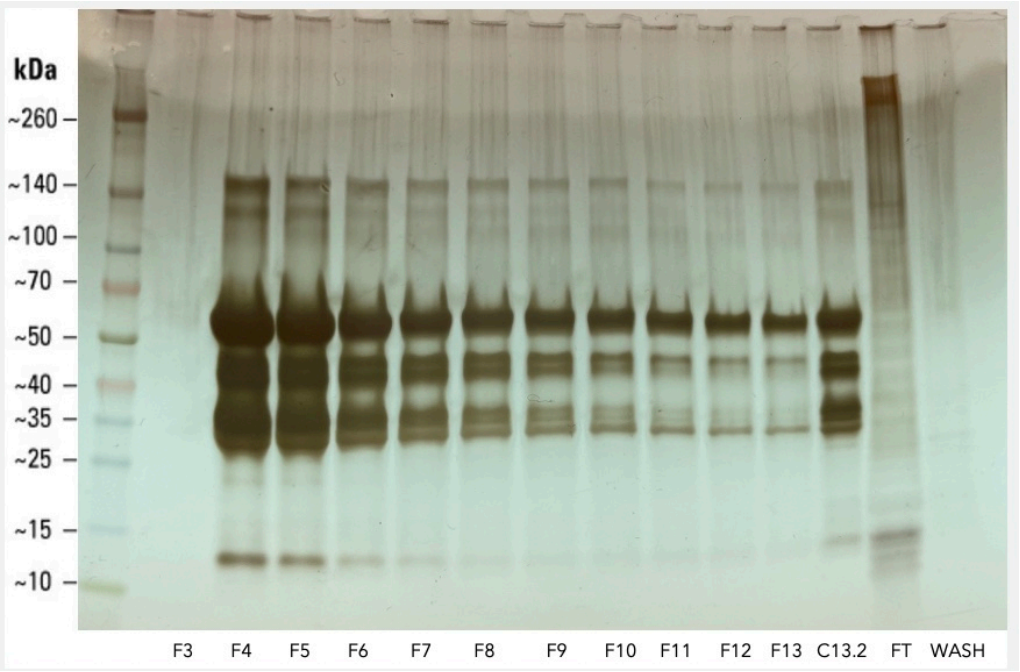

Figure 5.8: Silver stain of reduced C13.2 mAb purification fractions compared to pure C13.2 mAb, flow through and wash. Banding pattern from silver staining of reduced proteins from C13.2 fractions, Pure C13.2, flow through (FT) and wash. Three bands were present in the fractions and pure sample, the band at 55 kDa inferred as the heavy chain, 28 kDa the light chain, and the middle 45 kDa double bands as heavy-chain derived products. Left: molecular marker in kDa. The FT contained faint bands from the supernatant proteins.

5.4.7. Quantification of mAbs

Total protein from the purified mAbs was quantified using BCA assay. A standard curve of BSA was generated for interpolation of unknown sample protein concentrations. (Figure 5.9). Using the equation rearranged in Figures 5.9A and B, C13.2 was quantified at around 7.7 mg/mL and C13.7 at 6.1 mg/mL, respectively.

A

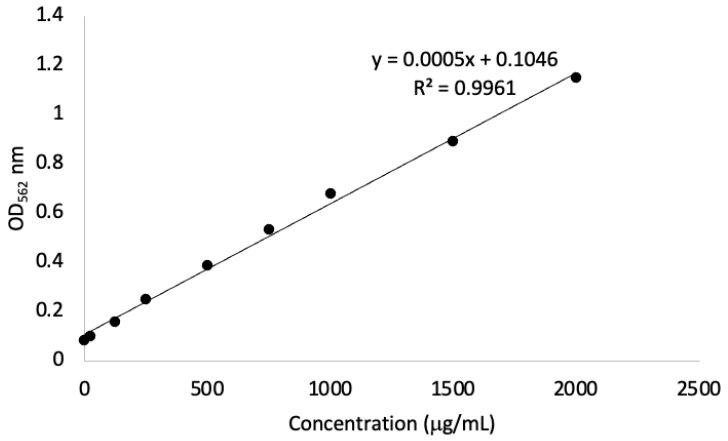

	Mean OD	Estimated concentration	Dilution factor	Sample concentration (µg/mL)	mg/mL
C13.2 1:10	0.488	765.8	10	7658	7.658
C13.2 1:20	0.219	228.8	20	4576	4.576
C13.2 1:40	0.142	73.8	40	2952	2.952

B

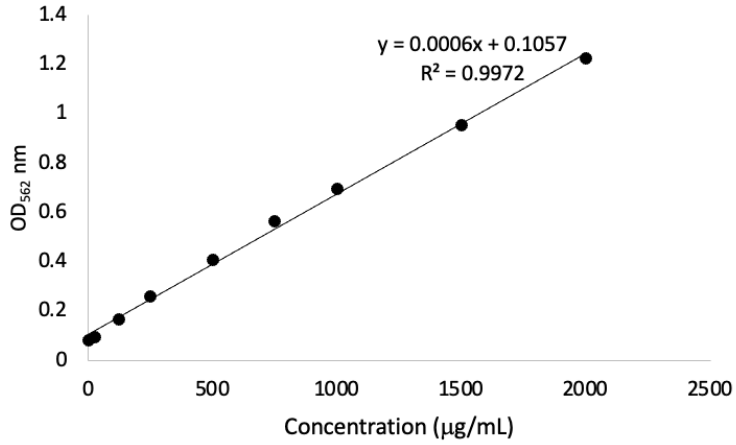

	Mean OD	Estimated Concentration	Dilution Factor	Sample concentration (µg/mL)	mg/mL
C13.7 1:10	0.485	632.167	10	6321.667	6.322
C13.7 1:20	0.286	299.667	20	5993.333	5.993
C13.7 1:40	0.198	153.833	40	6153.333	6.153

Figure 5.9: BCA assay for analysis and interpolation of total protein quantification of mAbs. A) C13.2. B) C13.7. Linear regression of standards from a known concentration, measured at OD_{562} nm. Y = mx + c derived from linear regression on the graph was used to interpolate total protein. Table shows mean OD_{562} nm, estimated interpolated concentration, dilution factor and concentration recorded in μg/mL and mg/mL (circled interpolation used).

IgG concentration of the total protein was quantified by IgG ELISA. The concentrations were derived the standard curves in Figure 5.10. Quantification of C13.2 revealed that 1.51 mg/mL of 7.7 mg/mL total protein was IgG, determining the preparation purity at approximately 20%. C13.7 was around 31% pure, with IgG forming 1.95 mg/mL out of 6.1 mg/mL total protein.

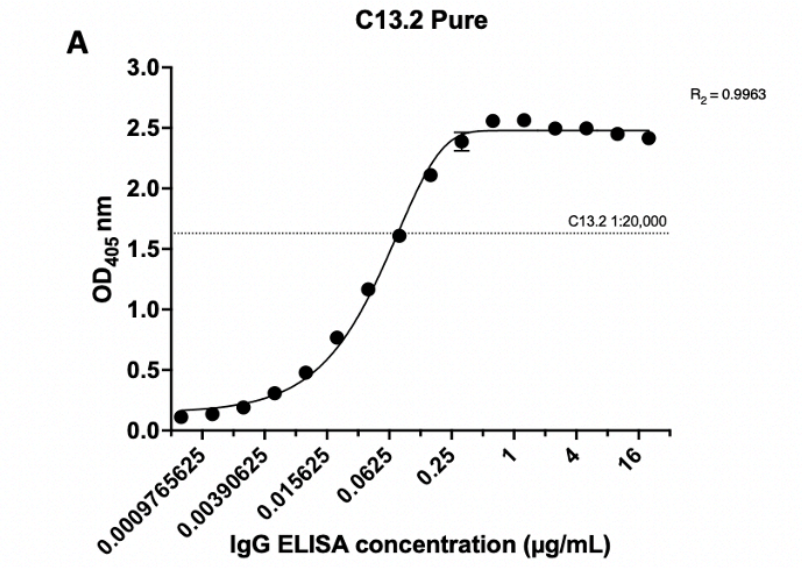

	Mean OD	Interpolated value from curve	Dilution factor	μg/mL	mg/mL
C13.2 PURE 1:10000	1.998	0.1179	10000	1179.777	1.179
C13.2 PURE 1:20000	1.630	0.0755	20000	1510.438	1.510
C13.2 PURE 1:40000	1.221	0.0461	40000	1845.378	1.845
C13.2 PURE 1:80000	0.788	0.0240	80000	1921.997	1.921
C13.2 PURE 1:100000	0.695	0.0200	100000	2000.202	2.000

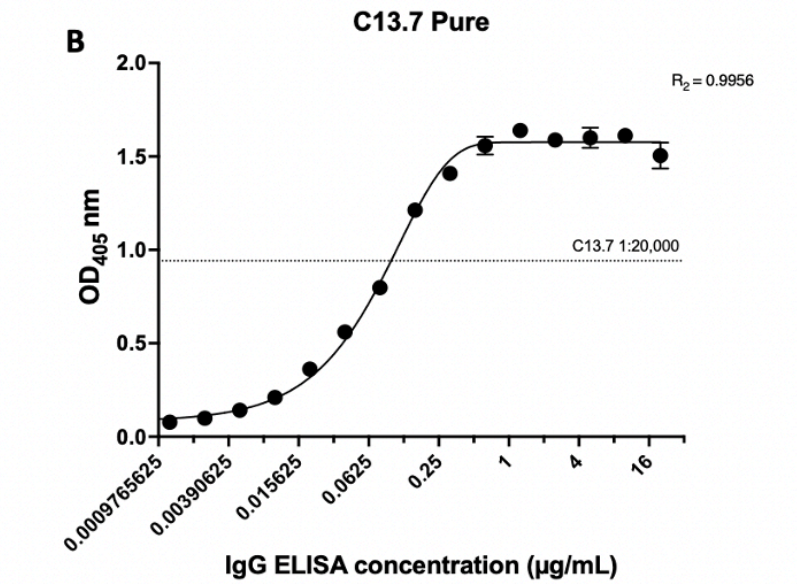

	Mean OD	Interpolated value from curve	Dilution factor	µg/mL	mg/mL
C13.7 PURE: 1:1000	1.402	0.2443	1000	244.315	0.240
C13.7 PURE: 1:20000	0.941	0.0973	20,000	1945.813	1.950
C13.7 PURE: 1:40000	0.636	0.0527	40,000	2108.684	2.110
C13.7 PURE: 1:80000	0.451	0.0323	80,000	2579.816	2.580
C13.7 PURE: 1:100000	1.402	0.0268	100,000	2677.666	2.680

Figure 5.10: IgG ELISA interpolation of purified Expi293 expressed mAbs. A) C13.2. B) C13.7. Absorbance measured at OD_{405} nm and concentration measured in µg/mL. Concentration of mAbs interpolated from a non-linear fit to standards of a known concentration, represented as a dotted line, at the dilution used to determine concentrations. Error bars demark standard deviation, N=2. Tables below each graph display mean optical density OD_{405} nm, interpolated X value, dilution factor and concentration in µg/mL and mg/mL.

5.4.8. Analysing mAb expression

The expression of each mAb was examined to confirm successful purification, and to identify any impurities that may have arisen during the mAb production. A silver stain of C13.7 in comparison to C13.2 showed the presence of the similar additional impure bands, between 30 and 45 kDa that were observed in the fractions of the previous silver stain (Figure 5.8), albeit with less intensity in C13.7 compared to C13.2 which was expected with a purer preparation. The higher intensity band in Figure 5.11 at approximately 55 kDa was inferred as the heavy chain, and the singular band at 28 kDa as the light chain.

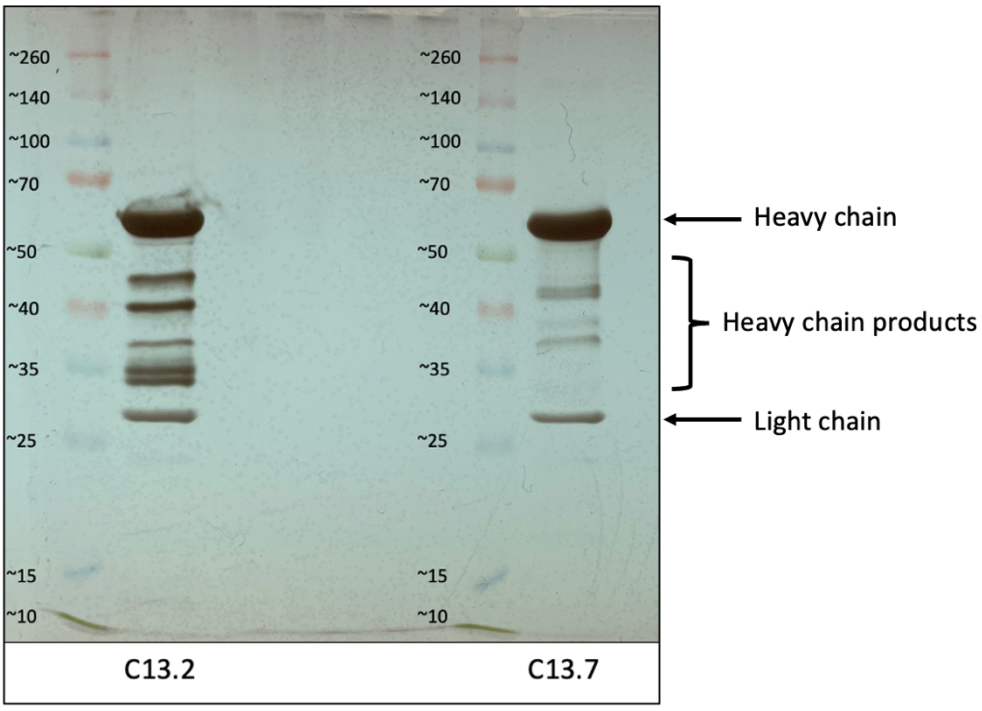

Figure 5.11: Silver stain of reduced purified C13.2 (left) and C13.7 (right). The thick intense band at 55 kDa inferred as heavy chain and faint band at 28 kDa the light chain. Bands at 30, 35, 37, 40 and 45 kDa in C13.2 inferred as heavy chain derived products. Bands at 37, 38, and 45 kDa in C13.7 inferred as heavy chain derived products. Molecular marker (M) in kDa.

To ascertain whether these additional bands between the heavy and light chains were non-specific products binding to the column during purification, western blots detecting the light and heavy chains were performed. Figure 5.12A, detecting reduced lambda light chains, showed a discrete band of the light chain in both mAb preparations at 28 kDa. On the contrary, Figure 5.12B, detecting reduced gamma chains, showed an intense band at 55 kDa as expected, but also the presence of additional heavy chain derived products. The additional bands in Figure 5.12B match those present in the silver stain, Figure 5.11, confirming the impurities as heavy chain-derived by-products which would have bound to protein G during the column affinity purification. These heavy chain-derived products would not be detected in the IgG ELISA as detection was performed using an anti-lambda light chain antibody. This

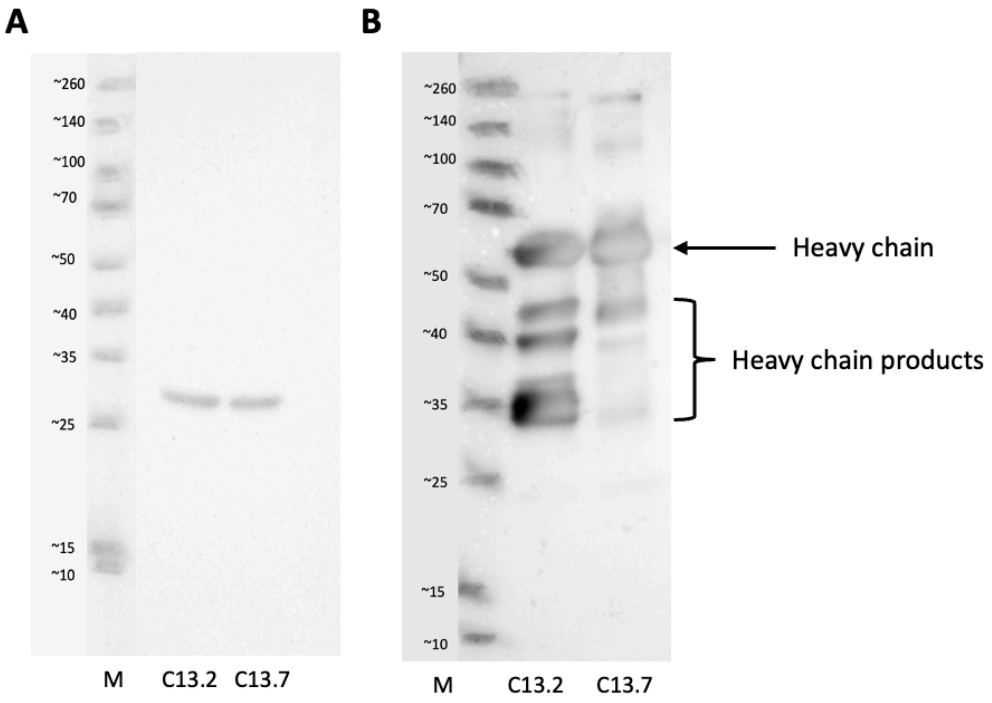

Figure 5.12: Western blot of mAbs C13.2 and C13.7, reduced, detecting expression of A) antibody light chains, at 28 kDa, and B) antibody heavy chains, at 55 kDa. Additional bands at 35, 40 and 45 kDa in B were heavy chain derived by products. Molecular marker (M) in kDa.

could explain why the IgG out of the total protein concentration was low for both preparations.

5.4.9. Characterising the binding profiles of C13.2 and C13.7

Subsequent binding experiments sought to determine the binding profiles of C13.2 and C13.7 mAb. ELISAs were performed for all variants of interest at the time including a breakdown of SARS-CoV-2 Lineage A into the trimer, full-length spike, S1 and RBD, adding to the binding ELISA experiment from Figure 5.4. A greater dilution series was performed to produce full curves whereby the lowest concentration of mAb would reach 0% proportion of binding. Binding curves generated by from the ELISAs revealed C13.2 showed higher levels of binding to the majority of SARS-CoV-2 antigens compared to C13.7, however, C13.2 did not bind to SARS-CoV-2 BA.5 (Figure 5.13). EC_{50}s for C13.2 ranged from 4-1043 ng/mL, whereas EC_{50}s of C13.7 ranged from 3-55 ng/mL. Interestingly, both mAbs showed the strongest binding to SARS-CoV-2 Lineage

A full-length spike (C13.2 EC_{50} of 4 ng/mL and C13.7 EC_{50} of 3 ng/mL).

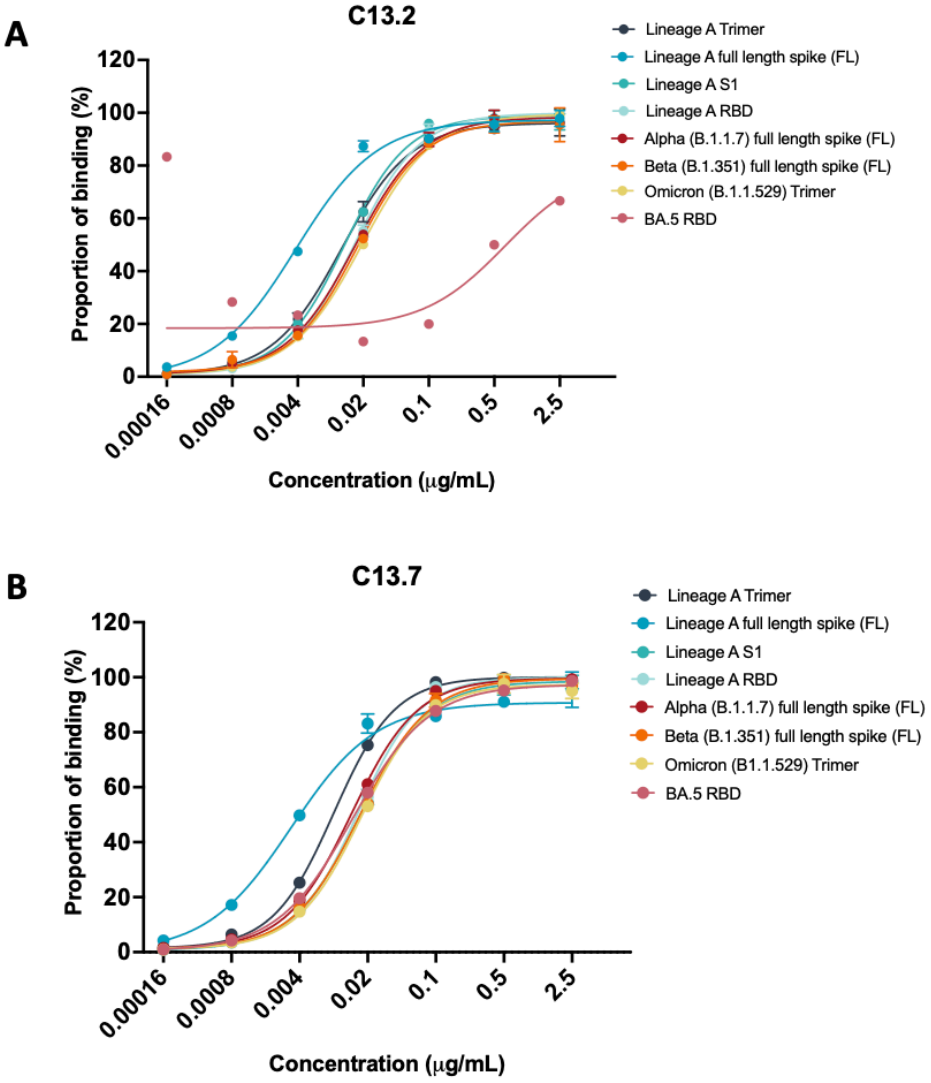

Figure 5.13: Binding ELISA curves to SARS-CoV-2 variants for mAbs C13.2 and C13.7. Binding curves of proportion of binding (%), whereby 100% was the highest optical density at 405 nm, and wells with no mAb as 0%. Curves generated from a non-linear fit of normalised, 5-fold dilution series of A) C13.2 mAb, and B) C13.7 mAb. Concentration measured in μg/mL. Curves were generated against SARS-CoV-2 lineage A trimer, full length spike (FL), S1, and RBD; Alpha (B.1.1.7) full length spike (FL); Beta (B.1.351) full length (FL), Omicron (B.1.1.529) trimer, and BA.5 (RBD). Error bars demark standard deviation, N=2.

Considering binding was observed for SARS-CoV-2 Lineage A RBD, it was predicted that the mAbs would interfere with ACE2 binding, thus an ACE2 inhibition ELISA was performed for both mAbs. Binding EC_{50}s to the SARS-CoV-2 antigens can be found in Table 5.1.

ACE2 was identified as an essential receptor for SARS-CoV-2 entry due to its interaction with the RBD. MAbs binding to the RBD are therefore likely to inhibit or alter this interaction. An ELISA detecting ACE2 was optimised (data not shown) and performed to determine whether this was true for C13.2 and C13.7. Unexpectedly, both mAbs were unable to fully abolish ACE2 binding, with ACE2 binding plateauing (Figure 3.14). At the highest C13.2 concentration of 2.5 μg/mL, 40% of ACE2 binding was recorded to SARS-CoV-2 Lineage A full length spike and RBD, and 68% to Lineage A trimer. Similarly, at the highest mAb concentration of C13.7, there was 48% of binding to ACE2 for SARS-CoV-2 Lineage A RBD, 65% to trimer, and 70% to full length spike. This suggests ACE2-spike interactions are occurring in the presence of each mAb. Binding EC_{50}s can be found in Table 5.1.

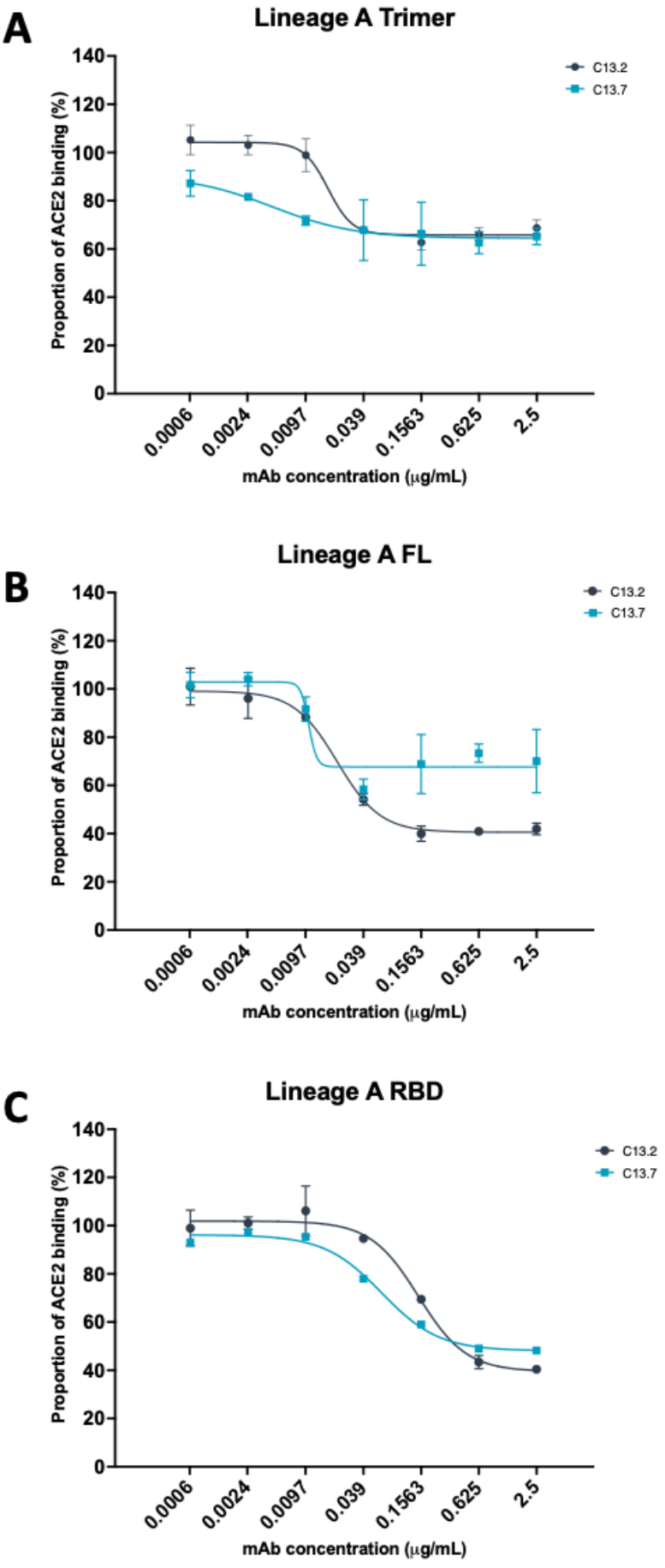
A
Lineage A Trimer
C13.2
C13.7
Proportion of ACE2 binding (%)
140
120
100
80
60
40
20
0
0.0006
0.0024
0.0097
0.039
0.1563
0.625
2.5
mAb concentration (μg/mL)
B
Lineage A FL
C13.2
C13.7
Proportion of ACE2 binding (%)
mAb concentration (μg/mL)
C
Lineage A RBD
C13.2
C13.7
Proportion of ACE2 binding (%)
mAb concentration (μg/mL)

Figure 5.14: ACE2 ELISA curves to SARS-CoV-2 Lineage A spike proteins for mAbs C13.2 and C13.7. Binding curves of proportion of ACE2 binding (%), whereby 100% was the highest optical density at 405 nm, and wells with no ACE2 as 0%. Curves generated from a non-linear fit of normalised ACE2 binding during a 5-fold dilution series of C13.2 mAb and C13.7 mAb diluted in soluble ACE2 for A) Lineage A trimer, B) Lineage A full length (FL), C) Lineage A RBD. Concentration measured in μg/mL. Error bars demark standard deviation, N=2.

5.4.10. Investigating C13.2 and C13.7 binding epitopes through competition ELISA

Investigations into C13.2 and C13.7 binding sites were achieved by generating Fab versions of C13.2 and C13.7 to perform competition ELISAs in which the mAb version would be detected. Primers were developed to produce Fc deletions in the heavy chain plasmids. The Fab plasmids were transformed and screened for positive colonies. Figure 5.15A shows the positive colonies for C13.2 heavy chain Fc deletion, colony 3 was the only unsuccessful colony for this modification at a band size of 2000 base pairs, whereas the positive colonies screened were around 1000 base pairs. All colonies were successful for the Fc deletion of the C13.7 heavy chain plasmid, with a band size of 1000 base pairs (Figure 5.15B).

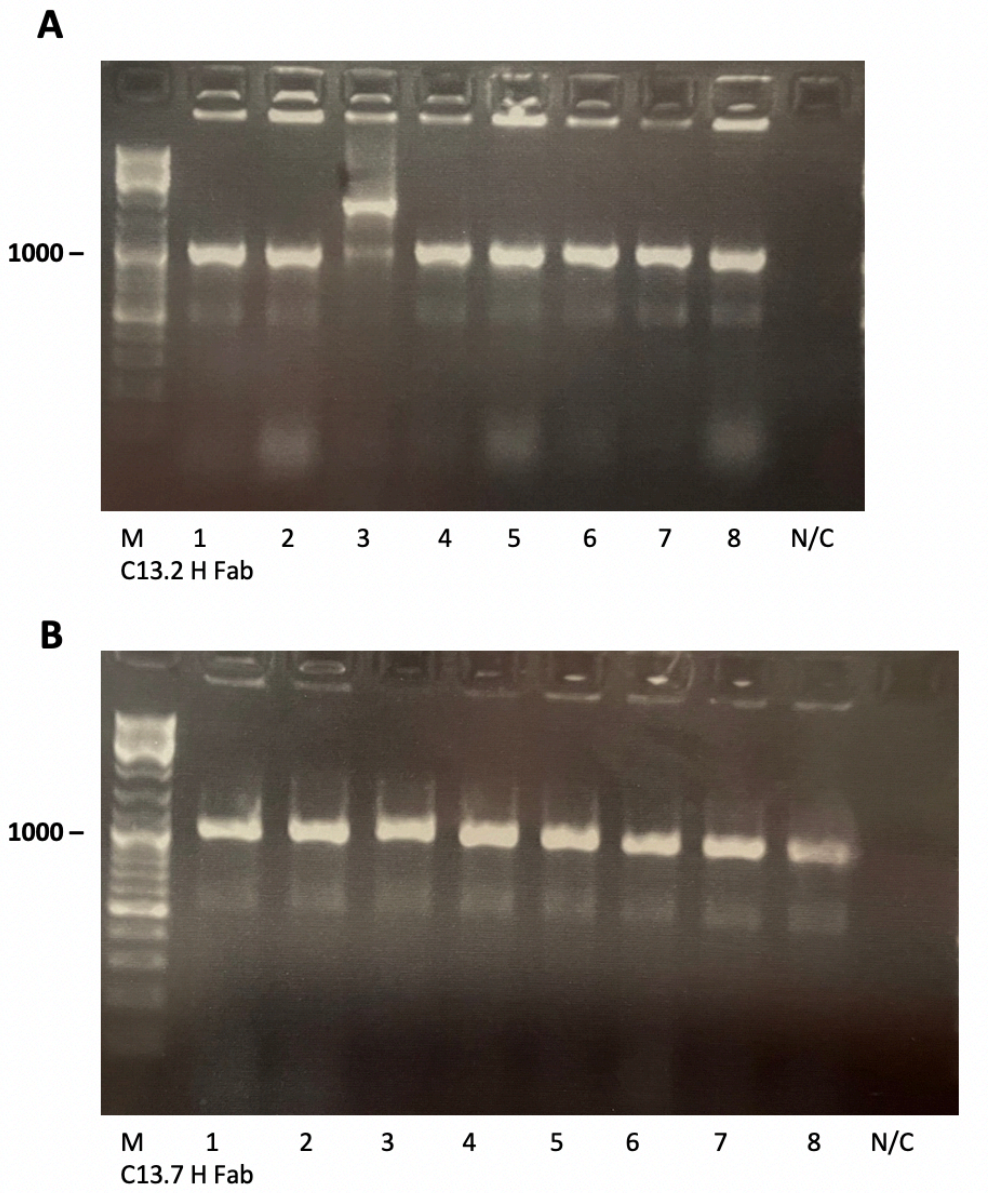

Figure 5.15: Screening colonies of C13.2 and C13.7 heavy chain plasmid Fc deletion to Fab. A) C13.2 H Fab clones 1-8. Positive colonies, 1, 2, 4-8 produced a band around 1000 base pairs whereas the negative colony 3, with full Fc, produced a band around 2000 base pairs. B) C13.7 H Fab clones 1-8. All colonies were positive producing a band around 1000 base pairs. A+B) M = 10 Kb DNA molecular marker. N/C = negative control.

Expi293 cells were transfected with C13.2 and C13.7 Fab plasmids and the light chain plasmid, and supernatant harvested, by Dr. Joseph Chappell. C13.2 Fab and C13.7 Fab were tested in a five-fold dilution series for their binding

against SARS-CoV-2 Lineage A trimer, and dilution EC_{50}s were determined. Similar to the mAbs, the EC_{50} of C13.2 Fab to SARS-CoV-2 Lineage A trimer was 1:2500, a lower concentration, compared to the EC_{50} of C13.7 Fab to SARS-CoV-2 Lineage A trimer which was 1:1150 (data not shown). This suggested the binding profiles had not been altered with this modification.

Competition ELISAs were performed with an excess of Fab, diluted 1:25. If potential additive effects or inhibition was present between two candidates an excess of Fab was expected to exaggerate the trend. Figure 5.16A and B shows binding curves of detected mAb using a diluent of excess Fab. Despite over-saturating the assay with Fab, there was modest impact on binding compared to the binding of uninhibited mAb (C13.2: Figure 5.16A) (C13.7: Figure 5.16B), suggesting no competition between C13.2 and C13.7 for SARS-CoV-2 Lineage A trimer.

In addition, the mAbs were tested for potential inhibition or additive effect with a panel of 14 SARS-CoV-2 spike reactive bovine Fab, previously isolated by Dr. Theocharis Tsoleridis using single B-cell sorting. Figure 5.16C shows the analysis of these results, generated by single points whereby the EC_{50} of each mAb was in the presence of Fab diluted 1:25. Fab interactions with mAb were compared to the uninhibited EC_{50} of each mAb and colour-coded depending on potential additive or inhibited effect. As expected, the Fab versus mAb of C13.2 generated inhibition, as did the Fab versus mAb of C13.7, confirming that the modification of these mAbs did not alter the binding to SARS-CoV-2 Lineage A trimer. All candidates in the Fab panel appeared to enhance the binding of each mAb with the exception of 103 which inhibited C13.2. Fab 103 was recorded to bind to the RBD suggesting it binds to residues involved in C13.2 binding. This suggests 103 occupies a similar epitope to C13.2 and may have greater affinity for the RBD compared to C13.2. It should, however, be noted that as Fab was used in excess, the results in Figure 5.16C serve as indications, and not accurate values, of potential additive effects or inhibition.

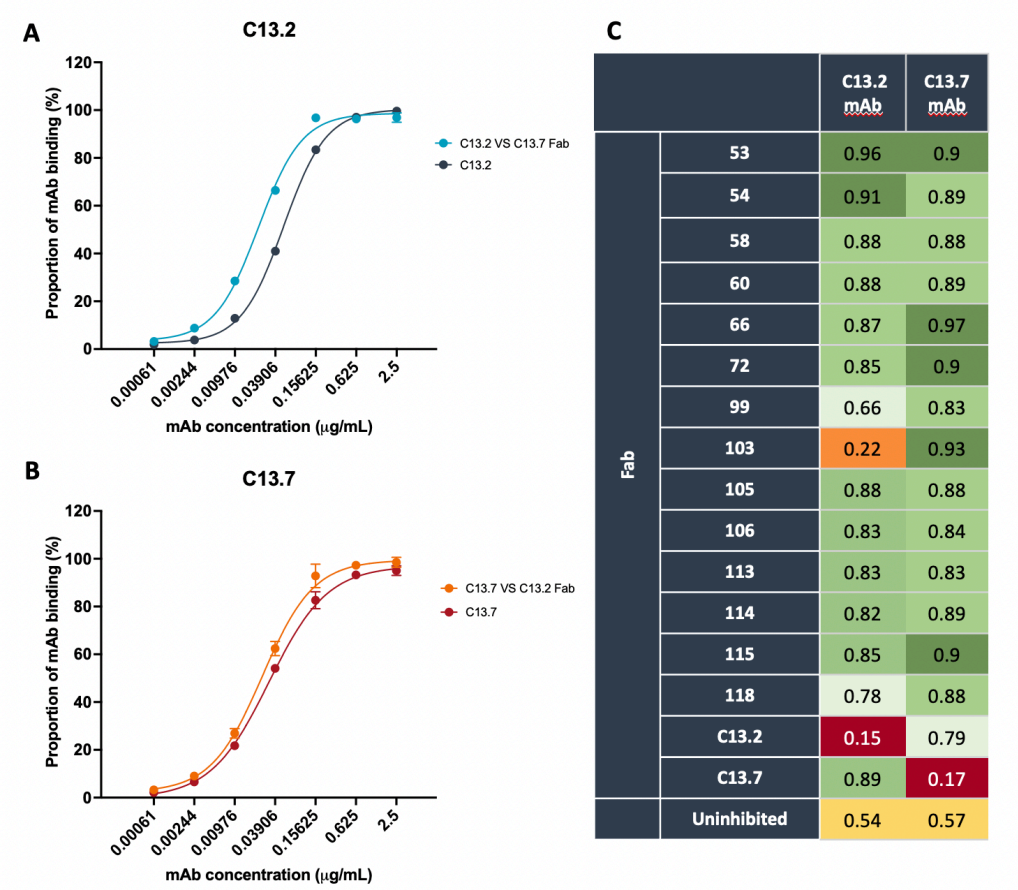

Figure 5.16: Competition ELISA between A) C13.2 mAb and C13.7 Fab, B) C13.7 mAb and C13.2 Fab, C) C13.2 and C13.7 mAb against the Fab panel (gifted by Dr. Theocharis Tsoleridis) measured as mean optical density at 405 nm. A-B) Non-linear curves analysed as proportion of mAb binding (%) measured at concentration of mAb (µg/mL) diluted in excess Fab (1:25), compared to uninhibited mAb (A: C13.2 or B: C13.7). Error bars demark standard deviation, N=2. C) Mean optical density measured at OD405 nm, colour coded to reflect potential additive effects (green) or inhibition (red), yellow neutral. Uninhibited mAbs served as comparison EC_{50}. MAb against autologous Fab served as inhibition control.

5.4.11. C13.2 and C13.7 neutralisation of pseudotyped SARS-CoV variants

Considering the little impact C13.2 and C13.7 had on ACE2 binding, it was predicted that RBD-ACE2 interactions were still permitted in the presence of C13.2 or C13.7. This was therefore thought to hinder neutralisation, and thus neutralisation would not reach 100%. Neutralisation was performed through

pseudotyping of SARS-CoV-1 (Frankfurt strain) and SARS-CoV-2 variants. The mAbs were able to reach 100% neutralisation to the majority of pseudotyped variants suggesting there may be an alternative explanation for the ACE2 ELISA data (Figure 5.14). C13.2 potently neutralised the initial variants of SARS-CoV-2 (Figure 5.17) as expected from the single point neutralisation data (Figure 5.4). This included Lineage A, Alpha (B.1.1.7), Beta (B.1.351), Gamma (P1), Delta (B.1.617.2) and Omicron (B.1.1.529). C13.2 neutralisation was completely abolished by Omicron sublineage variant, BA.5. A more recent subvariant of Omicron, XBB, generated from a recombination event between BA.2.10.1 and BA.2.75 was tested as a pseudotype. C13.2 was able to neutralise pseudoviruses of XBB, albeit with less potency than the other variants at an IC_{50} of 289 ng/mL. Neutralisation to the closely related strain SARS-CoV-1, responsible for outbreaks in 2002-2004, was tested to determine any cross-reactivity. However, no neutralisation to SARS-CoV-1 was observed for C13.2. IC_{50}s can be found in Table 5.1.

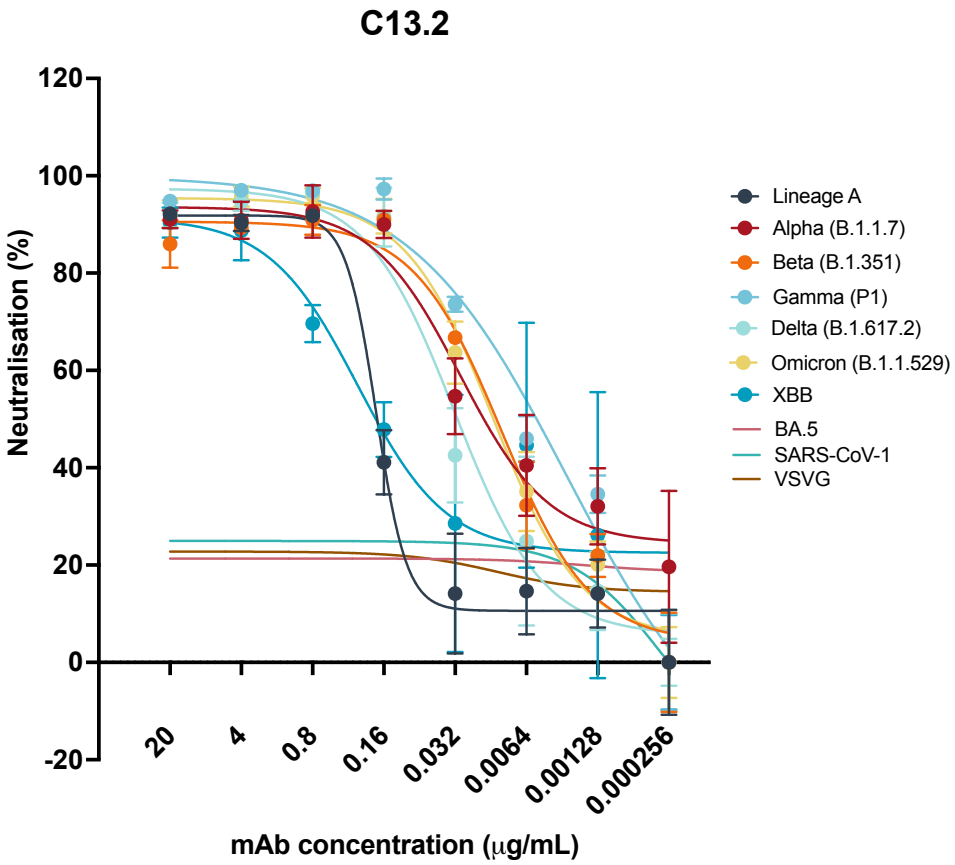

Figure 5.17: C13.2 Pseudovirus neutralisation assay. Pseudoviruses tested SARS-CoV-2: Lineage A, Alpha (B.1.1.7), Beta (B.1.351), Gamma (P1), Delta (B.1.617.2), Omicron (B.1.1.529), BA.5, XBB, and SARS-CoV-1: Frankfurt strain. Non-linear curves from normalised RLU data to positive and negative cell only controls, analysed as neutralisation (%) from a 5-fold dilution series of mAb (μg/mL). IC_{50}s ranged between 3-289 ng/mL. VSVg served as a negative control. Error bars demark standard deviation, N=3. Goodness of fit: $R_2 > 0.92$, except XBB where $R_2 = 0.7$.

MAb C13.7 was tested for neutralisation against all pseudotype variants previously mentioned. C13.7 exhibited a greater breadth of neutralisation (Figure 5.18); however, the potency was reduced in comparison to C13.2 (Figure 5.17), confirming trends observed in Figure 5.5. Interestingly, C13.7 was able to neutralise current variants of concern, including newer variants of BA.5 and XBB at 94 and 1,062 ng/mL, respectively. Unexpectedly, C13.7 was

able to neutralise pseudoviruses of SARS-CoV-1 at an IC_{50} of 11 ng/mL. IC_{50}s can be found in Table 5.1.

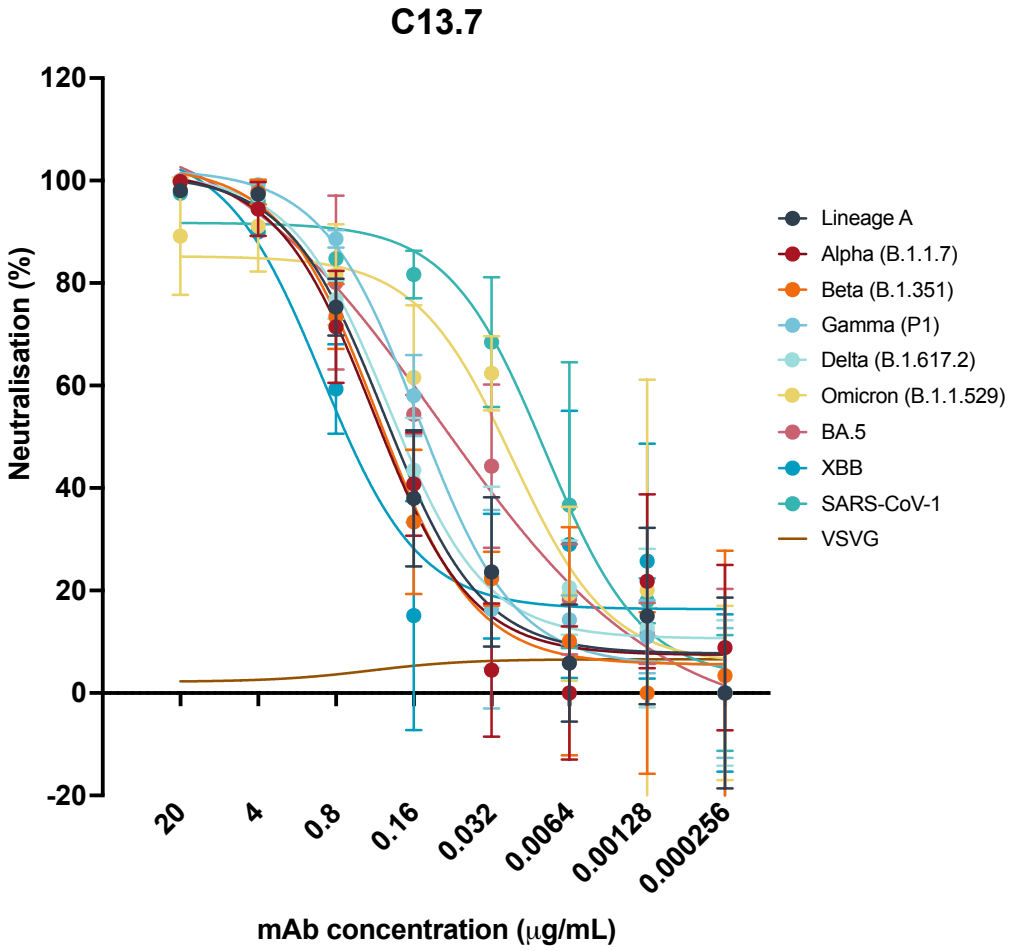

Figure 5.18: C13.7 Pseudovirus neutralisation assay. Pseudoviruses tested SARS-CoV-2: Lineage A, Alpha (B.1.1.7), Beta (B.1.351), Gamma (P1), Delta (B.1.617.2), Omicron (B.1.1.529), BA.5, XBB, and SARS-CoV-1: Frankfurt strain. Non-linear curves from normalised RLU data to positive and negative cell only controls and analysed as neutralisation (%) from a 5-fold dilution series of mAb (μg/mL). IC_{50}s ranged between 11 and 1062 ng/mL. VSVg served as a negative control. Error bars demark standard deviation, N=3. Goodness of fit: $R_2 > 0.9$, except XBB where $R_2 = 0.8$ and Omicron BA.1 where $R_2 = 0.78$.

Table 5.1 summarises the binding data and pseudotype neutralisation data, collating previous SARS-CoV-2 variant binding with the most recent binding data. In summary, C13.2 and C13.7 bound to the SARS-CoV-2 antigens with similar EC_{50}s, except for BA.5 RBD in which C13.2 did not bind (Figure 5.13A). This trend was reflected by the inability of C13.2 to neutralise pseudotypes of BA.5. Despite the presence of ACE2 binding to RBD, EC_{50}s of SARS-CoV-2 Lineage A trimer and full-length spike and each mAb remained relatively similar to their uninhibited binding values. This pattern however is not reflected for the EC_{50} values between binding data and ACE2 data for SARS-CoV-2 Lineage A RBD, whereby each mAb had higher EC_{50} values. This suggests binding of both mAbs may occur only partially within the RBD-ACE2 binding site.

Overall, C13.2 neutralised the variants with greater potency with IC_{50}s ranging between 3 ng/mL to 289 ng/mL. C13.2 had one of the lowest potencies against SARS-CoV-2 Lineage A trimer, at 190 ng/mL, which it was raised against. In contrast, the greatest potency was recorded for the Gamma (P1) variant with an IC_{50} of 3 ng/mL, showing a similar trend to the single point neutralisation of Figure 5.5. Despite the inability to neutralise BA.5, C13.2 effectively neutralised the BA.2 Lineage recombinant variant, XBB, with an IC_{50} of 289 ng/mL.

Even though C13.7 exhibited clear similarities between binding and ACE2 data to C13.2, neutralisation potency was reduced. However, C13.7 possessed greater neutralisation breadth. IC_{50}s ranged from 11 ng/mL to 1 μg/mL. The reduced neutralisation was expected following the data in Figure 5.5 whereby C13.7 showed less potent neutralisation to all variants compared to C13.2. Furthermore, as XBB had an impact on C13.2 neutralisation, C13.7 neutralisation to XBB was expected to be reduced. C13.7 showed strong binding to XBB RBD, yet this did not translate into neutralisation, and the reverse of this was observed with C13.2 suggesting binding and neutralisation curves require repeating to determine the accurate EC_{50}s and IC_{50}s. As reflected in the binding data (Figure 5.13B), C13.7 was also able to neutralise

pseudoviruses of SARS-CoV-2 BA.5, at a potent IC_{50} of 94 ng/mL. Most strikingly, was that C13.7 neutralised SARS-CoV-1 pseudoviruses with a potent IC_{50} of 11 ng/mL. This warranted further investigation into potential cross-reactivity with closely related strains.

Table 5.1: Summary of C13.2 and C13.7 mAb binding and neutralisation data to SARS-CoV-1 and SARS-CoV-2 variants. Measured as EC_{50} for binding data and IC_{50} for neutralisation data, measured as μg/mL. NA = not applicable, ND = no data. Colours represent spectrum of EC_{50}/ IC_{50} with green dictating low values and red as high values.

Assay	mAB	Lineage A trimer	Lineage A FL	Lineage A S1	Lineage A RBD	Alpha (B.1.1.7)	Beta (B.1.351)	Gamma (P1)	Delta (B.1.617)	Omicron (B.1.1.529) trimer	BA.5 RBD	SARS-COV-1	XBB RBD
Binding	13.7	0.009	0.003	0.017	0.016	0.014	0.017	ND	ND	0.017	0.014	ND	0.055
	13.2	0.012	0.004	0.013	0.016	0.016	0.017	ND	ND	0.019	NA	ND	1.043
ACE2 inhibition	13.7	0.004	0.005	ND	0.061	0.002	0.004	ND	ND	ND	ND	ND	ND
	13.2	0.017	0.021	ND	0.146	0.003	0.005	ND	ND	ND	NA	ND	ND
PV neutralisation	13.7	0.296	NA	NA	NA	0.368	0.339	0.137	0.283	0.100	0.094	0.011	1.062
	13.2	0.190	NA	NA	NA	0.034	0.013	0.003	0.032	0.014	NA	NA	0.289
		Lineage A				Alpha (B.1.1.7)	Beta (B.1.351)	Gamma (P1)	Delta (B.1.617)	Omicron (B.1.1.529)	BA.5	SARS-COV-1	XBB

5.4.12. C13.7 binds a pan-sarbecovirus RBD epitope

Discovering that C13.7 exhibited cross-reactivity to SARS-CoV-1 and SARS-CoV-2 instigated an investigation into reactivity to closely related *Sarbecovirus* strain RBDs. A panel of 14 *Sarbecovirus* RBD strains and eight SARS-CoV-2 RBD variants were gifted by Dr. Chengcheng Fan (Caltech) to determine the extent of cross-reactivity. RBD proteins were expressed, purified, and quantified prior to performing the RBD ELISAs. An anti-avi-tag antibody ELISA, performed by Dr. Joshua Duncan, served as a positive control for the expressed proteins (Appendix III). A phylogenetic tree has been provided in Figure 5.19C, sourced from studies by Fan et al. (Fan et al., 2022), for observations between the binding of strains.

Remarkably, C13.7 bound to all *Sarbecovirus* RBDs with EC_{50}s ranging between 34 and 74 ng/mL (Figure 5.19A). Interestingly, the weakest binding was clustered to RBD of Yunnan (2011) and Rs4081, distant relatives in the Bat Southeast Asian clade 2. The strongest binding was observed across SARS-CoV and SARS-CoV-2 related clades of 1, and Bat non-Southeast Asian strains, which formed a cluster away from clade 2. Additionally, binding was observed for all SARS-CoV-2 RBD variants, with EC_{50}s ranging between 38 and 86 ng/mL (Figure 5.19B). Perhaps most strikingly is the EC_{50} value (at 38 ng/mL) to SARS-CoV-2 BA.5 sublineage, BQ.1.1, which was discovered in late 2022. C13.7, despite being raised against SARS-CoV-2 Lineage A, retained strong activity against the highly variable Omicron variant, and later evolved sublineages.

To ascertain whether the binding was skewed to RBDs of *Sarbecovirus* strains or SARS-CoV-2 variants, the EC_{50}s were compared. The analysis of this is presented in Figure 5.19D where there was no significant difference between the two groups suggesting equal, broad binding to all RBDs tested.

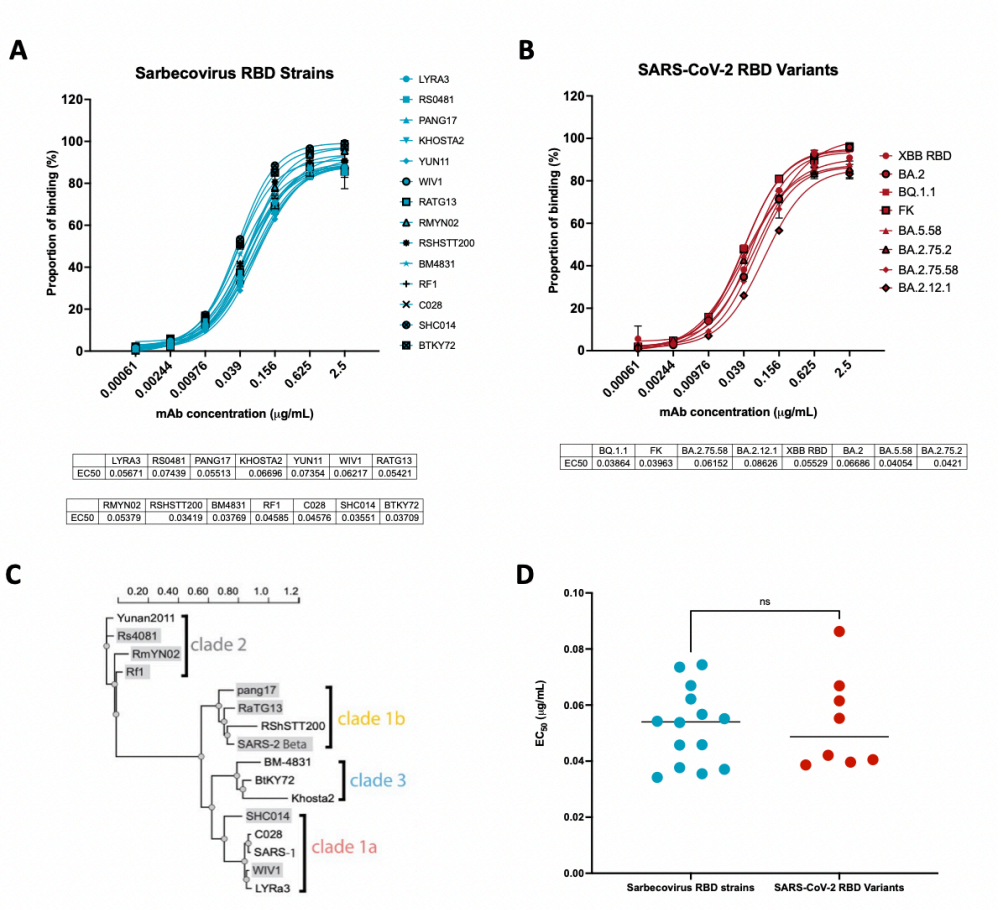

	LYRA3	RS0481	PANG17	KHOSTA2	YUN11	WIV1	RATG13
EC50	0.05671	0.07439	0.05513	0.06696	0.07354	0.06217	0.05421

	RMYN02	RSHSTT200	BM4831	RF1	C028	SHC014	BTKY72
EC50	0.05379	0.03419	0.03769	0.04585	0.04576	0.03551	0.03709

	BQ.1.1	FK	BA.2.75.58	BA.2.12.1	XBB RBD	BA.2	BA.5.58	BA.2.75.2
EC50	0.03864	0.03963	0.06152	0.08626	0.05529	0.06686	0.04054	0.0421

Figure 5.19: C13.7 mAb binding to *Sarbecovirus* RBD panel and SARS-CoV-2 RBD variants. A) *Sarbecovirus* RBD binding curves as proportion of binding (%), whereby 100% was the highest optical density and 0% wells without mAb. Curves generated from a non-linear fit of normalised, 4-fold dilution series of C13.7 mAb (µg/mL). EC_{50}s ranged between 34 and 74 ng/mL. B) SARS-CoV-2 RBD variants binding curves as proportion of binding (%), whereby 100% was the highest optical density and 0% wells without mAb. Curves generated from a non-linear fit of normalised, 4-fold dilution series of C13.7 mAb (µg/mL). EC_{50}s ranged between 38 and 86 ng/mL C) Phylogenetic tree of *Sarbecovirus* RBD strains and their clades (Fan et al., 2022). D) Comparison of *Sarbecovirus* RBD panel and SARS-CoV-2 RBD variants EC_{50}s analysed as unpaired T test. Significance at $P > 0.05$. A-B) Error bars demark standard deviation, N=2.

Considering C13.2 did not neutralise pseudotypes of SARS-CoV-1, binding to the *Sarbecovirus* panel was unexpected. This was confirmed by Sophie Wartnaby who performed the RBD ELISA with C13.2 (Figure 5.20). With the exception of Pang17 (Figure 5.20A), no binding was observed between C13.2 and *Sarbecovirus* RBDs. Reduction of binding was also observed for SARS-CoV-2 RBD strains, particularly to newer variants such as BQ.1.1 and XBB (Figure 5.20B), thus accurate EC_{50}s could not be accurately determined for these strains and variants.

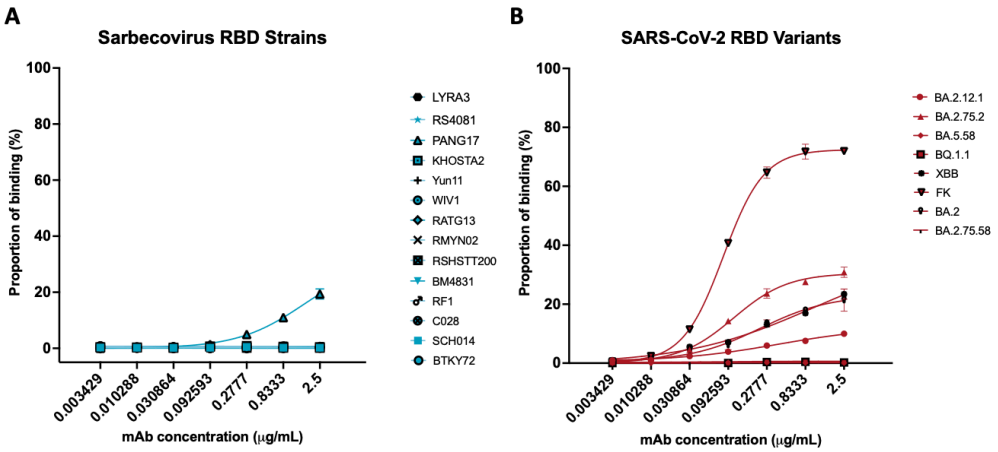

Figure 5.20: C13.2 mAb binding to *Sarbecovirus* RBD panel and SARS-CoV-2 RBD variants. A) *Sarbecovirus* RBD Binding curves as proportion of binding (%), whereby 100% was the highest optical density and 0% wells without mAb. Curves generated from a non-linear fit of normalised, 4-fold dilution series of C13.2 mAb (μg/mL). B) SARS-CoV-2 RBD variants Binding curves as proportion of binding (%), whereby 100% was the highest optical density and 0% wells without mAb. Curves generated from a non-linear fit of normalised, 4-fold dilution series of C13.2 mAb (μg/mL). A-B) Error bars demark standard deviation, N=2.

5.4.13. Structural analysis of C13.2 and C13.7

To further understand the modality of binding from the antibodies and gain insights into the tertiary and quaternary structures of the ultralong CDRH3s, structural work was performed by Dr. Chengcheng Fan at Caltech. Dr. Fan's work confirmed C13.2 as an RBD binding antibody (Figure 5.21). In Figure

5.21A C13.2 is visualised as orange, binding to two monomeric RBDs of a single trimer, locking them in a down conformation, from the side and top perspectives. Figure 5.21B shows C13.2 CDRH3 extending from the Fab as a looping paratope structure (left) and its interaction with a single SARS-CoV-2 RBD, appearing to partially obstruct the RBD (right). Further structural analyses highlighting the residues involved in ACE2 binding are thought to shed light on this and may provide an explanation for the ACE2 ELISA data. The most recent structural data, Figure 5.21C, shows the C13.7 Fab structure independently with the CDRH3 forming a paratope structure protruding from the heavy chain (yellow). In Figure 5.21C, the beta pleated sheets of the ascending and descending stalk supporting the knob of the CDRH3 can be observed. Further analysis of the folding of the CDRH3 will provide insights into the pairing of the cysteines and the disulphide bridges they form.

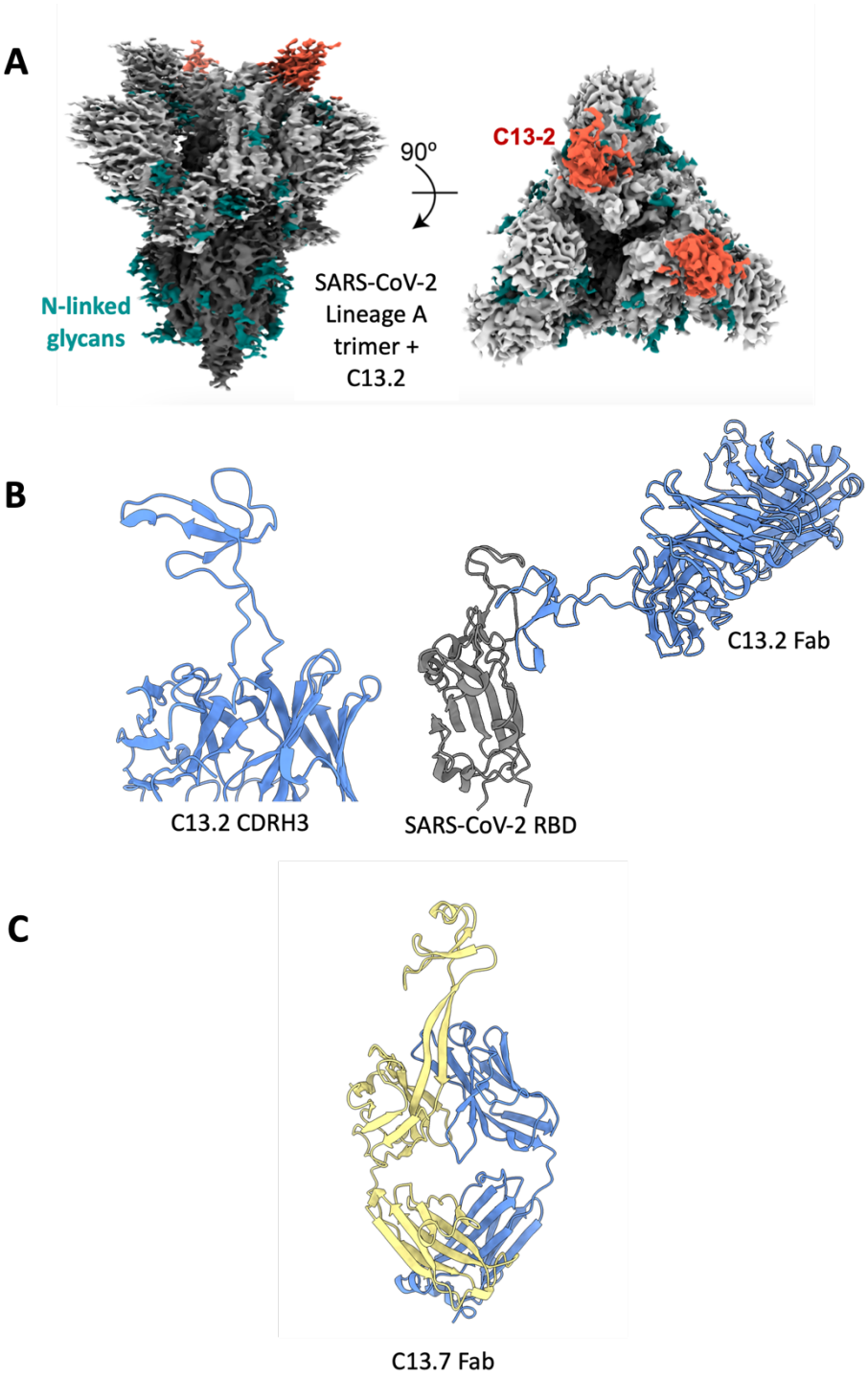

Figure 5.21: EM densities of single-particle cryo-EM structures of C13.2. and C13.7. A) C13.2 (orange)-spike (grey) complex shown from the side (left) and top (right). B) C13.2 as cartoon diagrams of the CDRH3 structure (left), and C13.2 Fab (light blue) interaction with the SARS-CoV-2 Lineage A RBD (grey) (right). C) C13.7 as cartoon diagram of Fab, light chain (blue) and heavy chain (yellow) with the CDRH3 protruding from the Fab.

5.5. Discussion

The employment of therapeutic mAbs for infectious diseases is likely to increase in popularity following their advantage of rapid development and deployment during the COVID-19 pandemic. In the case of SARS-CoV-2, the median time for disease onset to hospitalisation is between five and seven days (Zhou et al., 2020a), and eight to twelve days for ARDS (Li et al., 2020). This highlights an ideal time frame for the delivery of therapeutic mAb to limit infection spread into the lower respiratory tract, thus reducing the establishment of severe disease (Cruz-Teran et al., 2021). Nevertheless, the development of mAbs is faced by challenges in the pipeline such as cost, competition from alternative therapies, and the complexity of escape mutants (Salazar et al., 2017). Further challenges stem from the development, distribution, and implementation since the majority of research laboratories do not have certification to work on live viruses and thus rely on pseudotyped assays. Therefore, the efficacy assessment of mAbs results in a bottleneck (Laustsen et al., 2022). Advances in technology have enabled exploration into new avenues, for instance, harnessing mechanisms from other species, and modification of current therapies to extend their potential. This chapter discussed the characterisation and analysis of two ultralong chimeric antibodies to determine their reactivity and *in vitro* neutralisation to pseudotyped SARS-CoV-2 variants, and potential cross-reactivity to *Sarbecovirus* strains.

Bias to SARS-CoV-2 Lineage A trimer from FACS, validation of the ultralong Fab phage display libraires, and enrichment from the two rounds of biopanning resulted in two ultralong Fab candidates of interest from the bovine repertoires. C13.2 and C13.7 phage clones, initially identified from validation of the library, were selected for characterisation based on high affinity to SARS-CoV-2 Lineage A trimer in the case of C13.2, and cross-reactivity in the case of C13.7. As potential interest for clinical or diagnostic use, these Fabs were modified into chimeric IgG, with the aim of reducing their antigenicity without modifying their binding capabilities. IgG isotype was

chosen for a long half-life and the desired therapeutic effector mechanisms such as complement activation and immune cell recruitment which are important in the response to viral challenge (Waldmann, 2019, Kang and Jung, 2019). As IgA plays an important part in protecting mucosal membranes, chimeric bovine mAbs with the Fc as IgA would be beneficial to explore. IgG antibodies were produced by subcloning the heavy and light chains into cassettes within mammalian pCDNA3 vectors to achieve this. Cloning of the heavy chain was a challenge as the heavy chains from the phagemid lacked an upstream section of heavy chain constant region required for expression. To overcome this, primers were designed to PCR linearise a plasmid harbouring this segment of desired DNA, and to amplify the heavy chains with corresponding homology arms for seamless cloning into the expression vectors. Transient transfection of the heavy and light chain plasmids resulted in two chimeric antibodies consisting of a human constant IgG region and bovine ultralong Fab.

Identification of an antibody candidate is the initial step for developing an antibody therapy, subsequently followed by investigations into large-scale reproducibility. Obtaining high levels of expression ensures manufacturing of the product is financially viable (Kelley, 2009). This is particularly important for chimeric mAbs where altering promotor regions from the native host and expressing in alternative cell lines may influence the level of expression. Using mammalian expression for mAb production is common to ensure precise folding, post-translational modifications such as glycosylation, and assembly. Specifically, glycosylation which is involved in complement-dependent cytotoxicity and antibody-dependent cell-mediated cytotoxicity (Zheng et al., 2011). Fabs from phage are documented to have higher stability such that conversion to full antibodies rarely impairs the binding activity (Bradbury et al., 2011). Expression of C13.2 and C13.7 in Expi293 generated high yields and did not alter the binding of C13.2 and C13.7 to SARS-CoV-2 Lineage A trimer (Figures 5.4 and 5.5), therefore chimeric modification and mammalian expression were successful.

Impurities such as aggregates, DNA and host cell proteins were removed to reduce toxicity or non-specific binding (Liu et al., 2010). This was imperative for accurate characterisation and would be a requirement if mAbs were intended for future diagnostic or therapeutic uses. Protein G affinity was performed to purify preparations of C13.2 and C13.7, and preparations were subsequently quantified using BCA total protein and IgG ELISA quantification (Figures 5.7, 5.9 and 5.10). The purity of preparations was analysed by performing silver staining of reduced preparations, and impurities were analysed through western blotting (Figures 5.8, 5.11 and 5.12). Western blotting also served as confirmation of protein expression. The impurities were identified as heavy chain derived products with the bands present in the silver stain corresponding to the additional bands observed in the western blot in Figure 5.12B, suggesting over-secretion of the heavy chain. A molar ratio of 3:1 of light chain to heavy chain plasmids was used implying that future experiments may be modified to reduce this. Contrarily, the expression of the heavy chain derived products may be occurring through proteolysis of Fc fusion leading to partial cleavage of the expressed protein early on in culture. The addition of protease inhibitors during the transfection has been recorded to combat the proteolysis of recombinant proteins in mammalian cell culture (Chakrabarti et al., 2016), therefore this may be an option for future production of these mAbs. Alternatively, size exclusion chromatography could be used after the expression of mAb resulting in the separation of IgG from heavy chain derived products and impurities (Liu et al., 2009). Impure antibodies may have an impact on EC_{50} and IC_{50} absolute values, therefore optimised expression and purification are recommended for the downstream development of mAbs from this study.

The emergence of novel variants during the pandemic such as Delta (B.1.617.2) and Omicron (B1.1.529), were documented to have increased pathogenicity or transmissibility of the virus, respectively (Chakraborty et al., 2022). Mutations can alter characteristics such as antigenicity resulting in variants with immune evasion to vaccine and natural immunity, and or

monoclonal antibodies (Mileto et al., 2022, Touret et al., 2023, Tuekprakhon et al., 2022). Preliminary experiments of C13.2 and C13.7 binding to SARS-CoV-2 antigens revealed binding of the mAbs was not limited to SARS-CoV-2 Lineage A trimer (Figure 5.4). Potent binding was observed to SARS-CoV-2 variants Alpha (B.1.1.7), Beta (B.1.351), and Omicron (B.1.1.529), the latter of which was recorded to have more than 30 mutations within the spike protein (Chakraborty et al., 2022) compared to Lineage A. Binding was translated to neutralisation. C13.2 and C13.7 neutralised pseudotypes of SARS-CoV-2 Lineage A, Alpha (B.1.1.7), Beta (B.1.351), Omicron (B.1.1.529), Delta (B.1.617.2) and Gamma (P1) (Figure 5.5). As the pandemic developed giving rise to new variants, the binding of the mAbs were tested for their efficacy. C13.2 binding was abolished following the emergence of BA.5 and its mutations. As C13.2 is an RBD binding antibody it was suspected that the three mutations in the RBD of BA.5, L452R, F486V and wild-type amino acid at Q493, influenced this loss in binding. Due to this, it was predicted that C13.2 would not neutralise BA.5. On the other hand, C13.7 retained binding to BA.5 suggesting mutations gained by BA.5 did not influence C13.7 binding, thus may not be involved in C13.7's paratope. The level of potency and differences in binding profiles of C13.2 and C13.7 suggested they bound to unique epitopes.

Considering both mAbs exhibited binding to SARS-CoV-2 Lineage A RBD, it was thought that mAb binding to the RBD would interfere with ACE2 binding. Investigation of this revealed ACE2 binding to SARS-CoV-2 RBD in the presence of mAb high concentration. This trend was observed for both mAbs but was more exaggerated in C13.7. This suggested that mAbs may only partially inhibit ACE2 binding, or bind the RBD in a certain conformation, for instance, binding to a certain number of RBD monomers in the trimer. This is supported by the EC_{50}s to SARS-CoV-2 Lineage A RBD in the ACE2 ELISA which are higher than those recorded in the binding ELISA (Table 5.1). It was predicted that 100% neutralisation would not be achieved for these mAbs. However, ACE2 binding in the presence of neutralising mAbs is not

uncommon, with other studies identifying mAbs with mechanisms to bind and neutralise SARS-CoV-2 without completely interfering with ACE2 binding. For instance, Starr et al. (Starr et al., 2021a) identified mAb, S2H97, which inhibited ACE2-mediated entry by receptor-independent conversion of the spike. This proposed mechanism resulted in the premature refolding of the spike into its post-fusion state prior to the interaction with ACE2. In this situation, the RBD may be required to undergo extensive opening to expose the epitope. In an alternative study (Pinto et al., 2021), mAb S2P6, also did not interfere with ACE2 binding. The proposed mechanism of this mAb is suspected to interfere with the stem helix bundle of SARS-CoV-2 spike, sterically inhibiting fusion with host cells. S2P6 broadly neutralised pseudotypes of strains from *Sarbecoviruses, Merbecoviruses, and Embecoviruses*, targeting the S2 subunit refolding. Moreover, B9-scFV, discovered by Burke et al. (Burke et al., 2022), isolated by a bovine immune repertoire, does not directly interfere with ACE2 binding to the RBD but recognises a site within the RBD resulting in the destabilisation of the trimer. RBD binding antibodies can neutralise SARS-CoV-2 variants without interfering with ACE2, suggesting that ACE2 inhibition may not be a requisite for neutralisation.

Binding EC_{50}s were not reflected in IC_{50}s, which were generally higher, except for Beta (B.1.351) and Omicron (B.1.1.529) for C13.2. C13.2 outperformed C13.7 in most variant pseudovirus neutralisation assays but failed to neutralise SARS-CoV-1, and SARS-CoV-2 BA.5, confirming the binding data in Figure 5.13. Structural studies and site-directed mutagenesis to revert the BA.5 mutations one by one, or in combination, may provide further insight into defining the binding epitope of C13.2. Despite exhibiting similar EC_{50}s to the variants of Lineage A, Alpha (B.1.1.7), Beta (B.1.351), and Omicron (B.1.1.529), C13.2 had greater potency over C13.7, however, C13.7 demonstrated more breadth. The EC_{50} of C13.7 to XBB was higher than the binding data to the other variants, at 55 ng/mL compared to 3-17 ng/mL suggesting this novel variant may contain mutations that hinder the binding

of C13.7. Neutralisation to pseudotypes of XBB was observed for both mAbs, albeit with less potency than the other variants. The IC_{50} of C13.7 to XBB was 1 μg/mL compared to the other variants ranging between 11-368 ng/mL. Due to time constraints, repeats of the neutralisation assays of mAbs to XBB were not performed and therefore these experiments are recommended to be repeated to determine the accuracy of these values. C13.7 neutralisation of pseudotypes of SARS-CoV-1 was of the greatest interest considering these antibodies were raised against SARS-CoV-2 Lineage A, thus not exposed to earlier related strains, highlighting the power of the bovine immune repertoire to generate broadly neutralising antibodies. Further investigations are warranted to understand the neutralisation mechanisms utilised by C13.2 and C13.7 as little ACE2 interference was observed, yet 100% neutralisation was reached. Perhaps these mAbs perform with similar modalities to S2H97, by destabilising the trimer prior to cellular entry, however, determining this may require further structural studies that can image the interaction between SARS-CoV-2 and each mAb.

To further characterise the binding profiles competition ELISAs were performed. No competition, however, potential additive effects, were observed between C13.2 and C13.7 suggesting each had a unique binding epitope. A panel of 14 Fabs were tested for inhibition or additive effects, and one mAb to Fab interaction became of interest. Inhibition was observed between C13.2 and 103, both RBD binders, suggesting they occupy the same or overlapping epitope within the RBD. A caveat of this assay design is that Fab preparations were not purified, thus an accurate EC_{50} could not be equal to the mAb EC_{50}, which would be required for measuring true inhibition or additive effects. Thus, trends of additive effects observed in Figure 5.16C may be artefacts of the assay. Purification of Fab preparations for future experiments may highlight potential interactions between these mAbs and begin to group mAbs depending on the epitope they bind. In addition, analysis of competition using well characterised mAbs such as S2H97 and S2P6 may provide further insight of the binding epitopes of C13.2 and C13.7.

Preclinical and clinical mAbs to SARS-CoV-2 are recorded to have exceptional potencies, exceeding those previously in clinical trials to viral agents (Tang et al., 2019, Ali et al., 2018). Despite this, mutations of 417, 439, 452, 455, 478, 484, 493, and 501 of the RBD have severely reduced the efficacy of current therapeutic mAbs and vaccines. The search for broadly neutralising, pan-*Sarbecovirus* targeting mAbs, has identified candidates with similar characteristics such as C118, C022 (Jette et al., 2021), S2X259 (Tortorici et al., 2021), and E7 (Chia et al., 2023). These studies identify certain residues that are conserved across *Sarbecovirus* strains, suggesting a target for therapeutics. Mutational hotspots of Q493, F486 and R408 are of interest as they may be required to maintain viral fitness and may be involved in forming quaternary epitopes which are highly conserved across *Sarbecoviruses* (Chia et al., 2023*).* The pan-*Sarbecovirus* mAbs identified, however, were donor-derived, thus requiring convalescence from either a natural or vaccine-induced immunity. E7, was isolated from a SARS-CoV-1 recovered individual who received the BNT162b2 mRNA vaccine, thus requiring two different antigen exposures. Evidently, this method of isolation is not ideal for infectious diseases with related strains of high mortality rates. SARS-CoV-1 recorded case fatality rate of around 10% (Guarner, 2020), therefore finding cross-reactive donors from infections of high fatality would be increasingly challenging. Contrarily, bovine ultralong antibodies are rapidly generated following exposure to a pathogen and are recorded to exhibit cross clade neutralisation to challenging disease agents (Sok et al., 2017). Ultralong regions are able to recognise highly conserved regions, targeting sites of vulnerability on viral antigens. The breadth of binding of C13.7 extended across three *Sarbecovirus* clades, binding to 14 *Sarbecovirus* strain RBDs and a further eight SARS-CoV-2 RBDs with sub micromolar affinities (Figure 5.19), suggests C13.7 may be employed as a pan-*Sarbecovirus* mAb, if discovered to neutralise within a reasonable concentration range. C13.7, thought to target a seemingly conserved epitope within the RBD of *Sarbecoviruses,* is remarkable given the modest library size of around 4,200 B-cells, and that it was raised against SARS-CoV-2 Lineage A.

The current data suggests C13.2 and C13.7 have unique binding epitopes; therefore, structural studies were performed to unveil binding mechanisms. Collaborators from Caltech were able to generate cryo-EM structures of C13.2 and C13.7 providing insights into the epitope they bind to. From the structures in Figure 5.21A, C13.2 likely binds to two SARS-CoV-2 RBD monomers of the trimer in a down confirmation. This would leave one RBD available for ACE2 binding, thus providing a potential explanation for the ACE2 binding data. However, steric hindrance of this interaction may restrict the ability of this RBD to bind to ACE2 which may result in complete neutralisation. ACE2 can be found both as membrane-bound and soluble, which may alter binding to the RBD (Yeung et al., 2021). This may result in contradictory data from ACE2 usage in different assays and could explain why the neutralisation data in this study does not support the ACE2 ELISA data. A mAb analysed by Dr. Fan, M8a-28, binds to SARS-CoV-2 RBD with a similar conformation, locking all three RBDs, rather than two, in the down confirmation (Fan et al., 2022). M8a-28 shares similarities with C13.2, recorded to be a potent neutraliser to SARS-CoV-2 variants only. Interestingly, M8a-28 targets epitopes outside of the ACE2 receptor binding footprint. As a class 3 antibody, it binds to a non-occluded epitope that exhibits high levels of variation among *Sarbecoviruses.* Hence, future variant substitutes were predicted to abrogate the efficacy of M8a-28. If C13.2 is a class 3 antibody, this was likely the cause for the loss of efficacy to SARS-CoV-2 BA.5. This may be a possibility as no binding was observed to the *Sarbecovirus* RBD panel with the exception of modest reactivity to Pang17 (Figure 5.20A). Moreover, C13.2 had clear reductions in binding to the SARS-CoV-2 RBD variants of Figure 5.20B compared to the parental variants they evolved from, further supporting the notion that C13.2 could be a class 3 antibody. However, this is purely speculative without further structural analyses. An initial cryo-EM structure of C13.7 Fab shows the CDRH3 paratope structure protruding from the Fab, with the beta ribbon of the ascending and descending strands supporting the knob of the CDRH3 (figure 5.21C). The Fab in complex with SARS-CoV-2 could not be obtained for C13.7, suspected to be due to its mode

of binding, thus resulting in the destabilisation of the spike. C13.7 mechanism of binding to the RBD may occur similar to mAbs described to have pan-*Sarbecovirus* binding activity, thus binding to an occluded epitope (class 1 or 4 (Song et al., 2023)). More recent studies by Song et al. predict a potential site 'v' in class 2 antibodies, which is thought to be highly conserved between *Sarbecoviruses* (Song et al., 2023), highlighting another class that C13.7 may be attributed to. In the absence of the cryo-EM structure in complex with SARS-CoV-2 RBD, the binding of C13.7, and thus the prediction of its mechanism of neutralisation remains unknown. Extensive literature (Haakenson et al., 2018, Smider and Smider, 2020, Deiss et al., 2019) highlights the importance of cysteines in the formation of disulphide bonds, which are documented to be integral to the unique paratope structures formed in bovine ultralong antibodies. Considering three cysteines within C13.7 CDRH3 are adjacent to one another, disulphide bridges are suspected to form between each of these cysteines and others present in the CDRH3, which may form two or three globular loops. The initial C13.7 Fab structure indicates that this may be the case. Such a complex structure may bind to conserved, distal residues, binding an epitope that may be unattainable for a singular human mAb. If this site is conserved between *Sarbecovirus* RBDs, in which the RBD binding ELISA data suggests, then this may be a therapeutic site to target for *Sarbecoviruses.* To this end, future studies and analyses of C13.7 are recommended to explore its cryo-EM structure to confirm this, as well as *in vitro* live-virus studies and *in vivo* models to determine its clinical potential.

Indeed, *in vitro* neutralisation does not always directly translate to *in vivo*. Many mAbs with promising preliminary data fail during clinical trials. For instance, IV infusion of motavizumab to RSV (Ramilo et al., 2014), and KZ52 to Ebola (Oswald et al., 2007). However, if the neutralisation obtained for C13.7 during this study translates into *in vivo* neutralisation, various modifications may be required for its employment as a therapeutic. Studies by Sok et al. (Sok et al., 2017) previously demonstrated attempts to reduce

immunogenicity by transplantation of bovine knobs onto human scaffolds of long CDRH3-bearing human scaffolds to deliver the agent. However, further optimisation may be required for manufacturing or to gain stability. Moreover, CDRH3s may be utilised alone where effector functions are not required (Macpherson et al., 2021a), providing a multitude of avenues for bovine ultralong antibody modifications.

Recommendations for future experiments regarding C13.7 involve the grafting of C13.7 CDRH3 to a human IgG scaffold that may support the ultralong structure. Given that these structures can function independently it is theorised that this may work to humanise instead of generating chimeric antibodies which may be immunogenic, particularly where multiple doses may be required. Previously documented as the longest CDRH3 in humans, PG16 harbours a 28-residue CDRH3, suggesting this VDJ may tolerate a long CDRH3. It is worth investigating the stability of C13.7 CDRH3 incorporated in a natural or synthesised scaffold consisting of PG16 germlines IGHV3-33, IGHD3-3, and IGHJ6-03 to determine the possibility of this modification (Pancera et al., 2010). Efficacy of C13.7 modifications, and as a chimeric mAb, will need to be tested against live virus and *in vivo*, to determine any clinical potential.

Developments of mAbs for clinical or diagnostic use are still required to outweigh the disadvantages commonly associated with mAb therapy. For instance, the main issues arise from higher production costs and competition from other treatments. Further challenges to overcome include the bottleneck of efficacy assessments due to the infectious nature of viruses (Laustsen et al., 2022) and regulatory approval which can influence delays in distribution and administration (Liao and Li, 2022). However, the advantages of mAbs warrant further focus on their development. MAbs can be used in a diagnostic and prophylactic setting, initially identifying disease susceptibility and subsequently administration following disease onset to curtail to hyperinflammatory stage associated with severe disease. Advances in delivery indeed provide a promising future for clinically therapeutic mAbs, with

options to deliver by vector, and recently, via inhalation. For instance, inhaled delivery of Omalizumab (humanised mAb to Influenza) was recorded to be fast acting and exhibit superior efficacy compared to the same mAb administered intraperitoneally *in vivo*. Increased potency was observed with a lower dosage and at a later time point within the infection (Leyva-Grado et al., 2015). Such advances, particularly to a mAb that exhibits cross clade reactivity, may have importance in the diagnosis and treatment of infectious respiratory viruses.

5.6. Conclusion

Bovine ultralong mAbs, particularly if generated rapidly from pathogenic exposure, may be useful in identifying conserved cross clade epitopes of challenging viral agents. The discovery and characterisation of C13.7, and its continued characterisation may result in a therapeutic mAb for the diagnosis, and potential treatment of future *Sarbecoviruses.* If discovered to neutralise across *Sarbecoviruses,* both *in vitro* live virus studies, and *in vivo* animal models, may identify a candidate in which developments such as scaffolds, and newly emerging delivery methods can be applied. The success of a broadly neutralising bovine ultralong mAb, rapidly developed through a high throughput system like phage display, and deployed, has great promise for future therapeutics.

Chapter 6 General Discussion

The recurrent zoonotic spillovers of coronaviruses urgently call for broadly neutralising antibodies that can accompany the antigenic evolution of pathogens. The development and rapid deployment of mAbs in response to the pandemic by SARS-CoV-2 reduced severe disease, and in doing so, ultimately prevented deaths (Focosi et al., 2022). Despite the successful deployment of mAbs for treating infectious diseases, there is a need to identify exceptional, high-quality mAbs with broadly neutralising traits that can withstand viral evolution.

Treatments to SARS-CoV-2 have faltered in the challenges presented by the emergence of each novel variant. The disease heterogeneity of COVID-19 is theorised to have generated mixed results in patients for many treatments (Group, 2021). For instance, antivirals such as Paxlovid, approved for use in the UK and USA in December 2021, was associated with viral resurgence of up to 10%, and with one in eight experiencing high viral titres post-treatment (Deo et al., 2022, Boucau et al., 2023). Antivirals are most effective when delivered promptly to reduce viral load, and are heavily reliant on rapid diagnostics with a low level of detection (Singh and de Wit, 2022), therefore, are only a short term solution.

Vaccines and their boosters, developed at a faster timescale than traditionally, were recorded to reduce transmissibility, and protect from severe disease. However, current vaccines do not produce sterilising immunity, therefore, leading to reinfections and leaving individuals such as the immunocompromised vulnerable (Krammer, 2020). Booster doses derived from the Lineage A variant induced high antibody titres but lacked specificity in the B-cell response to subsequent variants, thus reducing protection against reinfection from evolving variants (Goel et al., 2021b). Newly emerging variants have impacted antibody mediated durability from natural, vaccinated, and hybrid immunity, with titres waning over time and reinfections reported between 3-63 months (Zhou et al., 2021, Liu et al., 2021, McCallum et al., 2021a, Wibmer et al., 2021, Chen et al., 2021,

Goldberg et al., 2022, Perez-Alos et al., 2022, Townsend et al., 2021). This called the need for bivalent vaccines as part of a booster programme, requiring regular updating to extend humoral immunity and match the antigenic evolution of the virus.

Comparatively, mAbs were reported to have higher success in viral clearance compared to therapies such as antivirals and can act complementary to vaccines (Zheng et al., 2022). However, antibody responses to viral infections commonly form a trade-off between potency and breadth (Corti et al., 2010, Wagh et al., 2016). In the case of SARS-CoV-2, the most potent antibodies competed with ACE2 for the RBD (Barnes et al., 2020a, Dejnirattisai et al., 2021, Huang et al., 2021, Liu et al., 2020, Piccoli et al., 2020). This region readily accumulated mutations thus impacting the efficacies of vaccines and approved mAb treatments. Diligent tracking of novel variants identified mutations associated with selective fitness, either by increasing transmissibility, enhanced viral affinity for ACE2, and or antibody evasion (Yurkovetskiy et al., 2020, Plante et al., 2021, Edara et al., 2021, Zhou et al., 2021, Planas et al., 2021, Chakraborty et al., 2022, Uraki et al., 2023a). For instance, mutational hotspots of Q493, F486 and R408 are of interest as they may be required to maintain viral fitness and may be involved in forming quaternary epitopes which are highly conserved across *Sarbecoviruses* (Chia et al., 2023). MAbs approved for therapeutic use, mainly isolated from convalescent donors, were often variant specific, thus susceptible to immune escape by the emergence of novel variants (Brouwer et al., 2020, Cao et al., 2020, Chen et al., 2020, Ju et al., 2020, Liu et al., 2020, Noy-Porat et al., 2020, Robbiani et al., 2020, Rogers et al., 2020, Seydoux et al., 2020, Wan et al., 2020, Zost et al., 2020, Pan et al., 2021, Wrapp et al., 2020b, Pinto et al., 2020). This was observed for mAbs Bamlanivimab (LY-CoV555 and LY-CoV016; Eli Lilly) (Starr et al., 2021b), Bebtelovimab (LY-CoV1404; Eli Lilly) (Wang et al., 2022), Imdevimab (REGN-COV2; Regenron) (Dejnirattisai et al., 2022), Tixagevimab and Cilgavimab (Evusheld), with Sotrovimab recorded to be the only mAb retaining modest reactivity to the most recent variants BQ.1.1 and

XBB.1.5 (Imai et al., 2023, Widyasari and Kim, 2023, Iacobucci, 2023). Given that these new variants will likely establish dominance within the population and emerging variants will probably derive from newly dominant strains, retention of neutralisation by Sotrovimab is of great concern. During this time, research into S2 targeting antibodies, recognising a conserved region within coronavirus spikes, were reported to offer cross-reactivity, however, tended to be less potent (Sauer et al., 2021, Shah et al., 2021, Wang et al., 2021a). In addition to S2 mAbs, research into soluble ACE2-fusion to Fc were explored, such as MDR504 recorded to neutralise SARS-CoV-2 variants and retain a longer half-life than soluble ACE2, however, have not yet been investigated for broad reactivity to other *Sarbecoviruses* (Iwanaga et al., 2020).

In severe cases, mAb and antiviral treatments have been commonly used in combination (Takashita et al., 2022, Mouffak et al., 2021). This has been a requirement for the immunocompromised who often cannot receive vaccinations or have suboptimal responses and thus develop persistent infections. In immunocompromised patients, such as those diagnosed with leukaemia or lymphoma, responses to vaccination are documented to be suboptimal (Lanzafame et al., 2023). Moreover, persistent infections in the immunocompromised are suspected to serve as a source for new variants. For example, SARS-CoV-2 mutations have been linked to resistance to Sotrovimab in patients receiving this mAb for treatment (Huygens et al., 2023). In addition to the immunocompromised, there are multiple reports of post-acute sequelae of COVID-19, referred to as 'Long COVID' (Lopez-Leon et al., 2021). Associated with low levels of seroconversion, low baseline IgG and few spike-specific memory B-cells, Long COVID is estimated to occur in 10% of infections (Augustin et al., 2021, Davis et al., 2023), thus, may represent a significant public health challenge. Vaccination is thought to reduce the duration (Tran et al., 2023) and provide partial protection from Long COVID (Al-Aly et al., 2022). Despite this, antibody waning has been documented in these individuals

(Nomura et al., 2021), suggesting a need for robust therapeutics to complement vaccines for COVID-19.

The search for mAbs that confer broad reactivity and retain potent neutralisation has identified candidates isolated from convalescent donors, generally through a combination of natural and vaccinated immunity. E7, C118, C022, S2H97, and S2X259 recognise cross clades strains and confer broad *Sarbecovirus* neutralisation (Jette et al., 2021, Tortorici et al., 2021, Starr et al., 2021a). However, the mAb recorded to exhibit the most extensive cross-reactivity, E7, required two different antigen exposures – a SARS-CoV-1 natural infection and the BNT162b2 mRNA vaccine, suggesting priming from similar strains are required to establish a broadly neutralising antibody response in humans.

The development of therapeutic mAbs faces challenges in the pipeline such as cost, competition from alternative therapies, and the complexity of viral escape mutants (Salazar et al., 2017). Animal antibodies are commonly overlooked as antibody therapeutics due to their levels of immunogenicity, and thus have higher risk (Harding et al., 2010). However, in the context of challenging disease agents, natural immunity and passive immunity often fall short (Tannock et al., 2020, Fauci and Marston, 2015, Wiedermann et al., 2016), leaving many susceptible to reinfection. A recently explored avenue into bovine ultralong antibodies highlights an untapped reservoir of naturally occurring antibodies recorded to exhibit characteristics conferring broad reactivity (Berens et al., 1997, Burke et al., 2022, Dong et al., 2019, Saini et al., 2003, Sinclair et al., 1997, Wang et al., 2013, Zhao et al., 2006, Sok et al., 2017). Bovine ultralong CDRH3 form unique paratope structures documented to bind to challenging epitopes, specifically in the context of challenging viral agents such as HIV. The longest recorded human mAb, PG16, is recorded to neutralise across eight clades of HIV (Walker et al., 2009), whereas bovine ultralong antibody NC Cow 1 neutralised 11 clades of HIV. Furthermore, PG16 was obtained from a HIV positive patient with an infection for at least three years. However, the bovine ultralong antibody, NC Cow 1, was isolated from a

cow that established 79% cross clade neutralisation by day 77 of the study. Neutralisation continued to rise with subsequent booster immunisations. This suggests bovine broadly neutralising ultralong antibodies can be rapidly generated from a single antigen in comparison to human antibodies which require years of priming and somatic hypermutation to gain cross-reactivity (Sok et al., 2017).

This study aimed to move beyond traditional antibody therapies and investigate bovine ultralong antibodies, recorded to be a rich, naturally occurring source, which if tapped into may aid in the search for broadly neutralising therapeutics. Considering ultralong antibodies of broad reactivity can be rapidly elicited to the exposure of a pathogen, this study aimed to generate a high throughput method to isolate bovine ultralong antibodies to SARS-CoV-2 Lineage A trimer from two sources of hyperimmune cows. Harnessing the versatility of phage display, the expression on p3 of M13 bacteriophage successfully supported the ultralong Fab structures, and thus, the selection of high affinity binders could be isolated through biopanning. Upon the success of generating bovine ultralong phage display libraries with representative diversity of the source, the study aimed to isolate Fabs of interest and characterise the bovine ultralong antibodies in a human Fc scaffold. This project aimed to deepen the current understanding of bovine ultralong antibodies, design an effective display mechanism for their isolation, and identify avenues for their modifications for use in identifying conserved epitopes, as diagnostics, and if conferring broad neutralisation, prophylactic use.

The most extensively applied system of displaying antibodies is phage display, due to low propagation costs, genetic stability, ease of handling, and a high level of adaptability to suit experimental design, enabling the production of large libraries without compromising on the diversity of the source (Parmley and Smith, 1989, Hoogenboom et al., 1991). In this study, the sources of library construction were two bulk-sorted B-cells reactive to SARS-CoV-2 Lineage A trimer from two hyperimmunised cows. Libraries generated from

hyperimmune sources benefit from affinity matured antibodies, which have high affinity towards the target (Noy-Porat et al., 2020). Hyperimmune libraries are commonly derived from convalescent donors, however, this study used an animal source, thus required ethics to perform bovine immunisations. However, the bovine immune repertoire has the ability to generate highly diverse antibodies, using a singular germline during heavy chain recombination, such that exposure to a pathogen can rapidly generate multiple candidates of high affinity to the target (Sok et al., 2017). Although this study used a source that had witnessed multiple immunisations, preliminary data from the serum early on the immunisation schedule indicated reactivity to SARS-CoV-2 Lineage A trimer and SARS-CoV-1 (data not shown). This reactivity may be through a polyclonal response or individual cross-reactive antibodies.

Phage display offers a flexible platform for the display of a multitude of antibody formats (Parmley and Smith, 1988). The experimental design was carefully tailored to accomplish the aims of this study. Bovine ultralong antibodies were chosen to be expressed as Fab for several reasons. Fab fusions have less of a tendency to dimerise (Griffiths and Duncan, 1998) and are thought to be more stable. Moreover, bovine light chains are thought to contain structural features that optimise ultralong heavy chain binding (Arun et al., 1996, Pasman et al., 2010, Saini et al., 2003, Ramirez Valdez et al., 2023). It should be noted however, that bovine heavy chains have been reported to function independently (Sok et al., 2017). The versatility of employing a phagemid vector resulted in the successful generation of two bovine ultralong heavy chain libraries on p3 of M13 bacteriophage. Display on the minor coat protein resulted in the expression of unique Fab at low valency, enabling the selection of high affinity Fab to the target (Breitling et al., 1991, Smith and Petrenko, 1997, Lowman et al., 1991, Sidhu, 2001). During library construction, adjustments were made for optimisation, and removal of bias were performed during amplification, assembly, cloning, and transformation. This included growth on solid media throughout the process

to avoid reductions in diversity during consecutive amplifications (Castel et al., 2011), and the use of TG1 cell lines for cloning efficiency. Validation of these adjustments ensured heavy chain representation of the libraries. To achieve this, colony screening and sequencing throughout the process identified areas where improvements to the process could be made. For instance, PCR linearising the vector to reduce the presence of light chain only vectors. NGS was beneficial tool in this study, resulting in the analysis of library construction, identifying areas of bias and ensuring source representation to mitigate loss of diversity, as well as identifying clonal variation within the population.

The analysis of library construction gained insights into several recommendations for future phage display of bovine ultralong Fabs. Library representation is of the utmost importance for successfully constructing a phage display library. Steps are recommended to safeguard the integrity and representation of the library source. For example, cloning efficiency, despite the initial library size, should aim to be at the highest achievable, this ensures rarer clones in the population have an equal chance of being represented. Where possible, construction is recommended to be validated, through Western blotting, ELISA and NGS. Specifically, the use of Illumina services covering longer reads which can result in the identification of rarer, longer heavy chain sequences. Furthermore, NGS data should be analysed through an antibody database of high integrity, or multiple databases to ensure accuracy of diversity inference. NGS can be advantageous for the tracking of clones that are well represented, and underrepresented, in the population, thus theories regarding population diversity can be inferred from this. Future advances in NGS technology and its costs, as well as the expansion and validation of databases, are thought to be beneficial for the analysis of phage display studies in the future. Perhaps a caveat to note for natural libraries is the lack of control over clonal variation. Variations in expression, due to translational, transportation, or stability differences of the fusion, may have generated a selection and amplification bias, particularly if certain sequences

form a greater percentage in the repertoire (McCafferty, 1996, Barbas et al., 1991, Lowman et al., 1991). Although this is not necessarily within control, it requires consideration when analysing the diversity and output of biopanning.

The versatility of phage display continues through the process of biopanning, which can be altered and modified to isolate a range of antibodies of varying affinities (Smith and Petrenko, 1997). The construction of C13 and C18 phage display libraries resulted in two libraries that were subsequently employed for high throughput screening of bovine ultralong Fab. Effective panning of a library required careful consideration of the display format, the quality of the library and its target, the number of panning rounds and the level of stringency and elution. The quality of the library was thoroughly assessed in Chapter 3 and biopanning optimisation assessed in Chapter 4. For biopanning, a high-quality target was paramount for selecting binders with high specificity to the target and are unlikely to non-specifically bind to off target motifs. Immobilised targets using passive adsorption is the most widely used mechanism for target presentation, with indirect immobilisation as preferable compared to direct immobilisation. Converse to most of the current literature (Dundas et al., 2013, Ivanov et al., 1992, Ledsgaard et al., 2018, Ledsgaard et al., 2022b), this study found non-specific binding to the capture protein Neutravidin, resulting in the use of direct immobilisation of targets for biopanning. In between biopanning rounds, modifications to the saturant and washing steps reduced the likelihood of non-specific binding and acted to increase the stringency between biopanning rounds.

This study was unique in that the source was previously enriched to spike-specific cells through FACS, therefore the first round of biopanning against SARS-CoV-2 Lineage A trimer acted as a second round of enrichment, and ultimately resulted in the discrimination between low and high affinity binders. This enabled investigations into cross-reactivity by cross-panning to SARS-CoV-2 BA.5 trimer following R1 biopanning. The C13 library performed as predicted, with increased levels of binding to SARS-CoV-2 Lineage A trimer after R1. Interestingly, R1 enrichment increased library binding to SARS-CoV-2

BA.5 trimer. Furthermore, enrichment was observed when comparing R1 binding to SARS-CoV-2 BA.5 to the pre-panned library, suggesting enrichment of cross-reactive phage within the population. This was confirmed following R2 panning. Unexpectedly, C18 library did not follow these trends, or identify an ultralong candidate to either of the SARS-CoV-2 baits. This is a likely result, and a good example, of how a poorer quality library can reduce the success of the panning stage. Indeed, immunisation with SARS-CoV-2 antigens stimulated the production of non-ultralong antibodies, which were selected for, thus ultralong antibodies present in the C18 library may not have had a high level of binding to the targets. This methodology provides a framework for the high throughput selection of broadly reactive bovine ultralong antibodies to challenging disease agents within a rapid time scale. Particularly in a pandemic setting, phage display of bovine ultralong Fab could be easily modified to cross pan for conserved epitopes, thus enabling the development and characterisation of a mAb with resistance to viral evasion.

The validation of the libraries resulted in two candidates of interest, which were also selected through biopanning rounds. C13.2 phage, which presented with the highest affinity to SARS-CoV-2 Lineage A trimer, and C13.7 phage which exhibited cross-reactivity, and thus bound to SARS-CoV-2 Lineage A and SARS-CoV-2 BA.5 trimers. Validation steps determined binding was specific to SARS-CoV-2 glycoprotein, which warranted further investigations into the Fab, thus potentially identifying a broadly reactive antibody to SARS-CoV-2. Phage display relies on *E. coli* which limits the display of more complex molecules like IgG (Kay et al., 1996). Therefore, phage display often requires a subsequent cloning step to modify Fab or scFv of interest into full immunoglobulin. C13.2 and C13.7 were modified into chimeric bovine-human antibodies for subsequent characterisation. Analysis of C13.2 and C13.7 mAb expression determined that the yield exceeded previous in-house expression of ultralong chimeric bovine mAbs. A probable explanation for this is that during the phage display process, bovine Fab with biophysiological properties such as exhibiting a higher level of expression may have been selected,

therefore eliminating Fab that expresses poorly. In the realm of therapeutic mAbs, obtaining high levels of expression is crucial for ensuring manufacturing of the product is financially viable (Kelley, 2009). MAbs were purified, filtered, and desalted prior to downstream analysis by silver stain and Western blot. For both mAbs, the heavy chain was discovered to be over-secreted, resulting in heavy chain derived products. Several suggestions to overcome this outline the use of protease inhibitors, reducing the molar ratio of heavy chain to light chain, and size exclusion chromatography for future purer mAb extractions.

Characterisation of the binding profiles of each mAb identified binding to SARS-CoV-2 variant spike proteins, with the exception of SARS-CoV-2 BA.5 RBD for C13.2. Considering binding was observed to the RBD, it was expected that mAbs would compete with ACE2. This was not the case for either mAb, whereby ACE2 binding to SARS-CoV-2 RBD occurred in the presence of high mAb concentration. This suggested that mAbs may only partially inhibit ACE2 binding, or bind the RBD in a certain conformation, for instance, binding to a certain number of RBD monomers in the trimer. This resulted in the theory that neutralisation would not reach 100% as ACE2 binding would be permitted. In light of the ACE2 experiments and binding profiles to SARS-CoV-2 variants, the mAbs were tested for competition, thus providing insights into their binding epitopes. The initial competition ELISAs suggested the two mAbs bind unique epitopes and may have an additive effect. Comparisons to an in-house derived Fab panel identified strong inhibition between C13.2 and Fab 103, a previously characterised RBD binder, thus it is probable that they occupy the same, or an overlapping epitope within the RBD. It was recommended that the competition ELISAs require repeating to establish trends of true additive effect or inhibition, with the caveat that Fabs were not purified and so could not be accurately quantified, thus current data only serves as an indication of trends.

Pseudovirus neutralisation was observed for all variants, with the exception of C13.2 to SARS-CoV-2 BA.5 trimer, as expected from the binding ELISA data.

C13.2 exhibited greater neutralisation potency compared to C13.7, however, C13.7 presented a greater neutralisation breadth to pseudoviruses of SARS-CoV-2 variants. The least potent neutralisation for both mAbs was to the recent variant of XBB, suggesting SARS-CoV-2 is still evolving to evade antibody responses, and, or, responding to the selective pressure of current therapeutic mAbs. The most compelling result was that C13.7 also neutralised pseudoviruses of SARS-CoV-1, indicating cross clade recognition. This was of interest as both these clones were found in the initial library which had low source representation and were subsequently found to be well represented in the source. Perhaps the most conflicting was between the pseudovirus neutralisation and ACE2 data with both mAbs reaching 100% neutralisation for most variants suggesting there may be an alternative explanation for the ACE2 data. Given mechanisms of human antibody neutralisation to SARS-CoV-2 have been documented to occur with little to no interference of ACE2 binding, (Starr et al., 2021a, Pinto et al., 2020), it is probable that C13.2 and C13.7 may achieve neutralisation in a similar way. Determining the mechanism by which these mAbs neutralise requires in-depth structural analysis, and live virus *in vitro* studies to confirm the pseudovirus neutralisation results.

Investigating the cross-reactivity of C13.7 discovered that C13.7 bound to 14 *Sarbecovirus* strain RBDs ranging clades 1 to 3, and a further eight SARS-CoV-2 RBDs, with high affinities, leading to the conclusion that C13.7 may be employed as a pan-*Sarbecovirus* mAb, if discovered to neutralise these strains within a reasonable concentration range. Demonstrating the power of the bovine immune repertoire, C13.7 is thought to target a seemingly conserved epitope within the RBD of *Sarbecoviruses,* which is remarkable, given the modest library size of around 4,200 B-cells and that it was raised against the original variant, SARS-CoV-2 Lineage A, thus not exposed to relatives or later variants.

Towards the end of this study, collaborators at Caltech performed structural studies on mAbs C13.2 and C13.7. Results indicated a potential mechanism of

binding for C13.2, providing insights into its binding epitope. C13.2 binds to two SARS-CoV-2 RBD monomers of the trimer in a down confirmation, potentially allowing one monomer to interact with ACE2, which supports the ACE2 data. Contradictory to this, steric hindrance may act in preventing binding, thereby enabling full neutralisation which was observed in the pseudovirus neutralisation data in Chapter 5. Further analysis of the structural data is suspected to shed light on this. Despite obtaining a Fab structure of C13.7, the structure of C13.7 in complex with SARS-CoV-2 RBD could not be obtained suspected to be due to its mode of binding. C13.7 mechanism of binding to the RBD may occur similar to mAbs described to have pan-*Sarbecovirus* binding activity, thus binding to occluded epitopes within the RBD. The even number of cysteines in the sequence in conjunction with their pairing in the Fab structure, sheds light on the tertiary structure of C13.7's CDRH3. Such a complex structure may bind to conserved, distal residues within the RBD, binding to an epitope that may be unattainable for a singular human mAb. The epitope in which C13.7 binds, suspected to be conserved between *Sarbecovirus* RBDs, may be a therapeutic site to target for *Sarbecoviruses*. To this end, further structural studies of C13.7 and *Sarbecovirus* RBD binding ELISAs to strains from other clades are recommended to try to obtain its structure in complex with SARS-CoV-2 RBD to unveil its method of binding, and to determine whether the epitope is conserved across *Sarbecoviruses*, respectively.

The current literature suggests bovine ultralong antibodies are highly versatile, easily modified to chimeric mAbs or work independently (Sok et al., 2017, Macpherson et al., 2021b, Macpherson et al., 2020, Huang et al., 2023). Grafting of C13.7 CDRH3 into a human IgG scaffold capable of stabilising such structures may be a viable option for therapeutics, particularly where Fc receptor functions can generate a more desired immune response (Sok et al., 2017). Humanising C13.7 would serve to reduce immunogenicity thus allowing for multiple dosages as a therapeutic. This may have advantages as complementary treatment alongside vaccines for the immunocompromised

and those with Long COVID or in which vaccination generates a suboptimal response. Efficacy of C13.7 grafts, and as a chimeric mAb, will need to be tested against *in vitro* live virus and *in vivo*, to determine any clinical potential. Given that SARS-CoV-2 continues to evolve in fitness and current treatments are reducing in efficacy, it is of utmost importance that mAbs conferring broad protection are escalated through the clinical pipeline. Specifically, current emerging variants are derived from recombination events (Tamura et al., 2023), potentially emerging within immunocompromised individuals, implying a viable treatment for these individuals is urgently needed.

MAbs are powerful agents in a diagnostic and prophylactic setting, initially identifying disease susceptibility and subsequently, administration following disease onset to curtail severe disease. Advances in modifications and delivery indeed provide a promising future for clinical therapeutic mAbs, with various options to humanise and deliver, for instance, by vector, and recently, via inhalation (Leyva-Grado et al., 2015). This research, however, extends beyond this pandemic of SARS-CoV-2, addressing the wider challenge of combatting viral agents. The combination of harnessing the screening advantages of phage display to a complex source such as bovine ultralong antibodies demonstrates how this could be applied in any viral challenge to rapidly produce mAbs conferring broad protection, influencing the use of bovine mAbs as therapeutics to viral entities. Moreover, bovine ultralong mAbs, particularly if generated rapidly from pathogenic exposure, may be useful in identifying conserved cross clade epitopes of challenging viral agents to aid in the development of vaccines. In a pandemic setting, time is of the essence. Given COVID-19 vaccines were produced in just under a year, there is a need for a treatment that can be employed during this time to reduce preventable deaths. A bovine ultralong candidate, like C13.7, may be rapidly isolated through a high throughput system like phage display, and if discovered to confer broad protection, may be deployed as a therapeutic in the arsenal of tools against future viral pandemic threats.

Appendix I – HIV Fab fused to truncated gene 3 protein

HIV Phage amino acid sequence from IgH to end of gene 3:
EEFKMKYLLPTAAAGLLLLAAQPAMAQVQLRESGPSLVKPSQTLSLTCTVSGFSLSDKAVGWVR
QAPGKALEWLGSIDAAGNTGYNPGLKSRLSITKDNSKSQVSLSVNSVSNEDSATYYCITAHQKTN
KKECPEDYTYNPRCPQQYGWSDCDCMGDRFGGYCRQDGCSNYIHRSTYEWYVSAWQGLLVT
VSSASTTAPKVYPLSSCCGDKSSSTVTLGCLVSSYMPEPVTVTWNSGALKSGVHTFPAVLQSSGL
YSLSSMVTVPGSTSGQTFTCNVAHPASSTKVDKAVDPTCKPSPAGGGSGGGSGGGSEGGGSEG
GGSEGGGSEGGGSGGGSGSGDFDYEKMANANKGAMTENADENALQSDAKGKLDSVATDYG
AAIDGFIGDVSGLANGNGATGXFAGSNSQMAQVGDGX = 39.14 kDa

Appendix II - C13.2 and C13.7 Heavy chain in the phagemid



Annotated C13.2 Heavy chain in the phagemid vector.

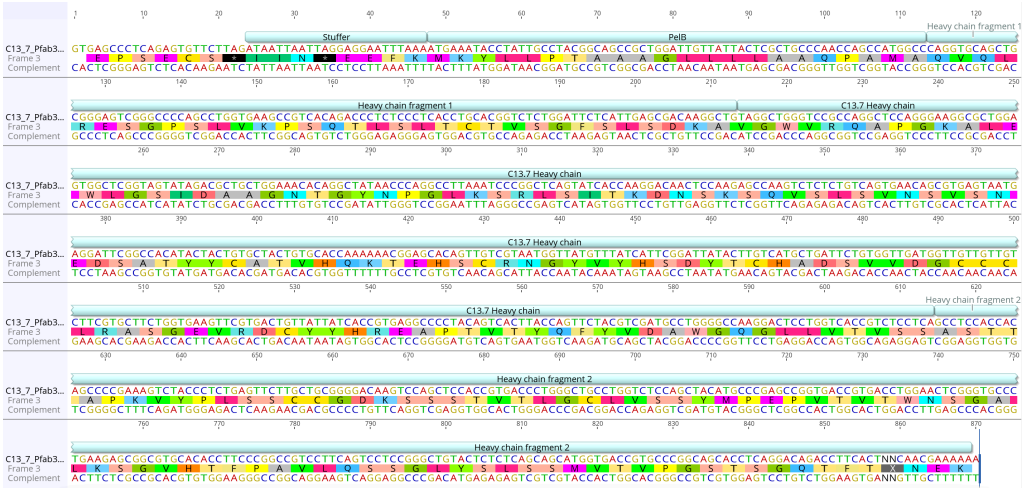

Annotated C13.7 Heavy chain in the phagemid vector.

Appendix III – RBD BCA assay and Anti-avi-tag ELISA

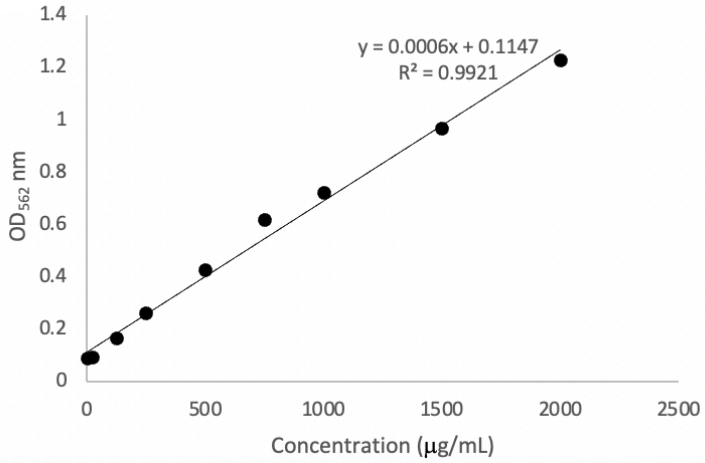

	Estimated concentration	Mean OD	Dilution Factor	μg/mL	mg/mL	Average mg/mL
LYRA 3 1:2	194.7273	0.227	2	389.454684	0.38945468	0.33907837
LYRA 3 1:5	57.74041	0.148	5	288.70205	0.28870205	
RSHSTT200 1:2	314.3742	0.296	2	628.748312	0.62874831	0.64079642
RSHSTT200 1:5	130.5689	0.19	5	652.844528	0.65284453	
RATG13 1:2	250.2157	0.259	2	500.431439	0.50043144	0.53328769
RATG13 1:5	113.2288	0.18	5	566.143938	0.56614394	
KHOSTA2 1:2	338.6503	0.31	2	677.300643	0.67730064	0.6087172
KHOSTA2 1:5	108.0268	0.177	5	540.133761	0.54013376	
BM4831 1:2	291.832	0.283	2	583.664006	0.58366401	0.59007657
BM4831 1:5	119.2978	0.1835	5	596.489144	0.59648914	
RF1 1:2	220.7375	0.242	2	441.475038	0.44147504	0.41494138
RF1 1:5	77.68155	0.1595	5	388.407728	0.38840773	
C028 1:2	256.2848	0.2625	2	512.569522	0.51256952	0.46566123
C028 1:5	83.75059	0.163	5	418.752935	0.41875293	
BA.5.58 1:2	418.4149	0.356	2	836.829728	0.83682973	0.75784222
BA.5.58 1:5	135.7709	0.193	5	678.854705	0.6788547	
BA.2.75.2 1:2	187.7913	0.223	2	375.58259	0.37558259	0.34514741
BA.2.75.2 1:5	62.94245	0.151	5	314.712227	0.31471223	
SHC014 1:2	506.8495	0.407	2	1013.69893	1.01369893	1.05435823
SHC014 1:5	219.0035	0.241	5	1095.01754	1.09501754	
BA.2.75.58 1:2	420.1489	0.357	2	840.297752	0.84029775	0.89612966
BA.2.75.58 1:5	190.3923	0.2245	5	951.961563	0.95196156	
FK 1:2	265.8218	0.268	2	531.643652	0.53164365	0.4470206
FK 1:5	72.47951	0.1565	5	362.397552	0.36239755	
XBB 1:2	272.7579	0.272	2	545.515746	0.54551575	0.46912925
XBB 1:5	78.54855	0.16	5	392.742758	0.39274276	
BQ.1.1 1:2	219.8705	0.2415	2	439.741026	0.43974103	0.37505911
BQ.1.1 1:5	62.07544	0.1505	5	310.377198	0.3103772	
BA.2.12.1 1:2	250.2157	0.259	2	500.431439	0.50043144	0.44441958
BA.2.12.1 1:5	77.68155	0.1595	5	388.407728	0.38840773	
BA.2 1:2	169.5842	0.2125	2	339.168342	0.33916834	0.27275242
BA.2 1:5	41.2673	0.1385	5	206.33649	0.20633649	
RMYN02 1:2	368.1285	0.327	2	736.257044	0.73625704	0.65553552
RMYN02 1:5	114.9628	0.181	5	574.813997	0.574814	
YUN11 1:2	172.1852	0.214	2	344.370377	0.34437038	0.2406732
YUN11 1:5	27.3952	0.1305	5	136.976018	0.13697602	
PANG17 1:2	480.8393	0.392	2	961.678578	0.96167858	0.82676919
PANG17 1:5	138.372	0.1945	5	691.859793	0.69185979	
BTKY72 1:2	362.9265	0.324	2	725.852973	0.72585297	0.57663798
BTKY72 1:5	85.4846	0.164	5	427.422994	0.42742299	
WIV1 1:2	336.0493037	0.3085	2	672.098607	0.67209861	0.59744613
WIV1 1:5	104.5587286	0.175	5	522.793643	0.52279364	

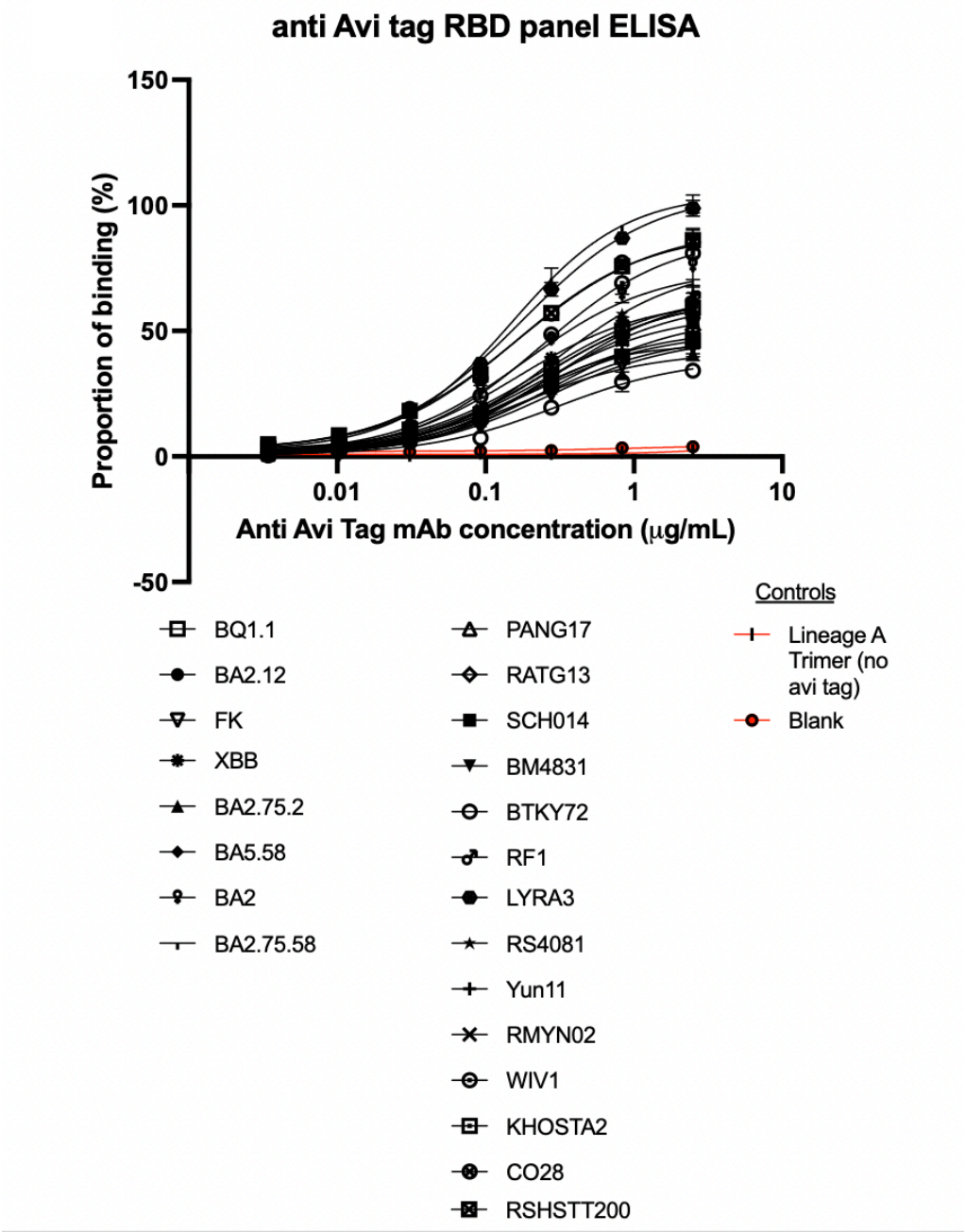

Appendix IV – Jack and Dougal



References

ABOU-NADER, M. & BENEDIK, M. J. 2010. Rapid generation of random mutant libraries. *Bioeng Bugs,* 1**,** 337-40.

ABRAHAM, R., BUXBAUM, S., LINK, J., SMITH, R., VENTI, C. & DARSLEY, M. 1996. Determination of binding constants of diabodies directed against prostate-specific antigen using electrochemiluminescence-based immunoassays. *J Mol Recognit,* 9**,** 456-61.

ADLER, A. S., BEDINGER, D., ADAMS, M. S., ASENSIO, M. A., EDGAR, R. C., LEONG, R., LEONG, J., MIZRAHI, R. A., SPINDLER, M. J., BANDI, S. R., HUANG, H., TAWDE, P., BRAMS, P. & JOHNSON, D. S. 2018. A natively paired antibody library yields drug leads with higher sensitivity and specificity than a randomly paired antibody library. *MAbs,* 10**,** 431-443.

AGHEBATI-MALEKI, L., BAKHSHINEJAD, B., BARADARAN, B., MOTALLEBNEZHAD, M., AGHEBATI-MALEKI, A., NICKHO, H., YOUSEFI, M. & MAJIDI, J. 2016. Phage display as a promising approach for vaccine development. *J Biomed Sci,* 23**,** 66.

AKKAYA, M., KWAK, K. & PIERCE, S. K. 2020. B cell memory: building two walls of protection against pathogens. *Nat Rev Immunol,* 20**,** 229-238.

AL-ALY, Z., BOWE, B. & XIE, Y. 2022. Long COVID after breakthrough SARS-CoV-2 infection. *Nat Med,* 28**,** 1461-1467.

ALAMYAR, E. E. A. 2010. *IMGT/HighV-QUEST: A High-Throughput System and Web Portal for the Analysis of Rearranged Nucleotide Sequences of Antigen Receptors* [Online]. Available: https://www.imgt.org/IMGTindex/IMGTHighV-QUEST.php [Accessed].

ALANAGREH, L., ALZOUGHOOL, F. & ATOUM, M. 2020. The Human Coronavirus Disease COVID-19: Its Origin, Characteristics, and Insights into Potential Drugs and Its Mechanisms. *Pathogens,* 9.

ALFALEH, M. A., ALSAAB, H. O., MAHMOUD, A. B., ALKAYYAL, A. A., JONES, M. L., MAHLER, S. M. & HASHEM, A. M. 2020. Phage Display Derived Monoclonal Antibodies: From Bench to Bedside. *Front Immunol,* 11**,** 1986.

ALI, S. O., TAKAS, T., NYBORG, A., SHOEMAKER, K., KALLEWAARD, N. L., CHIONG, R., DUBOVSKY, F. & MALLORY, R. M. 2018. Evaluation of MEDI8852, an Anti-Influenza A Monoclonal Antibody, in Treating Acute Uncomplicated Influenza. *Antimicrob Agents Chemother,* 62.

ANDERSON, E. M., GOODWIN, E. C., VERMA, A., AREVALO, C. P., BOLTON, M. J., WEIRICK, M. E., GOUMA, S., MCALLISTER, C. M., CHRISTENSEN, S. R., WEAVER, J., HICKS, P., MANZONI, T. B., ONIYIDE, O., RAMAGE, H., MATHEW, D., BAXTER, A. E., OLDRIDGE, D. A., GREENPLATE, A. R., WU, J. E., ALANIO, C., D'ANDREA, K., KUTHURU, O., DOUGHERTY, J., PATTEKAR, A., KIM, J., HAN, N., APOSTOLIDIS, S. A., HUANG, A. C., VELLA, L. A., KURI-CERVANTES, L., PAMPENA, M. B., UNIT, U. P. C. P., BETTS, M. R., WHERRY, E. J., MEYER, N. J., CHERRY, S., BATES, P., RADER, D. J. & HENSLEY, S. E. 2021. Seasonal human coronavirus antibodies are boosted upon SARS-CoV-2 infection but not associated with protection. *Cell,* 184**,** 1858-1864 e10.

ANDRABI, R., BHIMAN, J. N. & BURTON, D. R. 2018. Strategies for a multi-stage neutralizing antibody-based HIV vaccine. *Curr Opin Immunol,* 53**,** 143-151.

ARISTIZÁBAL, B. & GONZÁLEZ, Á. 2013. Innate immune system. *Autoimmunity: From Bench to Bedside [Internet].* El Rosario University Press.

ARUN, S. S., BREUER, W. & HERMANNS, W. 1996. Immunohistochemical examination of light-chain expression (lambda/kappa ratio) in canine, feline, equine, bovine and porcine plasma cells. *Zentralbl Veterinarmed A,* 43**,** 573-6.

AUGUSTIN, M., SCHOMMERS, P., STECHER, M., DEWALD, F., GIESELMANN, L., GRUELL, H., HORN, C., VANSHYLLA, K., CRISTANZIANO, V. D., OSEBOLD, L., ROVENTA, M., RIAZ, T., TSCHERNOSTER, N., ALTMUELLER, J., ROSE, L., SALOMON, S., PRIESNER, V., LUERS, J. C., ALBUS, C., ROSENKRANZ, S., GATHOF, B., FATKENHEUER, G., HALLEK, M., KLEIN, F., SUAREZ, I. & LEHMANN, C. 2021. Post-COVID syndrome in non-hospitalised patients with COVID-19: a longitudinal prospective cohort study. *Lancet Reg Health Eur,* 6**,** 100122.

BARBAS, C. F., 3RD, BAIN, J. D., HOEKSTRA, D. M. & LERNER, R. A. 1992. Semisynthetic combinatorial antibody libraries: a chemical solution to the diversity problem. *Proc Natl Acad Sci U S A,* 89**,** 4457-61.

BARBAS, C. F., 3RD, HU, D., DUNLOP, N., SAWYER, L., CABABA, D., HENDRY, R. M., NARA, P. L. & BURTON, D. R. 1994. In vitro evolution of a neutralizing human antibody to human immunodeficiency virus type 1 to enhance affinity and broaden strain cross-reactivity. *Proc Natl Acad Sci U S A,* 91**,** 3809-13.

BARBAS, C. F., 3RD, KANG, A. S., LERNER, R. A. & BENKOVIC, S. J. 1991. Assembly of combinatorial antibody libraries on phage surfaces: the gene III site. *Proc Natl Acad Sci U S A,* 88**,** 7978-82.

BARBAS, C. F., BURTON, D., SCOTT, J. & SILVERMAN, G. 2001. Phage display. *A Laboratory Manual*.

BARDERAS, R., DESMET, J., TIMMERMAN, P., MELOEN, R. & CASAL, J. I. 2008. Affinity maturation of antibodies assisted by in silico modeling. *Proc Natl Acad Sci U S A,* 105**,** 9029-34.

BARNES, C. O., JETTE, C. A., ABERNATHY, M. E., DAM, K. A., ESSWEIN, S. R., GRISTICK, H. B., MALYUTIN, A. G., SHARAF, N. G., HUEY-TUBMAN, K. E., LEE, Y. E., ROBBIANI, D. F., NUSSENZWEIG, M. C., WEST, A. P., JR. & BJORKMAN, P. J. 2020a. SARS-CoV-2 neutralizing antibody structures inform therapeutic strategies. *Nature,* 588**,** 682-687.

BARNES, C. O., WEST, A. P., JR., HUEY-TUBMAN, K. E., HOFFMANN, M. A. G., SHARAF, N. G., HOFFMAN, P. R., KORANDA, N., GRISTICK, H. B., GAEBLER, C., MUECKSCH, F., LORENZI, J. C. C., FINKIN, S., HAGGLOF, T., HURLEY, A., MILLARD, K. G., WEISBLUM, Y., SCHMIDT, F., HATZIIOANNOU, T., BIENIASZ, P. D., CASKEY, M., ROBBIANI, D. F., NUSSENZWEIG, M. C. & BJORKMAN, P. J. 2020b. Structures of Human Antibodies Bound to SARS-CoV-2 Spike Reveal Common Epitopes and Recurrent Features of Antibodies. *Cell,* 182**,** 828-842 e16.

BASS, S., GREENE, R. & WELLS, J. A. 1990. Hormone phage: an enrichment method for variant proteins with altered binding properties. *Proteins,* 8**,** 309-14.

BASSING, C. H., SWAT, W. & ALT, F. W. 2002. The mechanism and regulation of chromosomal V(D)J recombination. *Cell,* 109 Suppl**,** S45-55.

BAZAN, J., CALKOSINSKI, I. & GAMIAN, A. 2012. Phage display--a powerful technique for immunotherapy: 1. Introduction and potential of therapeutic applications. *Hum Vaccin Immunother,* 8**,** 1817-28.

BENTON, D. J., WROBEL, A. G., XU, P., ROUSTAN, C., MARTIN, S. R., ROSENTHAL, P. B., SKEHEL, J. J. & GAMBLIN, S. J. 2020. Receptor binding and priming of the spike protein of SARS-CoV-2 for membrane fusion. *Nature*.

BERENS, S. J., WYLIE, D. E. & LOPEZ, O. J. 1997. Use of a single VH family and long CDR3s in the variable region of cattle Ig heavy chains. *Int Immunol,* 9**,** 189-99.

BLAIR, H. A. 2020. Ibalizumab: A Review in Multidrug-Resistant HIV-1 Infection. *Drugs,* 80**,** 189-196.

BLANCO-MELO, D., NILSSON-PAYANT, B. E., LIU, W. C., UHL, S., HOAGLAND, D., MØLLER, R., JORDAN, T. X., OISHI, K., PANIS, M., SACHS, D., WANG, T. T., SCHWARTZ, R. E., LIM, J. K., ALBRECHT, R. A. & TENOEVER, B. R. 2020. Imbalanced Host Response to SARS-CoV-2 Drives Development of COVID-19. *Cell,* 181**,** 1036-1045.e9.

BODER, E. T. & WITTRUP, K. D. 1997. Yeast surface display for screening combinatorial polypeptide libraries. *Nat Biotechnol,* 15**,** 553-7.

BOUCAU, J., UDDIN, R., MARINO, C., REGAN, J., FLYNN, J. P., CHOUDHARY, M. C., CHEN, G., STUCKWISCH, A. M., MATHEWS, J., LIEW, M. Y., SINGH, A., REYNOLDS, Z., IYER, S. L., CHAMBERLIN, G. C., VYAS, T. D., VYAS, J. M., TURBETT, S. E., LI, J. Z., LEMIEUX, J. E., BARCZAK, A. K. & SIEDNER, M. J. 2023. Characterization of Virologic Rebound Following Nirmatrelvir-Ritonavir Treatment for Coronavirus Disease 2019 (COVID-19). *Clin Infect Dis,* 76**,** e526-e529.

BOURNAZOS, S. & RAVETCH, J. V. 2017. Anti-retroviral antibody FcgammaR-mediated effector functions. *Immunol Rev,* 275**,** 285-295.

BOYD, S. D. & JOSHI, S. A. 2014. High-Throughput DNA Sequencing Analysis of Antibody Repertoires. *Microbiol Spectr,* 2.

BRADBURY, A. R., SIDHU, S., DUBEL, S. & MCCAFFERTY, J. 2011. Beyond natural antibodies: the power of in vitro display technologies. *Nat Biotechnol,* 29**,** 245-54.

BRADBURY, A. R. M., TRINKLEIN, N. D., THIE, H., WILKINSON, I. C., TANDON, A. K., ANDERSON, S., BLADEN, C. L., JONES, B., ALDRED, S. F., BESTAGNO, M., BURRONE, O., MAYNARD, J., FERRARA, F., TRIMMER, J. S., GORNEMANN, J., GLANVILLE, J., WOLF, P., FRENZEL, A., WONG, J., KOH, X. Y., ENG, H. Y., LANE, D., LEFRANC, M. P., CLARK, M. & DUBEL, S. 2018. When monoclonal antibodies are not monospecific: Hybridomas frequently express additional functional variable regions. *MAbs,* 10**,** 539-546.

BRATKOVIC, T. 2010. Progress in phage display: evolution of the technique and its application. *Cell Mol Life Sci,* 67**,** 749-67.

BRAUN, J., LOYAL, L., FRENTSCH, M., WENDISCH, D., GEORG, P., KURTH, F., HIPPENSTIEL, S., DINGELDEY, M., KRUSE, B., FAUCHERE, F., BAYSAL, E., MANGOLD, M., HENZE, L., LAUSTER, R., MALL, M. A., BEYER, K., ROHMEL, J., VOIGT, S., SCHMITZ, J., MILTENYI, S., DEMUTH, I., MULLER, M. A., HOCKE, A., WITZENRATH, M., SUTTORP, N., KERN, F., REIMER, U., WENSCHUH, H., DROSTEN, C., CORMAN, V. M., GIESECKE-THIEL, C., SANDER, L. E. & THIEL, A. 2020. SARS-CoV-2-reactive T cells in healthy donors and patients with COVID-19. *Nature,* 587**,** 270-274.

BREITLING, F., DUBEL, S., SEEHAUS, T., KLEWINGHAUS, I. & LITTLE, M. 1991. A surface expression vector for antibody screening. *Gene,* 104**,** 147-53.

BROCHOT, E., DEMEY, B., TOUZE, A., BELOUZARD, S., DUBUISSON, J., SCHMIT, J. L., DUVERLIE, G., FRANCOIS, C., CASTELAIN, S. & HELLE, F. 2020. Anti-spike, Anti-nucleocapsid and Neutralizing Antibodies in SARS-CoV-2 Inpatients and Asymptomatic Individuals. *Front Microbiol,* 11**,** 584251.

BROUWER, P. J. M., CANIELS, T. G., VAN DER STRATEN, K., SNITSELAAR, J. L., ALDON, Y., BANGARU, S., TORRES, J. L., OKBA, N. M. A., CLAIREAUX, M., KERSTER, G., BENTLAGE, A. E. H., VAN HAAREN, M. M., GUERRA, D., BURGER, J. A., SCHERMER, E. E., VERHEUL, K. D., VAN DER VELDE, N., VAN DER KOOI, A., VAN SCHOOTEN, J., VAN BREEMEN, M. J., BIJL, T. P. L., SLIEPEN, K., AARTSE,

A., DERKING, R., BONTJER, I., KOOTSTRA, N. A., WIERSINGA, W. J., VIDARSSON, G., HAAGMANS, B. L., WARD, A. B., DE BREE, G. J., SANDERS, R. W. & VAN GILS, M. J. 2020. Potent neutralizing antibodies from COVID-19 patients define multiple targets of vulnerability. *Science,* 369**,** 643-650.

BRUGGEMANN, M., OSBORN, M. J., MA, B., HAYRE, J., AVIS, S., LUNDSTROM, B. & BUELOW, R. 2015. Human antibody production in transgenic animals. *Arch Immunol Ther Exp (Warsz),* 63**,** 101-8.

BURKE, M. J., SCOTT, J. N. F., MINSHULL, T. C., GAO, Z., MANFIELD, I., SAVIC, S., STOCKLEY, P. G., CALABRESE, A. N. & BOYES, J. 2022. A bovine antibody possessing an ultralong complementarity-determining region CDRH3 targets a highly conserved epitope in sarbecovirus spike proteins. *J Biol Chem,* 298**,** 102624.

CAI, X. & GAREN, A. 1995. Anti-melanoma antibodies from melanoma patients immunized with genetically modified autologous tumor cells: selection of specific antibodies from single-chain Fv fusion phage libraries. *Proc Natl Acad Sci U S A,* 92**,** 6537-41.

CALLAWAY, E. 2021. COVID super-immunity: one of the pandemic's great puzzles. *Nature,* 598**,** 393-394.

CALY, L., DRUCE, J. D., CATTON, M. G., JANS, D. A. & WAGSTAFF, K. M. 2020. The FDA-approved drug ivermectin inhibits the replication of SARS-CoV-2 in vitro. *Antiviral Res,* 178**,** 104787.

CANAS, L. S., MOLTENI, E., DENG, J., SUDRE, C. H., MURRAY, B., KERFOOT, E., ANTONELLI, M., RJOOB, K., CAPDEVILA PUJOL, J., POLIDORI, L., MAY, A., OSTERDAHL, M. F., WHISTON, R., CHEETHAM, N. J., BOWYER, V., SPECTOR, T. D., HAMMERS, A., DUNCAN, E. L., OURSELIN, S., STEVES, C. J. & MODAT, M. 2023. Profiling post-COVID-19 condition across different variants of SARS-CoV-2: a prospective longitudinal study in unvaccinated wild-type, unvaccinated alpha-variant, and vaccinated delta-variant populations. *Lancet Digit Health*.

CAO, Y., SU, B., GUO, X., SUN, W., DENG, Y., BAO, L., ZHU, Q., ZHANG, X., ZHENG, Y., GENG, C., CHAI, X., HE, R., LI, X., LV, Q., ZHU, H., DENG, W., XU, Y., WANG, Y., QIAO, L., TAN, Y., SONG, L., WANG, G., DU, X., GAO, N., LIU, J., XIAO, J., SU, X. D., DU, Z., FENG, Y., QIN, C., QIN, C., JIN, R. & XIE, X. S. 2020. Potent Neutralizing Antibodies against SARS-CoV-2 Identified by High-Throughput Single-Cell Sequencing of Convalescent Patients' B Cells. *Cell,* 182**,** 73-84 e16.

CARVALHO, A., HENRIQUES, A. R., QUEIROS, P., RODRIGUES, J., MENDONCA, N., RODRIGUES, A. M., CANHAO, H., DE SOUSA, G., ANTUNES, F. & GUIMARAES, M. 2022. Persistence of IgG COVID-19 antibodies: A longitudinal analysis. *Front Public Health,* 10**,** 1069898.

CASKEY, M., KLEIN, F., LORENZI, J. C., SEAMAN, M. S., WEST, A. P., JR., BUCKLEY, N., KREMER, G., NOGUEIRA, L., BRAUNSCHWEIG, M., SCHEID, J. F., HORWITZ, J. A., SHIMELIOVICH, I., BEN-AVRAHAM, S., WITMER-PACK, M., PLATTEN, M., LEHMANN, C., BURKE, L. A., HAWTHORNE, T., GORELICK, R. J., WALKER, B. D., KELER, T., GULICK, R. M., FATKENHEUER, G., SCHLESINGER, S. J. & NUSSENZWEIG, M. C. 2015. Viraemia suppressed in HIV-1-infected humans by broadly neutralizing antibody 3BNC117. *Nature,* 522**,** 487-91.

CASTEL, G., CHTEOUI, M., HEYD, B. & TORDO, N. 2011. Phage display of combinatorial peptide libraries: application to antiviral research. *Molecules,* 16**,** 3499-518.

CAVALLARI, M. 2017. Rapid and Direct VHH and Target Identification by Staphylococcal Surface Display Libraries. *Int J Mol Sci,* 18.

CHAI, D., WANG, G., FANG, L., LI, H., LIU, S., ZHU, H. & ZHENG, J. 2020. The optimization system for preparation of TG1 competent cells and electrotransformation. *Microbiologyopen,* 9**,** e1043.

CHAKRABARTI, S., BARROW, C. J., KANWAR, R. K., RAMANA, V. & KANWAR, J. R. 2016. Studies to Prevent Degradation of Recombinant Fc-Fusion Protein Expressed in Mammalian Cell Line and Protein Characterization. *Int J Mol Sci,* 17.

CHAKRABORTY, C., BHATTACHARYA, M., SHARMA, A. R. & MALLIK, B. 2022. Omicron (B.1.1.529) - A new heavily mutated variant: Mapped location and probable properties of its mutations with an emphasis on S-glycoprotein. *Int J Biol Macromol,* 219**,** 980-997.

CHANG, A., TING, J. P., ESPADA, A., BROUGHTON, H., MOLINA-MARTIN, M. & AFSHAR, S. 2020. A novel phage display vector for selection of target-specific peptides. *Protein Eng Des Sel,* 33.

CHASTEEN, L., AYRISS, J., PAVLIK, P. & BRADBURY, A. R. 2006. Eliminating helper phage from phage display. *Nucleic Acids Res,* 34**,** e145.

CHEN, R. E., ZHANG, X., CASE, J. B., WINKLER, E. S., LIU, Y., VANBLARGAN, L. A., LIU, J., ERRICO, J. M., XIE, X., SURYADEVARA, N., GILCHUK, P., ZOST, S. J., TAHAN, S., DROIT, L., TURNER, J. S., KIM, W., SCHMITZ, A. J., THAPA, M., WANG, D., BOON, A. C. M., PRESTI, R. M., O'HALLORAN, J. A., KIM, A. H. J., DEEPAK, P., PINTO, D., FREMONT, D. H., CROWE, J. E., JR., CORTI, D., VIRGIN, H. W., ELLEBEDY, A. H., SHI, P. Y. & DIAMOND, M. S. 2021. Resistance of SARS-CoV-2 variants to neutralization by monoclonal and serum-derived polyclonal antibodies. *Nat Med,* 27**,** 717-726.

CHEN, W. C. & MURAWSKY, C. M. 2018. Strategies for Generating Diverse Antibody Repertoires Using Transgenic Animals Expressing Human Antibodies. *Front Immunol,* 9**,** 460.

CHEN, X., LI, R., PAN, Z., QIAN, C., YANG, Y., YOU, R., ZHAO, J., LIU, P., GAO, L., LI, Z., HUANG, Q., XU, L., TANG, J., TIAN, Q., YAO, W., HU, L., YAN, X., ZHOU, X., WU, Y., DENG, K., ZHANG, Z., QIAN, Z., CHEN, Y. & YE, L. 2020. Human monoclonal antibodies block the binding of SARS-CoV-2 spike protein to angiotensin converting enzyme 2 receptor. *Cell Mol Immunol,* 17**,** 647-649.

CHIA, W. N., TAN, C. W., TAN, A. W. K., YOUNG, B., STARR, T. N., LOPEZ, E., FIBRIANSAH, G., BARR, J., CHENG, S., YEOH, A. Y., YAP, W. C., LIM, B. L., NG, T. S., SIA, W. R., ZHU, F., CHEN, S., ZHANG, J., KWEK, M. S. S., GREANEY, A. J., CHEN, M., AU, G. G., PARADKAR, P. N., PEIRIS, M., CHUNG, A. W., BLOOM, J. D., LYE, D., LOK, S. & WANG, L. F. 2023. Potent pan huACE2-dependent sarbecovirus neutralizing monoclonal antibodies isolated from a BNT162b2-vaccinated SARS survivor. *Sci Adv,* 9**,** eade3470.

CHOO, Y. & KLUG, A. 1994. Toward a code for the interactions of zinc fingers with DNA: selection of randomized fingers displayed on phage. *Proc Natl Acad Sci U S A,* 91**,** 11163-7.

CLACKSON, T., HOOGENBOOM, H. R., GRIFFITHS, A. D. & WINTER, G. 1991. Making antibody fragments using phage display libraries. *Nature,* 352**,** 624-8.

CORTI, D., SUGUITAN, A. L., JR., PINNA, D., SILACCI, C., FERNANDEZ-RODRIGUEZ, B. M., VANZETTA, F., SANTOS, C., LUKE, C. J., TORRES-VELEZ, F. J., TEMPERTON, N. J., WEISS, R. A., SALLUSTO, F., SUBBARAO, K. & LANZAVECCHIA, A. 2010. Heterosubtypic neutralizing antibodies are produced by individuals immunized with a seasonal influenza vaccine. *J Clin Invest,* 120**,** 1663-73.

COUTARD, B., VALLE, C., DE LAMBALLERIE, X., CANARD, B., SEIDAH, N. G. & DECROLY, E. 2020. The spike glycoprotein of the new coronavirus 2019-nCoV contains a

furin-like cleavage site absent in CoV of the same clade. *Antiviral Res,* 176**,** 104742.

COX, R. J. & BROKSTAD, K. A. 2020. Not just antibodies: B cells and T cells mediate immunity to COVID-19. *Nat Rev Immunol,* 20**,** 581-582.

CRAMERI, R. & SUTER, M. 1993. Display of biologically active proteins on the surface of filamentous phages: a cDNA cloning system for selection of functional gene products linked to the genetic information responsible for their production. *Gene,* 137**,** 69-75.

CRUZ-TERAN, C., TIRUTHANI, K., MCSWEENEY, M., MA, A., PICKLES, R. & LAI, S. K. 2021. Challenges and opportunities for antiviral monoclonal antibodies as COVID-19 therapy. *Adv Drug Deliv Rev,* 169**,** 100-117.

CWIRLA, S. E., PETERS, E. A., BARRETT, R. W. & DOWER, W. J. 1990. Peptides on phage: a vast library of peptides for identifying ligands. *Proc Natl Acad Sci U S A,* 87**,** 6378-82.

DAN, J. M., MATEUS, J., KATO, Y., HASTIE, K. M., YU, E. D., FALITI, C. E., GRIFONI, A., RAMIREZ, S. I., HAUPT, S., FRAZIER, A., NAKAO, C., RAYAPROLU, V., RAWLINGS, S. A., PETERS, B., KRAMMER, F., SIMON, V., SAPHIRE, E. O., SMITH, D. M., WEISKOPF, D., SETTE, A. & CROTTY, S. 2021. Immunological memory to SARS-CoV-2 assessed for up to 8 months after infection. *Science,* 371.

DAVIES, E. L., SMITH, J. S., BIRKETT, C. R., MANSER, J. M., ANDERSON-DEAR, D. V. & YOUNG, J. R. 1995. Selection of specific phage-display antibodies using libraries derived from chicken immunoglobulin genes. *J Immunol Methods,* 186**,** 125-35.

DAVIS, H. E., MCCORKELL, L., VOGEL, J. M. & TOPOL, E. J. 2023. Author Correction: Long COVID: major findings, mechanisms and recommendations. *Nat Rev Microbiol,* 21**,** 408.

DE HAARD, H. J., VAN NEER, N., REURS, A., HUFTON, S. E., ROOVERS, R. C., HENDERIKX, P., DE BRUINE, A. P., ARENDS, J. W. & HOOGENBOOM, H. R. 1999. A large non-immunized human Fab fragment phage library that permits rapid isolation and kinetic analysis of high affinity antibodies. *J Biol Chem,* 274**,** 18218-30.

DE WIT, E., VAN DOREMALEN, N., FALZARANO, D. & MUNSTER, V. J. 2016. SARS and MERS: recent insights into emerging coronaviruses. *Nature reviews microbiology,* 14**,** 523-534.

DECANNIERE, K., DESMYTER, A., LAUWEREYS, M., GHAHROUDI, M. A., MUYLDERMANS, S. & WYNS, L. 1999. A single-domain antibody fragment in complex with RNase A: non-canonical loop structures and nanomolar affinity using two CDR loops. *Structure,* 7**,** 361-70.

DEISS, T. C., VADNAIS, M., WANG, F., CHEN, P. L., TORKAMANI, A., MWANGI, W., LEFRANC, M. P., CRISCITIELLO, M. F. & SMIDER, V. V. 2019. Immunogenetic factors driving formation of ultralong VH CDR3 in Bos taurus antibodies. *Cell Mol Immunol,* 16**,** 53-64.

DEJNIRATTISAI, W., HUO, J., ZHOU, D., ZAHRADNIK, J., SUPASA, P., LIU, C., DUYVESTEYN, H. M. E., GINN, H. M., MENTZER, A. J., TUEKPRAKHON, A., NUTALAI, R., WANG, B., DIJOKAITE, A., KHAN, S., AVINOAM, O., BAHAR, M., SKELLY, D., ADELE, S., JOHNSON, S. A., AMINI, A., RITTER, T. G., MASON, C., DOLD, C., PAN, D., ASSADI, S., BELLASS, A., OMO-DARE, N., KOECKERLING, D., FLAXMAN, A., JENKIN, D., ALEY, P. K., VOYSEY, M., COSTA CLEMENS, S. A., NAVECA, F. G., NASCIMENTO, V., NASCIMENTO, F., FERNANDES DA COSTA, C., RESENDE, P. C., PAUVOLID-CORREA, A., SIQUEIRA, M. M., BAILLIE, V.,

SERAFIN, N., KWATRA, G., DA SILVA, K., MADHI, S. A., NUNES, M. C., MALIK, T., OPENSHAW, P. J. M., BAILLIE, J. K., SEMPLE, M. G., TOWNSEND, A. R., HUANG, K. A., TAN, T. K., CARROLL, M. W., KLENERMAN, P., BARNES, E., DUNACHIE, S. J., CONSTANTINIDES, B., WEBSTER, H., CROOK, D., POLLARD, A. J., LAMBE, T., CONSORTIUM, O., CONSORTIUM, I. C., PATERSON, N. G., WILLIAMS, M. A., HALL, D. R., FRY, E. E., MONGKOLSAPAYA, J., REN, J., SCHREIBER, G., STUART, D. I. & SCREATON, G. R. 2022. SARS-CoV-2 Omicron-B.1.1.529 leads to widespread escape from neutralizing antibody responses. *Cell,* 185**,** 467-484 e15.

DEJNIRATTISAI, W., ZHOU, D., GINN, H. M., DUYVESTEYN, H. M. E., SUPASA, P., CASE, J. B., ZHAO, Y., WALTER, T. S., MENTZER, A. J., LIU, C., WANG, B., PAESEN, G. C., SLON-CAMPOS, J., LOPEZ-CAMACHO, C., KAFAI, N. M., BAILEY, A. L., CHEN, R. E., YING, B., THOMPSON, C., BOLTON, J., FYFE, A., GUPTA, S., TAN, T. K., GILBERT-JARAMILLO, J., JAMES, W., KNIGHT, M., CARROLL, M. W., SKELLY, D., DOLD, C., PENG, Y., LEVIN, R., DONG, T., POLLARD, A. J., KNIGHT, J. C., KLENERMAN, P., TEMPERTON, N., HALL, D. R., WILLIAMS, M. A., PATERSON, N. G., BERTRAM, F. K. R., SIEBERT, C. A., CLARE, D. K., HOWE, A., RADECKE, J., SONG, Y., TOWNSEND, A. R., HUANG, K. A., FRY, E. E., MONGKOLSAPAYA, J., DIAMOND, M. S., REN, J., STUART, D. I. & SCREATON, G. R. 2021. The antigenic anatomy of SARS-CoV-2 receptor binding domain. *Cell,* 184**,** 2183-2200 e22.

DEL VALLE, D. M., KIM-SCHULZE, S., HUANG, H. H., BECKMANN, N. D., NIRENBERG, S., WANG, B., LAVIN, Y., SWARTZ, T. H., MADDURI, D., STOCK, A., MARRON, T. U., XIE, H., PATEL, M., TUBALLES, K., VAN OEKELEN, O., RAHMAN, A., KOVATCH, P., ABERG, J. A., SCHADT, E., JAGANNATH, S., MAZUMDAR, M., CHARNEY, A. W., FIRPO-BETANCOURT, A., MENDU, D. R., JHANG, J., REICH, D., SIGEL, K., CORDON-CARDO, C., FELDMANN, M., PAREKH, S., MERAD, M. & GNJATIC, S. 2020. An inflammatory cytokine signature predicts COVID-19 severity and survival. *Nat Med,* 26**,** 1636-1643.

DEO, R., CHOUDHARY, M. C., MOSER, C., RITZ, J., DAAR, E. S., WOHL, D. A., GRENINGER, A. L., ERON, J. J., CURRIER, J. S., HUGHES, M. D., SMITH, D. M., CHEW, K. W., LI, J. Z. & TEAM, A.-A. S. 2022. Viral and Symptom Rebound in Untreated COVID-19 Infection. *medRxiv*.

DEPARTMENT, S. R. 2023. *Impact of the coronavirus pandemic on the global economy - Statistics & Facts* [Online]. Available: https://www.statista.com/topics/6139/covid-19-impact-on-the-global-economy/#topicHeader__wrapper [Accessed].

DIEBOLDER, P. & KRAWCZYK, A. 2018. Detailed protocols for the selection of antiviral human antibodies from combinatorial immune phage display libraries. *Antibody Engineering***,** 75.

DONG, J., FINN, J. A., LARSEN, P. A., SMITH, T. P. L. & CROWE, J. E. 2019. Structural Diversity of Ultralong CDRH3s in Seven Bovine Antibody Heavy Chains. *Front Immunol,* 10**,** 558.

DOOLEY, H., FLAJNIK, M. F. & PORTER, A. J. 2003. Selection and characterization of naturally occurring single-domain (IgNAR) antibody fragments from immunized sharks by phage display. *Mol Immunol,* 40**,** 25-33.

DRIOUICH, J. S., BERNADIN, O., TOURET, F., DE LAMBALLERIE, X. & NOUGAIREDE, A. 2023. Activity of Sotrovimab against BQ.1.1 and XBB.1 Omicron sublineages in a hamster model. *Antiviral Res,* 215**,** 105638.

DUAN, J., YAN, X., GUO, X., CAO, W., HAN, W., QI, C., FENG, J., YANG, D., GAO, G. & JIN, G. 2005. A human SARS-CoV neutralizing antibody against epitope on S2 protein. *Biochem Biophys Res Commun,* 333**,** 186-93.

DUNDAS, C. M., DEMONTE, D. & PARK, S. 2013. Streptavidin-biotin technology: improvements and innovations in chemical and biological applications. *Appl Microbiol Biotechnol,* 97**,** 9343-53.

DYSON, M. R., MASTERS, E., PAZERAITIS, D., PERERA, R. L., SYRJANEN, J. L., SURADE, S., THORSTEINSON, N., PARTHIBAN, K., JONES, P. C., SATTAR, M., WOZNIAK-KNOPP, G., RUEKER, F., LEAH, R. & MCCAFFERTY, J. 2020. Beyond affinity: selection of antibody variants with optimal biophysical properties and reduced immunogenicity from mammalian display libraries. *MAbs,* 12**,** 1829335.

EDARA, V. V., NORWOOD, C., FLOYD, K., LAI, L., DAVIS-GARDNER, M. E., HUDSON, W. H., MANTUS, G., NYHOFF, L. E., ADELMAN, M. W., FINEMAN, R., PATEL, S., BYRAM, R., GOMES, D. N., MICHAEL, G., ABDULLAHI, H., BEYDOUN, N., PANGANIBAN, B., MCNAIR, N., HELLMEISTER, K., PITTS, J., WINTERS, J., KLEINHENZ, J., USHER, J., O'KEEFE, J. B., PIANTADOSI, A., WAGGONER, J. J., BABIKER, A., STEPHENS, D. S., ANDERSON, E. J., EDUPUGANTI, S., ROUPHAEL, N., AHMED, R., WRAMMERT, J. & SUTHAR, M. S. 2021. Infection- and vaccine-induced antibody binding and neutralization of the B.1.351 SARS-CoV-2 variant. *Cell Host Microbe,* 29**,** 516-521 e3.

EDOUARD MATHIEU, H. R., LUCAS RODÉS-GUIRAO, CAMERON APPEL, CHARLIE GIATTINO, JOE HASELL, BOBBIE MACDONALD, SALONI DATTANI, DIANA BELTEKIAN, ESTEBAN ORTIZ-OSPINA AND MAX ROSER 2020. Coronavirus Pandemic (COVID-19).

EISENHARDT, S. U., SCHWARZ, M., BASSLER, N. & PETER, K. 2007. Subtractive single-chain antibody (scFv) phage-display: tailoring phage-display for high specificity against function-specific conformations of cell membrane molecules. *Nat Protoc,* 2**,** 3063-73.

EKIERT, D. C., BHABHA, G., ELSLIGER, M. A., FRIESEN, R. H., JONGENEELEN, M., THROSBY, M., GOUDSMIT, J. & WILSON, I. A. 2009. Antibody recognition of a highly conserved influenza virus epitope. *Science,* 324**,** 246-51.

EKMAN, A., NIKU, M., LILJAVIRTA, J. & IIVANAINEN, A. 2009. Bos taurus genome sequence reveals the assortment of immunoglobulin and surrogate light chain genes in domestic cattle. *BMC Immunol,* 10**,** 22.

FAN, C., COHEN, A. A., PARK, M., HUNG, A. F., KEEFFE, J. R., GNANAPRAGASAM, P. N. P., LEE, Y. E., GAO, H., KAKUTANI, L. M., WU, Z., KLEANTHOUS, H., MALECEK, K. E., WILLIAMS, J. C. & BJORKMAN, P. J. 2022. Neutralizing monoclonal antibodies elicited by mosaic RBD nanoparticles bind conserved sarbecovirus epitopes. *Immunity,* 55**,** 2419-2435 e10.

FAUCI, A. S. & MARSTON, H. D. 2015. Toward an HIV vaccine: A scientific journey. *Science,* 349**,** 386-387.

FEHR, A. R. & PERLMAN, S. 2015. Coronaviruses: an overview of their replication and pathogenesis. *Methods Mol Biol,* 1282**,** 1-23.

FOCOSI, D., MCCONNELL, S., CASADEVALL, A., CAPPELLO, E., VALDISERRA, G. & TUCCORI, M. 2022. Monoclonal antibody therapies against SARS-CoV-2. *Lancet Infect Dis,* 22**,** e311-e326.

FRANCISCO, J. A., CAMPBELL, R., IVERSON, B. L. & GEORGIOU, G. 1993. Production and fluorescence-activated cell sorting of Escherichia coli expressing a functional antibody fragment on the external surface. *Proc Natl Acad Sci U S A,* 90**,** 10444-8.

FRENZEL, A., SCHIRRMANN, T. & HUST, M. 2016. Phage display-derived human antibodies in clinical development and therapy. *MAbs,* 8**,** 1177-1194.

GAEBLER, C., WANG, Z., LORENZI, J. C. C., MUECKSCH, F., FINKIN, S., TOKUYAMA, M., CHO, A., JANKOVIC, M., SCHAEFER-BABAJEW, D., OLIVEIRA, T. Y., CIPOLLA, M., VIANT, C., BARNES, C. O., BRAM, Y., BRETON, G., HAGGLOF, T., MENDOZA, P., HURLEY, A., TURROJA, M., GORDON, K., MILLARD, K. G., RAMOS, V., SCHMIDT, F., WEISBLUM, Y., JHA, D., TANKELEVICH, M., MARTINEZ-DELGADO, G., YEE, J., PATEL, R., DIZON, J., UNSON-O'BRIEN, C., SHIMELIOVICH, I., ROBBIANI, D. F., ZHAO, Z., GAZUMYAN, A., SCHWARTZ, R. E., HATZIIOANNOU, T., BJORKMAN, P. J., MEHANDRU, S., BIENIASZ, P. D., CASKEY, M. & NUSSENZWEIG, M. C. 2021. Evolution of antibody immunity to SARS-CoV-2. *Nature,* 591**,** 639-644.

GAGIC, D., CIRIC, M., WEN, W. X., NG, F. & RAKONJAC, J. 2016. Exploring the Secretomes of Microbes and Microbial Communities Using Filamentous Phage Display. *Front Microbiol,* 7**,** 429.

GAZIT, S., SHLEZINGER, R., PEREZ, G., LOTAN, R., PERETZ, A., BEN-TOV, A., HERZEL, E., ALAPI, H., COHEN, D., MUHSEN, K., CHODICK, G. & PATALON, T. 2022. Severe Acute Respiratory Syndrome Coronavirus 2 (SARS-CoV-2) Naturally Acquired Immunity versus Vaccine-induced Immunity, Reinfections versus Breakthrough Infections: A Retrospective Cohort Study. *Clin Infect Dis,* 75**,** e545-e551.

GIANG, E., DORNER, M., PRENTOE, J. C., DREUX, M., EVANS, M. J., BUKH, J., RICE, C. M., PLOSS, A., BURTON, D. R. & LAW, M. 2012. Human broadly neutralizing antibodies to the envelope glycoprotein complex of hepatitis C virus. *Proc Natl Acad Sci U S A,* 109**,** 6205-10.

GOEL, R. R., APOSTOLIDIS, S. A., PAINTER, M. M., MATHEW, D., PATTEKAR, A., KUTHURU, O., GOUMA, S., HICKS, P., MENG, W., ROSENFELD, A. M., DYSINGER, S., LUNDGREEN, K. A., KURI-CERVANTES, L., ADAMSKI, S., HICKS, A., KORTE, S., OLDRIDGE, D. A., BAXTER, A. E., GILES, J. R., WEIRICK, M. E., MCALLISTER, C. M., DOUGHERTY, J., LONG, S., D'ANDREA, K., HAMILTON, J. T., BETTS, M. R., LUNING PRAK, E. T., BATES, P., HENSLEY, S. E., GREENPLATE, A. R. & WHERRY, E. J. 2021a. Distinct antibody and memory B cell responses in SARS-CoV-2 naive and recovered individuals following mRNA vaccination. *Sci Immunol,* 6.

GOEL, R. R., PAINTER, M. M., APOSTOLIDIS, S. A., MATHEW, D., MENG, W., ROSENFELD, A. M., LUNDGREEN, K. A., REYNALDI, A., KHOURY, D. S., PATTEKAR, A., GOUMA, S., KURI-CERVANTES, L., HICKS, P., DYSINGER, S., HICKS, A., SHARMA, H., HERRING, S., KORTE, S., BAXTER, A. E., OLDRIDGE, D. A., GILES, J. R., WEIRICK, M. E., MCALLISTER, C. M., AWOFOLAJU, M., TANENBAUM, N., DRAPEAU, E. M., DOUGHERTY, J., LONG, S., D'ANDREA, K., HAMILTON, J. T., MCLAUGHLIN, M., WILLIAMS, J. C., ADAMSKI, S., KUTHURU, O., DAGGER, U. P. C. P. U., FRANK, I., BETTS, M. R., VELLA, L. A., GRIFONI, A., WEISKOPF, D., SETTE, A., HENSLEY, S. E., DAVENPORT, M. P., BATES, P., LUNING PRAK, E. T., GREENPLATE, A. R. & WHERRY, E. J. 2021b. mRNA vaccines induce durable immune memory to SARS-CoV-2 and variants of concern. *Science,* 374**,** abm0829.

GOLDBERG, Y., MANDEL, M., BAR-ON, Y. M., BODENHEIMER, O., FREEDMAN, L. S., ASH, N., ALROY-PREIS, S., HUPPERT, A. & MILO, R. 2022. Protection and Waning of Natural and Hybrid Immunity to SARS-CoV-2. *N Engl J Med,* 386**,** 2201-2212.

GOURLEY, T. S., WHERRY, E. J., MASOPUST, D. & AHMED, R. 2004. Generation and maintenance of immunological memory. *Semin Immunol,* 16**,** 323-33.
GOV.UK 2022. Investigation of SARS-CoV-2 variants: technical briefings. SARS-CoV-2 variants of concern and variants under investigation in England: technical briefings 44.
GRAHAM, C., SEOW, J., HUETTNER, I., KHAN, H., KOUPHOU, N., ACORS, S., WINSTONE, H., PICKERING, S., GALAO, R. P., DUPONT, L., LISTA, M. J., JIMENEZ-GUARDENO, J. M., LAING, A. G., WU, Y., JOSEPH, M., MUIR, L., VAN GILS, M. J., NG, W. M., DUYVESTEYN, H. M. E., ZHAO, Y., BOWDEN, T. A., SHANKAR-HARI, M., ROSA, A., CHEREPANOV, P., MCCOY, L. E., HAYDAY, A. C., NEIL, S. J. D., MALIM, M. H. & DOORES, K. J. 2021. Neutralization potency of monoclonal antibodies recognizing dominant and subdominant epitopes on SARS-CoV-2 Spike is impacted by the B.1.1.7 variant. *Immunity,* 54**,** 1276-1289 e6.
GRANT, C. F., LEFEVRE, E. A., CARR, B. V., PRENTICE, H., GUBBINS, S., POLLARD, A. J., CHARREYRE, C. & CHARLESTON, B. 2012. Assessment of T-dependent and T-independent immune responses in cattle using a B cell ELISPOT assay. *Vet Res,* 43**,** 68.
GREIG, S. L. 2016. Obiltoxaximab: First Global Approval. *Drugs,* 76**,** 823-30.
GRIFFITHS, A. D. & DUNCAN, A. R. 1998. Strategies for selection of antibodies by phage display. *Curr Opin Biotechnol,* 9**,** 102-8.
GRIFFITHS, A. D., MALMQVIST, M., MARKS, J. D., BYE, J. M., EMBLETON, M. J., MCCAFFERTY, J., BAIER, M., HOLLIGER, K. P., GORICK, B. D., HUGHES-JONES, N. C. & ET AL. 1993. Human anti-self antibodies with high specificity from phage display libraries. *EMBO J,* 12**,** 725-34.
GRIFFITHS, A. D., WILLIAMS, S. C., HARTLEY, O., TOMLINSON, I. M., WATERHOUSE, P., CROSBY, W. L., KONTERMANN, R. E., JONES, P. T., LOW, N. M., ALLISON, T. J. & ET AL. 1994. Isolation of high affinity human antibodies directly from large synthetic repertoires. *EMBO J,* 13**,** 3245-60.
GRIFONI, A., WEISKOPF, D., RAMIREZ, S. I., MATEUS, J., DAN, J. M., MODERBACHER, C. R., RAWLINGS, S. A., SUTHERLAND, A., PREMKUMAR, L., JADI, R. S., MARRAMA, D., DE SILVA, A. M., FRAZIER, A., CARLIN, A. F., GREENBAUM, J. A., PETERS, B., KRAMMER, F., SMITH, D. M., CROTTY, S. & SETTE, A. 2020. Targets of T Cell Responses to SARS-CoV-2 Coronavirus in Humans with COVID-19 Disease and Unexposed Individuals. *Cell,* 181**,** 1489-1501 e15.
GROUP, R. C. 2021. Convalescent plasma in patients admitted to hospital with COVID-19 (RECOVERY): a randomised controlled, open-label, platform trial. *Lancet,* 397**,** 2049-2059.
GUARNER, J. 2020. Three Emerging Coronaviruses in Two Decades: The Story of SARS, MERS, and Now COVID-19. *American Journal of Clinical Pathology,* 153**,** 420-421.
GUPTA, P., KAMATH, A. V., PARK, S., CHIU, H., LUTMAN, J., MAIA, M., TAN, M. W., XU, M., SWEM, L. & DENG, R. 2016. Preclinical pharmacokinetics of MHAA4549A, a human monoclonal antibody to influenza A virus, and the prediction of its efficacious clinical dose for the treatment of patients hospitalized with influenza A. *MAbs,* 8**,** 991-7.
HAAKENSON, J. K., HUANG, R. & SMIDER, V. V. 2018. Diversity in the Cow Ultralong CDR H3 Antibody Repertoire. *Front Immunol,* 9**,** 1262.
HADJADJ, J., YATIM, N., BARNABEI, L., CORNEAU, A., BOUSSIER, J., SMITH, N., PÉRÉ, H., CHARBIT, B., BONDET, V., CHENEVIER-GOBEAUX, C., BREILLAT, P., CARLIER, N., GAUZIT, R., MORBIEU, C., PÈNE, F., MARIN, N., ROCHE, N.,

SZWEBEL, T. A., MERKLING, S. H., TRELUYER, J. M., VEYER, D., MOUTHON, L., BLANC, C., THARAUX, P. L., ROZENBERG, F., FISCHER, A., DUFFY, D., RIEUX-LAUCAT, F., KERNÉIS, S. & TERRIER, B. 2020. Impaired type I interferon activity and inflammatory responses in severe COVID-19 patients. *Science,* 369**,** 718-724.

HARDING, F. A., STICKLER, M. M., RAZO, J. & DUBRIDGE, R. B. 2010. The immunogenicity of humanized and fully human antibodies: residual immunogenicity resides in the CDR regions. *MAbs,* 2**,** 256-65.

HAWKINS, R. E., RUSSELL, S. J. & WINTER, G. 1992. Selection of phage antibodies by binding affinity. Mimicking affinity maturation. *J Mol Biol,* 226**,** 889-96.

HAWLISCH, H., MULLER, M., FRANK, R., BAUTSCH, W., KLOS, A. & KOHL, J. 2001. Site-specific anti-C3a receptor single-chain antibodies selected by differential panning on cellulose sheets. *Anal Biochem,* 293**,** 142-5.

HMILA, I., ABDALLAH, R. B., SAERENS, D., BENLASFAR, Z., CONRATH, K., AYEB, M. E., MUYLDERMANS, S. & BOUHAOUALA-ZAHAR, B. 2008. VHH, bivalent domains and chimeric Heavy chain-only antibodies with high neutralizing efficacy for scorpion toxin AahI'. *Mol Immunol,* 45**,** 3847-56.

HOET, R. M., COHEN, E. H., KENT, R. B., ROOKEY, K., SCHOONBROODT, S., HOGAN, S., REM, L., FRANS, N., DAUKANDT, M., PIETERS, H., VAN HEGELSOM, R., NEER, N. C., NASTRI, H. G., RONDON, I. J., LEEDS, J. A., HUFTON, S. E., HUANG, L., KASHIN, I., DEVLIN, M., KUANG, G., STEUKERS, M., VISWANATHAN, M., NIXON, A. E., SEXTON, D. J., HOOGENBOOM, H. R. & LADNER, R. C. 2005. Generation of high-affinity human antibodies by combining donor-derived and synthetic complementarity-determining-region diversity. *Nat Biotechnol,* 23**,** 344-8.

HOFFMANN, M., KLEINE-WEBER, H., SCHROEDER, S., KRÜGER, N., HERRLER, T., ERICHSEN, S., SCHIERGENS, T. S., HERRLER, G., WU, N. H., NITSCHE, A., MÜLLER, M. A., DROSTEN, C. & PÖHLMANN, S. 2020. SARS-CoV-2 Cell Entry Depends on ACE2 and TMPRSS2 and Is Blocked by a Clinically Proven Protease Inhibitor. *Cell,* 181**,** 271-280.e8.

HOGAN, S., ROOKEY, K. & LADNER, R. 2005. URSA: ultra rapid selection of antibodies from an antibody phage display library. *Biotechniques,* 38**,** 536, 538.

HOOGENBOOM, H. R. 2002. Overview of antibody phage-display technology and its applications. *Antibody phage display: methods and protocols***,** 1-37.

HOOGENBOOM, H. R., DE BRUINE, A. P., HUFTON, S. E., HOET, R. M., ARENDS, J. W. & ROOVERS, R. C. 1998. Antibody phage display technology and its applications. *Immunotechnology,* 4**,** 1-20.

HOOGENBOOM, H. R., GRIFFITHS, A. D., JOHNSON, K. S., CHISWELL, D. J., HUDSON, P. & WINTER, G. 1991. Multi-subunit proteins on the surface of filamentous phage: methodologies for displaying antibody (Fab) heavy and light chains. *Nucleic Acids Res,* 19**,** 4133-7.

HOY, S. M. 2019. Sintilimab: First Global Approval. *Drugs,* 79**,** 341-346.

HOZUMI, N. & TONEGAWA, S. 2004. Evidence for somatic rearrangement of immunoglobulin genes coding for variable and constant regions. 1976 [classical article]. *J Immunol,* 173**,** 4260-4.

HU, D., ZHU, Z., LI, S., DENG, Y., WU, Y., ZHANG, N., PURI, V., WANG, C., ZOU, P., LEI, C., TIAN, X., WANG, Y., ZHAO, Q., LI, W., PRABAKARAN, P., FENG, Y., CARDOSA, J., QIN, C., ZHOU, X., DIMITROV, D. S. & YING, T. 2019. A broadly neutralizing germline-like human monoclonal antibody against dengue virus envelope domain III. *PLoS Pathog,* 15**,** e1007836.

HUANG, I. C., BOSCH, B. J., LI, F., LI, W., LEE, K. H., GHIRAN, S., VASILIEVA, N., DERMODY, T. S., HARRISON, S. C., DORMITZER, P. R., FARZAN, M., ROTTIER, P. J. & CHOE, H. 2006. SARS coronavirus, but not human coronavirus NL63, utilizes cathepsin L to infect ACE2-expressing cells. *J Biol Chem,* 281**,** 3198-203.

HUANG, J. X., BISHOP-HURLEY, S. L. & COOPER, M. A. 2012. Development of anti-infectives using phage display: biological agents against bacteria, viruses, and parasites. *Antimicrob Agents Chemother,* 56**,** 4569-82.

HUANG, K. A., TAN, T. K., CHEN, T. H., HUANG, C. G., HARVEY, R., HUSSAIN, S., CHEN, C. P., HARDING, A., GILBERT-JARAMILLO, J., LIU, X., KNIGHT, M., SCHIMANSKI, L., SHIH, S. R., LIN, Y. C., CHENG, C. Y., CHENG, S. H., HUANG, Y. C., LIN, T. Y., JAN, J. T., MA, C., JAMES, W., DANIELS, R. S., MCCAULEY, J. W., RIJAL, P. & TOWNSEND, A. R. 2021. Breadth and function of antibody response to acute SARS-CoV-2 infection in humans. *PLoS Pathog,* 17**,** e1009352.

HUANG, R., WARNER JENKINS, G., KIM, Y., STANFIELD, R. L., SINGH, A., MARTINEZ-YAMOUT, M., KROON, G. J., TORRES, J. L., JACKSON, A. M., KELLEY, A., SHAABANI, N., ZENG, B., BACICA, M., CHEN, W., WARNER, C., RADOICIC, J., JOH, J., DINALI PERERA, K., SANG, H., KIM, T., YAO, J., ZHAO, F., SOK, D., BURTON, D. R., ALLEN, J., HARRIMAN, W., MWANGI, W., CHUNG, D., TEIJARO, J. R., WARD, A. B., DYSON, H. J., WRIGHT, P. E., WILSON, I. A., CHANG, K. O., MCGREGOR, D. & SMIDER, V. V. 2023. The smallest functional antibody fragment: Ultralong CDR H3 antibody knob regions potently neutralize SARS-CoV-2. *Proc Natl Acad Sci U S A,* 120**,** e2303455120.

HURLBURT, N. K., SEYDOUX, E., WAN, Y. H., EDARA, V. V., STUART, A. B., FENG, J., SUTHAR, M. S., MCGUIRE, A. T., STAMATATOS, L. & PANCERA, M. 2020. Structural basis for potent neutralization of SARS-CoV-2 and role of antibody affinity maturation. *Nat Commun,* 11**,** 5413.

HUST, M., MAISS, E., JACOBSEN, H. J. & REINARD, T. 2002. The production of a genus-specific recombinant antibody (scFv) using a recombinant potyvirus protease. *J Virol Methods,* 106**,** 225-33.

HUYGENS, S., OUDE MUNNINK, B., GHARBHARAN, A., KOOPMANS, M. & RIJNDERS, B. 2023. Sotrovimab Resistance and Viral Persistence After Treatment of Immunocompromised Patients Infected With the Severe Acute Respiratory Syndrome Coronavirus 2 Omicron Variant. *Clin Infect Dis,* 76**,** e507-e509.

IACOBUCCI, G. 2023. Covid-19: FDA removes US authorisation for antibody drug Evusheld. *BMJ,* 380**,** 264.

IMAI, M., ITO, M., KISO, M., YAMAYOSHI, S., URAKI, R., FUKUSHI, S., WATANABE, S., SUZUKI, T., MAEDA, K., SAKAI-TAGAWA, Y., IWATSUKI-HORIMOTO, K., HALFMANN, P. J. & KAWAOKA, Y. 2023. Efficacy of Antiviral Agents against Omicron Subvariants BQ.1.1 and XBB. *N Engl J Med,* 388**,** 89-91.

IVANOV, V., SUVOROVA, Z., TCHIKIN, L., KOZHICH, A. & IVANOV, V. 1992. Effective method for synthetic peptide immobilization that increases the sensitivity and specificity of ELISA procedures. *Journal of immunological methods,* 153**,** 229-233.

IWANAGA, N., COOPER, L., RONG, L., BEDDINGFIELD, B., CRABTREE, J., TRIPP, R. A., QIN, X. & KOLLS, J. K. 2020. Novel ACE2-IgG1 fusions with improved in vitro and in vivo activity against SARS-CoV2. *bioRxiv*.

IYER, A. S., JONES, F. K., NODOUSHANI, A., KELLY, M., BECKER, M., SLATER, D., MILLS, R., TENG, E., KAMRUZZAMAN, M., GARCIA-BELTRAN, W. F., ASTUDILLO, M., YANG, D., MILLER, T. E., OLIVER, E., FISCHINGER, S., ATYEO, C., IAFRATE, A. J.,

CALDERWOOD, S. B., LAUER, S. A., YU, J., LI, Z., FELDMAN, J., HAUSER, B. M., CARADONNA, T. M., BRANDA, J. A., TURBETT, S. E., LAROCQUE, R. C., MELLON, G., BAROUCH, D. H., SCHMIDT, A. G., AZMAN, A. S., ALTER, G., RYAN, E. T., HARRIS, J. B. & CHARLES, R. C. 2020. Persistence and decay of human antibody responses to the receptor binding domain of SARS-CoV-2 spike protein in COVID-19 patients. *Sci Immunol,* 5.

JACKSON, C. B., FARZAN, M., CHEN, B. & CHOE, H. 2022. Mechanisms of SARS-CoV-2 entry into cells. *Nature reviews Molecular cell biology,* 23**,** 3-20.

JAIMES, J., MILLET, J. & WHITTAKER, G. 2020. Proteolytic Cleavage of the SARS-CoV-2 Spike Protein and the Role of the Novel S1/S2 Site. *SSRN***,** 3581359.

JAROSZEWICZ, W., MORCINEK-ORLOWSKA, J., PIERZYNOWSKA, K., GAFFKE, L. & WEGRZYN, G. 2022. Phage display and other peptide display technologies. *FEMS Microbiol Rev,* 46.

JERNE, N. K. 1955. The Natural-Selection Theory of Antibody Formation. *Proc Natl Acad Sci U S A,* 41**,** 849-57.

JETTE, C. A., COHEN, A. A., GNANAPRAGASAM, P. N. P., MUECKSCH, F., LEE, Y. E., HUEY-TUBMAN, K. E., SCHMIDT, F., HATZIIOANNOU, T., BIENIASZ, P. D., NUSSENZWEIG, M. C., WEST, A. P., JR., KEEFFE, J. R., BJORKMAN, P. J. & BARNES, C. O. 2021. Broad cross-reactivity across sarbecoviruses exhibited by a subset of COVID-19 donor-derived neutralizing antibodies. *Cell Rep,* 37**,** 110188.

JU, B., ZHANG, Q., GE, J., WANG, R., SUN, J., GE, X., YU, J., SHAN, S., ZHOU, B., SONG, S., TANG, X., YU, J., LAN, J., YUAN, J., WANG, H., ZHAO, J., ZHANG, S., WANG, Y., SHI, X., LIU, L., ZHAO, J., WANG, X., ZHANG, Z. & ZHANG, L. 2020. Human neutralizing antibodies elicited by SARS-CoV-2 infection. *Nature,* 584**,** 115-119.

KALELI, N. E., KARADAG, M. & KALYONCU, S. 2019. Phage display derived therapeutic antibodies have enriched aliphatic content: Insights for developability issues. *Proteins,* 87**,** 607-618.

KANEKO, N., KUO, H. H., BOUCAU, J., FARMER, J. R., ALLARD-CHAMARD, H., MAHAJAN, V. S., PIECHOCKA-TROCHA, A., LEFTERI, K., OSBORN, M., BALS, J., BARTSCH, Y. C., BONHEUR, N., CARADONNA, T. M., CHEVALIER, J., CHOWDHURY, F., DIEFENBACH, T. J., EINKAUF, K., FALLON, J., FELDMAN, J., FINN, K. K., GARCIA-BRONCANO, P., HARTANA, C. A., HAUSER, B. M., JIANG, C., KAPLONEK, P., KARPELL, M., KOSCHER, E. C., LIAN, X., LIU, H., LIU, J., LY, N. L., MICHELL, A. R., RASSADKINA, Y., SEIGER, K., SESSA, L., SHIN, S., SINGH, N., SUN, W., SUN, X., TICHELI, H. J., WARING, M. T., ZHU, A. L., ALTER, G., LI, J. Z., LINGWOOD, D., SCHMIDT, A. G., LICHTERFELD, M., WALKER, B. D., YU, X. G., PADERA, R. F., JR., PILLAI, S. & MASSACHUSETTS CONSORTIUM ON PATHOGEN READINESS SPECIMEN WORKING, G. 2020. Loss of Bcl-6-Expressing T Follicular Helper Cells and Germinal Centers in COVID-19. *Cell,* 183**,** 143-157 e13.

KANG, T. H. & JUNG, S. T. 2019. Boosting therapeutic potency of antibodies by taming Fc domain functions. *Exp Mol Med,* 51**,** 1-9.

KARA, E., NIELSEN, N. V., EGGERTSDOTTIR, B., THIEDE, B., KANSE, S. M. & LOSET, G. A. 2020. Design and Characterization of a New pVII Combinatorial Phage Display Peptide Library for Protease Substrate Mining Using Factor VII Activating Protease (FSAP) as Model. *Chembiochem,* 21**,** 1875-1884.

KATAKURA, Y., ZHUANG, G., UCHIDA, S., FURUTA, T., OMASA, T., KISHIMOTO, M. & SUGA, K.-I. 2002. Analysis and optimization of biopanning process of phage display libraries. ACS Publications.

KAY, B. K., WINTER, J. & MCCAFFERTY, J. 1996. *Phage display of peptides and proteins: a laboratory manual*, Elsevier.
KAZA, V. K. & NATHAN, B. 2023. Inclusion of Rabishield in the WHO guidelines for rabies postexposure prophylaxis. *Indian J Pharmacol,* 55**,** 141-142.
KE, Z., OTON, J., QU, K., CORTESE, M., ZILA, V., MCKEANE, L., NAKANE, T., ZIVANOV, J., NEUFELDT, C. J., CERIKAN, B., LU, J. M., PEUKES, J., XIONG, X., KRAUSSLICH, H. G., SCHERES, S. H. W., BARTENSCHLAGER, R. & BRIGGS, J. A. G. 2020. Structures and distributions of SARS-CoV-2 spike proteins on intact virions. *Nature,* 588**,** 498-502.
KECK, J. G., MAKINO, S., SOE, L. H., FLEMING, J. O., STOHLMAN, S. A. & LAI, M. M. 1987. RNA recombination of coronavirus. *Adv Exp Med Biol,* 218**,** 99-107.
KELLEY, B. 2009. Industrialization of mAb production technology: the bioprocessing industry at a crossroads. *MAbs,* 1**,** 443-52.
KHAILANY, R. A., SAFDAR, M. & OZASLAN, M. 2020. Genomic characterization of a novel SARS-CoV-2. *Gene Rep***,** 100682.
KIM, J. W., MIN, S. W., LEE, J., SHIN, H. G., CHOI, H. L., YANG, H. R., LEE, J. H., CHO, Y. B., SHIM, H. & LEE, S. 2022. Development and Characterization of Phage-Display-Derived Novel Human Monoclonal Antibodies against the Receptor Binding Domain of SARS-CoV-2. *Biomedicines,* 10.
KISHCHENKO, G., BATLIWALA, H. & MAKOWSKI, L. 1994. Structure of a foreign peptide displayed on the surface of bacteriophage M13. *J Mol Biol,* 241**,** 208-13.
KLEWINGHAUS, D., PEKAR, L., ARRAS, P., KRAH, S., VALLDORF, B., KOLMAR, H. & ZIELONKA, S. 2021. Grabbing the Bull by Both Horns: Bovine Ultralong CDR-H3 Paratopes Enable Engineering of 'Almost Natural' Common Light Chain Bispecific Antibodies Suitable For Effector Cell Redirection. *Front Immunol,* 12**,** 801368.
KOHLER, G. & MILSTEIN, C. 1975. Continuous cultures of fused cells secreting antibody of predefined specificity. *Nature,* 256**,** 495-7.
KOTI, M., KATAEVA, G. & KAUSHIK, A. K. 2008. Organization of D(H)-gene locus is distinct in cattle. *Dev Biol (Basel),* 132**,** 307-313.
KOTI, M., KATAEVA, G. & KAUSHIK, A. K. 2010. Novel atypical nucleotide insertions specifically at VH-DH junction generate exceptionally long CDR3H in cattle antibodies. *Mol Immunol,* 47**,** 2119-28.
KRAMMER, F. 2020. SARS-CoV-2 vaccines in development. *Nature,* 586**,** 516-527.
KRISTENSEN, P. & WINTER, G. 1998. Proteolytic selection for protein folding using filamentous bacteriophages. *Fold Des,* 3**,** 321-8.
KUGLER, J., WILKE, S., MEIER, D., TOMSZAK, F., FRENZEL, A., SCHIRRMANN, T., DUBEL, S., GARRITSEN, H., HOCK, B., TOLEIKIS, L., SCHUTTE, M. & HUST, M. 2015. Generation and analysis of the improved human HAL9/10 antibody phage display libraries. *BMC Biotechnol,* 15**,** 10.
KUMAR, R., KUMARI, R., KHAN, L., SANKHYAN, A., PARRAY, H. A., TIWARI, A., WIG, N., SINHA, S. & LUTHRA, K. 2019. Isolation and Characterization of Cross-Neutralizing Human Anti-V3 Single-Chain Variable Fragments (scFvs) Against HIV-1 from an Antigen Preselected Phage Library. *Appl Biochem Biotechnol,* 187**,** 1011-1027.
KWAK, K., AKKAYA, M. & PIERCE, S. K. 2019. B cell signaling in context. *Nat Immunol,* 20**,** 963-969.
LAIDLAW, B. J. & ELLEBEDY, A. H. 2022. The germinal centre B cell response to SARS-CoV-2. *Nat Rev Immunol,* 22**,** 7-18.

LAM, T. T., JIA, N., ZHANG, Y. W., SHUM, M. H., JIANG, J. F., ZHU, H. C., TONG, Y. G., SHI, Y. X., NI, X. B., LIAO, Y. S., LI, W. J., JIANG, B. G., WEI, W., YUAN, T. T., ZHENG, K., CUI, X. M., LI, J., PEI, G. Q., QIANG, X., CHEUNG, W. Y., LI, L. F., SUN, F. F., QIN, S., HUANG, J. C., LEUNG, G. M., HOLMES, E. C., HU, Y. L., GUAN, Y. & CAO, W. C. 2020. Identifying SARS-CoV-2-related coronaviruses in Malayan pangolins. *Nature,* 583**,** 282-285.

LANZAFAME, M., GOTTARDI, M., GUELLA, L., COLLINI, L., COSTA, G., GUELLA, A. & VENTO, S. 2023. Successful treatment of persistent SARS-CoV-2 infection with nirmatrelvir/ritonavir plus sotrovimab in four immunocompromised patients. *J Chemother***,** 1-4.

LARSEN, P. A., CAMPBELL, C. R. & YODER, A. D. 2014. Next-generation approaches to advancing eco-immunogenomic research in critically endangered primates. *Mol Ecol Resour,* 14**,** 1198-209.

LAUSTSEN, A. H., BOHN, M. F. & LJUNGARS, A. 2022. The challenges with developing therapeutic monoclonal antibodies for pandemic application. *Expert Opin Drug Discov,* 17**,** 5-8.

LAUSTSEN, A. H., LAURIDSEN, L. P., LOMONTE, B., ANDERSEN, M. R. & LOHSE, B. 2017. Pitfalls to avoid when using phage display for snake toxins. *Toxicon,* 126**,** 79-89.

LE BERT, N., TAN, A. T., KUNASEGARAN, K., THAM, C. Y. L., HAFEZI, M., CHIA, A., CHNG, M. H. Y., LIN, M., TAN, N., LINSTER, M., CHIA, W. N., CHEN, M. I., WANG, L. F., OOI, E. E., KALIMUDDIN, S., TAMBYAH, P. A., LOW, J. G., TAN, Y. J. & BERTOLETTI, A. 2020. SARS-CoV-2-specific T cell immunity in cases of COVID-19 and SARS, and uninfected controls. *Nature,* 584**,** 457-462.

LEDSGAARD, L., KILSTRUP, M., KARATT-VELLATT, A., MCCAFFERTY, J. & LAUSTSEN, A. H. 2018. Basics of Antibody Phage Display Technology. *Toxins (Basel),* 10.

LEDSGAARD, L., LAUSTSEN, A. H., PUS, U., WADE, J., VILLAR, P., BODDUM, K., SLAVNY, P., MASTERS, E. W., ARIAS, A. S., OSCOZ, S., GRIFFITHS, D. T., LUTHER, A. M., LINDHOLM, M., LEAH, R. A., MOLLER, M. S., ALI, H., MCCAFFERTY, J., LOMONTE, B., GUTIERREZ, J. M. & KARATT-VELLATT, A. 2022a. In vitro discovery of a human monoclonal antibody that neutralizes lethality of cobra snake venom. *MAbs,* 14**,** 2085536.

LEDSGAARD, L., LJUNGARS, A., RIMBAULT, C., SORENSEN, C. V., TULIKA, T., WADE, J., WOUTERS, Y., MCCAFFERTY, J. & LAUSTSEN, A. H. 2022b. Advances in antibody phage display technology. *Drug Discov Today,* 27**,** 2151-2169.

LEYVA-GRADO, V. H., TAN, G. S., LEON, P. E., YONDOLA, M. & PALESE, P. 2015. Direct administration in the respiratory tract improves efficacy of broadly neutralizing anti-influenza virus monoclonal antibodies. *Antimicrob Agents Chemother,* 59**,** 4162-72.

LI, F. 2016. Structure, Function, and Evolution of Coronavirus Spike Proteins. *Annu Rev Virol,* 3**,** 237-261.

LI, K., WANG, S., CAO, Y., BAO, H., LI, P., SUN, P., BAI, X., FU, Y., MA, X., ZHANG, J., LI, D., CHEN, Y., LIU, X., AN, F., WU, F., LU, Z. & LIU, Z. 2019. Development of Foot-and-Mouth Disease Virus-Neutralizing Monoclonal Antibodies Derived From Plasmablasts of Infected Cattle and Their Germline Gene Usage. *Front Immunol,* 10**,** 2870.

LI, W., SHI, Z., YU, M., REN, W., SMITH, C., EPSTEIN, J. H., WANG, H., CRAMERI, G., HU, Z., ZHANG, H., ZHANG, J., MCEACHERN, J., FIELD, H., DASZAK, P., EATON, B. T., ZHANG, S. & WANG, L. F. 2005. Bats are natural reservoirs of SARS-like coronaviruses. *Science,* 310**,** 676-9.

LI, X., GENG, M., PENG, Y., MENG, L. & LU, S. 2020. Molecular immune pathogenesis and diagnosis of COVID-19. *J Pharm Anal,* 10**,** 102-108.
LIAO, H. & LI, Z. 2022. Clinical Development and Regulatory Pathways of Monoclonal Antibodies in Japan. *Ther Innov Regul Sci,* 56**,** 173-183.
LILJAVIRTA, J., NIKU, M., PESSA-MORIKAWA, T., EKMAN, A. & IIVANAINEN, A. 2014. Expansion of the preimmune antibody repertoire by junctional diversity in Bos taurus. *PLoS One,* 9**,** e99808.
LIM, C. C., WOO, P. C. Y. & LIM, T. S. 2019. Development of a Phage Display Panning Strategy Utilizing Crude Antigens: Isolation of MERS-CoV Nucleoprotein human antibodies. *Sci Rep,* 9**,** 6088.
LIU, H., GAZA-BULSECO, G. & CHUMSAE, C. 2009. Analysis of reduced monoclonal antibodies using size exclusion chromatography coupled with mass spectrometry. *J Am Soc Mass Spectrom,* 20**,** 2258-64.
LIU, H. F., MA, J., WINTER, C. & BAYER, R. 2010. Recovery and purification process development for monoclonal antibody production. *MAbs,* 2**,** 480-99.
LIU, L., WANG, P., NAIR, M. S., YU, J., RAPP, M., WANG, Q., LUO, Y., CHAN, J. F., SAHI, V., FIGUEROA, A., GUO, X. V., CERUTTI, G., BIMELA, J., GORMAN, J., ZHOU, T., CHEN, Z., YUEN, K. Y., KWONG, P. D., SODROSKI, J. G., YIN, M. T., SHENG, Z., HUANG, Y., SHAPIRO, L. & HO, D. D. 2020. Potent neutralizing antibodies against multiple epitopes on SARS-CoV-2 spike. *Nature,* 584**,** 450-456.
LIU, P., HAN, L., WANG, F., PETRENKO, V. A. & LIU, A. 2016. Gold nanoprobe functionalized with specific fusion protein selection from phage display and its application in rapid, selective and sensitive colorimetric biosensing of Staphylococcus aureus. *Biosens Bioelectron,* 82**,** 195-203.
LIU, Z., VANBLARGAN, L. A., BLOYET, L. M., ROTHLAUF, P. W., CHEN, R. E., STUMPF, S., ZHAO, H., ERRICO, J. M., THEEL, E. S., LIEBESKIND, M. J., ALFORD, B., BUCHSER, W. J., ELLEBEDY, A. H., FREMONT, D. H., DIAMOND, M. S. & WHELAN, S. P. J. 2021. Identification of SARS-CoV-2 spike mutations that attenuate monoclonal and serum antibody neutralization. *Cell Host Microbe,* 29**,** 477-488 e4.
LONG, Q. X., LIU, B. Z., DENG, H. J., WU, G. C., DENG, K., CHEN, Y. K., LIAO, P., QIU, J. F., LIN, Y., CAI, X. F., WANG, D. Q., HU, Y., REN, J. H., TANG, N., XU, Y. Y., YU, L. H., MO, Z., GONG, F., ZHANG, X. L., TIAN, W. G., HU, L., ZHANG, X. X., XIANG, J. L., DU, H. X., LIU, H. W., LANG, C. H., LUO, X. H., WU, S. B., CUI, X. P., ZHOU, Z., ZHU, M. M., WANG, J., XUE, C. J., LI, X. F., WANG, L., LI, Z. J., WANG, K., NIU, C. C., YANG, Q. J., TANG, X. J., ZHANG, Y., LIU, X. M., LI, J. J., ZHANG, D. C., ZHANG, F., LIU, P., YUAN, J., LI, Q., HU, J. L., CHEN, J. & HUANG, A. L. 2020. Antibody responses to SARS-CoV-2 in patients with COVID-19. *Nat Med,* 26**,** 845-848.
LOPEZ, O., PEREZ, C. & WYLIE, D. 1998. A single VH family and long CDR3s are the targets for hypermutation in bovine immunoglobulin heavy chains. *Immunol Rev,* 162**,** 55-66.
LOPEZ-LEON, S., WEGMAN-OSTROSKY, T., PERELMAN, C., SEPULVEDA, R., REBOLLEDO, P. A., CUAPIO, A. & VILLAPOL, S. 2021. More than 50 long-term effects of COVID-19: a systematic review and meta-analysis. *Sci Rep,* 11**,** 16144.
LOSET, G. A., BOGEN, B. & SANDLIE, I. 2011. Expanding the versatility of phage display I: efficient display of peptide-tags on protein VII of the filamentous phage. *PLoS One,* 6**,** e14702.
LOWE, D., WILKINSON, T., VAUGHAN, T. & WOOD, C. 2012. Antibody Drug Discovery. *Molecular Medicine and Medicinal Chemistry***,** 85-119.

LOWMAN, H. B., BASS, S. H., SIMPSON, N. & WELLS, J. A. 1991. Selecting high-affinity binding proteins by monovalent phage display. *Biochemistry,* 30**,** 10832-8.

LOZANO-OJALVO, D., CAMARA, C., LOPEZ-GRANADOS, E., NOZAL, P., DEL PINO-MOLINA, L., BRAVO-GALLEGO, L. Y., PAZ-ARTAL, E., PION, M., CORREA-ROCHA, R., ORTIZ, A., LOPEZ-HOYOS, M., IRIBARREN, M. E., PORTOLES, J., ROJO-PORTOLES, M. P., OJEDA, G., CERVERA, I., GONZALEZ-PEREZ, M., BODEGA-MAYOR, I., MONTES-CASADO, M., PORTOLES, P., PEREZ-OLMEDA, M., OTEO, J., SANCHEZ-TARJUELO, R., POTHULA, V., SCHWARZ, M., BRAHMACHARY, M., TAN, A. T., LE BERT, N., BERIN, C., BERTOLETTI, A., GUCCIONE, E. & OCHANDO, J. 2021. Differential effects of the second SARS-CoV-2 mRNA vaccine dose on T cell immunity in naive and COVID-19 recovered individuals. *Cell Rep,* 36**,** 109570.

LU, R., ZHAO, X., LI, J., NIU, P., YANG, B., WU, H., WANG, W., SONG, H., HUANG, B., ZHU, N., BI, Y., MA, X., ZHAN, F., WANG, L., HU, T., ZHOU, H., HU, Z., ZHOU, W., ZHAO, L., CHEN, J., MENG, Y., WANG, J., LIN, Y., YUAN, J., XIE, Z., MA, J., LIU, W. J., WANG, D., XU, W., HOLMES, E. C., GAO, G. F., WU, G., CHEN, W., SHI, W. & TAN, W. 2020a. Genomic characterisation and epidemiology of 2019 novel coronavirus: implications for virus origins and receptor binding. *Lancet,* 395**,** 565-574.

LU, R. M., HWANG, Y. C., LIU, I. J., LEE, C. C., TSAI, H. Z., LI, H. J. & WU, H. C. 2020b. Development of therapeutic antibodies for the treatment of diseases. *J Biomed Sci,* 27**,** 1.

MA, L., QIN, T., CHU, D., CHENG, X., WANG, J., WANG, X., WANG, P., HAN, H., REN, L., AITKEN, R., HAMMARSTRÖM, L., LI, N. & ZHAO, Y. 2016. Internal Duplications of DH, JH, and C Region Genes Create an Unusual IgH Gene Locus in Cattle. *J Immunol,* 196**,** 4358-66.

MACAGNO, A., BERNASCONI, N. L., VANZETTA, F., DANDER, E., SARASINI, A., REVELLO, M. G., GERNA, G., SALLUSTO, F. & LANZAVECCHIA, A. 2010. Isolation of human monoclonal antibodies that potently neutralize human cytomegalovirus infection by targeting different epitopes on the gH/gL/UL128-131A complex. *J Virol,* 84**,** 1005-13.

MACPHERSON, A., BIRTLEY, J. R., BROADBRIDGE, R. J., BRADY, K., SCHULZE, M. E. D., TANG, Y., JOYCE, C., SAUNDERS, K., BOGLE, G., HORTON, J., KELM, S., TAYLOR, R. D., FRANKLIN, R. J., SELBY, M. D., LAABEI, M., WONFOR, T., HOLD, A., STANLEY, P., VADYSIRISACK, D., SHI, J., VAN DEN ELSEN, J. & LAWSON, A. D. G. 2021a. The Chemical Synthesis of Knob Domain Antibody Fragments. *ACS Chem Biol,* 16**,** 1757-1769.

MACPHERSON, A., LAABEI, M., AHDASH, Z., GRAEWERT, M. A., BIRTLEY, J. R., SCHULZE, M. E., CRENNELL, S., ROBINSON, S. A., HOLMES, B., OLEINIKOVAS, V., NILSSON, P. H., SNOWDEN, J., ELLIS, V., MOLLNES, T. E., DEANE, C. M., SVERGUN, D., LAWSON, A. D. & VAN DEN ELSEN, J. M. 2021b. The allosteric modulation of complement C5 by knob domain peptides. *Elife,* 10.

MACPHERSON, A., SCOTT-TUCKER, A., SPILIOTOPOULOS, A., SIMPSON, C., STANIFORTH, J., HOLD, A., SNOWDEN, J., MANNING, L., VAN DEN ELSEN, J. & LAWSON, A. D. G. 2020. Isolation of antigen-specific, disulphide-rich knob domain peptides from bovine antibodies. *PLoS Biol,* 18**,** e3000821.

MALMBORG, A. C., DUENAS, M., OHLIN, M., SODERLIND, E. & BORREBAECK, C. A. 1996. Selection of binders from phage displayed antibody libraries using the BIAcore biosensor. *J Immunol Methods,* 198**,** 51-7.

MANDRUP, O. A., FRIIS, N. A., LYKKEMARK, S., JUST, J. & KRISTENSEN, P. 2013. A novel heavy domain antibody library with functionally optimized complementarity determining regions. *PLoS One,* 8**,** e76834.

MANLEY, K., ANDERSON, J., YANG, F., SZUSTAKOWSKI, J., OAKELEY, E. J., COMPTON, T. & FEIRE, A. L. 2011. Human cytomegalovirus escapes a naturally occurring neutralizing antibody by incorporating it into assembling virions. *Cell Host Microbe,* 10**,** 197-209.

MARINTCHEVA, B. 2017. *Harnessing the power of viruses*, Academic Press.

MARKS, J. D., HOOGENBOOM, H. R., BONNERT, T. P., MCCAFFERTY, J., GRIFFITHS, A. D. & WINTER, G. 1991. By-passing immunization. Human antibodies from V-gene libraries displayed on phage. *J Mol Biol,* 222**,** 581-97.

MAROVICH, M., MASCOLA, J. R. & COHEN, M. S. 2020. Monoclonal Antibodies for Prevention and Treatment of COVID-19. *JAMA,* 324**,** 131-132.

MATEUS, J., GRIFONI, A., TARKE, A., SIDNEY, J., RAMIREZ, S. I., DAN, J. M., BURGER, Z. C., RAWLINGS, S. A., SMITH, D. M., PHILLIPS, E., MALLAL, S., LAMMERS, M., RUBIRO, P., QUIAMBAO, L., SUTHERLAND, A., YU, E. D., DA SILVA ANTUNES, R., GREENBAUM, J., FRAZIER, A., MARKMANN, A. J., PREMKUMAR, L., DE SILVA, A., PETERS, B., CROTTY, S., SETTE, A. & WEISKOPF, D. 2020. Selective and cross-reactive SARS-CoV-2 T cell epitopes in unexposed humans. *Science,* 370**,** 89-94.

MATHEW, D., GILES, J. R., BAXTER, A. E., OLDRIDGE, D. A., GREENPLATE, A. R., WU, J. E., ALANIO, C., KURI-CERVANTES, L., PAMPENA, M. B., D'ANDREA, K., MANNE, S., CHEN, Z., HUANG, Y. J., REILLY, J. P., WEISMAN, A. R., ITTNER, C. A. G., KUTHURU, O., DOUGHERTY, J., NZINGHA, K., HAN, N., KIM, J., PATTEKAR, A., GOODWIN, E. C., ANDERSON, E. M., WEIRICK, M. E., GOUMA, S., AREVALO, C. P., BOLTON, M. J., CHEN, F., LACEY, S. F., RAMAGE, H., CHERRY, S., HENSLEY, S. E., APOSTOLIDIS, S. A., HUANG, A. C., VELLA, L. A., UNIT, U. P. C. P., BETTS, M. R., MEYER, N. J. & WHERRY, E. J. 2020. Deep immune profiling of COVID-19 patients reveals distinct immunotypes with therapeutic implications. *Science,* 369.

MAZOR, Y., VAN BLARCOM, T., MABRY, R., IVERSON, B. L. & GEORGIOU, G. 2007. Isolation of engineered, full-length antibodies from libraries expressed in Escherichia coli. *Nat Biotechnol,* 25**,** 563-5.

MCCAFFERTY, J. 1996. Phage display: factors affecting panning efficiency. *Phage display of peptides and proteins.* Elsevier.

MCCAFFERTY, J., GRIFFITHS, A. D., WINTER, G. & CHISWELL, D. J. 1990. Phage antibodies: filamentous phage displaying antibody variable domains. *Nature,* 348**,** 552-4.

MCCAFFERTY, J. & JOHNSON, K. S. 1996. CHAPTER 6 - Construction and Screening of Antibody Display Libraries. *In:* KAY, B. K., WINTER, J. & MCCAFFERTY, J. (eds.) *Phage Display of Peptides and Proteins.* Burlington: Academic Press.

MCCALLUM, M., BASSI, J., DE MARCO, A., CHEN, A., WALLS, A. C., DI IULIO, J., TORTORICI, M. A., NAVARRO, M. J., SILACCI-FREGNI, C., SALIBA, C., SPROUSE, K. R., AGOSTINI, M., PINTO, D., CULAP, K., BIANCHI, S., JACONI, S., CAMERONI, E., BOWEN, J. E., TILLES, S. W., PIZZUTO, M. S., GUASTALLA, S. B., BONA, G., PELLANDA, A. F., GARZONI, C., VAN VOORHIS, W. C., ROSEN, L. E., SNELL, G., TELENTI, A., VIRGIN, H. W., PICCOLI, L., CORTI, D. & VEESLER, D. 2021a. SARS-CoV-2 immune evasion by the B.1.427/B.1.429 variant of concern. *Science,* 373**,** 648-654.

MCCALLUM, M., MARCO, A., LEMPP, F., TORTORICI, M. A., PINTO, D., WALLS, A. C., BELTRAMELLO, M., CHEN, A., LIU, Z., ZATTA, F., ZEPEDA, S., DI IULIO, J.,

BOWEN, J. E., MONTIEL-RUIZ, M., ZHOU, J., ROSEN, L. E., BIANCHI, S., GUARINO, B., FREGNI, C. S., ABDELNABI, R., CAROLINE FOO, S. Y., ROTHLAUF, P. W., BLOYET, L. M., BENIGNI, F., CAMERONI, E., NEYTS, J., RIVA, A., SNELL, G., TELENTI, A., WHELAN, S. P. J., VIRGIN, H. W., CORTI, D., PIZZUTO, M. S. & VEESLER, D. 2021b. N-terminal domain antigenic mapping reveals a site of vulnerability for SARS-CoV-2. *bioRxiv*.

MCCLURE, C. P., URBANOWICZ, R. A., KING, B. J., CANO-CRESPO, S., TARR, A. W. & BALL, J. K. 2016. Flexible and rapid construction of viral chimeras applied to hepatitis C virus. *J Gen Virol,* 97**,** 2187-2193.

MCCONNELL, S. J., DINH, T., LE, M. H. & SPINELLA, D. G. 1999. Biopanning phage display libraries using magnetic beads vs. polystyrene plates. *Biotechniques,* 26**,** 208-10, 214.

MCLELLAN, J. S., CHEN, M., KIM, A., YANG, Y., GRAHAM, B. S. & KWONG, P. D. 2010. Structural basis of respiratory syncytial virus neutralization by motavizumab. *Nat Struct Mol Biol,* 17**,** 248-50.

MEOLA, A., DELMASTRO, P., MONACI, P., LUZZAGO, A., NICOSIA, A., FELICI, F., CORTESE, R. & GALFRE, G. 1995. Derivation of vaccines from mimotopes. Immunologic properties of human hepatitis B virus surface antigen mimotopes displayed on filamentous phage. *J Immunol,* 154**,** 3162-72.

MILETO, D., MICHELI, V., FENIZIA, C., CUTRERA, M., GAGLIARDI, G., MANCON, A., BRACCHITTA, F., DE SILVESTRI, A., RIZZARDINI, G., LOMBARDI, A., BIASIN, M. & GISMONDO, M. R. 2022. Reduced neutralization of SARS-CoV-2 Omicron variant by BNT162b2 vaccinees' sera: a preliminary evaluation. *Emerg Microbes Infect,* 11**,** 790-792.

MOSS, P. 2022. The T cell immune response against SARS-CoV-2. *Nat Immunol,* 23**,** 186-193.

MOUFFAK, S., SHUBBAR, Q., SALEH, E. & EL-AWADY, R. 2021. Recent advances in management of COVID-19: A review. *Biomed Pharmacother,* 143**,** 112107.

NAQVI, A. A. T., FATIMA, K., MOHAMMAD, T., FATIMA, U., SINGH, I. K., SINGH, A., ATIF, S. M., HARIPRASAD, G., HASAN, G. M. & HASSAN, M. I. 2020. Insights into SARS-CoV-2 genome, structure, evolution, pathogenesis and therapies: Structural genomics approach. *Biochim Biophys Acta Mol Basis Dis,* 1866**,** 165878.

NELSON, R. S. & VALADON, P. 2017. A universal phage display system for the seamless construction of Fab libraries. *J Immunol Methods,* 450**,** 41-49.

NEUMAN, B. W. & BUCHMEIER, M. J. 2016. Supramolecular Architecture of the Coronavirus Particle. *Adv Virus Res,* 96**,** 1-27.

NEUMAN, B. W., KISS, G., KUNDING, A. H., BHELLA, D., BAKSH, M. F., CONNELLY, S., DROESE, B., KLAUS, J. P., MAKINO, S., SAWICKI, S. G., SIDDELL, S. G., STAMOU, D. G., WILSON, I. A., KUHN, P. & BUCHMEIER, M. J. 2011. A structural analysis of M protein in coronavirus assembly and morphology. *J Struct Biol,* 174**,** 11-22.

NG, K. W., FAULKNER, N., CORNISH, G. H., ROSA, A., HARVEY, R., HUSSAIN, S., ULFERTS, R., EARL, C., WROBEL, A. G., BENTON, D. J., ROUSTAN, C., BOLLAND, W., THOMPSON, R., AGUA-DOCE, A., HOBSON, P., HEANEY, J., RICKMAN, H., PARASKEVOPOULOU, S., HOULIHAN, C. F., THOMSON, K., SANCHEZ, E., SHIN, G. Y., SPYER, M. J., JOSHI, D., O'REILLY, N., WALKER, P. A., KJAER, S., RIDDELL, A., MOORE, C., JEBSON, B. R., WILKINSON, M., MARSHALL, L. R., ROSSER, E. C., RADZISZEWSKA, A., PECKHAM, H., CIURTIN, C., WEDDERBURN, L. R., BEALE, R., SWANTON, C., GANDHI, S., STOCKINGER, B., MCCAULEY, J., GAMBLIN, S. J., MCCOY, L. E., CHEREPANOV, P., NASTOULI,

E. & KASSIOTIS, G. 2020. Preexisting and de novo humoral immunity to SARS-CoV-2 in humans. *Science,* 370**,** 1339-1343.
NGUYEN, V. K., HAMERS, R., WYNS, L. & MUYLDERMANS, S. 2000. Camel heavy-chain antibodies: diverse germline V(H)H and specific mechanisms enlarge the antigen-binding repertoire. *EMBO J,* 19**,** 921-30.
NGUYEN-CONTANT, P., EMBONG, A. K., KANAGAIAH, P., CHAVES, F. A., YANG, H., BRANCHE, A. R., TOPHAM, D. J. & SANGSTER, M. Y. 2020. S Protein-Reactive IgG and Memory B Cell Production after Human SARS-CoV-2 Infection Includes Broad Reactivity to the S2 Subunit. *mBio,* 11.
NIKU, M., LILJAVIRTA, J., DURKIN, K., SCHRODERUS, E. & IIVANAINEN, A. 2012. The bovine genomic DNA sequence data reveal three IGHV subgroups, only one of which is functionally expressed. *Dev Comp Immunol,* 37**,** 457-61.
NILSSON, N., MALMBORG, A. C. & BORREBAECK, C. A. 2000. The phage infection process: a functional role for the distal linker region of bacteriophage protein 3. *J Virol,* 74**,** 4229-35.
NISSIM, A., HOOGENBOOM, H. R., TOMLINSON, I. M., FLYNN, G., MIDGLEY, C., LANE, D. & WINTER, G. 1994. Antibody fragments from a 'single pot' phage display library as immunochemical reagents. *EMBO J,* 13**,** 692-8.
NOMURA, Y., SAWAHATA, M., NAKAMURA, Y., KOIKE, R., KATSUBE, O., HAGIWARA, K., NIHO, S., MASUDA, N., TANAKA, T. & SUGIYAMA, K. 2021. Attenuation of antibody titers from 3 to 6 months after the second dose of the BNT162b2 vaccine depends on sex, with age and smoking risk factors for lower antibody titers at 6 months. *Vaccines,* 9**,** 1500.
NOREN, C. J., ANTHONY-CAHILL, S. J., GRIFFITH, M. C. & SCHULTZ, P. G. 1989. A general method for site-specific incorporation of unnatural amino acids into proteins. *Science,* 244**,** 182-8.
NOY-PORAT, T., MAKDASI, E., ALCALAY, R., MECHALY, A., LEVY, Y., BERCOVICH-KINORI, A., ZAUBERMAN, A., TAMIR, H., YAHALOM-RONEN, Y., ISRAELI, M., EPSTEIN, E., ACHDOUT, H., MELAMED, S., CHITLARU, T., WEISS, S., PERETZ, E., ROSEN, O., PARAN, N., YITZHAKI, S., SHAPIRA, S. C., ISRAELY, T., MAZOR, O. & ROSENFELD, R. 2020. A panel of human neutralizing mAbs targeting SARS-CoV-2 spike at multiple epitopes. *Nat Commun,* 11**,** 4303.
O'CALLAGHAN, R., BRADLEY, R. & PARANCHYCH, W. 1973. The effect of M13 phage infection upon the F pili of E. coli. *Virology,* 54**,** 220-9.
OLIVIERO, B., VARCHETTA, S., MELE, D., MANTOVANI, S., CERINO, A., PEROTTI, C. G., LUDOVISI, S. & MONDELLI, M. U. 2020. Expansion of atypical memory B cells is a prominent feature of COVID-19. *Cell Mol Immunol,* 17**,** 1101-1103.
OSWALD, W. B., GEISBERT, T. W., DAVIS, K. J., GEISBERT, J. B., SULLIVAN, N. J., JAHRLING, P. B., PARREN, P. W. & BURTON, D. R. 2007. Neutralizing antibody fails to impact the course of Ebola virus infection in monkeys. *PLoS Pathog,* 3**,** e9.
PAN, Y., DU, J., LIU, J., WU, H., GUI, F., ZHANG, N., DENG, X., SONG, G., LI, Y., LU, J., WU, X., ZHAN, S., JING, Z., WANG, J., YANG, Y., LIU, J., CHEN, Y., CHEN, Q., ZHANG, H., HU, H., DUAN, K., WANG, M., WANG, Q. & YANG, X. 2021. Screening of potent neutralizing antibodies against SARS-CoV-2 using convalescent patients-derived phage-display libraries. *Cell Discov,* 7**,** 57.
PANCERA, M., MCLELLAN, J. S., WU, X., ZHU, J., CHANGELA, A., SCHMIDT, S. D., YANG, Y., ZHOU, T., PHOGAT, S., MASCOLA, J. R. & KWONG, P. D. 2010. Crystal structure of PG16 and chimeric dissection with somatically related PG9: structure-function analysis of two quaternary-specific antibodies that effectively neutralize HIV-1. *J Virol,* 84**,** 8098-110.

PARMLEY, S. F. & SMITH, G. P. 1988. Antibody-selectable filamentous fd phage vectors: affinity purification of target genes. *Gene,* 73**,** 305-18.

PARMLEY, S. F. & SMITH, G. P. 1989. Filamentous fusion phage cloning vectors for the study of epitopes and design of vaccines. *Adv Exp Med Biol,* 251**,** 215-8.

PASMAN, Y., SAINI, S. S., SMITH, E. & KAUSHIK, A. K. 2010. Organization and genomic complexity of bovine lambda-light chain gene locus. *Vet Immunol Immunopathol,* 135**,** 306-13.

PEACOCK, T. P., GOLDHILL, D. H., ZHOU, J., BAILLON, L., FRISE, R., SWANN, O. C., KUGATHASAN, R., PENN, R., BROWN, J. C., SANCHEZ-DAVID, R. Y., BRAGA, L., WILLIAMSON, M. K., HASSARD, J. A., STALLER, E., HANLEY, B., OSBORN, M., GIACCA, M., DAVIDSON, A. D., MATTHEWS, D. A. & BARCLAY, W. S. 2021. The furin cleavage site in the SARS-CoV-2 spike protein is required for transmission in ferrets. *Nat Microbiol,* 6**,** 899-909.

PEKAR, J. E., MAGEE, A., PARKER, E., MOSHIRI, N., IZHIKEVICH, K., HAVENS, J. L., GANGAVARAPU, K., MALPICA SERRANO, L. M., CRITS-CHRISTOPH, A., MATTESON, N. L., ZELLER, M., LEVY, J. I., WANG, J. C., HUGHES, S., LEE, J., PARK, H., PARK, M. S., CHING ZI YAN, K., LIN, R. T. P., MAT ISA, M. N., NOOR, Y. M., VASYLYEVA, T. I., GARRY, R. F., HOLMES, E. C., RAMBAUT, A., SUCHARD, M. A., ANDERSEN, K. G., WOROBEY, M. & WERTHEIM, J. O. 2022. The molecular epidemiology of multiple zoonotic origins of SARS-CoV-2. *Science,* 377**,** 960-966.

PEKAR, L., KLEWINGHAUS, D., ARRAS, P., CARRARA, S. C., HARWARDT, J., KRAH, S., YANAKIEVA, D., TOLEIKIS, L., SMIDER, V. V., KOLMAR, H. & ZIELONKA, S. 2021. Milking the Cow: Cattle-Derived Chimeric Ultralong CDR-H3 Antibodies and Their Engineered CDR-H3-Only Knobbody Counterparts Targeting Epidermal Growth Factor Receptor Elicit Potent NK Cell-Mediated Cytotoxicity. *Front Immunol,* 12**,** 742418.

PELFRENE, E., MURA, M., CAVALEIRO SANCHES, A. & CAVALERI, M. 2019. Monoclonal antibodies as anti-infective products: a promising future? *Clin Microbiol Infect,* 25**,** 60-64.

PEREZ-ALOS, L., ARMENTEROS, J. J. A., MADSEN, J. R., HANSEN, C. B., JARLHELT, I., HAMM, S. R., HEFTDAL, L. D., PRIES-HEJE, M. M., MOLLER, D. L., FOGH, K., HASSELBALCH, R. B., ROSBJERG, A., BRUNAK, S., SORENSEN, E., LARSEN, M. A. H., OSTROWSKI, S. R., FRIKKE-SCHMIDT, R., BAYARRI-OLMOS, R., HILSTED, L. M., IVERSEN, K. K., BUNDGAARD, H., NIELSEN, S. D. & GARRED, P. 2022. Modeling of waning immunity after SARS-CoV-2 vaccination and influencing factors. *Nat Commun,* 13**,** 1614.

PERLMAN, S. & NETLAND, J. 2009. Coronaviruses post-SARS: update on replication and pathogenesis. *Nat Rev Microbiol,* 7**,** 439-50.

PHILIPP, D. & ADALBERT, K. 2017. Detailed Protocols for the Selection of Antiviral Human Antibodies from Combinatorial Immune Phage Display Libraries. *In:* THOMAS, B. (ed.) *Antibody Engineering.* Rijeka: IntechOpen.

PICCOLI, L., PARK, Y. J., TORTORICI, M. A., CZUDNOCHOWSKI, N., WALLS, A. C., BELTRAMELLO, M., SILACCI-FREGNI, C., PINTO, D., ROSEN, L. E., BOWEN, J. E., ACTON, O. J., JACONI, S., GUARINO, B., MINOLA, A., ZATTA, F., SPRUGASCI, N., BASSI, J., PETER, A., DE MARCO, A., NIX, J. C., MELE, F., JOVIC, S., RODRIGUEZ, B. F., GUPTA, S. V., JIN, F., PIUMATTI, G., LO PRESTI, G., PELLANDA, A. F., BIGGIOGERO, M., TARKOWSKI, M., PIZZUTO, M. S., CAMERONI, E., HAVENAR-DAUGHTON, C., SMITHEY, M., HONG, D., LEPORI, V., ALBANESE, E., CESCHI, A., BERNASCONI, E., ELZI, L., FERRARI, P., GARZONI, C., RIVA, A., SNELL, G., SALLUSTO, F., FINK, K., VIRGIN, H. W., LANZAVECCHIA,

A., CORTI, D. & VEESLER, D. 2020. Mapping Neutralizing and Immunodominant Sites on the SARS-CoV-2 Spike Receptor-Binding Domain by Structure-Guided High-Resolution Serology. *Cell,* 183**,** 1024-1042 e21.

PILZECKER, B. & JACOBS, H. 2019. Mutating for Good: DNA Damage Responses During Somatic Hypermutation. *Front Immunol,* 10**,** 438.

PINTO, D., PARK, Y. J., BELTRAMELLO, M., WALLS, A. C., TORTORICI, M. A., BIANCHI, S., JACONI, S., CULAP, K., ZATTA, F., DE MARCO, A., PETER, A., GUARINO, B., SPREAFICO, R., CAMERONI, E., CASE, J. B., CHEN, R. E., HAVENAR-DAUGHTON, C., SNELL, G., TELENTI, A., VIRGIN, H. W., LANZAVECCHIA, A., DIAMOND, M. S., FINK, K., VEESLER, D. & CORTI, D. 2020. Cross-neutralization of SARS-CoV-2 by a human monoclonal SARS-CoV antibody. *Nature,* 583**,** 290-295.

PINTO, D., SAUER, M. M., CZUDNOCHOWSKI, N., LOW, J. S., TORTORICI, M. A., HOUSLEY, M. P., NOACK, J., WALLS, A. C., BOWEN, J. E., GUARINO, B., ROSEN, L. E., IULIO, J. D., JERAK, J., KAISER, H., ISLAM, S., JACONI, S., SPRUGASCI, N., CULAP, K., ABDELNABI, R., FOO, C., COELMONT, L., BARTHA, I., BIANCHI, S., SILACCI-FREGNI, C., BASSI, J., MARZI, R., VETTI, E., CASSOTTA, A., CESCHI, A., FERRARI, P., CIPPÀ, P. E., GIANNINI, O., CERUTI, S., GARZONI, C., RIVA, A., BENIGNI, F., CAMERONI, E., PICCOLI, L., PIZZUTO, M. S., SMITHEY, M., HONG, D., TELENTI, A., LEMPP, F. A., NEYTS, J., HAVENAR-DAUGHTON, C., LANZAVECCHIA, A., SALLUSTO, F., SNELL, G., VIRGIN, H. W., BELTRAMELLO, M., CORTI, D. & VEESLER, D. 2021. A human antibody that broadly neutralizes betacoronaviruses protects against SARS-CoV-2 by blocking the fusion machinery. *bioRxiv***,** 2021.05.09.442808.

PLANAS, D., VEYER, D., BAIDALIUK, A., STAROPOLI, I., GUIVEL-BENHASSINE, F., RAJAH, M. M., PLANCHAIS, C., PORROT, F., ROBILLARD, N., PUECH, J., PROT, M., GALLAIS, F., GANTNER, P., VELAY, A., LE GUEN, J., KASSIS-CHIKHANI, N., EDRISS, D., BELEC, L., SEVE, A., COURTELLEMONT, L., PERE, H., HOCQUELOUX, L., FAFI-KREMER, S., PRAZUCK, T., MOUQUET, H., BRUEL, T., SIMON-LORIERE, E., REY, F. A. & SCHWARTZ, O. 2021. Reduced sensitivity of SARS-CoV-2 variant Delta to antibody neutralization. *Nature,* 596**,** 276-280.

PLANTE, J. A., MITCHELL, B. M., PLANTE, K. S., DEBBINK, K., WEAVER, S. C. & MENACHERY, V. D. 2021. The variant gambit: COVID-19's next move. *Cell Host Microbe,* 29**,** 508-515.

PRABAKARAN, P. & CHOWDHURY, P. S. 2020. Landscape of Non-canonical Cysteines in Human V(H) Repertoire Revealed by Immunogenetic Analysis. *Cell Rep,* 31**,** 107831.

PRASHAR, P., SWAIN, S., ADHIKARI, N., ARYAN, P., SINGH, A., KWATRA, M. & B, P. 2022. A novel high-throughput single B-cell cloning platform for isolation and characterization of high-affinity and potent SARS-CoV-2 neutralizing antibodies. *Antiviral Res,* 203**,** 105349.

PROMPETCHARA, E., KETLOY, C. & PALAGA, T. 2020. Immune responses in COVID-19 and potential vaccines: Lessons learned from SARS and MERS epidemic. *Asian Pac J Allergy Immunol,* 38**,** 1-9.

PUTNAM, F. W. 1969. Immunoglobulin structure: variability and homology. *Science,* 163**,** 633-44.

QIU, X., WONG, G., AUDET, J., BELLO, A., FERNANDO, L., ALIMONTI, J. B., FAUSTHER-BOVENDO, H., WEI, H., AVILES, J., HIATT, E., JOHNSON, A., MORTON, J., SWOPE, K., BOHOROV, O., BOHOROVA, N., GOODMAN, C., KIM, D., PAULY, M. H., VELASCO, J., PETTITT, J., OLINGER, G. G., WHALEY, K., XU, B., STRONG,

J. E., ZEITLIN, L. & KOBINGER, G. P. 2014. Reversion of advanced Ebola virus disease in nonhuman primates with ZMapp. *Nature,* 514**,** 47-53.

RAHBARNIA, L., FARAJNIA, S., BABAEI, H., MAJIDI, J., VEISI, K., TANOMAND, A. & AKBARI, B. 2016. Invert biopanning: A novel method for efficient and rapid isolation of scFvs by phage display technology. *Biologicals,* 44**,** 567-573.

RAMILO, O., LAGOS, R., SÁEZ-LLORENS, X., SUZICH, J., WANG, C. K., JENSEN, K. M., HARRIS, B. S., LOSONSKY, G. A., GRIFFIN, M. P. & GROUP, M. S. 2014. Motavizumab treatment of infants hospitalized with respiratory syncytial virus infection does not decrease viral load or severity of illness. *The Pediatric infectious disease journal,* 33**,** 703-709.

RAMIREZ VALDEZ, K., NZAU, B., DOREY-ROBINSON, D., JARMAN, M., NYAGWANGE, J., SCHWARTZ, J. C., FREIMANIS, G., STEYN, A. W., WARIMWE, G. M., MORRISON, L. J., MWANGI, W., CHARLESTON, B., BONNET-DI PLACIDO, M. & HAMMOND, J. A. 2023. A Customizable Suite of Methods to Sequence and Annotate Cattle Antibodies. *Vaccines (Basel),* 11.

RAYBOULD, M. I. J., MARKS, C., KRAWCZYK, K., TADDESE, B., NOWAK, J., LEWIS, A. P., BUJOTZEK, A., SHI, J. & DEANE, C. M. 2019. Five computational developability guidelines for therapeutic antibody profiling. *Proc Natl Acad Sci U S A,* 116**,** 4025-4030.

ROBBIANI, D. F., GAEBLER, C., MUECKSCH, F., LORENZI, J. C. C., WANG, Z., CHO, A., AGUDELO, M., BARNES, C. O., GAZUMYAN, A., FINKIN, S., HAGGLOF, T., OLIVEIRA, T. Y., VIANT, C., HURLEY, A., HOFFMANN, H. H., MILLARD, K. G., KOST, R. G., CIPOLLA, M., GORDON, K., BIANCHINI, F., CHEN, S. T., RAMOS, V., PATEL, R., DIZON, J., SHIMELIOVICH, I., MENDOZA, P., HARTWEGER, H., NOGUEIRA, L., PACK, M., HOROWITZ, J., SCHMIDT, F., WEISBLUM, Y., MICHAILIDIS, E., ASHBROOK, A. W., WALTARI, E., PAK, J. E., HUEY-TUBMAN, K. E., KORANDA, N., HOFFMAN, P. R., WEST, A. P., JR., RICE, C. M., HATZIIOANNOU, T., BJORKMAN, P. J., BIENIASZ, P. D., CASKEY, M. & NUSSENZWEIG, M. C. 2020. Convergent antibody responses to SARS-CoV-2 in convalescent individuals. *Nature,* 584**,** 437-442.

ROBBIE, G. J., CRISTE, R., DALL'ACQUA, W. F., JENSEN, K., PATEL, N. K., LOSONSKY, G. A. & GRIFFIN, M. P. 2013. A novel investigational Fc-modified humanized monoclonal antibody, motavizumab-YTE, has an extended half-life in healthy adults. *Antimicrob Agents Chemother,* 57**,** 6147-53.

ROGERS, T. F., ZHAO, F., HUANG, D., BEUTLER, N., BURNS, A., HE, W. T., LIMBO, O., SMITH, C., SONG, G., WOEHL, J., YANG, L., ABBOTT, R. K., CALLAGHAN, S., GARCIA, E., HURTADO, J., PARREN, M., PENG, L., RAMIREZ, S., RICKETTS, J., RICCIARDI, M. J., RAWLINGS, S. A., WU, N. C., YUAN, M., SMITH, D. M., NEMAZEE, D., TEIJARO, J. R., VOSS, J. E., WILSON, I. A., ANDRABI, R., BRINEY, B., LANDAIS, E., SOK, D., JARDINE, J. G. & BURTON, D. R. 2020. Isolation of potent SARS-CoV-2 neutralizing antibodies and protection from disease in a small animal model. *Science,* 369**,** 956-963.

ROLTGEN, K. & BOYD, S. D. 2021. Antibody and B cell responses to SARS-CoV-2 infection and vaccination. *Cell Host Microbe,* 29**,** 1063-1075.

ROLTGEN, K., POWELL, A. E., WIRZ, O. F., STEVENS, B. A., HOGAN, C. A., NAJEEB, J., HUNTER, M., WANG, H., SAHOO, M. K., HUANG, C., YAMAMOTO, F., MANOHAR, M., MANALAC, J., OTRELO-CARDOSO, A. R., PHAM, T. D., RUSTAGI, A., ROGERS, A. J., SHAH, N. H., BLISH, C. A., COCHRAN, J. R., JARDETZKY, T. S., ZEHNDER, J. L., WANG, T. T., NARASIMHAN, B., GOMBAR, S., TIBSHIRANI, R., NADEAU, K. C., KIM, P. S., PINSKY, B. A. & BOYD, S. D.

2020. Defining the features and duration of antibody responses to SARS-CoV-2 infection associated with disease severity and outcome. *Sci Immunol,* 5.

ROTH, D. B. 2014. V(D)J Recombination: Mechanism, Errors, and Fidelity. *Microbiol Spectr,* 2.

RUSSO, G., MEIER, D., HELMSING, S., WENZEL, E., OBERLE, F., FRENZEL, A. & HUST, M. 2018. Parallelized Antibody Selection in Microtiter Plates. *Methods Mol Biol,* 1701**,** 273-284.

SAFONOVA, Y. & PEVZNER, P. A. 2020. V(DD)J recombination is an important and evolutionarily conserved mechanism for generating antibodies with unusually long CDR3s. *Genome Res,* 30**,** 1547-1558.

SAINI, S. S., ALLORE, B., JACOBS, R. M. & KAUSHIK, A. 1999. Exceptionally long CDR3H region with multiple cysteine residues in functional bovine IgM antibodies. *Eur J Immunol,* 29**,** 2420-6.

SAINI, S. S., FARRUGIA, W., RAMSLAND, P. A. & KAUSHIK, A. K. 2003. Bovine IgM antibodies with exceptionally long complementarity-determining region 3 of the heavy chain share unique structural properties conferring restricted VH + Vlambda pairings. *Int Immunol,* 15**,** 845-53.

SAKHARKAR, M., RAPPAZZO, C. G., WIELAND-ALTER, W. F., HSIEH, C. L., WRAPP, D., ESTERMAN, E. S., KAKU, C. I., WEC, A. Z., GEOGHEGAN, J. C., MCLELLAN, J. S., CONNOR, R. I., WRIGHT, P. F. & WALKER, L. M. 2021. Prolonged evolution of the human B cell response to SARS-CoV-2 infection. *Sci Immunol,* 6.

SALAZAR, G., ZHANG, N., FU, T. M. & AN, Z. 2017. Antibody therapies for the prevention and treatment of viral infections. *NPJ Vaccines,* 2**,** 19.

SARIOL, A. & PERLMAN, S. 2020. Lessons for COVID-19 Immunity from Other Coronavirus Infections. *Immunity*.

SAUER, M. M., TORTORICI, M. A., PARK, Y. J., WALLS, A. C., HOMAD, L., ACTON, O. J., BOWEN, J. E., WANG, C., XIONG, X., DE VAN DER SCHUEREN, W., QUISPE, J., HOFFSTROM, B. G., BOSCH, B. J., MCGUIRE, A. T. & VEESLER, D. 2021. Structural basis for broad coronavirus neutralization. *Nat Struct Mol Biol,* 28**,** 478-486.

SAWICKI, S. G., SAWICKI, D. L. & SIDDELL, S. G. 2007. A contemporary view of coronavirus transcription. *J Virol,* 81**,** 20-9.

SAYLOR, C., DADACHOVA, E. & CASADEVALL, A. 2009. Monoclonal antibody-based therapies for microbial diseases. *Vaccine,* 27 Suppl 6**,** G38-46.

SCHANZ, M., LIECHTI, T., ZAGORDI, O., MIHO, E., REDDY, S. T., GÜNTHARD, H. F., TRKOLA, A. & HUBER, M. 2014. High-throughput sequencing of human immunoglobulin variable regions with subtype identification. *PLoS One,* 9**,** e111726.

SCOTT, J. K. & SMITH, G. P. 1990. Searching for peptide ligands with an epitope library. *Science,* 249**,** 386-90.

SELLMANN, C., PEKAR, L., BAUER, C., CIESIELSKI, E., KRAH, S., BECKER, S., TOLEIKIS, L., KUGLER, J., FRENZEL, A., VALLDORF, B., HUST, M. & ZIELONKA, S. 2020. A One-Step Process for the Construction of Phage Display scFv and VHH Libraries. *Mol Biotechnol,* 62**,** 228-239.

SEYDOUX, E., HOMAD, L. J., MACCAMY, A. J., PARKS, K. R., HURLBURT, N. K., JENNEWEIN, M. F., AKINS, N. R., STUART, A. B., WAN, Y. H., FENG, J., WHALEY, R. E., SINGH, S., BOECKH, M., COHEN, K. W., MCELRATH, M. J., ENGLUND, J. A., CHU, H. Y., PANCERA, M., MCGUIRE, A. T. & STAMATATOS, L. 2020. Analysis of a SARS-CoV-2-Infected Individual Reveals Development of Potent Neutralizing Antibodies with Limited Somatic Mutation. *Immunity,* 53**,** 98-105 e5.

SHAH, P., CANZIANI, G. A., CARTER, E. P. & CHAIKEN, I. 2021. The Case for S2: The Potential Benefits of the S2 Subunit of the SARS-CoV-2 Spike Protein as an Immunogen in Fighting the COVID-19 Pandemic. *Front Immunol,* 12**,** 637651.
SHAH, V. K., FIRMAL, P., ALAM, A., GANGULY, D. & CHATTOPADHYAY, S. 2020. Overview of Immune Response During SARS-CoV-2 Infection: Lessons From the Past. *Front Immunol,* 11**,** 1949.
SHRESTHA, L. B., FOSTER, C., RAWLINSON, W., TEDLA, N. & BULL, R. A. 2022. Evolution of the SARS-CoV-2 omicron variants BA.1 to BA.5: Implications for immune escape and transmission. *Rev Med Virol,* 32**,** e2381.
SHRESTHA, L. B., TEDLA, N. & BULL, R. A. 2021. Broadly-Neutralizing Antibodies Against Emerging SARS-CoV-2 Variants. *Front Immunol,* 12**,** 752003.
SIDHU, S. S. 2001. Engineering M13 for phage display. *Biomol Eng,* 18**,** 57-63.
SIMONS, G. F., KONINGS, R. N. & SCHOENMAKERS, J. G. 1981. Genes VI, VII, and IX of phage M13 code for minor capsid proteins of the virion. *Proc Natl Acad Sci U S A,* 78**,** 4194-8.
SINCLAIR, M. C., GILCHRIST, J. & AITKEN, R. 1997. Bovine IgG repertoire is dominated by a single diversified VH gene family. *J Immunol,* 159**,** 3883-9.
SINGH, A. K., SINGH, A., SINGH, R. & MISRA, A. 2021. Molnupiravir in COVID-19: A systematic review of literature. *Diabetes Metab Syndr,* 15**,** 102329.
SINGH, M. & DE WIT, E. 2022. Antiviral agents for the treatment of COVID-19: Progress and challenges. *Cell Rep Med,* 3**,** 100549.
SMIDER, B. A. & SMIDER, V. V. 2020. Formation of ultralong DH regions through genomic rearrangement. *BMC Immunol,* 21**,** 30.
SMITH, G. P. 1985. Filamentous Fusion Phage: Novel Expression Vectors That Display Cloned Antigens on the Virion Surface. *Science,* 228**,** 1315-1317.
SMITH, G. P. & PETRENKO, V. A. 1997. Phage Display. *Chem Rev,* 97**,** 391-410.
SOK, D., LE, K. M., VADNAIS, M., SAYE-FRANCISCO, K. L., JARDINE, J. G., TORRES, J. L., BERNDSEN, Z. T., KONG, L., STANFIELD, R., RUIZ, J., RAMOS, A., LIANG, C. H., CHEN, P. L., CRISCITIELLO, M. F., MWANGI, W., WILSON, I. A., WARD, A. B., SMIDER, V. V. & BURTON, D. R. 2017. Rapid elicitation of broadly neutralizing antibodies to HIV by immunization in cows. *Nature,* 548**,** 108-111.
SOKAL, A., CHAPPERT, P., BARBA-SPAETH, G., ROESER, A., FOURATI, S., AZZAOUI, I., VANDENBERGHE, A., FERNANDEZ, I., MEOLA, A., BOUVIER-ALIAS, M., CRICKX, E., BELDI-FERCHIOU, A., HUE, S., LANGUILLE, L., MICHEL, M., BALOUL, S., NOIZAT-PIRENNE, F., LUKA, M., MEGRET, J., MENAGER, M., PAWLOTSKY, J. M., FILLATREAU, S., REY, F. A., WEILL, J. C., REYNAUD, C. A. & MAHEVAS, M. 2021. Maturation and persistence of the anti-SARS-CoV-2 memory B cell response. *Cell,* 184**,** 1201-1213 e14.
SOLEMANI ZADEH, A., GRASSER, A., DINTER, H., HERMES, M. & SCHINDOWSKI, K. 2019. Efficient Construction and Effective Screening of Synthetic Domain Antibody Libraries. *Methods Protoc,* 2.
SONG, G., YUAN, M., LIU, H., CAPOZZOLA, T., LIN, R. N., TORRES, J. L., HE, W. T., MUSHARRAFIEH, R., DUEKER, K., ZHOU, P., CALLAGHAN, S., MISHRA, N., YONG, P., ANZANELLO, F., AVILLION, G., VO, A. L., LI, X., MAKHDOOMI, M., FENG, Z., ZHU, X., PENG, L., NEMAZEE, D., SAFONOVA, Y., BRINEY, B., WARD, A. B., BURTON, D. R., WILSON, I. A. & ANDRABI, R. 2023. Broadly neutralizing antibodies targeting a conserved silent face of spike RBD resist extreme SARS-CoV-2 antigenic drift. *bioRxiv*.
SPARKS, A. B., ADEY, N. B., CWIRLA, S. & KAY, B. K. 1996. *Screening phage-displayed random peptide libraries*, San Diego, CA: Academic Press.

SPENCER, S., BETHEA, D., RAJU, T. S., GILES-KOMAR, J. & FENG, Y. 2012. Solubility evaluation of murine hybridoma antibodies. *MAbs,* 4**,** 319-25.

STALEY, T. E. & BUSH, L. J. 1985. Receptor mechanisms of the neonatal intestine and their relationship to immunoglobulin absorption and disease. *J Dairy Sci,* 68**,** 184-205.

STANFIELD, R. L., DOOLEY, H., FLAJNIK, M. F. & WILSON, I. A. 2004. Crystal structure of a shark single-domain antibody V region in complex with lysozyme. *Science,* 305**,** 1770-3.

STANFIELD, R. L., HAAKENSON, J., DEISS, T. C., CRISCITIELLO, M. F., WILSON, I. A. & SMIDER, V. V. 2018. The Unusual Genetics and Biochemistry of Bovine Immunoglobulins. *Adv Immunol,* 137**,** 135-164.

STANFIELD, R. L., WILSON, I. A. & SMIDER, V. V. 2016. Conservation and diversity in the ultralong third heavy-chain complementarity-determining region of bovine antibodies. *Sci Immunol,* 1.

STANGEL, M. & PUL, R. 2006. Basic principles of intravenous immunoglobulin (IVIg) treatment. *J Neurol,* 253 Suppl 5**,** V18-24.

STARR, T. N., CZUDNOCHOWSKI, N., LIU, Z., ZATTA, F., PARK, Y. J., ADDETIA, A., PINTO, D., BELTRAMELLO, M., HERNANDEZ, P., GREANEY, A. J., MARZI, R., GLASS, W. G., ZHANG, I., DINGENS, A. S., BOWEN, J. E., TORTORICI, M. A., WALLS, A. C., WOJCECHOWSKYJ, J. A., DE MARCO, A., ROSEN, L. E., ZHOU, J., MONTIEL-RUIZ, M., KAISER, H., DILLEN, J. R., TUCKER, H., BASSI, J., SILACCI-FREGNI, C., HOUSLEY, M. P., DI IULIO, J., LOMBARDO, G., AGOSTINI, M., SPRUGASCI, N., CULAP, K., JACONI, S., MEURY, M., DELLOTA, E., JR., ABDELNABI, R., FOO, S. C., CAMERONI, E., STUMPF, S., CROLL, T. I., NIX, J. C., HAVENAR-DAUGHTON, C., PICCOLI, L., BENIGNI, F., NEYTS, J., TELENTI, A., LEMPP, F. A., PIZZUTO, M. S., CHODERA, J. D., HEBNER, C. M., VIRGIN, H. W., WHELAN, S. P. J., VEESLER, D., CORTI, D., BLOOM, J. D. & SNELL, G. 2021a. SARS-CoV-2 RBD antibodies that maximize breadth and resistance to escape. *Nature,* 597**,** 97-102.

STARR, T. N., GREANEY, A. J., DINGENS, A. S. & BLOOM, J. D. 2021b. Complete map of SARS-CoV-2 RBD mutations that escape the monoclonal antibody LY-CoV555 and its cocktail with LY-CoV016. *Cell Rep Med,* 2**,** 100255.

STAVNEZER, J., GUIKEMA, J. E. & SCHRADER, C. E. 2008. Mechanism and regulation of class switch recombination. *Annu Rev Immunol,* 26**,** 261-92.

STEPHENS, D. S. & MCELRATH, M. J. 2020. COVID-19 and the Path to Immunity. *JAMA,* 324**,** 1279-1281.

STIJLEMANS, B., CONRATH, K., CORTEZ-RETAMOZO, V., VAN XONG, H., WYNS, L., SENTER, P., REVETS, H., DE BAETSELIER, P., MUYLDERMANS, S. & MAGEZ, S. 2004. Efficient targeting of conserved cryptic epitopes of infectious agents by single domain antibodies. African trypanosomes as paradigm. *J Biol Chem,* 279**,** 1256-61.

SUTHAR, M. S., ZIMMERMAN, M. G., KAUFFMAN, R. C., MANTUS, G., LINDERMAN, S. L., HUDSON, W. H., VANDERHEIDEN, A., NYHOFF, L., DAVIS, C. W., ADEKUNLE, O., AFFER, M., SHERMAN, M., REYNOLDS, S., VERKERKE, H. P., ALTER, D. N., GUARNER, J., BRYKSIN, J., HORWATH, M. C., ARTHUR, C. M., SAAKADZE, N., SMITH, G. H., EDUPUGANTI, S., SCHERER, E. M., HELLMEISTER, K., CHENG, A., MORALES, J. A., NEISH, A. S., STOWELL, S. R., FRANK, F., ORTLUND, E., ANDERSON, E. J., MENACHERY, V. D., ROUPHAEL, N., MEHTA, A. K., STEPHENS, D. S., AHMED, R., ROBACK, J. D. & WRAMMERT, J. 2020. Rapid Generation of Neutralizing Antibody Responses in COVID-19 Patients. *Cell Rep Med,* 1**,** 100040.

SVILENOV, H. L., SACHERL, J., PROTZER, U., ZACHARIAS, M. & BUCHNER, J. 2021. Mechanistic principles of an ultra-long bovine CDR reveal strategies for antibody design. *Nat Commun,* 12**,** 6737.

SWIMMER, C., LEHAR, S. M., MCCAFFERTY, J., CHISWELL, D. J., BLATTLER, W. A. & GUILD, B. C. 1992. Phage display of ricin B chain and its single binding domains: system for screening galactose-binding mutants. *Proc Natl Acad Sci U S A,* 89**,** 3756-60.

TAKASHITA, E., KINOSHITA, N., YAMAYOSHI, S., SAKAI-TAGAWA, Y., FUJISAKI, S., ITO, M., IWATSUKI-HORIMOTO, K., CHIBA, S., HALFMANN, P., NAGAI, H., SAITO, M., ADACHI, E., SULLIVAN, D., PEKOSZ, A., WATANABE, S., MAEDA, K., IMAI, M., YOTSUYANAGI, H., MITSUYA, H., OHMAGARI, N., TAKEDA, M., HASEGAWA, H. & KAWAOKA, Y. 2022. Efficacy of Antibodies and Antiviral Drugs against Covid-19 Omicron Variant. *N Engl J Med,* 386**,** 995-998.

TAMURA, T., ITO, J., URIU, K., ZAHRADNIK, J., KIDA, I., ANRAKU, Y., NASSER, H., SHOFA, M., ODA, Y., LYTRAS, S., NAO, N., ITAKURA, Y., DEGUCHI, S., SUZUKI, R., WANG, L., BEGUM, M. M., KITA, S., YAJIMA, H., SASAKI, J., SASAKI-TABATA, K., SHIMIZU, R., TSUDA, M., KOSUGI, Y., FUJITA, S., PAN, L., SAUTER, D., YOSHIMATSU, K., SUZUKI, S., ASAKURA, H., NAGASHIMA, M., SADAMASU, K., YOSHIMURA, K., YAMAMOTO, Y., NAGAMOTO, T., SCHREIBER, G., MAENAKA, K., GENOTYPE TO PHENOTYPE JAPAN, C., HASHIGUCHI, T., IKEDA, T., FUKUHARA, T., SAITO, A., TANAKA, S., MATSUNO, K., TAKAYAMA, K. & SATO, K. 2023. Virological characteristics of the SARS-CoV-2 XBB variant derived from recombination of two Omicron subvariants. *Nat Commun,* 14**,** 2800.

TANG, A., CHEN, Z., COX, K. S., SU, H. P., CALLAHAN, C., FRIDMAN, A., ZHANG, L., PATEL, S. B., CEJAS, P. J., SWOYER, R., TOUCH, S., CITRON, M. P., GOVINDARAJAN, D., LUO, B., EDDINS, M., REID, J. C., SOISSON, S. M., GALLI, J., WANG, D., WEN, Z., HEIDECKER, G. J., CASIMIRO, D. R., DISTEFANO, D. J. & VORA, K. A. 2019. A potent broadly neutralizing human RSV antibody targets conserved site IV of the fusion glycoprotein. *Nat Commun,* 10**,** 4153.

TANG, T., BIDON, M., JAIMES, J. A., WHITTAKER, G. R. & DANIEL, S. 2020. Coronavirus membrane fusion mechanism offers a potential target for antiviral development. *Antiviral Res,* 178**,** 104792.

TANNE, J. H. 2022. Covid-19: BA.5 variant is now dominant in US as infections rise. *BMJ,* 378**,** o1770.

TANNOCK, G. A., KIM, H. & XUE, L. 2020. Why are vaccines against many human viral diseases still unavailable; an historic perspective? *J Med Virol,* 92**,** 129-138.

TIKUNOVA, N. V. & MOROZOVA, V. V. 2009. Phage display on the base of filamentous bacteriophages: application for recombinant antibodies selection. *Acta Naturae,* 1**,** 20-8.

TONG, P., GAUTAM, A., WINDSOR, I. W., TRAVERS, M., CHEN, Y., GARCIA, N., WHITEMAN, N. B., MCKAY, L. G. A., STORM, N., MALSICK, L. E., HONKO, A. N., LELIS, F. J. N., HABIBI, S., JENNI, S., CAI, Y., RENNICK, L. J., DUPREX, W. P., MCCARTHY, K. R., LAVINE, C. L., ZUO, T., LIN, J., ZUIANI, A., FELDMAN, J., MACDONALD, E. A., HAUSER, B. M., GRIFFTHS, A., SEAMAN, M. S., SCHMIDT, A. G., CHEN, B., NEUBERG, D., BAJIC, G., HARRISON, S. C. & WESEMANN, D. R. 2021. Memory B cell repertoire for recognition of evolving SARS-CoV-2 spike. *Cell,* 184**,** 4969-4980 e15.

TORTORICI, M. A., CZUDNOCHOWSKI, N., STARR, T. N., MARZI, R., WALLS, A. C., ZATTA, F., BOWEN, J. E., JACONI, S., DI IULIO, J., WANG, Z., DE MARCO, A., ZEPEDA, S. K., PINTO, D., LIU, Z., BELTRAMELLO, M., BARTHA, I., HOUSLEY, M.

P., LEMPP, F. A., ROSEN, L. E., DELLOTA, E., JR., KAISER, H., MONTIEL-RUIZ, M., ZHOU, J., ADDETIA, A., GUARINO, B., CULAP, K., SPRUGASCI, N., SALIBA, C., VETTI, E., GIACCHETTO-SASSELLI, I., FREGNI, C. S., ABDELNABI, R., FOO, S. C., HAVENAR-DAUGHTON, C., SCHMID, M. A., BENIGNI, F., CAMERONI, E., NEYTS, J., TELENTI, A., VIRGIN, H. W., WHELAN, S. P. J., SNELL, G., BLOOM, J. D., CORTI, D., VEESLER, D. & PIZZUTO, M. S. 2021. Broad sarbecovirus neutralization by a human monoclonal antibody. *Nature,* 597**,** 103-108.

TOURET, F., GIRAUD, E., BOURRET, J., DONATI, F., TRAN-RAJAU, J., CHIARAVALLI, J., LEMOINE, F., AGOU, F., SIMON-LORIERE, E., VAN DER WERF, S. & DE LAMBALLERIE, X. 2023. Enhanced neutralization escape to therapeutic monoclonal antibodies by SARS-CoV-2 omicron sub-lineages. *iScience,* 26**,** 106413.

TOWNSEND, J. P., HASSLER, H. B., WANG, Z., MIURA, S., SINGH, J., KUMAR, S., RUDDLE, N. H., GALVANI, A. P. & DORNBURG, A. 2021. The durability of immunity against reinfection by SARS-CoV-2: a comparative evolutionary study. *Lancet Microbe,* 2**,** e666-e675.

TRAGGIAI, E., BECKER, S., SUBBARAO, K., KOLESNIKOVA, L., UEMATSU, Y., GISMONDO, M. R., MURPHY, B. R., RAPPUOLI, R. & LANZAVECCHIA, A. 2004. An efficient method to make human monoclonal antibodies from memory B cells: potent neutralization of SARS coronavirus. *Nature medicine,* 10**,** 871-875.

TRAN, V. T., PERRODEAU, E., SALDANHA, J., PANE, I. & RAVAUD, P. 2023. Efficacy of first dose of covid-19 vaccine versus no vaccination on symptoms of patients with long covid: target trial emulation based on ComPaRe e-cohort. *BMJ Med,* 2**,** e000229.

TUEKPRAKHON, A., NUTALAI, R., DIJOKAITE-GURALIUC, A., ZHOU, D., GINN, H. M., SELVARAJ, M., LIU, C., MENTZER, A. J., SUPASA, P., DUYVESTEYN, H. M. E., DAS, R., SKELLY, D., RITTER, T. G., AMINI, A., BIBI, S., ADELE, S., JOHNSON, S. A., CONSTANTINIDES, B., WEBSTER, H., TEMPERTON, N., KLENERMAN, P., BARNES, E., DUNACHIE, S. J., CROOK, D., POLLARD, A. J., LAMBE, T., GOULDER, P., PATERSON, N. G., WILLIAMS, M. A., HALL, D. R., CONSORTIUM, O., CONSORTIUM, I. C., FRY, E. E., HUO, J., MONGKOLSAPAYA, J., REN, J., STUART, D. I. & SCREATON, G. R. 2022. Antibody escape of SARS-CoV-2 Omicron BA.4 and BA.5 from vaccine and BA.1 serum. *Cell,* 185**,** 2422-2433 e13.

TURNER, J. S., O'HALLORAN, J. A., KALAIDINA, E., KIM, W., SCHMITZ, A. J., ZHOU, J. Q., LEI, T., THAPA, M., CHEN, R. E., CASE, J. B., AMANAT, F., RAUSEO, A. M., HAILE, A., XIE, X., KLEBERT, M. K., SUESSEN, T., MIDDLETON, W. D., SHI, P. Y., KRAMMER, F., TEEFEY, S. A., DIAMOND, M. S., PRESTI, R. M. & ELLEBEDY, A. H. 2021. SARS-CoV-2 mRNA vaccines induce persistent human germinal centre responses. *Nature,* 596**,** 109-113.

URAKI, R., ITO, M., FURUSAWA, Y., YAMAYOSHI, S., IWATSUKI-HORIMOTO, K., ADACHI, E., SAITO, M., KOGA, M., TSUTSUMI, T., YAMAMOTO, S., OTANI, A., KISO, M., SAKAI-TAGAWA, Y., UEKI, H., YOTSUYANAGI, H., IMAI, M. & KAWAOKA, Y. 2023a. Humoral immune evasion of the omicron subvariants BQ.1.1 and XBB. *Lancet Infect Dis,* 23**,** 30-32.

URAKI, R., ITO, M., KISO, M., YAMAYOSHI, S., IWATSUKI-HORIMOTO, K., FURUSAWA, Y., SAKAI-TAGAWA, Y., IMAI, M., KOGA, M., YAMAMOTO, S., ADACHI, E., SAITO, M., TSUTSUMI, T., OTANI, A., KIKUCHI, T., YOTSUYANAGI, H., HALFMANN, P. J., PEKOSZ, A. & KAWAOKA, Y. 2023b. Antiviral and bivalent

vaccine efficacy against an omicron XBB.1.5 isolate. *Lancet Infect Dis,* 23**,** 402-403.
URQUHART, L. 2020. Top companies and drugs by sales in 2019. *Nat Rev Drug Discov,* 19**,** 228.
USMAN, M., YUYAN, L., HUSNAIN, M. & AKHTAR, M. W. 2023. COVID-19, travel restrictions and environmental consequences. *Environ Dev Sustain***,** 1-21.
VADNAIS, M. L. & SMIDER, V. V. 2016. Bos taurus ultralong CDR H3 antibodies. *Curr Opin Struct Biol,* 38**,** 62-7.
VALLDORF, B., HINZ, S. C., RUSSO, G., PEKAR, L., MOHR, L., KLEMM, J., DOERNER, A., KRAH, S., HUST, M. & ZIELONKA, S. 2022. Antibody display technologies: selecting the cream of the crop. *Biol Chem,* 403**,** 455-477.
VANHERCKE, T., AMPE, C., TIRRY, L. & DENOLF, P. 2005. Rescue and in situ selection and evaluation (RISE): a method for high-throughput panning of phage display libraries. *J Biomol Screen,* 10**,** 108-17.
VANSHYLLA, K., DI CRISTANZIANO, V., KLEIPASS, F., DEWALD, F., SCHOMMERS, P., GIESELMANN, L., GRUELL, H., SCHLOTZ, M., ERCANOGLU, M. S., STUMPF, R., MAYER, P., ZEHNER, M., HEGER, E., JOHANNIS, W., HORN, C., SUAREZ, I., JUNG, N., SALOMON, S., EBERHARDT, K. A., GATHOF, B., FATKENHEUER, G., PFEIFER, N., EGGELING, R., AUGUSTIN, M., LEHMANN, C. & KLEIN, F. 2021. Kinetics and correlates of the neutralizing antibody response to SARS-CoV-2 infection in humans. *Cell Host Microbe,* 29**,** 917-929 e4.
VAUGHAN, T. J., WILLIAMS, A. J., PRITCHARD, K., OSBOURN, J. K., POPE, A. R., EARNSHAW, J. C., MCCAFFERTY, J., HODITS, R. A., WILTON, J. & JOHNSON, K. S. 1996. Human antibodies with sub-nanomolar affinities isolated from a large non-immunized phage display library. *Nat Biotechnol,* 14**,** 309-14.
VODNIK, M., ZAGER, U., STRUKELJ, B. & LUNDER, M. 2011. Phage display: selecting straws instead of a needle from a haystack. *Molecules,* 16**,** 790-817.
W.H.O. 2023. *WHO Coronavirus (COVID-19) Dashboard* [Online]. Geneva (Switzerland): World Health Organisation. Available: https://covid19.who.int/ [Accessed 02nd August 2023].
WAGH, K., BHATTACHARYA, T., WILLIAMSON, C., ROBLES, A., BAYNE, M., GARRITY, J., RIST, M., RADEMEYER, C., YOON, H., LAPEDES, A., GAO, H., GREENE, K., LOUDER, M. K., KONG, R., KARIM, S. A., BURTON, D. R., BAROUCH, D. H., NUSSENZWEIG, M. C., MASCOLA, J. R., MORRIS, L., MONTEFIORI, D. C., KORBER, B. & SEAMAN, M. S. 2016. Optimal Combinations of Broadly Neutralizing Antibodies for Prevention and Treatment of HIV-1 Clade C Infection. *PLoS Pathog,* 12**,** e1005520.
WAJNBERG, A., AMANAT, F., FIRPO, A., ALTMAN, D. R., BAILEY, M. J., MANSOUR, M., MCMAHON, M., MEADE, P., MENDU, D. R., MUELLERS, K., STADLBAUER, D., STONE, K., STROHMEIER, S., SIMON, V., ABERG, J., REICH, D. L., KRAMMER, F. & CORDON-CARDO, C. 2020. Robust neutralizing antibodies to SARS-CoV-2 infection persist for months. *Science,* 370**,** 1227-1230.
WALDMANN, H. 2019. Human monoclonal antibodies: the benefits of humanization. *Human Monoclonal Antibodies: Methods and Protocols***,** 1-10.
WALKER, L. M., PHOGAT, S. K., CHAN-HUI, P. Y., WAGNER, D., PHUNG, P., GOSS, J. L., WRIN, T., SIMEK, M. D., FLING, S., MITCHAM, J. L., LEHRMAN, J. K., PRIDDY, F. H., OLSEN, O. A., FREY, S. M., HAMMOND, P. W., PROTOCOL, G. P. I., KAMINSKY, S., ZAMB, T., MOYLE, M., KOFF, W. C., POIGNARD, P. & BURTON, D. R. 2009. Broad and potent neutralizing antibodies from an African donor reveal a new HIV-1 vaccine target. *Science,* 326**,** 285-9.

WALLS, A. C., PARK, Y. J., TORTORICI, M. A., WALL, A., MCGUIRE, A. T. & VEESLER, D. 2020. Structure, Function, and Antigenicity of the SARS-CoV-2 Spike Glycoprotein. *Cell,* 181**,** 281-292.e6.

WALTHER, S., CZERNY, C. P. & DIESTERBECK, U. S. 2013. Exceptionally long CDR3H are not isotype restricted in bovine immunoglobulins. *PLoS One,* 8**,** e64234.

WALTHER, S., TIETZE, M., CZERNY, C. P., KÖNIG, S. & DIESTERBECK, U. S. 2016. Development of a Bioinformatics Framework for the Detection of Gene Conversion and the Analysis of Combinatorial Diversity in Immunoglobulin Heavy Chains in Four Cattle Breeds. *PLoS One,* 11**,** e0164567.

WAN, J., XING, S., DING, L., WANG, Y., GU, C., WU, Y., RONG, B., LI, C., WANG, S., CHEN, K., HE, C., ZHU, D., YUAN, S., QIU, C., ZHAO, C., NIE, L., GAO, Z., JIAO, J., ZHANG, X., WANG, X., YING, T., WANG, H., XIE, Y., LU, Y., XU, J. & LAN, F. 2020. Human-IgG-Neutralizing Monoclonal Antibodies Block the SARS-CoV-2 Infection. *Cell Rep,* 32**,** 107918.

WANG, C., LI, W., DRABEK, D., OKBA, N. M. A., VAN HAPEREN, R., OSTERHAUS, A. D. M. E., VAN KUPPEVELD, F. J. M., HAAGMANS, B. L., GROSVELD, F. & BOSCH, B. J. 2020a. A human monoclonal antibody blocking SARS-CoV-2 infection. *Nat Commun,* 11**,** 2251.

WANG, C., VAN HAPEREN, R., GUTIERREZ-ALVAREZ, J., LI, W., OKBA, N. M. A., ALBULESCU, I., WIDJAJA, I., VAN DIEREN, B., FERNANDEZ-DELGADO, R., SOLA, I., HURDISS, D. L., DARAMOLA, O., GROSVELD, F., VAN KUPPEVELD, F. J. M., HAAGMANS, B. L., ENJUANES, L., DRABEK, D. & BOSCH, B. J. 2021a. A conserved immunogenic and vulnerable site on the coronavirus spike protein delineated by cross-reactive monoclonal antibodies. *Nat Commun,* 12**,** 1715.

WANG, F., EKIERT, D. C., AHMAD, I., YU, W., ZHANG, Y., BAZIRGAN, O., TORKAMANI, A., RAUDSEPP, T., MWANGI, W., CRISCITIELLO, M. F., WILSON, I. A., SCHULTZ, P. G. & SMIDER, V. V. 2013. Reshaping antibody diversity. *Cell,* 153**,** 1379-93.

WANG, H., LI, X., LI, T., ZHANG, S., WANG, L., WU, X. & LIU, J. 2020b. The genetic sequence, origin, and diagnosis of SARS-CoV-2. *Eur J Clin Microbiol Infect Dis*.

WANG, M., CAO, R., ZHANG, L., YANG, X., LIU, J., XU, M., SHI, Z., HU, Z., ZHONG, W. & XIAO, G. 2020c. Remdesivir and chloroquine effectively inhibit the recently emerged novel coronavirus (2019-nCoV) in vitro. *Cell Res,* 30**,** 269-271.

WANG, Q., GUO, Y., IKETANI, S., NAIR, M. S., LI, Z., MOHRI, H., WANG, M., YU, J., BOWEN, A. D., CHANG, J. Y., SHAH, J. G., NGUYEN, N., CHEN, Z., MEYERS, K., YIN, M. T., SOBIESZCZYK, M. E., SHENG, Z., HUANG, Y., LIU, L. & HO, D. D. 2022. Antibody evasion by SARS-CoV-2 Omicron subvariants BA.2.12.1, BA.4 and BA.5. *Nature,* 608**,** 603-608.

WANG, Y. H., GRUNEWALD, M. & PERLMAN, S. 2020d. Coronaviruses: An Updated Overview of Their Replication and Pathogenesis. *Coronaviruses, 2 Edition,* 2203**,** 1-29.

WANG, Z., MUECKSCH, F., SCHAEFER-BABAJEW, D., FINKIN, S., VIANT, C., GAEBLER, C., HOFFMANN, H. H., BARNES, C. O., CIPOLLA, M., RAMOS, V., OLIVEIRA, T. Y., CHO, A., SCHMIDT, F., DA SILVA, J., BEDNARSKI, E., AGUADO, L., YEE, J., DAGA, M., TURROJA, M., MILLARD, K. G., JANKOVIC, M., GAZUMYAN, A., ZHAO, Z., RICE, C. M., BIENIASZ, P. D., CASKEY, M., HATZIIOANNOU, T. & NUSSENZWEIG, M. C. 2021b. Naturally enhanced neutralizing breadth against SARS-CoV-2 one year after infection. *Nature,* 595**,** 426-431.

WANG, Z., PAN, H. & JIANG, B. 2020e. Type I IFN deficiency: an immunological characteristic of severe COVID-19 patients. *Signal Transduct Target Ther,* 5**,** 198.

WEBER, M., BUJAK, E., PUTELLI, A., VILLA, A., MATASCI, M., GUALANDI, L., HEMMERLE, T., WULHFARD, S. & NERI, D. 2014. A highly functional synthetic phage display library containing over 40 billion human antibody clones. *PLoS One,* 9**,** e100000.

WEBSTER, R. E. 1996. CHAPTER 1 - Biology of the Filamentous Bacteriophage. *In:* KAY, B. K., WINTER, J. & MCCAFFERTY, J. (eds.) *Phage Display of Peptides and Proteins.* Burlington: Academic Press.

WESTENDORF, K., ZENTELIS, S., WANG, L., FOSTER, D., VAILLANCOURT, P., WIGGIN, M., LOVETT, E., VAN DER LEE, R., HENDLE, J., PUSTILNIK, A., SAUDER, J. M., KRAFT, L., HWANG, Y., SIEGEL, R. W., CHEN, J., HEINZ, B. A., HIGGS, R. E., KALLEWAARD, N. L., JEPSON, K., GOYA, R., SMITH, M. A., COLLINS, D. W., PELLACANI, D., XIANG, P., DE PUYRAIMOND, V., RICICOVA, M., DEVORKIN, L., PRITCHARD, C., O'NEILL, A., DALAL, K., PANWAR, P., DHUPAR, H., GARCES, F. A., COHEN, C. A., DYE, J. M., HUIE, K. E., BADGER, C. V., KOBASA, D., AUDET, J., FREITAS, J. J., HASSANALI, S., HUGHES, I., MUNOZ, L., PALMA, H. C., RAMAMURTHY, B., CROSS, R. W., GEISBERT, T. W., MENACHERY, V., LOKUGAMAGE, K., BORISEVICH, V., LANZ, I., ANDERSON, L., SIPAHIMALANI, P., CORBETT, K. S., YANG, E. S., ZHANG, Y., SHI, W., ZHOU, T., CHOE, M., MISASI, J., KWONG, P. D., SULLIVAN, N. J., GRAHAM, B. S., FERNANDEZ, T. L., HANSEN, C. L., FALCONER, E., MASCOLA, J. R., JONES, B. E. & BARNHART, B. C. 2022. LY-CoV1404 (bebtelovimab) potently neutralizes SARS-CoV-2 variants. *Cell Rep,* 39**,** 110812.

WHALEY, K. J. & ZEITLIN, L. 2022. Emerging antibody-based products for infectious diseases: Planning for metric ton manufacturing. *Hum Vaccin Immunother,* 18**,** 1930847.

WIBMER, C. K., AYRES, F., HERMANUS, T., MADZIVHANDILA, M., KGAGUDI, P., OOSTHUYSEN, B., LAMBSON, B. E., DE OLIVEIRA, T., VERMEULEN, M., VAN DER BERG, K., ROSSOUW, T., BOSWELL, M., UECKERMANN, V., MEIRING, S., VON GOTTBERG, A., COHEN, C., MORRIS, L., BHIMAN, J. N. & MOORE, P. L. 2021. SARS-CoV-2 501Y.V2 escapes neutralization by South African COVID-19 donor plasma. *Nat Med,* 27**,** 622-625.

WIDYASARI, K. & KIM, J. 2023. A Review of the Currently Available Antibody Therapy for the Treatment of Coronavirus Disease 2019 (COVID-19). *Antibodies (Basel),* 12.

WIEDERMANN, U., GARNER-SPITZER, E. & WAGNER, A. 2016. Primary vaccine failure to routine vaccines: Why and what to do? *Hum Vaccin Immunother,* 12**,** 239-43.

WILSON, P., STAMPER, C., DUGAN, H., LI, L., ASBY, N., HALFMANN, P., GUTHMILLER, J., ZHENG, N. Y., HUANG, M., STOVICEK, O., WANG, J., MADARIAGA, M. L., SHANMUGARAJAH, K., JANSEN, M., AMANAT, F., STEWART, I., CHANGROB, S., UTSET, H., HUANG, J., NELSON, C., DAI, Y. N., HALL, P., JEDRZEJCZAK, R., JOACHIMIAK, A., KRAMMER, F., FREMONT, D. & KAWAOKA, Y. 2020. Distinct B cell subsets give rise to antigen-specific antibody responses against SARS-CoV-2. *Res Sq*.

WINTER, G., GRIFFITHS, A. D., HAWKINS, R. E. & HOOGENBOOM, H. R. 1994. Making antibodies by phage display technology. *Annu Rev Immunol,* 12**,** 433-55.

WOROBEY, M., LEVY, J. I., MALPICA SERRANO, L., CRITS-CHRISTOPH, A., PEKAR, J. E., GOLDSTEIN, S. A., RASMUSSEN, A. L., KRAEMER, M. U. G., NEWMAN, C., KOOPMANS, M. P. G., SUCHARD, M. A., WERTHEIM, J. O., LEMEY, P., ROBERTSON, D. L., GARRY, R. F., HOLMES, E. C., RAMBAUT, A. & ANDERSEN,

K. G. 2022. The Huanan Seafood Wholesale Market in Wuhan was the early epicenter of the COVID-19 pandemic. *Science,* 377**,** 951-959.

WRAPP, D., DE VLIEGER, D., CORBETT, K. S., TORRES, G. M., WANG, N., VAN BREEDAM, W., ROOSE, K., VAN SCHIE, L., TEAM, V.-C. C.-R., HOFFMANN, M., POHLMANN, S., GRAHAM, B. S., CALLEWAERT, N., SCHEPENS, B., SAELENS, X. & MCLELLAN, J. S. 2020a. Structural Basis for Potent Neutralization of Betacoronaviruses by Single-Domain Camelid Antibodies. *Cell,* 181**,** 1436-1441.

WRAPP, D., WANG, N., CORBETT, K. S., GOLDSMITH, J. A., HSIEH, C. L., ABIONA, O., GRAHAM, B. S. & MCLELLAN, J. S. 2020b. Cryo-EM Structure of the 2019-nCoV Spike in the Prefusion Conformation. *bioRxiv*.

WU, L., OFICJALSKA, K., LAMBERT, M., FENNELL, B. J., DARMANIN-SHEEHAN, A., NÍ SHÚILLEABHÁIN, D., AUTIN, B., CUMMINS, E., TCHISTIAKOVA, L., BLOOM, L., PAULSEN, J., GILL, D., CUNNINGHAM, O. & FINLAY, W. J. J. 2012. Fundamental Characteristics of the Immunoglobulin VH Repertoire of Chickens in Comparison with Those of Humans, Mice, and Camelids. *The Journal of Immunology,* 188**,** 322-333.

WU, X., ZHOU, T., ZHU, J., ZHANG, B., GEORGIEV, I., WANG, C., CHEN, X., LONGO, N. S., LOUDER, M., MCKEE, K., O'DELL, S., PERFETTO, S., SCHMIDT, S. D., SHI, W., WU, L., YANG, Y., YANG, Z. Y., YANG, Z., ZHANG, Z., BONSIGNORI, M., CRUMP, J. A., KAPIGA, S. H., SAM, N. E., HAYNES, B. F., SIMEK, M., BURTON, D. R., KOFF, W. C., DORIA-ROSE, N. A., CONNORS, M., PROGRAM, N. C. S., MULLIKIN, J. C., NABEL, G. J., ROEDERER, M., SHAPIRO, L., KWONG, P. D. & MASCOLA, J. R. 2011. Focused evolution of HIV-1 neutralizing antibodies revealed by structures and deep sequencing. *Science,* 333**,** 1593-602.

XU, H., ZHONG, L., DENG, J., PENG, J., DAN, H., ZENG, X., LI, T. & CHEN, Q. 2020. High expression of ACE2 receptor of 2019-nCoV on the epithelial cells of oral mucosa. *Int J Oral Sci,* 12**,** 8.

XUE, B. A. B. D. A. H. J. A. U. A. V. A. K. L. A. U. V. N. A. L. S. 2014. Structural Disorder in Viral Proteins. *Chemical Reviews,* 114**,** 6880-6911.

YAN, X. & XU, Z. 2006. Ribosome-display technology: applications for directed evolution of functional proteins. *Drug Discov Today,* 11**,** 911-6.

YANG, F., LIU, L., NEUENSCHWANDER, P. F., IDELL, S., VANKAYALAPATI, R., JAIN, K. G., DU, K., JI, H. & YI, G. 2022. Phage Display-Derived Peptide for the Specific Binding of SARS-CoV-2. *ACS Omega,* 7**,** 3203-3211.

YANG, W., YOON, A., LEE, S., KIM, S., HAN, J. & CHUNG, J. 2017. Next-generation sequencing enables the discovery of more diverse positive clones from a phage-displayed antibody library. *Exp Mol Med,* 49**,** e308.

YEUNG, M. L., TENG, J. L. L., JIA, L., ZHANG, C., HUANG, C., CAI, J. P., ZHOU, R., CHAN, K. H., ZHAO, H., ZHU, L., SIU, K. L., FUNG, S. Y., YUNG, S., CHAN, T. M., TO, K. K., CHAN, J. F., CAI, Z., LAU, S. K. P., CHEN, Z., JIN, D. Y., WOO, P. C. Y. & YUEN, K. Y. 2021. Soluble ACE2-mediated cell entry of SARS-CoV-2 via interaction with proteins related to the renin-angiotensin system. *Cell,* 184**,** 2212-2228 e12.

YURKOVETSKIY, L., WANG, X., PASCAL, K. E., TOMKINS-TINCH, C., NYALILE, T., WANG, Y., BAUM, A., DIEHL, W. E., DAUPHIN, A., CARBONE, C., VEINOTTE, K., EGRI, S. B., SCHAFFNER, S. F., LEMIEUX, J. E., MUNRO, J., RAFIQUE, A., BARVE, A., SABETI, P. C., KYRATSOUS, C. A., DUDKINA, N., SHEN, K. & LUBAN, J. 2020. Structural and Functional Analysis of the D614G SARS-CoV-2 Spike Protein Variant. *bioRxiv*.

ZAMBRANO, N., FROECHLICH, G., LAZAREVIC, D., PASSARIELLO, M., NICOSIA, A., DE LORENZO, C., MORELLI, M. J. & SASSO, E. 2022. High-Throughput Monoclonal Antibody Discovery from Phage Libraries: Challenging the Current Preclinical Pipeline to Keep the Pace with the Increasing mAb Demand. *Cancers (Basel),* 14.

ZANOTTO, P. M., GIBBS, M. J., GOULD, E. A. & HOLMES, E. C. 1996. A reevaluation of the higher taxonomy of viruses based on RNA polymerases. *J Virol,* 70**,** 6083-96.

ZHANG, J., WU, Q., LIU, Z., WANG, Q., WU, J., HU, Y., BAI, T., XIE, T., HUANG, M., WU, T., PENG, D., HUANG, W., JIN, K., NIU, L., GUO, W., LUO, D., LEI, D., WU, Z., LI, G., HUANG, R., LIN, Y., XIE, X., HE, S., DENG, Y., LIU, J., LI, W., LU, Z., CHEN, H., ZENG, T., LUO, Q., LI, Y. P., WANG, Y., LIU, W. & QU, X. 2021a. Spike-specific circulating T follicular helper cell and cross-neutralizing antibody responses in COVID-19-convalescent individuals. *Nat Microbiol,* 6**,** 51-58.

ZHANG, M. Y., SHU, Y., PHOGAT, S., XIAO, X., CHAM, F., BOUMA, P., CHOUDHARY, A., FENG, Y. R., SANZ, I., RYBAK, S., BRODER, C. C., QUINNAN, G. V., EVANS, T. & DIMITROV, D. S. 2003. Broadly cross-reactive HIV neutralizing human monoclonal antibody Fab selected by sequential antigen panning of a phage display library. *J Immunol Methods,* 283**,** 17-25.

ZHANG, Q., XIANG, R., HUO, S., ZHOU, Y., JIANG, S., WANG, Q. & YU, F. 2021b. Molecular mechanism of interaction between SARS-CoV-2 and host cells and interventional therapy. *Signal transduction and targeted therapy,* 6**,** 233.

ZHAO, A., TOHIDKIA, M. R., SIEGEL, D. L., COUKOS, G. & OMIDI, Y. 2016. Phage antibody display libraries: a powerful antibody discovery platform for immunotherapy. *Crit Rev Biotechnol,* 36**,** 276-89.

ZHAO, Y., JACKSON, S. M. & AITKEN, R. 2006. The bovine antibody repertoire. *Dev Comp Immunol,* 30**,** 175-86.

ZHAO, Y., KACSKOVICS, I., RABBANI, H. & HAMMARSTROM, L. 2003. Physical mapping of the bovine immunoglobulin heavy chain constant region gene locus. *J Biol Chem,* 278**,** 35024-32.

ZHENG, B., GREEN, A. C. A., TAZARE, J., CURTIS, H. J., FISHER, L., NAB, L., SCHULTZE, A., MAHALINGASIVAM, V., PARKER, E. P. K., HULME, W. J., BACON, S. C. J., DEVITO, N. J., BATES, C., EVANS, D., INGLESBY, P., DRYSDALE, H., DAVY, S., COCKBURN, J., MORTON, C. E., HICKMAN, G., WARD, T., SMITH, R. M., PARRY, J., HESTER, F., HARPER, S., MEHRKAR, A., EGGO, R. M., WALKER, A. J., EVANS, S. J. W., DOUGLAS, I. J., MACKENNA, B., GOLDACRE, B. & TOMLINSON, L. A. 2022. Comparative effectiveness of sotrovimab and molnupiravir for prevention of severe covid-19 outcomes in patients in the community: observational cohort study with the OpenSAFELY platform. *BMJ,* 379**,** e071932.

ZHENG, K., BANTOG, C. & BAYER, R. 2011. The impact of glycosylation on monoclonal antibody conformation and stability. *MAbs,* 3**,** 568-76.

ZHOU, D., DEJNIRATTISAI, W., SUPASA, P., LIU, C., MENTZER, A. J., GINN, H. M., ZHAO, Y., DUYVESTEYN, H. M. E., TUEKPRAKHON, A., NUTALAI, R., WANG, B., PAESEN, G. C., LOPEZ-CAMACHO, C., SLON-CAMPOS, J., HALLIS, B., COOMBES, N., BEWLEY, K., CHARLTON, S., WALTER, T. S., SKELLY, D., LUMLEY, S. F., DOLD, C., LEVIN, R., DONG, T., POLLARD, A. J., KNIGHT, J. C., CROOK, D., LAMBE, T., CLUTTERBUCK, E., BIBI, S., FLAXMAN, A., BITTAYE, M., BELIJ-RAMMERSTORFER, S., GILBERT, S., JAMES, W., CARROLL, M. W., KLENERMAN, P., BARNES, E., DUNACHIE, S. J., FRY, E. E., MONGKOLSAPAYA, J., REN, J., STUART, D. I. & SCREATON, G. R. 2021. Evidence of escape of

SARS-CoV-2 variant B.1.351 from natural and vaccine-induced sera. *Cell,* 184**,** 2348-2361 e6.

ZHOU, D., ZHOU, R. & CHEN, Z. 2022. Human neutralizing antibodies for SARS-CoV-2 prevention and immunotherapy. *Immunother Adv,* 2**,** ltab027.

ZHOU, F., YU, T., DU, R., FAN, G., LIU, Y., LIU, Z., XIANG, J., WANG, Y., SONG, B., GU, X., GUAN, L., WEI, Y., LI, H., WU, X., XU, J., TU, S., ZHANG, Y., CHEN, H. & CAO, B. 2020a. Clinical course and risk factors for mortality of adult inpatients with COVID-19 in Wuhan, China: a retrospective cohort study. *Lancet,* 395**,** 1054-1062.

ZHOU, H., CHEN, X., HU, T., LI, J., SONG, H., LIU, Y., WANG, P., LIU, D., YANG, J., HOLMES, E. C., HUGHES, A. C., BI, Y. & SHI, W. 2020b. A Novel Bat Coronavirus Closely Related to SARS-CoV-2 Contains Natural Insertions at the S1/S2 Cleavage Site of the Spike Protein. *Curr Biol,* 30**,** 2196-2203.e3.

ZOST, S. J., GILCHUK, P., CHEN, R. E., CASE, J. B., REIDY, J. X., TRIVETTE, A., NARGI, R. S., SUTTON, R. E., SURYADEVARA, N., CHEN, E. C., BINSHTEIN, E., SHRIHARI, S., OSTROWSKI, M., CHU, H. Y., DIDIER, J. E., MACRENARIS, K. W., JONES, T., DAY, S., MYERS, L., EUN-HYUNG LEE, F., NGUYEN, D. C., SANZ, I., MARTINEZ, D. R., ROTHLAUF, P. W., BLOYET, L. M., WHELAN, S. P. J., BARIC, R. S., THACKRAY, L. B., DIAMOND, M. S., CARNAHAN, R. H. & CROWE, J. E., JR. 2020. Rapid isolation and profiling of a diverse panel of human monoclonal antibodies targeting the SARS-CoV-2 spike protein. *Nat Med,* 26**,** 1422-1427.